UNIVERSITÀ *DELLA* CALABRIA

Dipartimento di Farmacia e Scienze della Salute e della Nutrizione

Dottorato di Ricerca in

Medicina Traslazionale
Ciclo XXIX

STUDY OF ANTIMICROBIAL AND ANTICANCER ACTIVITY OF NEW SYNTHETIC AND NATURAL TOOLS

Settore Scientifico Disciplinare: BIO/10

Coordinatore:

Ch.mo Prof. Sebastiano ANDÒ

Supervisore:

Ch.ma Prof.ssa Anna Rita CAPPELLO

Dottorando:

Dott.ssa Dhanya DHANYALAYAM

Presentazione al Collegio dei docenti della dott.ssa Dhanya Dhanyalayam per il conseguimento del titolo di "Dottore di Ricerca in Medicina Traslazionale" (XXIX ciclo).

Le malattie infettive ed il cancro sono considerate, attualmente, i due gruppi di patologie che rappresentano la principale causa di morte, in tutto il mondo. La resistenza agli antibiotici rappresenta la minaccia più grande per il primo gruppo dal momento che, a livello mondiale, costantemente, emergono e si diffondono nuovi meccanismi di resistenza che minacciano la capacità di trattare le comuni malattie infettive. La resistenza alla chemioterapia e alle terapie mirate a livello molecolare rappresentano, invece, il grosso problema nei trattamenti terapici contro il cancro. Gli effetti collaterali dei chemioterapici e la tossicità nei confronti delle cellule sane costituiscono, inoltre, un'ulteriore minaccia al trattamento di questa patologia. A questo proposito, la ricerca scientifica e l'innovazione tecnologica sono orientati verso lo sviluppo di nuovi approcci terapeutici contro le malattie infettive ed il cancro.

Durante il dottorato di Ricerca in "Medicina Traslazionale" (XXIX ciclo) l'attività di ricerca della dott.ssa Dhanya Dhanyalayam è stata rivolta allo studio di composti naturali e neo-sintetizzati allo scopo di individuare nuove molecole con potenzialità antibatteriche, antiparassitarie ed antitumorali.

Nella prima parte del lavoro svolto, la dott.ssa Dhanyalayam ha valutato l'attività antimicrobica, *in vitro*, di una gamma di complessi dell'Argento neo-sintetizzati: Ioduro (N-metil-N- (2-idossi-ciclopentil-imidazol-2-ilidina) argento (I), Ioduro (N-metil-N- (2-idrossi-cicloesil) -imidazol-2-ilidina) argento (I) e Ioduro (N-metil-N- (2-idossi-2-fenil) etil-imidazolo-2-ilidina) argento (I), indicati rispettivamente con i nomi di AgL6, AgL18 ed AgL20.

Sin dai tempi antichi, i complessi metallici sono stati utilizzati come agenti antibatterici ed, in particolare, sono state ben riconosciute le proprietà battericide, fungicide e protozoicide dell'Argento, soprattutto nella forma di nitrato d'argento.

Diversi complessi dell'Argento si sono dimostrati efficaci nel trattamento di ferite aperte e suppurate, ustioni, osteomielite cronica e infezioni delle vie urinarie. Oggi la Sulfadiazina d'Argento (AgSD) rimane uno dei farmaci a base d'argento più comunemente utilizzate nella terapia delle ferite, anche se, a causa della sua citotossicità nei confronti di fibroblasti e cheratinociti, può provocare gravi effetti avversi, tra cui ritardi nella guarigione delle ferite stesse.

La dottoressa ha valutato l'attività antimicrobica dei nuovi complessi dell'Argento utilizzando, in primo luogo, il metodo di diffusione su piastra (Kirby-Bauer disc-diffusion test) contro due ceppi batterici Gram positivi (*Staphylococcus aureus e Streptococcus pyogenes*) e tre ceppi Gram negativi (*Escherichia coli, Klebsiella pneumoniae e Pseudomonas aeruginosa*). Le percentuali di inibizione dei nuovi complessi sono stati calcolati dai valori dei diametri di inibizione, misurati a concentrazioni

differenti di ciascuno di essi. Come controllo positivo ha utilizzato una cefalosporina commerciale (cefotaxime) e Argento-sulfadiazina (AgSD).

Il profilo di sensibilità antibiotica dei ceppi batterici ottenuto, ha dimostrato che, rispetto a cefotaxime, tra i tre complessi testati, solo AgL6 possedeva attività antimicrobica contro i microrganismi, ma solo ad elevata concentrazione. Allo scopo di definire meglio la capacità antibatterica di AgL6 la dottoressa ha condotto il test di diluizione in brodo liquido che le ha permesso di calcolare i valori della Minima Concentrazione Inibente (MIC), contro i diversi ceppi batterici testati. Purtroppo, i risultati ottenuti hanno evidenziato dei valori di MIC elevati e superiori a quelli riscontrati per i controlli positivi utilizzati. Risultati analoghi sono stati riportati nella valutazione della Minima Concentrazione Battericida (MBC).

Partendo dal presupposto che la bassa attività di AgL6 potrebbe essere dovuta ad un difficile ingresso del complesso nella cellula batterica, al fine di facilitarne l'assunzione, la dottoressa ha utilizzato un dispositivo farmaceutico orientato, un nanocarrier. Il nanocarrier biopolimerico è stato ottenuto mediante l'autoassemblaggio di destrano oleato coniugato, in cui la catena di destrano e i residui oleici rappresentano rispettivamente le parti idrofile e quelle idrofobe della struttura anfifilica. La dimensione nanometrica delle particelle è stata confermata da analisi DLS (diametro medio compreso tra 500-600 nm). Le nanoparticelle sono state, quindi, caricate con AgL6 e, successivamente, ne è stata valutata l'attività antibatterica. Da questi esperimenti la dottoressa ha ottenuto risultati molto interessanti, infatti, i valori di MIC sono risultati ridotti quattro volte sia per i batteri Gram positivi che per i Gram negativi, ad eccezione di *P. aeruginosa* in cui è stata riscontrata una riduzione del valore di MIC pari a due volte, rispetto al controllo. Sorprendentemente, i valori ottenuti sono risultati essere due volte inferiori rispetto a quelli diriscontrati dopo trattamento con AgSD.

Infine, allo scopo di comprendere se l'attività antibatterica osservata per AgL6 fosse dovuta ad una variazione della permeabilità della membrana esterna batterica indotta dal trattamento con il complesso, la dottoressa ha condotto degli esperimenti con Ioduro di Propidio (PI), colorante fluorescente impermeabile alla membrana. I risultati hanno mostrato, nei batteri trattati con dosi crescenti di AgL6, un aumento della fluorescenza dovuta a PI, dose dipendente, rispetto alle cellule non trattate, indicando una maggiore permeabilità della membrana.

Nel complesso gli studi condotti dalla dottoressa Dhanyalayam hanno evidenziato che il complesso AgL6 può essere considrato un buon candidato come agente antibatterico, soprattutto contro iceppi Gram negativi, di per sé resistenti a molte classi di antibiotici.

Secondo l'Organizzazione Mondiale della Sanità (OMS), 17 malattie causate da batteri e parassiti sono classificate come malattie tropicali trascurate (NTD). Tali patologie sono endemiche in 149

paesi tropicali e subtropicali ed interessano più di 1 miliardo di persone, di cui 875 milioni di bambini; sono caratterizzate da gravi dolori e disabilità a lungo termine e sono responsabili, ogni anno, di oltre 500.000 decessi. La Tripanosomiasi umana africana è una di queste patologie; è causata da due parassiti del genere *Trypanosoma; T. brucei rhodesiense* e *T. brucei gambiense* ed è considerata una malattia con un impatto socioeconomico devastante nell'Africa sub-sahariana infatti, se non trattata, si rivela fatale. Le terapie attuali presentano molti limiti, pertanto la ricerca farmaceutica è rivolta verso la scoperta di nuovi farmaci o nell'utilizzo di farmaci già da tempo impiegati nella la terapia di altre patologie, processo noto come "repurposing" del farmaco.

La dottoressa Dhanyalayam ha incentrato una parte dei suoi studi nella ricerca di molecole con attività tripanocida. In particolare, ha analizzato 2000 estratti naturali di Funghi ed Attinomiceti, ha selezionato quelli che hanno mostrato, *in vitro*, attività tripanocida e ne ha identificato il composto attivo, mediante cromatografia liquida e spettroscopia di massa. Tra le molecole attive, la dottoressa ha identificato la Chaetocina, noto inibitore della metilazione degli istoni, già utilizzata come farmaco antibatterico ed antitumorale e, nel suo lavoro di ricerca, ha valutato la possibilità che questa molecola potesse essere considerata anche un ipotetico agente tripanocida. I risultati sono stati sorprendenti, infatti la Chaetocina ha mostrato una buona attività trypanocida a concentrazioni molto basse con un valore di IC_{50} pari a 8.3 nM.

Al fine di far luce sul meccanismo d'azione della molecola sul Tripanosoma, la dottoressa ha condotto studi di immunofluorescenza che hanno evidenziato cambiamenti morfologici delle cellule e degradazione della cromatina, dopo trattamento con Chaetocina. L'analisi di citometria di flusso ha rivelato, invece, l'arresto del ciclo cellulare in fase G2.

Dagli studi, *in vitro*, effettuati dalla dott.ssa Dhanyalayam si può dedurre che la Chaetocina potrebbe essere considerata un potenziale agente tripanocida, ma saranno necessari ulteriori ricerche al fine di valutare se la molecola è in grado di attraversare la barriera emato-encefalica, infatti solo in questo caso potrà essere presa in considerazione quale ipotetico farmaco contro la Tripanosomiasi.

Inoltre, l'attività scientifica della dott.ssa Dhanya Dhanyalayam è stata rivolta allo studio degli effetti di un sale di fosfonio commerciale (11-metossi, 11-oxoundecil) trifenilfosfonium bromuro (MUTP) e di due sali di ossido di fosfina neo-sintetizzati, 3,3'-(metilfosforil) Cloruro dibenzenaminium e cloruro 3,3'-(fenilfosforil) dibenzaminium cloruro (SBAMPO e SBAPPO), sulla proliferazione in due linee cellulari tumorali umane: cellule di cancro al seno (MCF-7) e cellule di adenocarcinoma della cervice uterina (HeLa).

I sali di fosfonio sono una classe di molecole cationiche lipofiliche che si accumulano preferenzialmente nei mitocondri e inibiscono la crescita delle cellule tumorali umane. Infatti, il potenziale della membrana mitocondriale delle cellule tumorali, relativamente elevato rispetto a

quello delle cellule normali, induce i sali di fosfonio ad accumularsi preferenzialmente nei mitocondri e ad inibirne la funzione.

I risultati ottenuti dalla dott.ssa Dhanyalayam hanno evidenziato che solo MUTP presenta effetti antiproliferativi su entrambe le linee cellulari tumorali, senza compromettere la proliferazione delle linee cellulari non tumorali MCF-10A, utilizzate come controllo. In particolare, la dottoressa ha dimostrato che il trattamento con MUTP delle cellule MCF-7 compromette la normale progressione del ciclo cellulare. Infatti, studi di citometria di flusso hanno evidenziato un arresto del ciclo cellulare nella fase G1/S, dopo trattamento delle cellule MCF-7 con due concentrazioni di MUTP (0,5 and 2 μM) per per 24 h o 72 h. Tale risultato ha indotto la dottoressa ad indagare il possibile coinvolgimento del gene oncosoppressore p53 e del suo target naturale p21, inibitore di chinasi ciclina-dipendenti, nell'arresto della crescita cellulare e le ha permesso di dimostrare che dosi crescenti di MUTP inducono un incremento di p53, sia a livello di trascritto che di tradotto, con un concomitante aumento dell'espressione di p21.

Successivamente, per caratterizzare la funzione metabolica delle cellule MCF-7 dopo trattamento con MUTP, la dottoressa ha marcato le cellule con sonde metaboliche specifiche e le ha analizzate mediante FACS. I risultati hanno mostrato che il trattamento con MUTP determina una riduzione della massa mitocondriale, del potenziale di membrana e del rapporto potenziale/massa. In accordo con quanto riportato in letteratura, circa la relazione esistente tra riduzione del potenziale della membrana mitocondriale e specie reattive dell'ossigeno (ROS), la dottoressa ha riscontrato un aumentato livello di ROS, nelle cellule sottoposte a trattamento con MUTP. Un squilibrio bioenergetico, indotto da MUTP, nelle cellule trattate è stato ulteriormente confermato dalla riduzione dei livelli di espressione degli enzimi del pathway ossidativo mitocondriale (OXPHOS).

Infine, per definire il meccanismo di morte cellulare determinato dal sale di fosfonio oggetto di studio, la dottoressa ha indagato sul meccanismo di apoptosi utilizzando tre approcci differenti: il TUNEL test, il DNA Laddering e l'analisi di Western blot di caspasi-3, caspasi-9 e Bax, tre proteine coinvolte nel meccanismo intrinseco di apoptosi. I risultati ottenuti hanno confermato che il trattamento con MUTP induce l'attivazione della via intrinseca dell'apoptosi.

Considerati insieme, tutti questi dati hanno portato la dottoressa Dhanyalayam a dedurre che MUTP, essendo in grado di inibire, selettivamente, la proliferazione delle cellule neoplastiche determinandone la morte per apoptosi, potrebbe essere preso in considerazione quale potenziale agente antitumorale.

Durante l'intero periodo del dottorato di ricerca la dott.ssa Dhanya Dhanyalayam ha mostrato notevole interesse nell'apprendimento di numerose tecniche laboratoristiche, evidenziando buone capacità nella esecuzione dei protocolli sperimentali e nella valutazione dei dati ottenuti. Ha
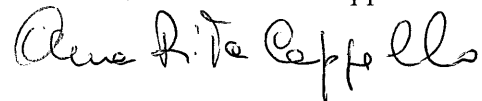
partecipato, inoltre, alle attività seminariali e didattico-formative organizzate dal Dipartimento di Farmacia e Scienze della Salute e della Nutrizione. L'esperienza maturata durante il ciclo di dottorato è stata accresciuta da un periodo di formazione svolto presso l'"Instituto de Investigación Biosanitaria de Granada" dell'Università di Granada, sotto la guida del prof. Jose Antonio Garcia Salcedo.

Il contributo scientifico della dottoressa è dimostrato dai lavori pubblicati (ed in corso di pubblicazione) su riviste internazionali la cui rilevanza scientifica della collocazione editoriale è di buon livello. Pertanto si esprime parere estremamente positivo sull'attività scientifica svolta dalla dott.ssa Dhanya Dhanyalayam.

Rende, 18-05-2017   **Docente Tutor**

                                                   Prof.ssa Anna Rita Cappello

To the most special person, My Husband,

Hariprasad Thangavel

ACKNOWLEDGEMENTS

This thesis has been written as a part of my three-year PhD at Department of Pharmacy Health and Nutritional science in the University of Calabria, Italy, between December 2013 and February 2017.

First and foremost, I praise God, the almighty for providing me this opportunity and granting me the capability to proceed successfully. This thesis appears in its current form due to the assistance, guidance and encouragement of several people. I would therefore like to offer my sincere thanks to all of them.

I would like to express my deep and sincere gratitude to **Prof. Sebastiano Ando**, my esteemed director of the Department of Pharmacy Health and Nutritional science, for accepting me as a PhD student and continuous support throughout my PhD.

I am deeply grateful to my supervisor, **Prof.ssa Anna Rita Cappello**, whose support and motivation from the initial to the final level enabled me to develop an understanding of the subject. Her understanding and thoughtful guidance have provided a good basis for this thesis. I could not have imagined having a better supervisor for my PhD study.

I would like to thank **Dott. Marco Fiorillo** for his advises and friendly assistance with various problems time to time. I greatly appreciate his time in teaching me some basics about some experiments during my initial days. Without his initiative, my PhD would not have been possible.

I express my sincere thanks to **Prof. Francesco Puoci** for developing and providing 'Pharmaceutically oriented vehicle' for my research investigations against bacterial species.

I express my sincere thanks to **Prof. Pasquale Longo, Prof.ssa Carmela Saturnino & Prof.ssa Maria Stefania Sinicropi** for their valuable insights and collaborative inputs to my research project.

Next, I cordially thank **Prof. Jose Antonio Garcia Salcedo**, for accepting me as a visiting scholar and giving me the opportunity to work in Genyo (Spain). I really had a valuable and enjoyable experience working with his team. His excellent guidance, encouragement and motivation have been of great value in this thesis.

I express my sincere thanks to a wonderful personality I have ever found, **Matilde Ortiz** for her personal and professional support during my stay in Genyo (Spain).

I express my sincere thanks to my dear friends in the lab, **Luca Frattaruolo, Biagio Armentano, Roberta Bartucci, Antonietta fazio & Emanuela Frega** for their kind support throughout my PhD.

I extend my special thanks to my bestie and colleague **Luigina Muto** for her kind support throughout my stay in Italy in many things.

I cannot finish without thanking my family. I warmly thank and appreciate my parents **Devi and Balakrishnan,** my sister **Dhanisha** and her husband **Nithin**, my adorable husband **Hariprasad Thangavel,** one of the best gift I have ever got**.** My sincere thanks to my affectionate in-laws **Malathi and Thangavel** and my lovely brother-in-law **Naveen Prasath**. All the support they have provided me over the years was the greatest gift anyone has ever given me.

CONTENTS

ABSTRACT

Infectious diseases and cancer are the two disease groups that representing the major cause of death worldwide. Unfortunately, antibiotic resistance is the biggest threat in the first case; in fact, new resistance mechanisms continuously are emerging and spreading globally, threatening the ability to treat common infectious diseases. A growing list of infections caused by bacteria, viruses, parasites etc. are becoming harder and harder to treat, and sometimes impossible, as antibiotics become less effective. Without urgent action, we are heading for a post-antibiotic era, in which common infections and minor injuries can once again kill the human population. Concerning cancer, Resistance to chemotherapy and molecularly targeted therapies is a major problem in current research. Drugs side effects and toxicity to normal body cells is also an important threat in cancer treatments. In this regard, these problems are at the forefront of scientific research and technological innovation and are leading to the development of new therapeutic approaches against cancer and infectious disease with fewer side effects and lesser resistance problems.

The aim of the present study was to investigate on the new compounds in order to find new possible therapeutic agents against bacteria, parasites and cancer.

Infectious diseases are caused by microorganisms such as bacteria, parasites, viruses etc.; in particular, bacterial infectious diseases are caused by either Gram +ve or Gram -ve bacteria. Certainly, antibiotics are the main weapon against infectious bacterial diseases; however, the uncontrolled use of antibiotics to control infections in humans, animals and in agriculture caused the development of drug resistance by bacterial populations. Besides this, infections caused by Gram -ve bacteria are difficult to treat due to the presence of a protective outer membrane consisting of lipopolysaccharides. Therefore, it is clear that there is a need to develop novel classes of antibacterial agents capable of killing bacteria through mechanisms unlike those of the known classes of antibiotics. Then, scientists are currently searching for new approaches to treat infectious diseases, particularly those caused by Gram -ve bacteria, focusing on exactly how the pathogens change and how drug resistance evolves.

Since ancient times, metal complexes have been used as antibacterial compounds, metallic silver and silver salts are good examples of this. Silver compounds are particularly interesting since their antibacterial activity can be altered by changing the ligand associated

with the silver complex. To date, among silver derivatives, silver sulfadiazine remains one of the most commonly-used antibacterial drugs. Therefore, metal N-heterocyclic carbene (M-NHC) complexes appeared as an emerging field of research in medicinal chemistry where NHC complexes of coinage metals (Cu, Au, and Ag) proved to be better antimicrobial agents. Herein, it was investigated the, *in vitro,* antibacterial activity of the newly synthesized silver (Ag) complexes, Iodide[N-methyl-N-(2-hydoxy-cyclopentyl-imidazole-2ylidine]silver(I), Iodide[N-methyl-N-(2-hydoxy-cyclohexyl)-imidazole-2-ylidine]silver(I) and Iodide[N-methyl-N-(2-hydoxy-2-phenyl)ethyl-imidazole-2-ylidine]silver(I), namely AgL6, AgL18 and AgL20, against two Gram +ve (*Staphylococcus aureus*, *Streptococcus pyogenes*) and three Gram -ve (*Escherichia coli*, *Klebsiella pneumoniae* and *Pseudomonas aeruginosa*) bacteria. Among these, AgL6 showed good antibacterial activity against both Gram +ve and Gram -ve bacteria. However, the minimum inhibitory concentration (MIC) value was 32 µg/mL for Gram +ve and 16 µg/mL for Gram -ve bacteria, which was higher than that displayed by commercial drug, used as control (Silver Sulfadiazine, AgSD).

We therefore hypothesized that the poor activity is due to the poor intake of the compound. In order to enhance its antibacterial activity, we have developed "a pharmaceutically-oriented device", a nanocarrier as a tool for targeted drug delivery. Here it was described, for the first time, the production of a polymer nanostructure in which dextran, a biopolymer, and oleate residues represent the hydrophilic and hydrophobic parts, respectively. This nanoparticle was loaded with AgL6 and the antibacterial activity has been investigated. The results were very interesting, with MIC values being reduced four-fold for both Gram +ve and Gram -ve bacteria. Surprisingly, these values were two-fold lower than for silver sulfadiazine. Briefly, our results showed that *K. pneumoniae* and *E. coli* are the most susceptible bacteria to AgL6, followed by *P. aeruginosa*.

In conclusion, the investigated compound AgL6 showed excellent potentiality against bacterial infections.

According to the World Health Organization (WHO), 17 diseases caused by bacteria and parasites have been classified as neglected tropical diseases (NTDs). NTDs are endemic in 149 tropical and subtropical countries and affect more than 1 billion people, including 875 million children. These diseases are responsible for over 500,000 deaths per year and are characterized by severe pain and long term disability. Human African Trypanosomiasis

(sleeping sickness) is an important disease among them and is caused by two parasites of the genus Trypanosome: *Trypanosome brucei rhodesiense* and *Trypanosome brucei gambiense*. Trypanosomiasis is a disease with a devastating socio-economic impact in sub-Saharan Africa through direct infection of humans and livestock. This disease is fatal if left untreated. Current therapy relies on five drugs that have many limitations among which acute toxicity, problems with oral absorption and emergence of trypanosomal resistance, this latter is a major concern owing to the absence of vaccines and therapeutic alternatives. Therefore pharmaceutical research is aimed at the discovery of new drugs, although the investment in this therapeutic area is not attractive owing to the prospect of poor financial returns. Many pharmaceutical industries have already utilized an opportunistic approach by utilizing drugs long since used for other diseases, a process known as "repurposing" of the drug. It is estimated that over half of the drugs used today are derived from natural sources.

In the present study, in a search for molecules with trypanocida activity, it was screened 2000 natural extracts from Fungi and Actinomycetes. The extracts showing activity were selected, and the active compound was identified by liquid chromatography and mass spectroscopy. Chaetocin is one of the molecules identified which showed good trypanocidal activity when tested *in vitro*. Chaetocin is already used as an antibacterial and anticancer drug, here it was repurposed as drug against trypanosomiasis. The results were very surprising because the trypanocidal activity was in the nanomolar range; the IC_{50} value was found to be 8.3 nM.

Next, it was investigated on its mechanism of action. In chaetocin treated cells, morphological changes and chromatin degradation were identified, by fluorescence microscopy and cell-cycle arrest during the G2 phase was proven by cytometry analysis. Finally, it was hypothesized that the enzyme histone methyl transferase, an important enzyme acting in the G2 phase, could be the target for this drug. This study displayed that chaetocin could have great potentiality in the fight against the deadly trypanosomiasis. However, further studies will be needed to reveal whether this compound can cross the blood-brain barrier.

In the third part of this thesis it was evaluated the synthesis and anticancer activity of some phosphonium salts. Phosphonium salts are a class of lipophilic cationic molecules that accumulate preferentially in mitochondria and inhibit the growth of human cancer cell lines.

3

The aim of the present study was to investigate the effects of a lipophilic phosphonium salt, (11-methoxy, 11-oxoundecyl)triphenylphosphonium bromide (MUTP) along with two other newly synthesized phosphine oxide salts, 3,3'-(methylphosphoryl)dibenzenaminium chloride and 3,3'-(phenylphosphoryl)dibenzenaminium chloride (SBAMPO and SBAPPO) on proliferation, in two human cancer cell lines: human breast cancer cells (MCF-7) and human uterine cervix adenocarcinoma cells (HeLa) and to elucidate their mechanism. The cancer cell mitochondrial membrane potential is relatively high when compared to normal cells, this force the phosphonium salts to accumulate, preferencially, in the mitochondria and inhibit their function. The results showed that only MUTP exhibits anti-proliferative effects on both cell lines, without affecting normal breast epithelial cell proliferation. More specifically, it was demonstrated that MUTP treatment of breast cancer cells is associated with impaired cell cycle progression, as determined by cytometry analysis. The G1/S cell cycle arrest was confirmed by an increased expression level of two proteins involved in cell cycle regulation, p21 and p53.

Recently, there has been a surge of interest in developing compounds selectively targeting mitochondria for the treatment of neoplasms. The critical role of mitochondria in cellular metabolism and respiration supports this therapeutic rationale. Dysfunction in the processes of energy production and metabolism contributes to attenuation of response to pro-apoptotic stimuli and increased ROS production both of which are implicated in the initiation and progression of most human cancers. Therefore, in order to characterize the mitochondrial function in MCF7 cells, after MUTP treatment, the cells were stained with specific metabolic probes and analyzed by FACS.

The outcomes displayed that MUTP treatment decreased mitochondrial mass and mitochondrial membrane potential and increased the ROS production. In agreement with these findings, the reduction in the expression of the mitochondrial oxidative pathway (OXPHOS) enzymes revealed a bioenergetics failure, induced by MUTP, in treated cells. TUNEL assay, DNA Laddering and Western blot analysis of caspase-3, caspase-9 and Bax confirmed the apoptotic effect of MUTP treatment.

Taken together, all these data suggest that MUTP may be capable of selectively targeting neoplastic cell growth and therefore has potential applications as an anticancer agent.

CHAPTER 1

AgL6: A New Silver Complex as Candidate Antibacterial Agent

1.1 INTRODUCTION

Bacterial diseases continue to present a major threat to human health. Infectious diseases (IDs) concern the whole world and can only be combated by internationally coordinated and interdisciplinary approaches [1]. Antibiotics are certainly an important weapon against IDs however, their wide use to control microbial infections in humans, animals and in agriculture has caused the development of resistance in bacterial populations. The drug discovery against bacterial diseases was in a peak during mid of the last century. After streptogramins and quinolones in 1962, no novel class of antibiotics were identified and approved for clinical use until the launch of linezolid in 2000 [2]. Some of the bacterial species continues to be a frequent cause of life threatening infections during the first two months of life. In the past 25 years, a steady increase in microbial infections was occurred therefore, serious attention has been directed towards the research and development of new antimicrobial drugs [3]. During the last decade's scientists discovered many new organisms and new strains of familiar bacteria. Such emerging bacterial diseases present a clear challenge to biomedical researchers. In addition, the emergence of antibiotic-resistant bacteria represents a serious problem that could be overcome by the development of novel antimicrobial agents.

In this chapter, we have demonstrated the antibacterial activity of a silver compound, namely AgL6. Before explaining about the promising antibacterial activity of this compound, it is good to mention some of the main features of two different groups of bacteria, Gram positive (Gram +ve) and Gram negative (Gram -ve). This information will be necessary to better understand the mechanism of action of these novel compounds. Danish physician Hans Christian Gram devised a method to differentiate two types of bacteria based on the structural differences in their cell walls. In his test, bacteria that retain the crystal violet dye do so because of a thick layer of peptidoglycan and are called Gram-positive bacteria. In contrast, Gram-negative bacteria do not retain the violet dye and are colored red or pink. Compared with Gram-positive bacteria, Gram-negative bacteria are more resistant against antibodies because of their impenetrable cell wall. The cell wall structure of bacteria have numerous differences. The cell wall is a rigid structure arranged immediately outside the cell membrane. It is one of the most important structures in the prokaryotes which determines

the pathogenicity of the organism and it is the site of action for many antibiotics. So, it is important to study the structure of the bacteria. The space which is found in between the cell membrane and outer membrane is called periplasmic place. The nature and composition of the periplasm and the periplasmic space differ between Gram +ve bacteria and Gram -ve bacteria. The fundamental element of the cell wall is peptidoglycan and it is made up of subunits which are identical to each other. They are two polysaccharide derivatives, the N-acetyl glucosamine and N-acetyl muramic acid, and many amino acids such as the D-glutamic acid, D-alanine and the meso-di amino pimelic acid. The presence of amino acids in the D form exerts a protective action against the attack of most peptidases. The skeleton of the polymer is composed of alternating residues of N-acetyl glucosamine and N-acetyl muramic acid.

The Gram +ve bacteria contain only one layer and it is 100-120 Armstrong thick. The majority of the cell wall is made up of peptidoglycan layer and it is sensitive to many antibiotics (**Figure 1**).
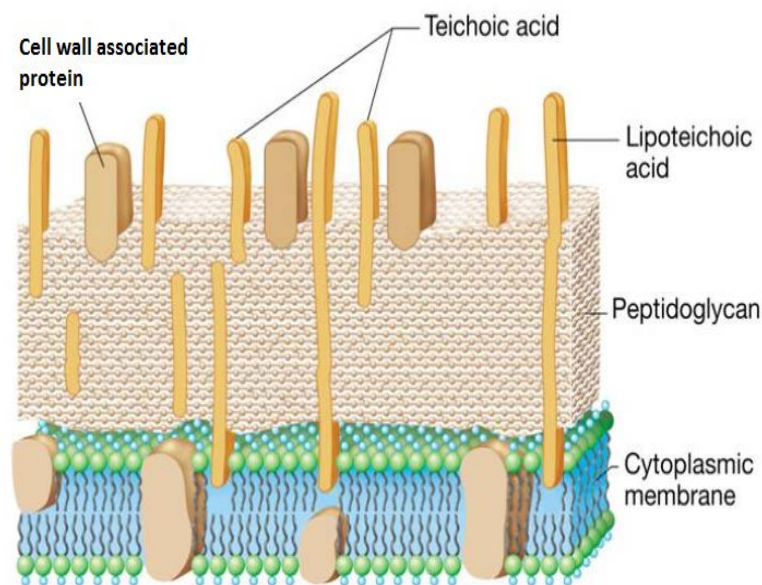
Figure 1. Structure of Gram +ve bacterial cell membrane

The Gram -ve bacteria contain two layers, an outer membrane and an inner membrane. It is 70-120 Armstrong thick (**Figure 2**). They are more resistant to antibiotics. It contains large number of lipopolysaccharides. These bacteria can produce endotoxins.
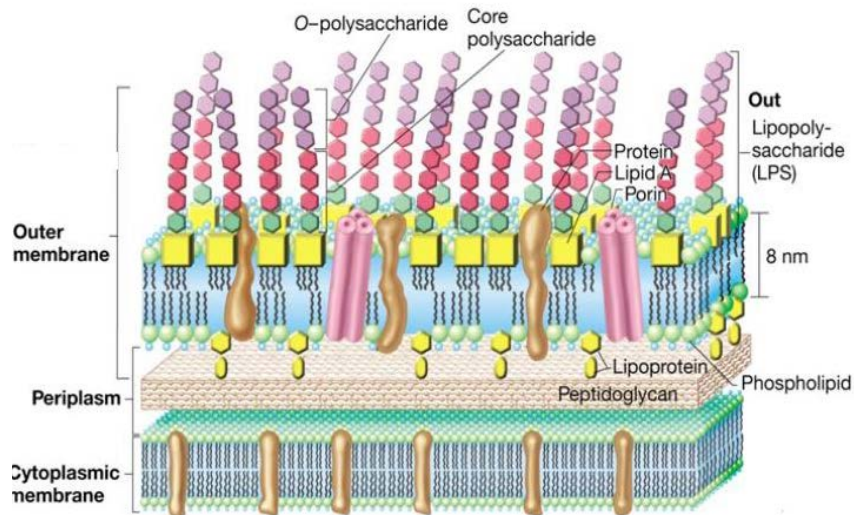
Figure 2. Structure of Gram -ve bacterial cell membrane.

The main reason behind the failure of bacterial disease treatment is the development of bacterial resistance. The uncontrolled use of antibiotics is the main reason behind this. Bacteria have highly effective defense mechanisms, giving them the ability to mutate over time and become resistant to many of the medicines available to treat them.

An important Gram +ve bacteria, *Staphylococcus aureus* is responsible for the hospital and community associated infection in the United States (US) and around the world. These infections are very difficult to treat due to the propensity to develop antibiotic resistance and it forms biofilm. For clinical use, no anti-biofilm agents are discovered yet [4]. Methicillin-resistant Staphylococcus aureus has been responsible for the serious hospital infections worldwide. According to the World Health Organization (WHO), approximately 5%–10% of patients throughout the world is facing some acquired nosocomial infection during hospitalization [5]. The discovery of new and effective antimicrobials or resistance modulators is necessary to combat the spread of resistance or to reverse the multi-drug resistance [6].

Multi-drug resistance of Gram -ve bacteria constitutes a major obstacle in the antibacterial fight worldwide. Three are the main mechanisms of multi-drug resistance: the capture by bacteria of resistance genes from the surrounding environment; the freezing of polymorphism in antibiotic target genes that imparts drug-resistance [7]; and the up-regulation of proteins involved in drug efflux [8, 9] or enzymatic inactivation [10]. Besides this

the infections, caused by Gram -ve bacteria, are difficult to treat because these organisms have a protective outer membrane consisting of lipopolysaccharides [11].

For this reason, there is an urgent need of new antimicrobial agents that express antibacterial activity, particularly against Gram -ve pathogens and that could be used to fight drug resistance.

1.1.1 Metal complexes as antibacterial agents

Metal complexes have been used as an antibacterial agent since ancient times. The antibacterial properties of silver and silver ions have been recognized before centuries. It exhibited bactericidal, fungicidal and protozoacidal   in sub micro molar range [12]. Particularly silver used in the treatment of infection in the form of silver nitrate, because of wide spectrum of activities [13, 14]. Several silver compounds have proven effective in the treatment of open wounds, and suppurating wounds, burns, chronic osteomyelitis, and urinary tract infections [13, 15, 16]. Silver sulfadiazine is a broad-spectrum antibiotic used to prevent bacterial infection in severe burns [17]. The inorganic salts and complexes of silver such as silver nitrate and silver sulfadiazine and its therapeutic use is fully recognized. The silver in the form of colloidal silver has been historically consumed as antibacterial agents. Like other nontraditional antibiotics, silver ions can act with multiple components of bacterial structure [18]. Although the cytotoxic effects of silver against Gram +ve and Gram -ve bacteria have long been established, the exact mechanisms of action are not completely understood [19].

Several literature data reported that the mechanism of action of silver ions is due to the strong electrostatic interaction between silver ions and electron donor group of proteins, such as thiols, that could lead to the inactivation of proteins [15, 20]. However, different papers indicated that silver ions could competitively bind to metal chelation site in the enzyme and displace the binding of inherent metal cations suitable for the proper functioning of the enzymes [21]. These enzymes are the critical regulators of cellular respiration, oxidation and cell wall integrity [22, 23]. Moreover, silver ions have the ability to bind with the nucleic acid bases of some bacteria and can cause a block in the replication process by condensing the nuclear DNA [15]. In addition, these ions can produce and accumulate reactive oxygen species in the bacterial cell, which can cause damage in the critical cellular functions

including chromatin condensation and ultimately disrupting all the key cellular functions [24]. Nowadays silver ions are used for water sterilization procedure, dental works and catheters. Disulfide bond containing amino acids, non-sulfur containing amino acids and sulfur containing compounds such as cystathione, cysteic acid, L-methionine, taurine and sodium thiosulfate were all unable to neutralize silver ions. This indicated that the interaction of silver ions with thiol group of enzymes and proteins plays an essential role in the antimicrobial action. In addition to their effect in bacterial enzymes, silver ions can deposit inside the vacuoles and cell wall as granules [25]. In *Vibrio cholera,* silver ions produce a massive leak of protons through the membrane of the bacterium and can cause complete de energization and ultimately death [26]. The silver zeolite in contact with bacterial cell can produce reactive oxygen species inside the cell and ultimately lead to bacterial cell death [27]. It is known that silver can act against two potential opportunistic pathogens namely *Pseudomonas aeruginosa* and *Aeromonas hydrophila* [28].

As we know that Gram -ve bacteria are mostly become resistant to antibiotics. Still the silver ion is a good choice to react with it. Silver can be used to enhance the action of some antibiotic against Gram -ve bacteria and strengthen the antibiotic arsenal for fighting bacterial infections [29]. Silver nanoparticles is another important thing which can be used as antibacterial. Nanoparticles have been used for numerous physical, chemical, biological and therapeutic applications. The free radical generation of silver nanoparticles on microbial growth inhibition was investigated and confirmed the activity of the nanoparticles on yeast and *Escherichia coli* [30, 31]. The antibacterial effects of silver nanoparticles are size-dependent, since the only nanoparticles that can directly interact with bacterial surface preferentially have a diameter of 1 to 10 nm [32].

So far, we were discussing about the advantages and possible mechanism of action of silver compounds on different bacteria. There are some disadvantages also. The main disadvantage of silver nanoparticles is the cytotoxicity. Nanoparticles can accumulate inside the body for a long period of time. Commercially using antibiotic form of silver is the silver sulfadiazine (AgSD), remains as an important drug used in wound therapy and in medicinal devices. Modak et al. combined two useful antibacterial agents, silver nitrate and sulfadiazine, to form an extremely useful agent Silvazine [33].

It is thought that Silvazine functions with the slow release of Ag+ as the primary biocide while sulfadiazine serves mostly to keep Ag+ in solution and to prevent the light-sensitive formation of black colloidal AgO on the skin surface, a serious cosmetic problem with AgNO3-based products [14]. Besides that, it can cause adverse side effects like gastrointestinal reactions, allergic reactions, delayed wound healing due to its cytotoxicity towards fibroblasts and keratinocytes [34]. In recent years, there has been a considerable trend toward the development of metal complexes having biological properties. Indeed, Silver-N-heterocyclic carbene complexes can release, slowly silver ions into the wound, enabling better prevention of infection and promoting healing.

Metal N-heterocyclic carbene (M-NHC) complexes have appeared as an emerging field of research in medicinal chemistry where NHC complexes of coinage metals (Cu, Au, and Ag) proved to be better anticancer and antimicrobial agents [35-37]. For their excellent chemical properties and quite easy synthesis, different examples of NHC complexes of silver, gold platinum or other transition metals have been evaluated, biologically, and they seem to have promising properties in biomedical sciences [38-43]. In particular, Ag-NHCs have long been used as antimicrobial agents for their high stability, as they can overcome the drawbacks associated with conventional silver antibiotics including resistance and fast loss of activity [44, 45].

As a result, herein we have investigated the *in vitro* antimicrobial activity of a range of newly synthesized silver (Ag) complexes, Iodide[N-methyl-N-(2-hydoxy-cyclopentyl-imidazole-2ylidine]silver(I), Iodide[N-methyl-N-(2-hydoxy-cyclohexyl)-imidazole-2-ylidine]silver(I) and Iodide[N-methyl-N-(2-hydoxy-2-phenyl)ethyl-imidazole-2-ylidine]silver(I), namely AgL6, AgL18 and AgL20 (**Figure 3**). Even though the results were surprising, we had to modify few things to make it more effective. For AgL6, in particular, we have developed a polymeric nanocarrier, in order to increase its efficacy, as described in the literature [46].
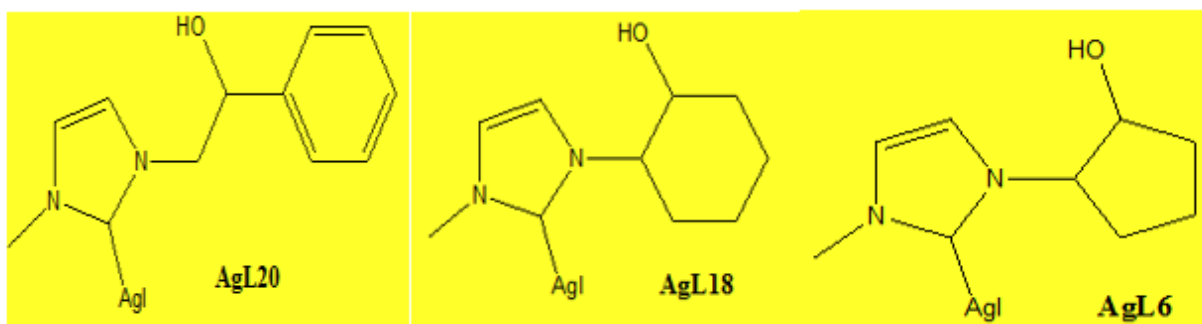
Figure 3. Structures of the silver compounds synthesized.

Lipids, polymers and organic particles are the main materials used for the synthesis of carrier molecules. Hydrogels, dendrimers, drug-polymer conjugates and polymer vesicles represent few examples of nanosized particles based on polymeric materials and used as drug delivery systems. Polymer vesicles are nanosized drug carriers auto assembled from amphiphilic block copolymers. They are organized in structures in which the hydrophobic parts are inserted in the middle of the membrane, while the hydrophilic parts are exposed on both the inner and outer surfaces, delimiting a central aqueous core separated from the outside environment [47]. This organization represents the major advantage of this kind of structure, that can encapsulate hydro soluble drugs in the aqueous core, and hydrophobic or amphiphilic compounds in the thick membrane. Despite a large number of scientific papers describing the development of polymer vesicles as drug delivery systems, only few have explored their application to antimicrobials [48, 49]. Here we describe for the first time the production of polymer vesicles in which dextran and oleate residues represents the hydrophilic and the hydrophobic parts, respectively. The nanoparticles were loaded with one of the newly synthesized Ag-based drug, whose antimicrobial activity was not investigated yet.

1.2 MATERIALS AND METHODS

1.2.1 Materials

Tryptic soy broth (TSB) and Tryptic soy agar (TSA) were manufactured by BD (Frankiln Lakes, NJ) and purchased from Fisher Scientific (Pittsburgh, PA); Bacto Agar (BD Biosciences); sterile filter paper disc (Oxoid™); Müller-Hinton broth II (Difco, Detroit, MI, USA) containing 2 g/L beef infusion solids, 17.5 g/L casein hydrolysate, 1.5 g/L starch; AgSD (Sigma-Aldrich, St. Louis, MO, USA); and Dimethyl sulfoxide, DMSO (Sigma-Aldrich, St. Louis, MO, USA). All these materials used for growing the pathogens and for testing antibacterial activity were exposed to UV radiation or sterilized in an autoclave prior to use, unless purchased as sterile.

1.2.2 Bacterial strains

The microbial strains used in this study were obtained from American Type Culture Collection center (ATCC, Manassas, VA). The ATCC identification number for each strain was as follows: *Escherichia coli* (ATCC 25922), *Klebisella pneumoniae* (ATCC 13883), *Pseudomonas aeruginosa* (ATCC 27853), *Staphylococcus aureus* (ATCC 25923) and *Streptococcus pyogenes* (ATCC 19615) and were provided by REMEL. Experiments were conducted in a dedicated laminar flow hood equipped with UV lamp. Lyophilized bacteria were reconstituted in TSB and cultured overnight at 37^0C. 1 ml aliquot of culture was grown in 100 ml of TSB for 2-4 h until reaching an optical density at 600 nm (OD 600) = O.15-0.3. The resulting culture was stored at -80^0C as 1 ml aliquots. For daily experiments, 1 ml of bacteria culture was grown in 100 ml of TSB overnight at 37^0c. And finally, the absorbance was adjusted to 0.5 McFarland standard (1.5 x 10^8 CFU/mL) as starting concentration in the experiment.

1.2.3 Evaluation of antibacterial activity

A, Disc diffusion susceptibility testing

The antimicrobial susceptibilities of the novel synthetic Ag complexes were evaluated using the Kirby-Bauer disc-diffusion method [50-52]. This test is otherwise called agar diffusion test. This test is used for testing the antibiotic sensitivity of bacteria. Because of convenience, efficiency and cost, the disk diffusion method is probably the most widely used method for determining antibacterial activity and resistance pattern of antibiotic. Normally

performed according to CLSI guidelines and results were interpreted using CLSI breakpoints [53, 54]. Cefotaxime discs (10 µg; from Oxoid™) and silver sulfadiazine (AgSD) discs (32 µg) were used as positive controls. This stock solutions were utilized to impregnate the blank antimicrobial susceptibility disks. Specifically, overnight cultures of bacteria tested, were adjusted to a turbidity of 0.5 McFarland standards (1.5×10^8 CFU/ml) before inoculation onto agar plates with sterile cotton swabs. A cotton swab dipped in the cell culture was streaked onto an agar plate surface in such a way as to obtain a uniform layer of bacteria across the whole surface. After 10-15 min, the commercially prepared discs (Cefotaxime or AgSD) and pre-impregnated with the novel complexes of silver discs were laid on the inoculated surface of the agar plates. The discs were lightly pressed on the surface of agar surfaces. The test antibiotic immediately begins to diffuse outward from the disks, creating a gradient of antibiotic concentration in the agar such that the highest concentration is found close to the disk with decreasing concentrations further away from the disk. After an overnight incubation, the bacterial growth around each disc is observed. If the test isolate is susceptible to a particular antibiotic, a clear area of "no growth" will be observed around that particular disk. The zone around an antibiotic disk that has no growth is referred to as the zone of inhibition since this approximates the minimum antibiotic concentration sufficient to prevent growth of the test isolate. This zone is then measured in millimeter and compared to a standard interpretation chart used to categorize the isolate as susceptible (S), intermediate (I) or resistant (R) (**Figure 4**) MIC measurement cannot be determined from this qualitative test, which simply classifies the isolate as susceptible, intermediate or resistant. Agar plates inoculated with bacteria tested with impregnated DMSO discs were used as controls. Analysis for each combination of bacteria tested and discs with positive controls and with several new compounds were repeated three times.
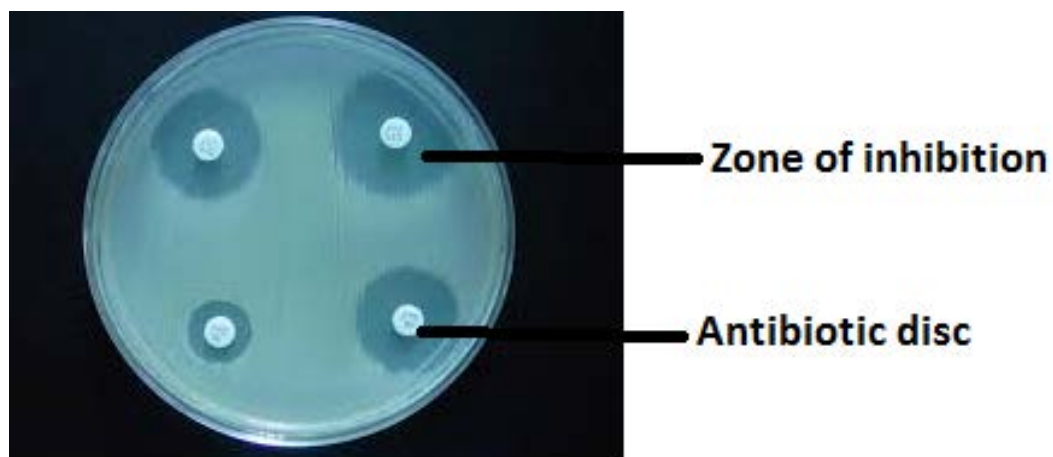
Figure 4. Antibiotic sensitivity test.

B, Determination of MIC (Minimum inhibitory concentration) and MBC (minimum bactericidal concentration)

Broth dilution method

The aim of the broth dilution method is to find out the lowest concentration of antibiotic needed to inhibit the complete growth of the bacterium that is MIC value. MIC of the antibacterial compounds was determined using the broth dilution method, according to CLSI guidelines [55]. The Broth dilution method involves subjecting the isolate to a series of concentrations of antimicrobial agents in a broth environment. First of all, make serial dilutions of Ag compounds in MHB medium. Then, the suspensions of the microorganisms, prepared from overnight cultures of bacteria in the MHB medium, at a concentration of 10^6 CFU/mL, were added to each dilution in a 1:1 ratio. Growth (or lack) of the microorganisms was determined visually after incubation for 24 h at 37 °C. AgSD and cefotaxime were also included as positive controls and DMSO served as negative control. The lowest concentration at which there was no visible growth (turbidity) was considered as the MIC value (**Figure 5**). The MIC is thus the minimum concentration of the antibiotic that will inhibit this particular isolate. The test is only valid if the positive control shows no growth and the negative control shows growth. The experiments were repeated three times.
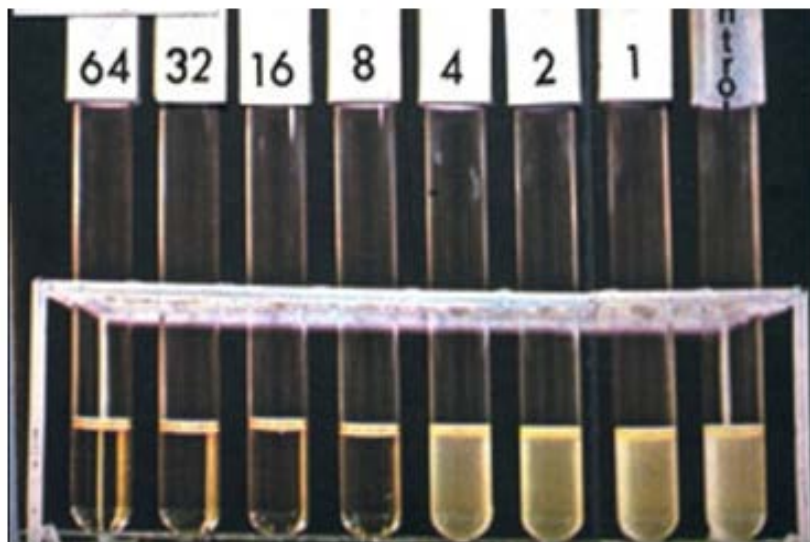
Figure 5. Broth dilution test with AgL6 in *E.coli.*

In order to determine the MBC, 10 µL aliquots of dilution representing the MIC value, and at least three of the more concentrated dilutions of the Ag complexes, cefotaxime and AgSD, were plated on Müller-Hinton agar. Then, the plates were incubated for 24 h, at 37°C. The MBC values were determined as the lowest concentration that causes at least a 99.9% decrease in CFU/ml^{-1} relative to the initial concentration [56].

1.2.4 Synthesis of the vehicle Dextran-oleate

A, Materials

The coupling of dextran and sodium oleate was achieved as follows: 500 mg of dextran were dissolved in 50 mL of DMSO. After complete dissolution, 100 mg of sodium oleate, 68 mg of DCC and 40 mg of DMAP, were added to the solution and left under magnetic stirring, for 4 h at 60 °C, and at room temperature overnight. In order to recover the oleate-grafted dextran, the purification step was performed by precipitating the reaction mixture in cold ethanol. Then the product was collected in dialysis membrane and dialyzed against a mixture ethanol/water 50:50 for 24 h and against distilled water for further 48 h. Finally, dextran oleate was recovered and freeze-dried to a powder.

B, Instrumentation

Absorption spectra were recorded with a UV-Vis JASCO V-530 spectrometer using 1 cm quartz cells. Particles size and distribution were determined by Dynamic Light Scattering

(DLS) analyses using a 90 Plus particle size analyzer (Brookhaven Instruments Corporation, New York, NY USA), at 25.0± 0.1 °C by measuring the autocorrelation function at 90°. The laser was operating at 658 nm. The distribution size was directly obtained from the instrument fitting data by the inverse "Laplace transformation" method and by Contin methods. The polydispersity index (P.I.) was used as a measure of the width of size distribution. P.I. less than 0.3 indicates a homogenous population of particles. Each sample was measured three times and the results are expressed as mean ± standard deviation. IR spectra were recorded as KBr pellets on a Jasco FT-IR 4200.

C, Dextran-oleate synthesis

The coupling of dextran and sodium oleate was achieved as follows: 500 mg of dextran were dissolved in 50 mL of DMSO. After complete dissolution, 100 mg of sodium oleate, 68 mg of DCC and 40 mg of DMAP, were added to the solution and left under magnetic stirring, for 4 h at 60 °C, and at room temperature overnight. In order to recover the oleate-grafted dextran, the purification step was performed by precipitating the reaction mixture in cold ethanol. Then the product was collected in dialysis membrane and dialyzed against a mixture ethanol/water 50:50 for 24 h and against distilled water for further 48 h. Finally, dextran oleate was recovered and freeze-dried to a powder.

1.2.5 Determination of the Critical Aggregation Concentration

The critical aggregation concentration (CAC) of the dextran oleate aqueous solution was determined by fluorescence method using pyrene as a nonpolar fluorescent probe. 24.0 μL of pyrene solution (2.5×10^{-5} M) in acetone were added in vials and evaporated under vacuum. Amounts of dextran oleate solution at various concentrations were added to the pyrene vials leading to a final pyrene concentration of 6.0×10^{-7} M. The mixture was kept under agitation for 4-5 h. Fluorescence measurements were conducted on each sample (excitation = 333 nm, emission = 350-500 nm) at a 90° angle in a 1 cm quartz cuvette. The average ratio of the intensity of the vibronic bands at 372 nm (I1) over 383 nm (I3), obtained from the fluorescence emission spectra of pyrene recorded at 25 °C, was plotted vs. log of the concentration for each sample. The CAC was determined as the polymer concentration at the intersection point of two regression lines.

1.2.6 Self-assembling of the polymer vesicle

5 mg of dextran oleate was dissolved in 10 mL of THF in a 50 mL round bottom flask. Next, 10 mL of phosphate buffer saline solution (0.01 M, pH 7.4) were gently poured along the flask walls. The organic solvent was removed using a rotary evaporator, under reduced pressure at 40°C and 40 rpm, yielding the dextran oleate vesicles suspension. AgL6 loaded vesicles were prepared as described above, by adding 1 mL of AgL6 solution to the phosphate buffer

1.2.7 Drug encapsulation efficiency

Drug encapsulation efficiency was determined using the dialysis method for separating the non-entrapped drug from dextran oleate vesicles (DOVs) [57]. According to this technique, 3 mL of AgL6-loaded DOVs dispersion were dropped into a dialysis bag immersed in 10 mL of distilled water and magnetically stirred. Free drug was dialyzed for 30 min each time. The dialysis was complete when no drug was detectable in the recipient solution. The encapsulation efficiency was expressed as the percentage of the drug entrapped into DOVs referred to the total amount of drug that is present in the non-dialyzed sample. It was determined by diluting 1 mL of dialyzed and 1 mL of non-dialyzed DOVs in 25 mL of methanol and obtaining two solutions whose concentrations are represented in equation 1 by [ND] and [D], respectively. The concentrations of AgL6 where calculated by measuring the absorbance of the two solutions between 200 nm and 400 nm. This procedure was necessary to breakdown DOVs.

Encapsulation efficiency percentage (%) = [ND]-[D]/[ND] X 100

1.2.8 *In vitro* diffusion study

In vitro diffusion studies were performed at 37 ± 0.5 °C using Franz diffusion cells (Disa, Milan, Italy; permeation area 0.4614 cm2). For this purpose, Strat-M® membrane (Merck-Millipore) was placed between the donor and receptor compartments of the Franz cells and, then, the compartments were clamped together ensuring that the shiny side of the membrane was facing the donor compartment. The receptor compartment was filled with 5.5 mL of phosphate buffer at pH 7.4 (1.0 × 10-3 M) and, after 20-30 min when the receptor solution reached 37ºC, 0.5 mL of the AgL6-loaded DOVs suspension were added to the donor

compartment, which was covered with Parafilm™ in order to prevent any loss. The content of the receptor compartment was removed at 1, 2, 4, 6, 8 and 24 hours for UV-Vis analysis and, at each time point, the amount withdrawn was replaced with fresh phosphate buffer. The in vitro diffusion experiments were performed in triplicate.

1.2.9 Evaluation of the membrane permeability in *Staphylococcus aureus*

Propidium iodide (PI) was used to monitor the permeability of the membrane. The increase in PI fluorescence is related to the increase in membrane permeability. *Staphylococcus aureus* overnight cultures were diluted in MHB in order to reach OD~ 0.6 at the wavelength of 600nm, then they were treated with AgL6 , incubated at 37 ° C by shaking at 300 rpm. After 30 minutes of treatment, 500 mL samples were collected, centrifuged at 3500 rpm, and the medium was removed and replaced with 1mM PI in PBS. The samples were incubated in the dark at room temperature for 15 min and then centrifuged at 3500 rpm. The supernatant was removed and replaced with 1X PBS. Bacterial cells were visualized using an OLYMPUS BX 41 microscope; the images were taken with CSV1.14 software using a CAMXC-30 for image acquisition. Fluorescent signal intensity was assessed using a fluorescent plate reader (ex. 530 nM; em. 620 nM).

1.2.10 Statistical analysis

Data is represented as the mean ± standard deviation (SD), taken over ≥ 3 independent experiments, with ≥ 3 technical replicates per experiment, unless otherwise stated. Statistical significance was measured using the analysis of variance (ANOVA) test or student t-test. $p \leq 0.05$ was considered significant and all statistical tests were two sided.

1.3   RESULTS AND DISCUSSION

1.3.1 Disc diffusion test

Antibacterial properties of silver complexes were evaluated against two Gram positive (*S. aureus*, *S. pyogenes*) and three Gram negative *(K. pneumoniae, P. aeruginosa, E. coli)* bacteria*.* The drug susceptibility patterns of the bacteria tested are shown in the **table 1**. The susceptibility of the novel complexes against pathogenic strains were calculated from inhibition diameters values, which was measured at 32, 64 and 128 µg of each tested compound. Then the inhibition zone diameters obtained was compared with that of positive controls, Cefotaxime and Silver sulfadiazine by using disc diffusion susceptibility test protocol. The final interpretation of the results enabled all the bacteria strains tested to be grouped into three categories, Sensitive(S), Intermediate (I) and Resistant (R). The antibiotic sensitivity profile of the bacterial strains showed that, among the Ag complexes tested, only AgL6 displayed antimicrobial activity against the microorganisms, but only when tested in large amounts, in comparison with Cefotaxime. However, a comparison of data obtained on the inhibition zones of the pathogenic bacteria proved that all five bacterial strains were Sensitive to 32, 64 and 128 µg of AgL6. Both AgL18 and AgL20 were less effective against these bacteria. Even though *E. coli, K. pneumoniae* and *P. aeruginosa* showed intermediate sensitivity to 128 µg of these compounds.

COMPOUNDS	μg	BACTERIAL STRAINS				
		Staphylococcus aureus ATCC 25923	*Streptococcus pyogenes* ATCC 19615	*Escherichia coli* ATCC 25922	*Klebsiella pneumoniae* ATCC 13883	*Pseudomonas aeruginosa* ATCC 27853
Cefotaxime	10	S	S	S	S	S
Silver sulfadiazine (AgSD)	32	S	S	S	S	S
AgL6	32	S	S	S	S	S
	64	S	S	S	S	S
	128	S	S	S	S	S
AgL18	32	R	R	R	R	R
	64	R	R	R	R	R
	128	R	R	I	I	I
AgL20	32	R	R	R	R	R
	64	R	R	R	R	R
	128	R	R	I	I	I

S: Sensitive, **I**: Intermediate, **R**: Resistant

Table 1. Antibiotic susceptibility profile.

1.3.2 Broth dilution method for calculating MIC and MBC

The Kirby-Bauer test could only test the bacterial susceptibility to various antimicrobial reagents at pre-designed dosage. Information such as minimal inhibitory concentration (MIC) of a specific compound could not be obtained from this test. Therefore, in order to determine MIC values for AgL6, the broth dilution method was performed. The MIC and MBC values for several bacterial strains are shown in **table 2**. As expected, the MIC determination results were in good agreement with the disc-diffusion susceptibility test. For example, in the disc-diffusion test, all five bacteria were found to be Sensitive to AgL6; in the dilution experiment, the MIC of this compound was found to be very high against all the strains, particularly against Gram +ve bacteria (MIC values were 32 μg/ml). The values obtained were greater than those reported for the commercial drugs Cefotaxime (MIC ranging between 0.5 and 4 μg/ml) and AgSD (MIC ranging between 8 and 32 μg/ml). Both of these commercial drugs were found to be Sensitive according to the Kirby-Bauer test. Similarly, minimal bactericidal concentration (MBC) values for AgL6 were also determined in bacterial cultures and the values were higher against Gram +ve bacteria than against Gram -ve bacteria.

COMPOUNDS	MIC MBC (μg/ml)	BACTERIAL STRAINS				
		Staphylococcus aureus ATCC 25923	*Streptococcus pyogenes* ATCC 19615	*Escherichia coli* ATCC 25922	*Klebsiella pneumoniae* ATCC 13883	*Pseudomonas aeruginosa* ATCC 27853
Cefotaxime	MIC	1	0.5	2	2	4
	MBC	1	1	4	2	8
Silver sulfadiazine (AgSD)	MIC	32	16	8	8	16
	MBC	32	32	16	16	16
AgL6	MIC	32	32	16	16	32
	MBC	64	64	32	32	32

Table 2. MIC (top rows) and MBC (bottom rows) values of the investigated compound.

Since limited cellular penetration could reduce the effectiveness of many antimicrobial treatments, we hypothesized that incorporating AgL6 into a "pharmaceutically-oriented device", such as dextran-oleate polymer vesicles, could improve its cellular uptake and, consequently, its antimicrobial activity

1.3.3 Polymer vesicles characterization

Evaluation by FT-IR spectra analyses has been performed in order to verify the coupling of oleate onto dextran backbone, comparing the FT-IR spectra of sodium oleate, dextran and dextran oleate conjugate. The sodium oleate spectrum (**Figure 6** - Trace B) shows a strong peak at 1560 cm-1, which is the typical signal of the C=O stretching vibration of the carboxylic salt group. It can be also observed the presence of strong signals between 2849 and 2950 cm-1 corresponding to stretching vibration of the C–H bond of the alkane portion of the molecule; while the double bond can be identified thanks to the band at 3030 cm-1, corresponding to the stretching vibration of =C–H bond. Dextran spectrum (**Figure 6** - Trace A), on the contrary, does not show any signal that can be ascribed to C=O double bond, which is obviously absent in dextran structure. But information about the conformation of the polysaccharide can be acquired in the region 600-950 cm-1. A peak in the 885-925 cm-1 region is the evidence of two CH in the axial position (AA), in the 825-855 cm-1 region the equatorial-axial position (EA), in the 790-825 cm-1 region in the equatorial-equatorial position (EE) and in 860-885 cm-1 region in the axial equatorial position (AE). The bands around 915 cm-1 and 850 cm-1, indicating AA and EA fragments, confirm the glucopyranosyl conformation, which

is not affected by oleate conjugation. In dextran oleate spectrum (**Figure 6** - Trace C), in fact, these peaks are preserved, while a new strong band appeared. It can be found around 1740 cm-1 indicating the presence of C=O bond stretching vibration of an ester group. This group came from the oleate moieties, but its spectroscopic signal has been shifted towards higher frequencies. This is certainly due to the new formation of the ester bond.
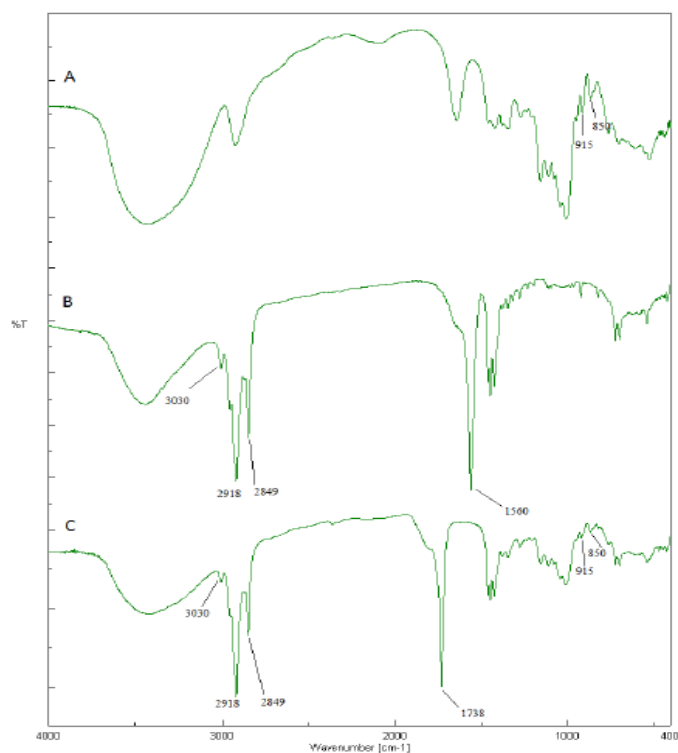
***Figu*re 6.** FT-IR spectra of (A) dextran, (B) sodium oleate and (C) dextran oleate.

The polymer nanovesicles were prepared by self-assembling procedure and their dimensions were analyzed by dynamic light scattering. The self-assembling technique involves the dissolution of the amphiphilic polymer in organic solvent, followed by the introduction of the aqueous phase, represented by phosphate buffer saline (PBS) solution at pH = 7.4. The apolar organic phase is then removed under reduced pressure decreasing the dissolution of the hydrophobic block of dextran oleate. This led to the increase of hydrophilicity of the phase and, consequently, to the self-assembly of the nanosized DOVs.

The dimensional characterization of DOVs and DOVs-AgL6 was performed with DLS, putting a small amount of polymer vesicles in the PBS solution at pH 7.4. The mean hydrodynamic diameter found was different for the two polymer batches: 525 nm and 613 nm for DOVs and DOVs-AgL6, respectively (**Figure 7**). Data collected in **table 3**, shows the

presence of monodisperse homogeneous population of both empty and AgL6-loaded vesicles. Polydispersity index value is, in fact, below 0.3 and the mean diameter is below 700 nm. There is a difference of almost 100 nm between the two systems and that can be ascribed to the presence of encapsulated drug. It seems that the presence of AgL6 in solution negatively affects the self-assembling of dextran oleate vesicles, resulting in larger nanoparticles. In particular, the Ag atoms can interfere with vesicles formation, due to its nature. However, the negative effect on DOVs dimension does not compromise their formation maintaining a mean diameter far below 1 μm.

Figure 7. Graph of size and size distribution obtained by DLS analysis of DOVs (Panel A) and DOVS-AgL6 (Panel B).

The amphiphilic character was conferred to dextran thanks to the conjugation with a hydrophobic group, i.e. the oleate residue. The so modified polysaccharide acquired the ability to self-assemble in an aqueous environment via hydrophobic interaction between lipidic moieties.

	Mean diameter	Polydispersity index
DOVs	525 ± 14 nm	0.214
DOVs-AgL6	613 ± 17 nm	0.268

Table 3. Dimensional data. DOVs size and size distribution of both empty and AgL6-loaded DOVs are expressed as mean diameter ± standard deviation and polydispersity index (P.I.).

The critical aggregation concentration (CAC) of dextran oleate in water was estimated from the dependence of pyrene fluorescence spectra (I372/I383 ratio) as a function of the polysaccharide- lipid concentration (**Figure 8**). A sharp change was observed from 14 μg/mL, which was considered to be the CAC.
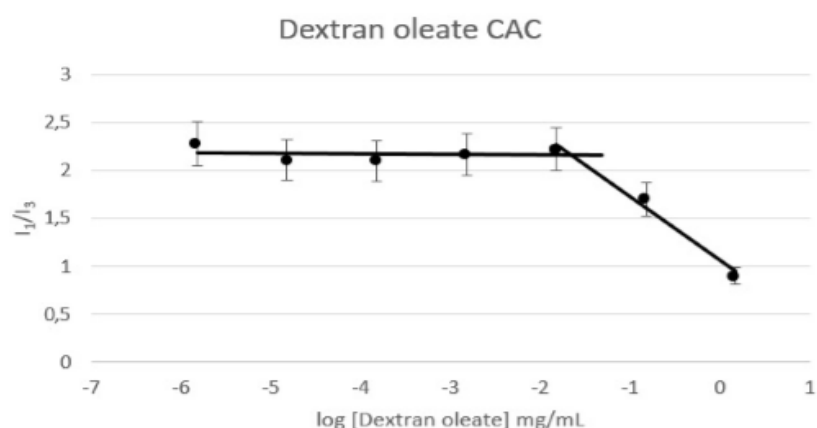
Figure 8. Ratio of pyrene I1/I3 band fluorescence at various concentrations of dextran oleate in water. The critical aggregation concentration was calculated as the intersection point of the two linear regions of the plots.

1.3.4 Drug encapsulation and release profile

Polymer nanovesicles possess the advantage of being optimal carrier for both hydrophobic and hydrophilic drugs, which can be loaded in the lipophilic membrane or in the aqueous core, respectively. Dextran oleate vesicles (DOVs) were loaded with AgL6 during self-assembling and drug encapsulation was measured by UV-Vis spectrophotometry after dialysis against distilled water. The encapsulation efficiency has been calculated according to the equation 1 reported in the experimental method section. The obtained value for AgL6 was ca. 76%, supporting the vesicular structure of the carrier. Strat-M® membranes, which are a synthetic model that is predictive of diffusion in human skin, were employed for transdermal diffusion testing. The diffusion of AgL6-loaded DOVs was compared to free AgL6 and the results are reported in **Figure 9**. From the release profile depicted in **figure 9**, it is evident an increased amount of AgL6 recovered in the acceptor compartment of Franz diffusion cells from DOVs-AgL6, since the time point of 2 h, if compared to free AgL6. The trend is much more evident in the following hours, since DOVs-AgL6 released almost 95% of its payload after 24 h. On the other hand, free AgL6 diffusion is limited and it is not complete at the end point.
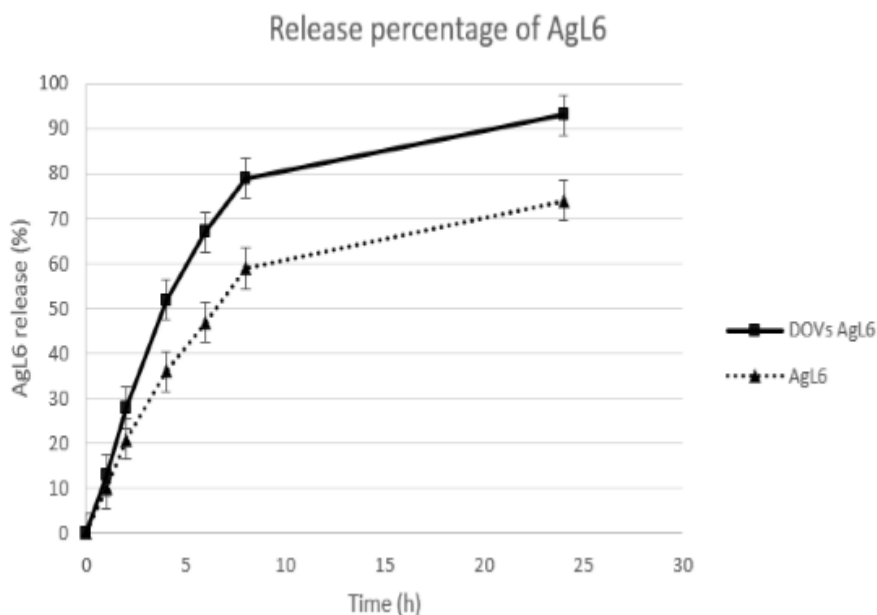
Figure 9. Transdermal diffusion profile of AgL6 and DOVs-AgL6.

1.3.5 Dextran-oleate as a 'pharmaceutically oriented-vehicle' improves AgL6 antibacterial activity

Since limited cellular penetration could reduce the effectiveness of many antimicrobial treatments. We hypothesized that incorporating AgL6 into a "pharmaceutically-oriented device" (Dextran-oleate) could improve its cellular uptake and, consequently, its antimicrobial activity. Literature data reported that the incorporation of novel synthetic compounds into suitable drug carriers can improve their antimicrobial effect and, consequently, may be a very promising strategy to enhance their cellular uptake [46]. The MIC and MBC values for the novel Ag complex, after its incorporation into the carrier confirmed our hypothesis, evidencing improved activity against all bacterial strains (**Table 4**). Indeed, all MIC and MBC values decreased four times against all bacteria tested, while only the MBC value, against *P. aeruginosa*, was reduced twofold. These values were found to be closer to those for cefotaxime and, surprisingly, twofold lower than for AgSD. In contrast, the vehicle alone did not exhibit antibacterial activity. Finally, our outcomes showed *K. pneumoniae* and *E. coli* to be the most sensitive microorganisms to AgL6, followed by *P. aeruginosa* while the GP bacteria were less sensitive to the novel complex.

COMPOUNDS	MIC MBC (µg/ml)	BACTERIAL STRAINS				
		Staphylococcus aureus ATCC 25923	*Streptococcus pyogenes* ATCC 19615	*Escherichia coli* ATCC 25922	*Klebsiella pneumoniae* ATCC 13883	*Pseudomonas aeruginosa* ATCC 27853
Cefotaxime	MIC	1	0.5	2	2	4
	MBC	1	1	4	2	8
Silver sulfadiazine (AgSD)	MIC	32	16	8	8	16
	MBC	32	32	16	16	16
Dextran-oleate	MIC	>128	>128	>128	>128	>128
	MBC	>128	>128	>128	>128	>128
Dextran-oleate AgL6	MIC	8	8	4	4	8
	MBC	16	16	8	8	16

Table 4. MIC (top rows) and MBC (bottom rows) values of AgL6 incorporated in Dextran-oleate, Vehicle alone, Cefotaxime and AgSD.

From the results, it was also observed that the MBC/MIC ratio offers information about the nature of the antibacterial activity. For example, when the MBC/MIC ratio is between 1 and 2, the sample is considered as a bactericidal agent. On the other hand, if the MBC/MIC ratio is higher than 2, the antimicrobial substance can be classified as a bacteriostatic agent [58]. In our present study, MBC/MIC ratios indicate that, rather than a bacteriostatic effect, dextran-oleate AgL6 acted as a strong bactericidal agent (**Table 5**).

Strains	MIC(µg/ml)		MBC(µg/ml)		MBC/MIC
	DO	DO-AgL6	DO	DO-AgL6	DO-AgL6
Staphylococcus aureus ATCC 25923	>128	8	>128	16	2
Streptococcus pyogenes ATCC 19615	>128	8	>128	16	2
Escherichia coli ATCC 25922	>128	4	>128	8	2
Klebsiella pneumoniae ATCC 13883	>128	4	>128	8	2
Pseudomonas aeruginosa ATCC 27853	>128	8	>128	16	2

DO: Dextran-oleate, DO-AgL6-Dextran -oleate AgL6.

Table 5. The ratios of MBC/MIC of dextran-oleate and dextran-oleate AgL6 against Gram +ve and Gram -ve bacterial strains.

1.3.6 AgL6 increases outer membrane permeability in *Staphylococcus aureus*

We next asked whether **AgL6** antimicrobial activity was due to morphological changes in the cell envelope, followed by an overall increase in outer membrane permeability. To this end, we used propidium iodide (PI), a membrane-impermeable fluorescent dye, on *Staphylococcus aureus* cells treated with different **AgL6** concentrations (1/2 MIC, MIC and 2MIC values), in order to detect a possible permeation of cell membrane [29]. After 30 minutes, the treated cells showed increased PI fluorescence relative to untreated cells, in a dose-dependent manner, indicating destabilization of the cellular envelope and increased membrane permeability (**Figure 10a**). The observed increase was quantified by detecting red fluorescent signal by a fluorescent plate reader (**Figure 10b**). Cells treated with **AgL6**, at MIC concentration, displayed red fluorescent signal three times increased, compared to untreated cells.
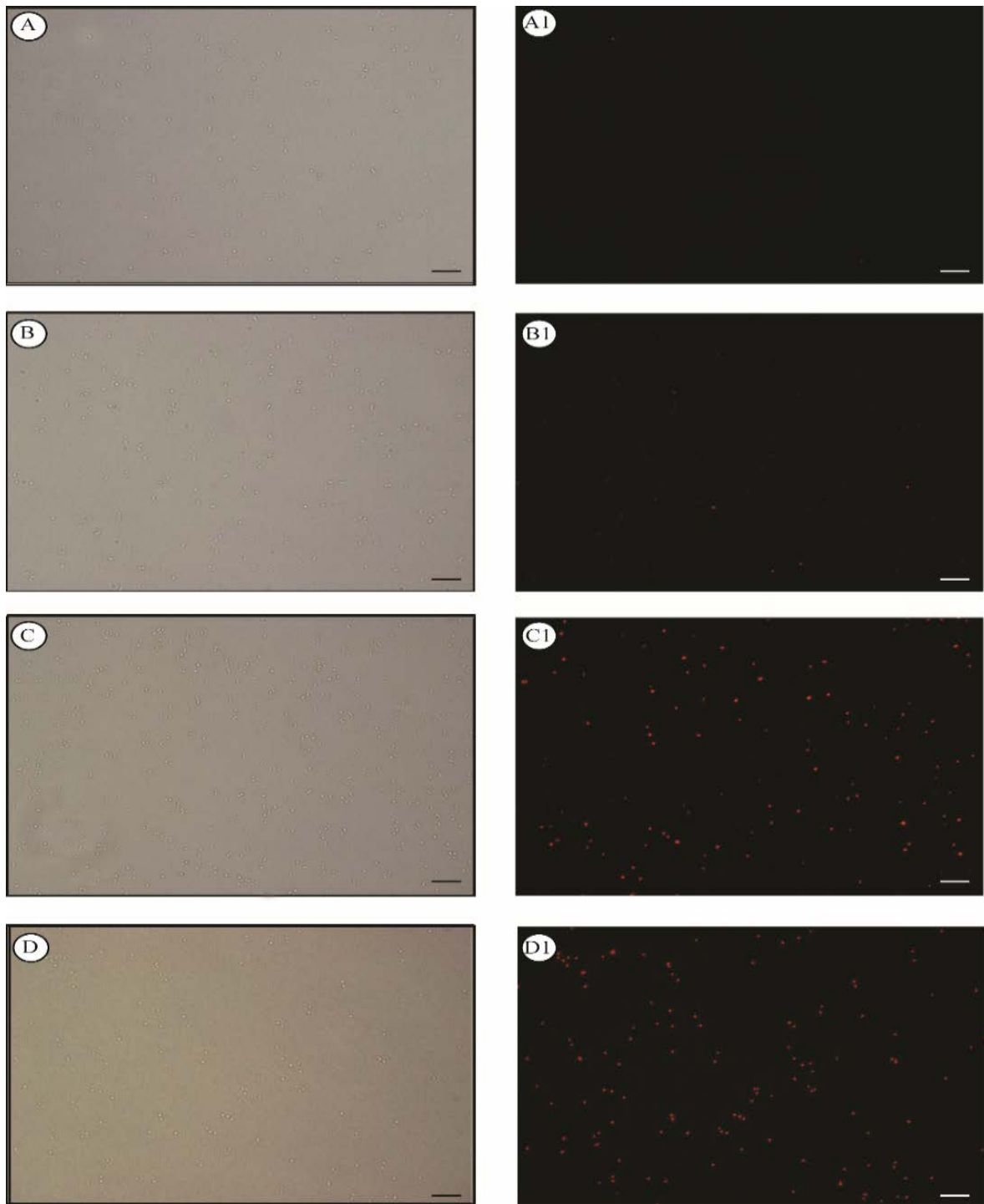
Figure 10a. AgL6 increases outer membrane permeability in *Staphylococcus aureus*.

Bright field and fluorescence microscopy of PI-stained untreated A1) cells and cells treated for 30 minutes with 4μg/ml (B1), 8 μg/ml (C1), 16 μg/ml (D1) 4b. Bacterial cells were visualized using an Olympus BX41 microscope and the images were taken with CSV1.14 software using a CAMXC-30 for image acquisition. The experiment repeated tree times for each sample. Scale Bars 12.5μm.
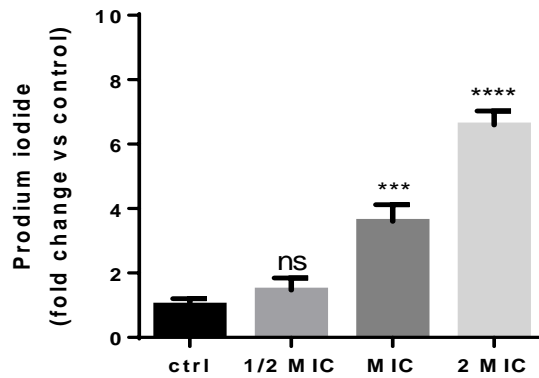
Figure 10b. AgL6 increases outer membrane permeability in *Staphylococcus aureus.*

Quantification of propidium iodide fluorescent signal intensity in untreated (control) or AgL6-treated cells was evaluated measuring red fluorescent signal by a fluorescent plate reader (ex.530; em.620) compared to untreated control sample. (***p < 0.0001, ****p°< 0.00001, one-way ANOVA and Student's t-test calculations).

1.4 CONCLUSION

The present study was aimed at investigating the antibacterial activity of silver N-heterocyclic carbene complexes: Iodide[N-methyl-N-(2-hydoxy-cyclopentyl-imidazole-2- ylidine]silver(I), Iodide[N-methyl-N-(2-hydoxy-cyclohexyl)-imidazole-2-ylidine]silver(1), Iodide[N-methyl-N-(2-hydoxy-2-phenyl)ethyl-imidazole-2-ylidine]silver(I), namely AgL6, AgL18 and AgL20 respectively. They were tested against both Gram +ve (*Staphylococcus aureus, Streptococcus pyogenes*) and Gram –ve (*Escherichia coli, Pseudomonas aeruginosa, Klebisella pneumoniae*) bacteria. One of the compounds was found to be the most active (AgL6), while there is a natural bacterial resistance towards AgL18 and AgL20. Indeed, we calculated the MIC values for this compound and it was found to be 32 μg against Gram +ve bacteria, 16μg for *E.coli* and *K.pneumoniae* and 32μg against *P.aeruginosa*. Even though it was a good result, the dose was higher, than the MIC values of positive controls.

We hypothesized that the most probable reason was the poor uptake of the compounds inside the cell. Literature data suggested that incorporation of some compounds in a vehicle could increase the drug uptake (Parisi et al. 2014). Therefore, we decided to incorporate AgL6 into a nanosystem. These systems have been proven to succeed as antimicrobial carrier due to targeted drug delivery at infection sites, reduced drug-resistance by microbial organism and increased therapeutic index. These actions reduce side effects and improve patient compliance thanks to the decreased frequency of administrations.

The biopolymeric nanocarrier developed for AgL6 delivery, was successfully obtained by self-assembly of dextran oleate conjugate, in which dextran chain and oleic residues represent the hydrophilic and the hydrophobic parts of the amphiphilic material, respectively. The nanometric dimension of the particles have been confirmed by DLS analyses (mean diameter ranging between 500-600 nm). We have demonstrated that this Nanosystem is an excellent tool that can greatly improve antibiotic activity of silver compound. The MIC and MBC values for the new Ag complex, after its incorporation into the carrier, evidenced improved antibacterial activity, indeed, all MIC values decreased four times against all bacteria tested except for *P. aeruginosa* in which reduced only 2 folds.

Finally, we hypothesized that the antibacterial activity observed for AgL6 could be due to an increase in the permeability of the bacterial outer membrane. To explore this, we used

propidium iodide (PI), a membrane-impermeable fluorescent dye that has been utilized to detect permeation of the cell membrane. The results showed, in AgL6-treated bacteria, an increased PI fluorescence, relative to untreated cells, indicating increased membrane permeability. Taken together all the data, we came to conclusion that AgL6 is a promising antibacterial agent.

1.5 BIBLIOGRAPHY

1. Becker k, Hu Y and Biller-Andorno N. (2006) Infectious diseases- a global challenge. *International journal of medical microbiology*. 296(4-5):179-85.

2. O'Shea R and Moser HE. (2008) Physico chemical properties of antibacterial compounds: Implications for dru delivery. *Journal of medicinal chemistry*. 51(10):2871-8.

3. Sopbue Fondjo E, Sorel DD, Jean-de-Dieu T, Joseph T, Sylvian K, Doriane N, Rodolphe CJ, Pepin NE, Jules-Roger K, Arnaud NN and Luca SB. (2016) Synthesis,Characterization, Antimicrobial and Antioxidant Activities of The Homocyclotrimer Of 4-Oxo-4h-Thieno[3,4-C]Chromene-3-Diazonium Sulfate. *Open Med Chem J.* 10:21-32.

4. Yang Z, Liu Y, Ahn J, Qiao Z, Endres JL, Gautam N, Huang Y, Li J, Zheng J, Alnouti Y, Bayles KW and Li R. (2016) Novel fluorinated pyrrolomycins as potent anti-staphylococcal biofilm agents: Design, synthesis, pharmacokinetics and antibacterial activities. *Eur J Med Chem*. 124:129-137.

5. de Moraes AC, Lima BA, de Faria AF, Brocchi M and Alves OL. (2015) Graphene oxide-silver nanocomposite as a promising biocidal agent against methicillin-resistant Staphylococcus aureus. *Int J Nanomedicine*. 10:6847-61.

6. Seukep JA, Sandjo LP, Ngadjui BT and Kuete V. (2016) Antibacterial and antibiotic-resistance modifying activity of the extracts and compounds from Nauclea pobeguinii against Gram-negative multi-drug resistant phenotypes. *BMC Complement Altern Med*. 16:193.

7. Andersson DI and Hughes D. (2011) Persistence of antibiotic resistance in bacterial populations. *FEMS Microbiol Rev*. 35(5):901-11.

8. Cox G and Wright GD. (2013) Intrinsic antibiotic resistance: mechanisms, origins, challenges and solutions. *Int J Med Microbiol*. 303(6-7):287-92.

9. Fajardo A, Martínez-Martín N, Mercadillo M, Galán JC, Ghysels B, Matthijs S, Cornelis P, Wiehlmann L, Tümmler B, Baquero F and Martínez JL. (2008) The neglected intrinsic resistome of bacterial pathogens. *PLoS One*. 3(2):e1619.

10. Abraham EP and Chain E. (1940) An Enzyme from Bacteria able to Destroy Penicillin. *Nature.* 146:837-837.

11. Pagès JM, James CE and Winterhalter M. (2008) The porin and the permeating antibiotic: a selective diffusion barrier in Gram-negative bacteria. *Nat Rev Microbiol*. 6(12):893-903.

12. Privett BJ, Deupree SM, Backlund CJ, Rao KS, Johnson CB, Coneski PN and Schoenfisch MH. (2010) Synergy of nitric oxide and silver sulfadiazine against gram-negative, gram-positive, and antibiotic-resistant pathogens. *Mol Pharm*. 7(6):2289-96.

13. Berger TJ, Spadaro JA, Bierman R, Chapin SE and Becker RO. (1976) Antifungal properties of electrically generated metallic ions. *Antimicrob Agents Chemother*. 10(5):856-60.

14. Klasen HJ. (2000) Historical review of the use of silver in the treatment of burns. I. Early uses. *Burns.* 26(2):117-30.

15. Feng QL, Wu J, Chen GQ, Cui FZ, Kim TN and Kim JO. (2000) A mechanistic study of the antibacterial effect of silver ions on Escherichia coli and Staphylococcus aureus. *J Biomed Mater Res*. 52(4):662-8.

16. Silver S1, Phung le T and Silver G. (2006) Silver as biocides in burn and wound dressings and bacterial resistance to silver compounds. *J Ind Microbiol Biotechnol.* 33(7):627-34.

17. Kalinowska-Lis U1, Szewczyk EM, Chęcińska L, Wojciechowski JM, Wolf WM and Ochocki J. (2014) Synthesis, characterization, and antimicrobial activity of silver(I) and copper(II) complexes of phosphate derivatives of pyridine and benzimidazole. *ChemMedChem*. (1):169-76.

18. Butler KS, Peeler DJ, Casey BJ, Dair BJ and Elespuru RK. (2015) Silver nanoparticles: correlating nanoparticle size and cellular uptake with genotoxicity. *Mutagenesis.* 30(4):577-91.

19. Kyros L1, Banti CN, Kourkoumelis N, Kubicki M, Sainis I and Hadjikakou SK. (2014) Synthesis, characterization, and binding properties towards CT-DNA and lipoxygenase of mixed-ligand silver(I) complexes with 2-mercaptothiazole and its derivatives and triphenylphosphine. *J Biol Inorg Chem*. 19(3):449-64.

20. Kim JY, Lee C, Cho M and Yoon J. (2008) Enhanced inactivation of E. coli and MS-2 phage by silver ions combined with UV-A and visible light irradiation*. Water Res*. 42(1-2):356-62.

21. Ghandour W, Hubbard JA, Deistung J, Hughes MN and Poole RK. (1988) The uptake of silver ions by Escherichia coli K12: toxic effects and interaction with copper ions. *Appl Microbiol Biotechnol*. 28: 559.

22. Bragg PD and Rainnie DJ. (1974) The effect of silver ions on the respiratory chain of Escherichia coli. *Can J Microbiol*. 20(6):883-9.

23. Slawson RM, Lohmeier-Vogel EM, Lee H and Trevors JT. (1994) Silver resistance in Pseudomonas stutzeri. *Biometals*. 7(1):30-40.

24. Choi O and Hu Z. (2008) Size dependent and reactive oxygen species related nanosilver toxicity to nitrifying bacteria. *Environ Sci Technol*. 42(12):4583-8.

25. Jung WK, Koo HC, Kim KW, Shin S, Kim SH and Park YH. (2008) Antibacterial activity and mechanism of action of the silver ion in *Staphylococcus aureus* and *Escherichia coli*. *Appl Environ Microbiol.* 74(7):2171-8.

26. Dibrov P, Dzioba J, Gosink KK and Häse CC. (2002) Chemiosmotic mechanism of antimicrobial activity of Ag(+) in Vibrio cholerae. *Antimicrob Agents Chemother*. 46(8):2668-70.

27. Matsumura Y, Yoshikata K, Kunisaki S and Tsuchido T. (2003) Mode of bactericidal action of silver zeolite and its comparison with that of silver nitrate. *Appl Environ Microbiol*. 69(7):4278-81.

28. Silvestry-Rodriguez N, Bright KR, Uhlmann DR, Slack DC and Gerba CP. (2007) Inactivation of *Pseudomonas aeruginosa* and Aeromonas hydrophila by silver in tap water. *J Environ Sci Health A Tox Hazard Subst Environ Eng*. 42(11):1579-84.

29. Morones-Ramirez JR, Winkler JA, Spina CS and Collins JJ. (2013) Silver enhances antibiotic activity against gram-negative bacteria. *Sci Transl Med.* 19:5(190).

30. Prabhu S and Poulose EK. (2012) Silver nanoparticles: mechanism of antimicrobial action, synthesis, medical applications, and toxicity effects. *Int Nano Lett*. 2:32.

31. Kim JS, Kuk E, Yu KN, Kim JH, Park SJ, Lee HJ, Kim SH, Park YK, Park YH, Hwang CY, Kim YK, Lee YS, Jeong DH and Cho MH. (2007) Antimicrobial effects of silver nanoparticles. *Nanomedicine.* 3(1):95-101.

32. Morones JR, Elechiguerra JL, Camacho A, Holt K, Kouri JB, Ramírez JT and Yacaman MJ. (2005) The bactericidal effect of silver nanoparticles. *Nanotechnology*. 16(10):2346-53.

33. Fox CL Jr and Modak SM. (1974) Mechanism of silver sulfadiazine action on burn wound infections. *Antimicrob Agents Chemother*. 5(6):582-8.

34. Kalinowska-Lis U, Felczak A, Chęcińska L, Szabłowska-Gadomska I, Patyna E, Małecki M, Lisowska K and Ochocki J. (2016) Antibacterial Activity and Cytotoxicity of Silver(I) Complexes of Pyridine and (Benz)Imidazole Derivatives. X-ray Crystal Structure of [Ag(2,6-di(CH2OH)py)2]NO3. *Molecules*. 21(2):87.

35. Iqbal MA, Haque RA, Ahamed MBK, Majid AA and Al-Rawi SS. (2013) Synthesis and anticancer activity of para-xylyl linked bis-benzimidazolium salts and respective Ag (I) Nheterocyclic carbene complexes. *Medicinal Chemistry Research*. 22:2455-2466.

36. Melaiye A, Simons RS, Milsted A, Pingitore F, Wesdemiotis C, Tessier CA and Youngs WJ. (2004) Formation of water-soluble pincer silver (I)-carbene complexes: a novel antimicrobial agent. *Journal of medicinal chemistry*. 47:973-977.

37. Tan SJ, Yan YK, Lee PPF and Lim KH. (2010) Copper, gold and silver compounds as potential new anti-tumor metallodrugs. *Future medicinal chemistry.* 2:1591-1608.

38. Bruno G, Nicolo F, Loschiavo S, Sinicropi MS and Tresoldi G. (1995) Synthesis and Spectroscopic Properties of Di-2-Pyridyl Sulfide (Dps) Compounds - Crystal-Structure of [Ru(Dps)2cl2]. *J Chem Soc Dalton*. 17-24.

39. Oehninger L, Rubbiani R and Ott I. (2013) N-Heterocyclic carbene metal complexes in medicinal chemistry. *Dalton transactions.* 42:3269-3284.

40. Patil SA, Patil SA, Patil R, Keri RS, Budagumpi S, Balakrishna GR and Tacke M. (2015) N-heterocyclic carbene metal complexes as bio-organometallic antimicrobial and anticancer drugs*. Future medicinal chemistry.* 7:1305-1333.

41. Saturnino C, Napoli M, Paolucci G, Bortoluzzi M, Popolo A, Pinto A and Longo P. (2010) Synthesis and cytotoxic activities of group 3 metal complexes having monoanionic tridentate ligands. *European journal of medicinal chemistry.* 45:4169-4174.

42. Saturnino C, Sirignano E, Botta A, Sinicropi MS, Caruso A, Pisano A, Lappano R, Maggiolini M and Longo P. (2014) New titanocene derivatives with high anti-proliferative activity against breast cancer cells. *Bioorganic and medicinal chemistry letters*. 24:136-140.

43. Sirignano E, Saturnino C, Botta A, Sinicropi MS, Caruso A, Pisano A, Lappano R, Maggiolini M and Longo P. (2013) Synthesis, characterization and cytotoxic activity on breast cancer cells of new half-titanocene derivatives. *Bioorganic and medicinal chemistry letters*. 23:3458-3462.

44. Sinicropi MS, Amantea D, Caruso A and Saturnino C. (2010) Chemical and biological properties of toxic metals and use of chelating agents for the pharmacological treatment of metal poisoning. *Archives of toxicology*. 84:501-520.

45. Sinicropi MS, Caruso A, Capasso A, Palladino C, Panno A and Saturnino C. (2010) Heavy metals: toxicity and carcinogenicity. *Pharmacology.* 2:329-333.

46. Parisi OI, Fiorillo M, Caruso A, Cappello AR, Saturnino C, Puoci F, Panno A, Dolce V, El-Kashef H and Sinicropi MS. (2014) Enhanced cellular uptake by "pharmaceutically oriented devices" of new simplified analogs of Linezolid with antimicrobial activity. *Int J Pharm*. 461(1-2):163-70.

47. Levine DH, Ghoroghchian PP, Freudenberg J, Zhang G, Therien MJ, Greene MI, Hammer DA and Murali R. (2008) Polymersomes: a new multi-functional tool for cancer diagnosis and therapy. *Methods.* 46:25-32.

48. Ahmed F, Pakunlu RI, Brannan A, Bates F, Minko T and Discher DE. (2006) Biodegradable polymersomes loaded with both paclitaxel and doxorubicin permeate and shrink tumors, inducing apoptosis in proportion to accumulated drug. *J Control Release*. 116(2):150-8.

49. Geilich BM, van de Ven AL, Singleton GL, Sepúlveda LJ, Sridhar S and Webster TJ. (2015) Silver nanoparticle-embedded polymersome nanocarriers for the treatment of antibiotic-resistant infections. *Nanoscale*. 7(8):3511-9.

50. Bauer A, Kirby W, Sherris JC and Turck M. (1966) Antibiotic susceptibility testing by a standardized single disk method. *American journal of clinical pathology*. 45:493.

51. Benson H. (1998) Antimicrobial sensitivity testing: the Kirby-Bauer method. Microbiological applications: *laboratory manual in general microbiology*, 7th edn. McGraw Hill, Boston, Massachusetts, 139-141.

52. Benson HJ. (1967) Microbiological applications; a laboratory manual in general microbiology.

53. Clinical and Laboratory Standards Institute. (2012) Performance Standard for Antimicrobial Disk Susceptibility Tests; Approved Standard. Document M02-A11 No. 1. Vol. 32. PA, USA: CLSI.

54. Clinical and Laboratory Standards Institute. (2013) Performance Standards for Antimicrobial Susceptibility Testing. Twentieth Informational Supplement M100-S23. Wayne, PA, USA: CLSI.

55. Clinical and Laboratory Standards Institute. (2012) Methods for dilution antimicrobial susceptibility test for bacteria that grow aerobically; approved standards. 9th 485 ed. Document M07-A9. CLSI, Wayne, PA.

56. Kalinowska-Lis U, Szewczyk EM, Chęcińska L, Wojciechowski JM, Wolf WM and Ochocki J. (2014) Synthesis, characterization, and antimicrobial activity of silver (I) and copper(II)

complexes of phosphate derivatives of pyridine and benzimidazole. *ChemMedChem.* 9:169-176.

57. Maestrelli F, González-Rodríguez ML, Rabasco AM and Mura P. (2005) Preparation and characterisation of liposomes encapsulating ketoprofen-cyclodextrin complexes for transdermal drug delivery. *Int J Pharm*. 298(1):55-67.

58. Clinical and Laboratory Standards Institute. (2015) Methods for Dilution Antimicrobial Susceptibility Tests for Bacteria that Grow Aerobically. Vol 35. 8th ed. Wayne, PA: USA: CLSI.

CHAPTER 2

CHAETOCIN: A Promising Natural Antiparasitic Agent

2.1 INTRODUCTION

2.1.1 Sleeping sickness

Human African trypanosomiasis (HAT), also known as sleeping sickness, is a disease with a devastating socio-economic impact in 36 Sub-Saharan African countries via direct infection of humans and livestock. Parasitic protozoa infects hundreds of millions of people every year and are collectively some of the most important causes of human misery. This is a vector-borne parasitic disease, caused by an infection with protozoan parasites belonging to the genus *Trypanosoma* and the species *Trypanosoma brucei*. They are transmitted to humans by the tsetse fly (*Glossina* species) [1]. Human African trypanosomiasis can take one of two forms, depending upon the parasite involved. *T. brucei gambiense* accounts for 98% of reported cases and is found in 24 countries in west and central Africa. *T. brucei rhodesiense* accounts for 2 % of cases and is found in 13 countries in eastern and southern Africa [2]. It is one of the main neglected tropical diseases. Without prompt diagnosis and treatment, the disease is usually fatal, as the parasites multiply in the body, cross the blood-brain barrier and invade the central nervous system. The signs and symptoms are generally the same for both forms, but they differ in terms of their frequency, severity, and kinetic appearance. Rhodesiense HAT is an acute disease that usually progresses to death within 6 months. Gambiense HAT has a more chronic progressive course, with an average duration of almost 3 years. The clinical signs and symptoms are nonspecific in both forms of the disease, and their appearance varies between individuals and foci.

2.1.2 Clinical features

This disease evolves through two clinically distinct stages which have a lethal outcome if left untreated. The first symptom of this disease starts at the site of the tsetse fly bite after a minimum of 5-10 days. This local skin reaction, known as trypanosomal chancre, is accompanied by lymphadenopathy and is more common in east African than in West African trypanosomiasis. The first stage is known as the haemolymphatic stage, where the parasites multiply in the subcutaneous tissue, blood and lymph. Fever, head ache, weight loss, swollen lymph nodes, joint pain and itching are the common signs. Hepatosplenomegaly and faint rash are the common nonspecific signs [3]. The second stage is known as the meninges-

encephalitic stage, in which the parasite crosses the blood-brain barrier (BBB) and invades the central nervous system. World Health Organization (WHO) defines this situation by the changes in the cerebrospinal fluid (CSF), such as increased white blood cells (WBC), increased CSF protein and the presence of trypanosomes [4]. In this stage, the patient shows significant neurological consequences, systemic deterioration, changes in behavior, confusion, poor coordination, sensory disturbances, and disorder of the sleep cycle which gives the disease its name and, ultimately, death [5].

2.1.3 Epidemiology

Sleeping sickness is a neglected tropical disease that occurs in impoverished rural parts of sub-Saharan Africa where tsetse flies can be found. Sleeping sickness threatens millions of people in 36 countries in sub-Saharan Africa. Many of the effected populations lives in remote rural areas with limited access to adequate health services, which complicates surveillance and therefore diagnosis and treatment of cases. In addition, displacement of populations, war and poverty are important factors that facilitate transmission [6]. There have been several epidemics in Africa over the last century [7]. Recent reports from the World Health Organization (WHO) reveal that the number of new cases have been reduced [8]. In 2000, WHO started a HAT control program in 24 endemic countries, providing them with technical assistance, access to diagnosis and treatment [9]. This decline in the number of cases has continued with 6,314 new cases reported in 2012 [10]. Despite such progress, only a fraction of the at-risk population in sub-Saharan Africa is under surveillance and relatively few cases are diagnosed annually [11, 12]. Since the number of new human African trypanosomiasis cases reported between 2000 and 2012 dropped by 73%, the WHO neglected tropical diseases roadmap targeted its elimination as a public health problem by 2020. However, HAT has proved capable of recurring after long periods in which the disease appeared to have been kept under control, which underlines the urgent need for more research and development in diagnosis, treatment, control and prevention.

2.1.4 Treatment

Trypanosomes have developed an antigenic variation strategy helped by the presence of variant surface glycoproteins (VSGs). This allows the parasite to evade the host's immune response and thus repopulate the host, resulting in the development of a long-lasting chronic

infection [13, 14]. Consequently, no vaccines have yet been produced. Current treatment options for HAT are based on the use of five chemotherapeutic agents: Pentamidine, Suramin, Melarsoprol, Eflornithine and Nifurtimox (all of which are on the Essential Medicine List for 2009). These drugs are donated to WHO by their producers (Bayer and Sanofi). These drugs have many limitations, including poor efficacy, acute toxicity, problems with oral absorption and drug resistance. As these drugs are not readily available, there is an urgent need for new medicines. Researchers are investigating new enzyme targets for the parasite, searching for more efficient and selective inhibitors, capable of causing parasite death but with lower toxicity for the host. Most often, the treatment depends on the stages of the infection and the parasite species. First-stage drugs may or may not be effective against second-stage disease. Further information on the five drugs is shown below.

A, Pentamidine (pentamidine isethionate)
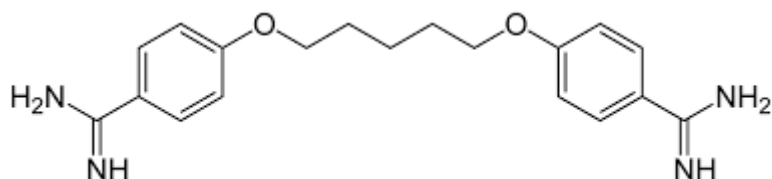
Figure 1. Structure of pentamidine.

One of the classic and most widely-used drugs is pentamidine, an aromatic diamidine compound introduced in 1940 (**Figure 1**). Recently, a trypanosome knockout strain revealed that a specific aquaglyceroporin is required for the high-affinity uptake of pentamidine [15]. Its uptake is mediated by the trypanosome adenosine P2 transporter (TbAT1/P2) in combination with two other transport proteins, namely the High-affinity pentamidine transporter (HAPT1) and the Low-affinity pentamidine transporter (LAPT1) [16-18].

Pentamidine is used for the treatment of early stages of African trypanosomiasis caused by *T. b. gambiense*. Recent studies show that this drug crosses the blood-brain barrier (BBB) but not in sufficient concentrations to kill the parasites. Unfortunately, it causes toxicity in at least half of patients, with life-threatening hypoglycemia being the most serious [19]. The routes of administration are parenteral or intramuscular, due to its poor oral absorption. Suramin may be used as an alternative drug in areas of pentamidine resistance. In addition to

the transporters mentioned above, two nucleoside transporters are present, i.e. NT11.1 and NT11.2, expressed in a heterologous system [20]. A thorough investigation is needed to enhance , but also to select the best drug combination therapies (combination with suramin, eflornithine etc.) [22].

It is necessary to emphasize that the altered function of classical surface transporters (TbAT1/P2 and HAPT1) is associated with the pentamidine resistance mechanism. It is also the reason for melarsoprol resistance, the major resistance in this field [23-26]. However, recent studies have shown a link between melarsoprol/pentamidine cross resistance and aquaglyceroporins (AQPs), channels which are permeable to water, glycerol and other small uncharged solutes, specifically AQP2 which controls the susceptibility to both drugs [27, 28].

B, Suramin
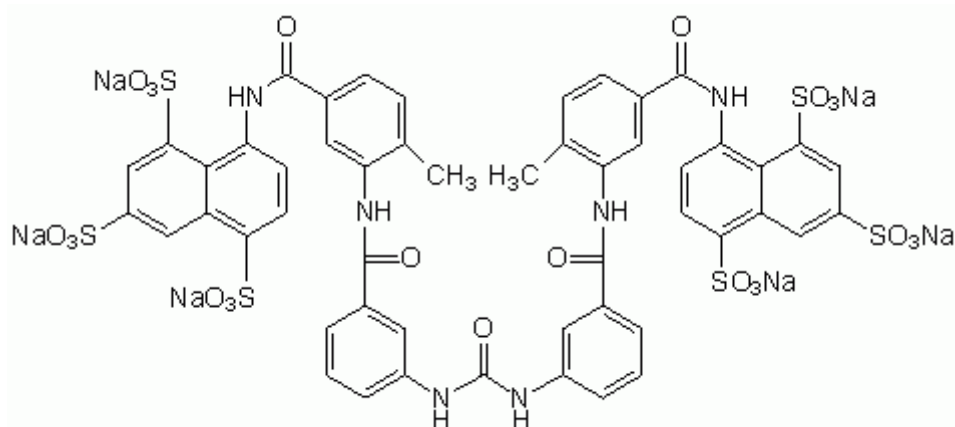
Figure 2. Structure of suramin.

Developed in 1920, suramin is used for the treatment of early stages of trypanosomiasis caused by *T. b. rhodesiense* and *T. b. gambiense* in the event of pentamidine resistance (**Figure 2**). It is a colourless polyanionic sulfonated naphthylamine. Because of its highly ionic nature, it cannot cross the BBB. As it is water-soluble, it can be administered via intravenous injection. Recent studies show that suramin is an inhibitor of cyclic diadenylate monophosphate cyclase, an important second messenger molecule in trypanosomes [32]. Suramin binds with high avidity to serum proteins, including low-density lipoprotein for which trypanosomes have a receptor used to accumulate this complex via receptor-mediated endocytosis [33]. So far, no resistance has been noted for this drug.

C, Melarsoprol
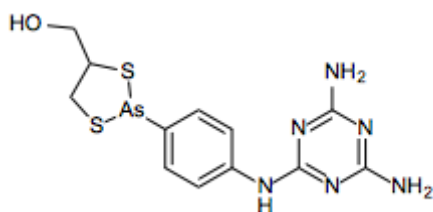
Figure 3. Structure of Melarsoprol.

Melarsoprol is an organic arsenic compound synthesised in the 1940s (**Figure 3**) used for the treatment of the final stages of HAT caused by either species. As this drug crosses the BBB and reaches high levels, it is used to treat the neurological stages of the disease [34]. It suffers from poor gastrointestinal absorption, while its solvent (propylene glycol) displays high toxicity when administered intramuscularly; the preferred route of administration is intravenous. Treatment elicits adverse reactions such as encephalopathic syndromes, leading to a death rate of 50-70% [35]. In order to reduce the side effects caused by this drug, one scientist added a disulphide chelating agent known as dimercaprol, making the active compound less toxic and yet still trypanosomicidal [36, 37]. Actually, Melarsoprol can also be formulated as Melarsoprol cyclodextrin inclusion complexes which have been tested on mice and are less toxic than the traditional form of melarsoprol [38].

D, Eflornithine (diethylfluoromethylornithine-DMFO)
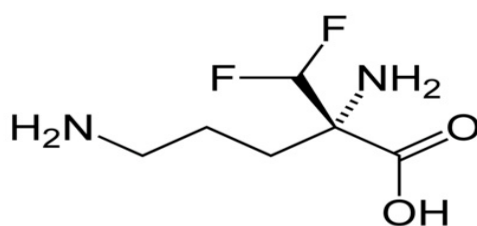
Figure 4. Structure of Eflornithine.

DMFO is the drug used to treat the second stages of HAT caused by *T. b. gambiense* (**Figure 4**). It can cross the BBB and is an inhibitor of ornithine decarboxylase, an enzyme essential for the polyamine biosynthetic pathway. Its main disadvantage is that its mode of administration requires costly equipment. Its side effects include diarrhoea, anaemia, leucopoenia, thrombocytopaenia, etc. Recently, scientists have assessed the efficacy and

safety of the Nifurtimox-eflornithine drug combination to make it easier to administer the drugs and to protect against the emergence of resistance [39]. Eflornithine resistance mechanisms have been associated with the loss of the amino acid transporter TbAAT6 gene which controls its uptake [40].

E, Nifurtimox
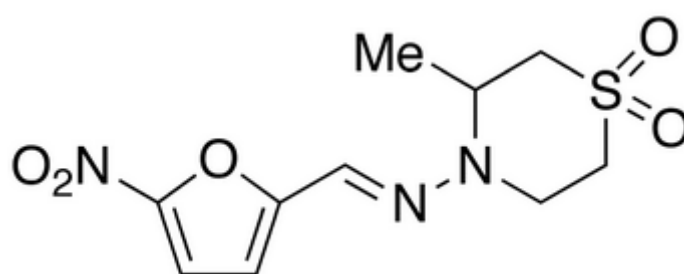
Figure 5. Structure of Nifurtimox.

Nifurtimox is a 5-nitrofuran used to treat HAT and American trypanosomiasis (Chagas disease) (**Figure 5**). This drug is readily absorbed in the gastrointestinal tract, so it can be administered orally. It can cause the formation of the superoxide ion which can damage DNA and alter the redox equilibrium. Its side effects are nausea, vomiting, myalgia, excitability, headache etc. It is a pro drug activated by the mitochondrially-localized type-1 nitroreductase. The downregulation of this gene is correlated with resistance mechanisms [41]. The combination of eflornithine and nifurtimox is less toxic and is used for the treatment of disease caused by *T. b. gambiense.*

2.1.5 *Trypanosoma brucei*

Trypanosoma is a genus of kinetoplastids, and a group of unicellular parasitic flagellate protozoans. It is characterized by the presence of DNA containing granules known as kinetoplasts in their large single mitochondrion. Most trypanosomes are heteroxenous, completing their life cycle in two different hosts and most are transmitted by a tsetse fly vector. The majority of the species are transmitted by blood-feeding invertebrates. In invertebrates, the parasites are found in the intestine, while in mammals they are found in the blood. Among *Trypanosoma*, the two human parasites are *T. cruzi*, the causative agent of Chagas disease, and *T. brucei*, the causative agent of HAT. In addition, *T. brucei* is the agent for nanaga, the cattle disease.

2.1.6 Life cycle of *Trypanosoma brucei*

The life cycle of *T.brucei* is complex and completes in two totally different hosts , mammalian host and tsetse fly host (**Figure 6**) Due to the large differences in the host this parasite undergo complex changes in cell morphology, gene expression and metabolism to allow the survival of the parasite in the two hosts.
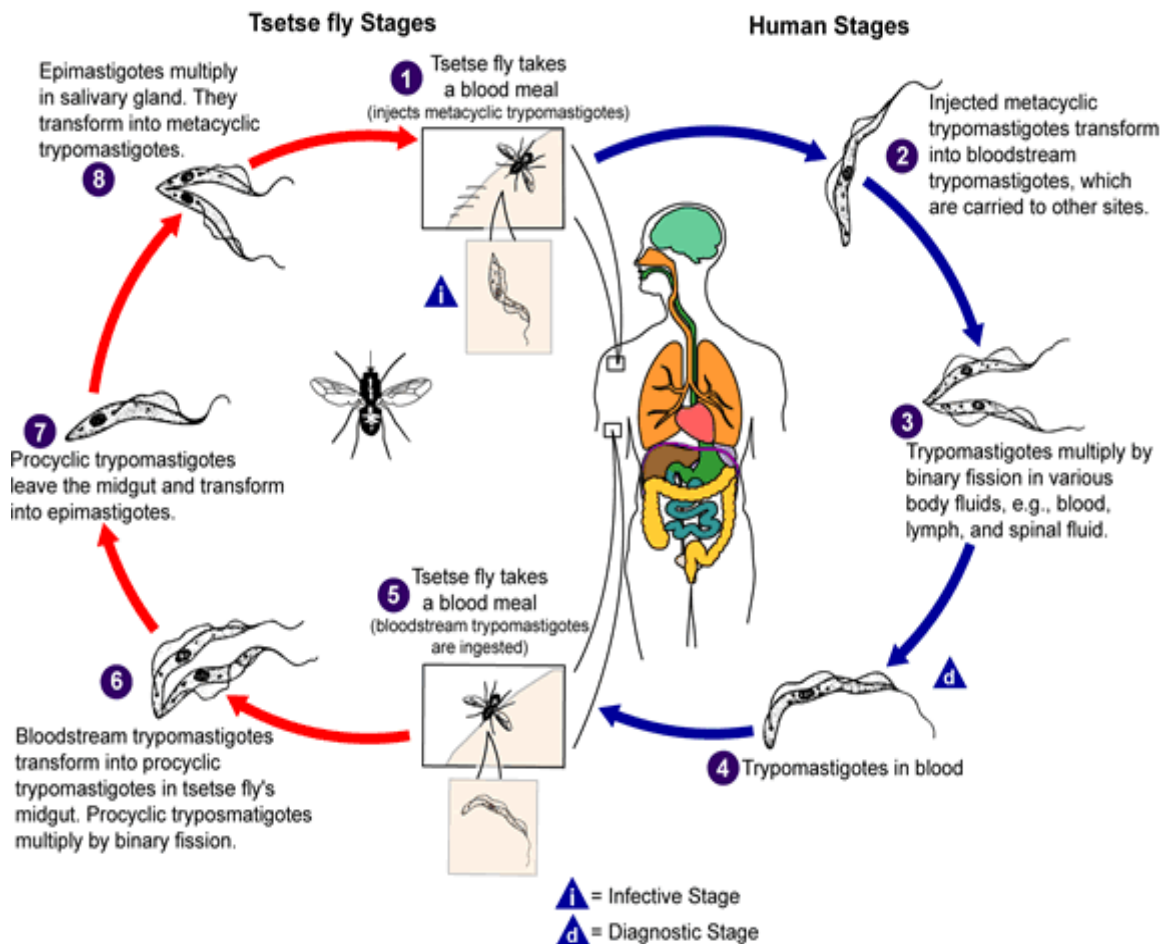
Figure 6. Life cycle diagram.

The life cycle begins when a tsetse fly bites a human and injects metacyclic trypomastigotes. This meta cyclic form rapidly transform into proliferative long slender blood forms which multiplies and invade the blood stream, lymphatic system and subcutaneous tissue and finally in spinal fluid. In mammals, this parasite lives freely in the blood and being able to evade host immune system through antigenic variation strategy. As this forms have an inactive mitochondrion it utilizes glucose from the blood of the host through glycolysis. This long slender form eventually differentiates into non-dividing short stumpy blood stream forms. These forms are preadapted to the gut of tsetse fly. When again tsetse fly bites, an

infected human and ingests blood stream trypomastigotes and transform into pro cyclic trypomastigotes in the fly's midgut. After proliferation, pro cyclic forms migrate from midgut to the salivary gland where they finally differentiate into infective non-proliferative metacyclic forms. The cycle again continues when this fly again bites and inject this form in to mammal [42].

2.1.7 Cellular structure

The cell organization of trypanosomes is similar to that of a typical eukaryotic cell. A single flagellum starts from the posterior end and extends towards the anterior end, which is physically attached to the cell body via an FAZ (Flagellum Attachment Zone). A basal body is present at the start of the flagellum.
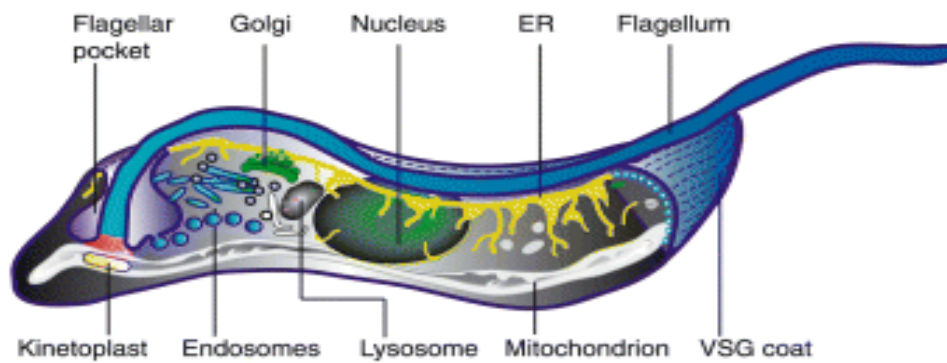
Figure 7. Schematic representation of the *T. brucei* bloodstream form.

Extracted from "Endocytosis, membrane recycling and sorting of GPI-anchored proteins: *Trypanosoma brucei* as a model system".

T. brucei contains a number of single copy organelles and structures: a single nucleus; a single flagellum which emerges from a membrane invagination known as flagellar pocket; a single golgi; a basal body associated with a pro basal body which is immature; a single large unique mitochondrial DNA referred to as kinetoplast; an endosomes; a lysosome and a VSG (Variant surface glycoproteins) which is a protein coat present throughout the cell membrane (**Figure 7**). All these structures must be accurately duplicated and segregated if cell division is going to generate viable progeny [43]. The flagellar pocket is the only site in the cell membrane where endocytosis and exocytosis occurs [44].

2.1.8 Cell cycle

The cell cycle consists of four phases in a typical eukaryotic cell: Go/G1 phase (Gap 0/ Gap 1 phase), S phase (synthesis phase), G2 phase (gap 2 or interphase) and M phase (mitotic phase) (**Figure 8**). During the G1 phase, the cell is growing and replicating cytoplasmic organelles, preparing for DNA replication by synthesizing the enzyme needed to make copies of the DNA. DNA will be replicated during the S phase. In the G2 phase, the biochemical activity of the cell increases and prepares for cell division. In the M phase, the cells divide into two daughter cells having the same copy of all the organelles. In mammals, the M phase is coupled with cytokinesis which starts just before the chromosome segregation is completed. The activation of each phase depends strictly on the completion of the previous phase. Cells which have stopped dividing will go to the G0 phase [45].
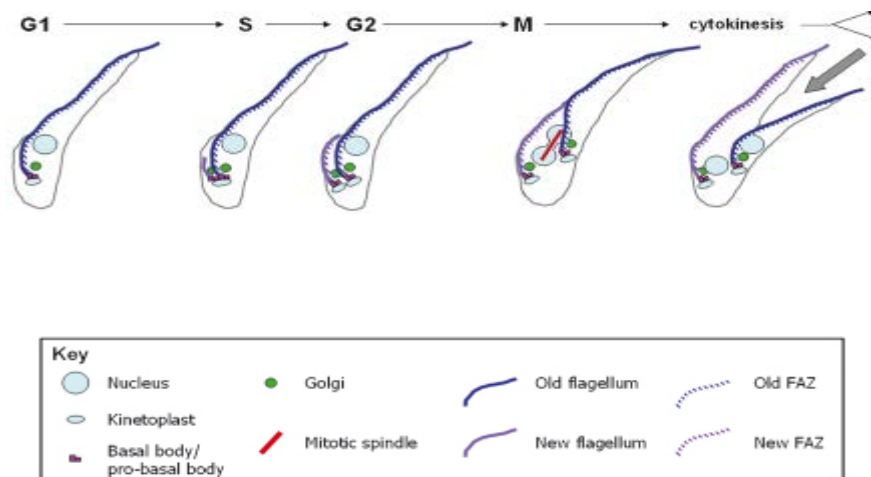
Figure 8 Representation of the cell-cycle stages of *T. brucei.*

In *T. brucei*'s G1 phase, the cell contains one nucleus, one kinetoplast, one flagellum and one Golgi apparatus. The first morphological change observed is the elongation of the probasal body and formation of a new flagellum. This is followed by Golgi duplication. In the S phase, the kinetoplast divides first, followed by the nucleus S phase. In the G2 phase, kinetoplast segregation occurs. Then the nucleus undergoes mitosis causing a cell with double genetic content which is followed by cytokinesis, producing two identical daughter cells.

2.1.9 Antigenic variation

As this parasite lives and multiplies extracellularly in the blood, it is exposed on a continuous basis to antibody challenge. The thick surface protein coat offers the parasite protection against host immunity, enabling it to escape from the immune response. Trypanosomes vary their surface coat, which consists of a single tightly-packed, highly immunogenic protein species covering its whole body. The ability is called antigenic variation. In the mammalian infective stage, this parasite expresses around 107 molecules anchored to the cell membrane through a glycosylphosphatidylinositol (GPI). Normally, the immune system has access to the N terminal of the VSG, antibodies are produced against this and parasites are eliminated by the immune system. But sometimes the parasites spontaneously change their VSG coat and survive the antibody-mediated response against the traditional VSG.

So far, no vaccines are available for treating HAT and it is unlikely that one will be produced in the future. Consequently, the treatment of HAT relies only on chemotherapy. However, current therapy is unsatisfactory: five different drugs are available commercially, but all have side effects and were developed in the early 20th century. Although they are effective, most of these drugs have little in common with the modern concepts of a drug in terms of toxicity, specificity, therapeutic regime duration of treatment and patient compliance. The evolution of drug resistance has worsened this scenario. Therefore, there is a clear need for cost-effective, novel and safe treatments.

This study is part of the search for new molecules with trypanocidal activity. We screened 2000 microbial extracts from Fungi and *Actinomycetes*, from the Medina Natural products library. Initially, 267 extracts (13.5%) showed activity. Liquid chromatography and mass spectrometry showed that 185 extracts contain potentially new compounds. From these molecules, we selected a known molecule, Chaetocin. The discovery of new uses for old drugs, previously used to treat other diseases, is a new and interesting approach by various pharmaceutical companies in the search for new medicines. We selected Chaetocin in an attempt to perform drug repositioning, i.e. to use an existing drug against some neglected tropical diseases (NTDs) in which the pharmacological industry is reluctant to invest vast sums [46]. We investigated and confirmed the activity of chaetocin against human trypanosomiasis and elucidated the mechanism of action behind it.

2.1.10 Chaetocin
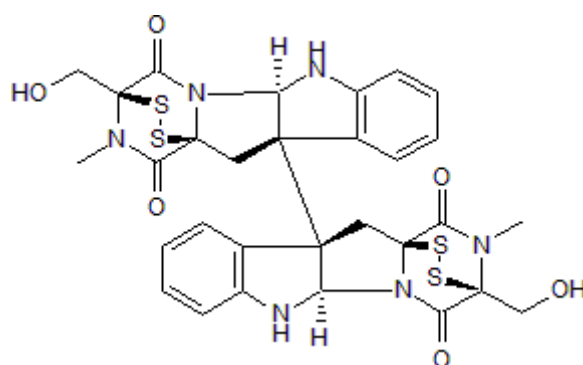
Figure 9. Structure of chaetocin.

Chaetocin is a fungal metabolite from *Chaetomium minutum* with antimicrobial and cytostatic activity (**Figure 9**). It belongs to the 3,6-epidithio-diketopiperazines class and is a molecular dimer made up of *cis*-fused five-membered rings. Chaetocin is a specific inhibitor of the lysine-specific histone methyl transferase SU(VAR)3-9 and acts as a competitive inhibitor of S-adenosylmethionine. The anticancer activity of chaetocin is due to the inhibition of thioredoxin reductase in HeLa cell lines [47]. Chaetocin inhibited the growth of human hepatoma grafts in nude mice. Immunohistochemical analyses revealed that chaetocin inhibits hypoxia-inducible factor-1a (HIF-1a) expression and vessel formation in tumours [48]. In recent studies, chaetocin has been shown to perform both apoptosis and autophagy in several hepatoma cell lines, including HepG2, Hep3B and Huh7 cell lines [49]. Here we demonstrate, for the first time, the promising trypanocidal activity of chaetocin and study its mechanism of action.

2.2 MATERIALS AND METHODS

2.2.1 Screening of the extracts and Identification of Chaetocin

2.2.1.1 Screening of 2000 extracts from fungi and actinomycetes

Actinomycetes and fungi are the main source of antibacterial, anticancer and anti-parasitic agents, hence they are widely used pharmacologically and commercially. These extracts are the secondary metabolites of actinomycetes and fungi, which are extracted using different microbiological methods. The initial screening was performed against both the procyclic (insect form) strain 427 and the blood form, strain 221, with extracts from actinomycetes and fungi. Out of 2000 extracts, 267 showed activity.

2.2.1.2 Determination of effectiveness by dose-response curve

267 active extracts were selected and their activities confirmed by dose-response curve. Of these, 33 showed good activity against the blood form and 14 showed activity against the insect form. The UV-LC-MS data for these metabolites when compared with the UV-LC-MS data for the known metabolites revealed that 30 extracts contained no known metabolites. We later selected just three extracts which showed activity against both forms of the parasite.

2.2.1.3 Semi preparative HPLC fractionation

The three extracts were fractionated based on their size/polarity and plated in duplicate for bioassay for each of the parasitic forms. Activities were co-related with the chromatogram peaks and the active peaks analyzed by LC-HRMS. The molecules identified for extract CF-258252 were Cordycepin, Curvicollide A, and Chaetocins A, B and C. Extract CF-090067 contains Trichothecinol and Trichothenin. Extract CF-010945 contains no compounds.

2.2.1.4 Cytotoxicity study in mammalian cells

The two extracts, which showed good activity against both forms of the parasite, were tested on normal human liver cells, THLE-2 (ATCC® CRL-2706™), by MTT assay. This is a colorimetric assay used for assessing cell viability by using tetrazolium dye, MTT 3-(4,5-dimethylthiazol-2-yl)-2,5-diphenyltetrazolium bromide. The NADPH dependent cellular oxidoreductase enzyme is capable of reducing tetrazolium dye into insoluble formazan which

will give it a purple colour. The deeper the colour, the more cells are present. In this assay, a specified quantity of human cells (THLE-2) are plated in 96 well plates and treated with the two extracts in different concentrations. After 20 hours of incubation, the MTT dye was added in specific concentration and incubated again for 2 hours at 37^0C and read on a plate reader at a wavelength of 535 nM.

2.2.2 Trypanocidal effect of Chaetocin in *T. brucei*

2.2.2.1 Parasites and cell culture

All of the experiments were performed with the bloodstream forms of trypanosomes which were taken from frozen stocks and grown in axenic culture at 37^0C and 5 % CO_2 in HMI-9 media supplemented with 10 % heat-inactivated foetal bovine serum (Gibco). Bloodstream *T. b.brueci AnTat 1.1* (Institute of Tropical Medicine, Antwerp, Belgium) was used throughout the *in vivo* experiment.

2.2.2.2 Anti-proliferative assay and calculation of IC50 value

The growth of the bloodstream forms of the trypanosomes was monitored for some days under appropriate culture conditions. Subculturing started at an initial density of 1×10^4 parasites/ml. The parasites were maintained at 37^0C and 5 % CO_2 in HMI-9 medium. The growth of the parasites was determined daily by counting them with an optical microscope using a Neubauer chamber.

Chaetocin susceptibility was assessed using Resazurin sodium salt (SIGMA- ALDRICH), modifying the protocol developed by Raz et al [50]. During the exponential growth phase, the parasites were seeded into 96 well plates in 50 µL of medium at an initial density of 1×10^4 cells. Later, they were incubated with different concentrations of chaetocin ranging from 0.8 µM to 0.001 µM for 20 hours at 37^0C and 5 % CO_2. Two rows of blank and one column of positive control were maintained in the plate. Thereafter, 20 µL of 0.5 mM resazurin was added to each well and incubated again, under the same conditions, for a further 4 hours. Then, the reaction was stopped by adding SDS 3% solution and immediately read on a Glomax multi detection system (Promega) using an excitation wavelength of 525 nM and an emission wavelength of 580 nM. Each concentration was tested in six wells and the experiment was repeated six times. Half-inhibitory concentration was calculated using the GraphPad Prism

software and defined as the concentration of the drug required to diminish the fluorescence output by 50 %.

2.2.2.3 Analysis of structural changes by flourescence microscopy

In order to understand the structural changes caused by treating the parasite with chaetocin, we performed the fluorescence microscopy technique. The parasites were incubated in a medium containing chaetocin at (10 nM) at 37^0 C and 5 % CO_2 for different time periods. After incubation, the parasites were precipitated by centrifugation at 13000 rpm for 4 minutes. The supernatant was removed and 100 µL of 4 % paraformaldehyde (PFA) and 100µL of phosphate buffered saline (PBS) were added to the pellet and incubated at 4^0 C overnight for fixation. The next day, the Eppendorf tube was centrifuged at the same rpm and the pellet resuspended in 50 µL of PBS. 50 µL of parasites were spread on poly-L-lysine coated slides and incubated at room temperature for 30 minutes in a wet chamber [46]. Then, 5 µL of DAPI were placed on the slide, a coverslip was carefully applied and observed under a Zeiss Axio Imager A.1 fluorescence microscope with Zen Blue software. 100 cells were counted at each time interval. Parasites were classified according to the number of nuclei (N) and kinetoplasts (K).

2.2.2.4 Cell cycle analysis by florescence activated cell sorting

In order to assess how chaetocin interferes with the cell-cycle stages of trypanosomes, we conducted an experiment with propidium Iodide solution (PI). Parasites were seeded at a density of 1×10^4 cells/ml and treated at different time intervals; after, they were centrifuged, at different treatment times. Then, 100 µL of PBS and 900 µL of 70% ice cold ethanol were added to the pellet, which was incubated in ice at 4^0C for 10 minutes. Thereafter, it was washed with PBS and centrifuged at 13000 rpm for 4 minutes. The supernatant was removed and the pellet incubated with 200µl of solution containing PI 40 µg/ml, Ribonuclease A, RNAse A-100µg/ml in PBS for 30 minutes at 37^0C [35]. The analysis was performed using the BD FACSCANTO 2 flow cytometer. The number of cells at G1, S and G2/M were estimated using the BD FACSDIVA software. The experiment was performed in triplicate and repeated four times.

2.2.2.5 Chaetocin uptake by trypanosomes

Uptake of chaetocin by the parasites was determined using the flow cytometer. It is known that parasites take up suramin by endocytosis [28]. It is also known that the endocytosis process will be inhibited at a temperature of 4^0C. The parasite takes up pentamidine by means of a transporter, so temperature has no effect on drug uptake. Parasites at specific concentrations were treated with chaetocin and pentamidine and incubated at both 37^0C and 4^0C for 1 and 2 hours, respectively. After incubation, cells were precipitated by centrifugation at 13000 rpm for 4 minutes. After removing the supernatant, 200 µL of PI solution (40µG/mL) were added and put into an Eppendorf tube at 37^0C, for 30 minutes and analyzed by flow cytometer.

2.2.2.6 Analysis of cytotoxicity in normal liver cells

In order to evaluate the toxicity of chaetocin in normal human cells, we selected normal liver cells for the cytotoxicity assays. The MTT assay was performed as described above, using different concentrations of chaetocin from 20 to 200 nM.

2.3 RESULTS AND DISCUSSION

2.3.1 Screening of the extracts and Identification of Chaetocin

2.3.1.1 Initial screening of 2000 extracts form fungi and actinomycetes

A
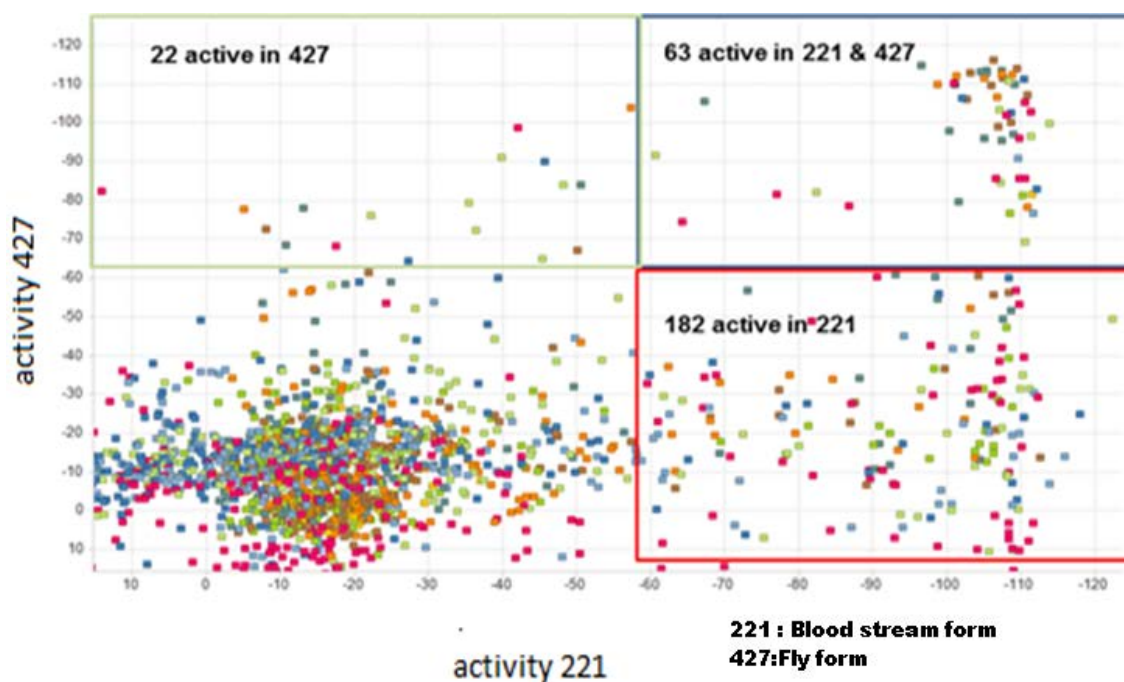
B

Natural extract	Assay	Procyclic & Blood	Blood	Procyclic	Total
Actinomycetes	960	35	59	8	102
Fungi	1040	28	123	14	165
Total	2000	63	82	22	267

Figure 10. **(A)** The result of the initial screening of 2000 natural extracts from fungi and actinomycetes. The X axis indicates the extracts showing activity against the bloodstream forms of the parasite and the Y axis shows activity against the fly form of the parasite. **(B)** The table showing the activity of 2000 extracts from fungi and actinomycetes against the bloodstream and fly forms of trypanosomes.

Initial screening of the extracts from fungi and actinomycetes showed trypanocidal effects against the bloodstream and fly forms of trypanosomes. Out of 2000, 267 extracts showed activity (13.5%): 102 extracts from *Actinomycetes* and 165 extracts from Fungi. 35 extracts from *Actinomycetes* showed activity against both forms of parasite, as did 28 extracts from Fungi (**Figure 10**). Next, we performed liquid chromatography and mass spectrometry to identify the molecules present in those extracts, evidencing that 185 extracts contained new molecules.

2.3.1.2 Dose-response assay

In order to confirm the results of the initial screening, we performed a dose-response curve assay. The parasites were seeded at a specific concentration and incubated with compounds at different concentrations. The results obtained were shown in **figure 11**.
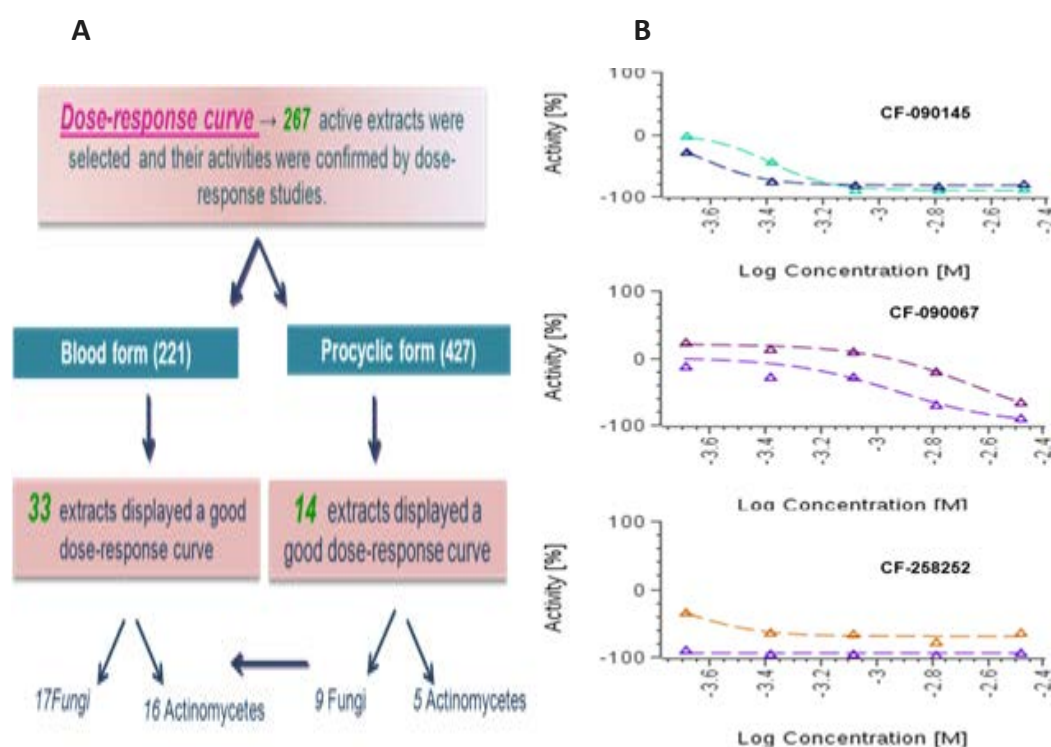
Figure 11. **(A)** Summary of the dose-response curve. 33 extracts showed activity against the bloodstream form (i.e. extracts 221) and 14 showed a good dose-response curve against the insect form of the parasite (i.e. no. 427). In all, 33 extracts showed activity against 221, 17 extracts from fungi and 16 extracts from actinomycetes. In all, 14 extracts showed activity against 427, 9 from fungi and five from actinomycetes. **(B)** Dose-response curve of the three extracts which showed good activity against both mammalian and insect forms. These extracts were selected for further studies.

2.3.1.3 Identification of molecules from three extracts

In order to understand the active molecules, present in the three extracts, we fractionated the extracts based on their size and polarity. Carried out bio assay for both blood and insect forms of parasite. All the fractions were plated in duplicate with each plate for each form of the parasite. Activity were detected for both forms and it was correlated with chromatogram peaks and the active peaks were analyzed by Liquid Chromatography-High resolution mass spectrometry (LC-HRMS). Out of three extracts, in one extract no molecules were identified. The results were shown in **figure 12**.

A,

B,

C,

trichothecinol A

trichothecin
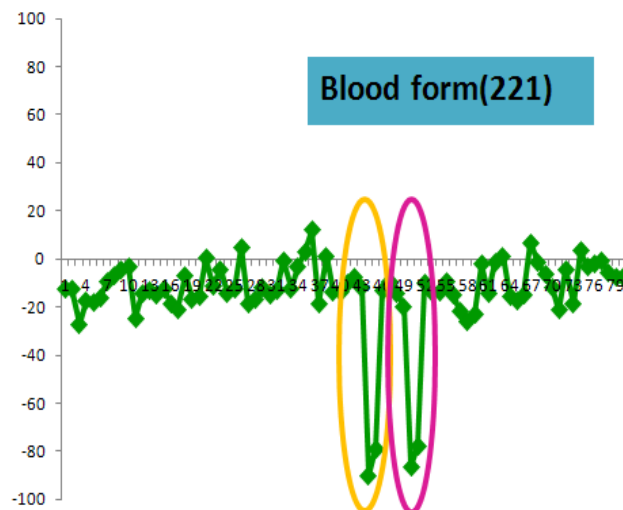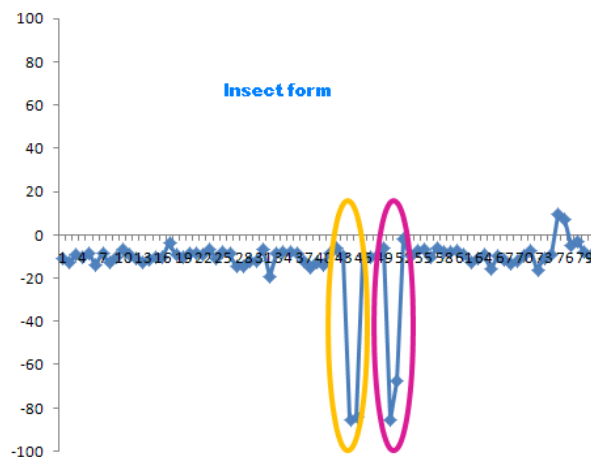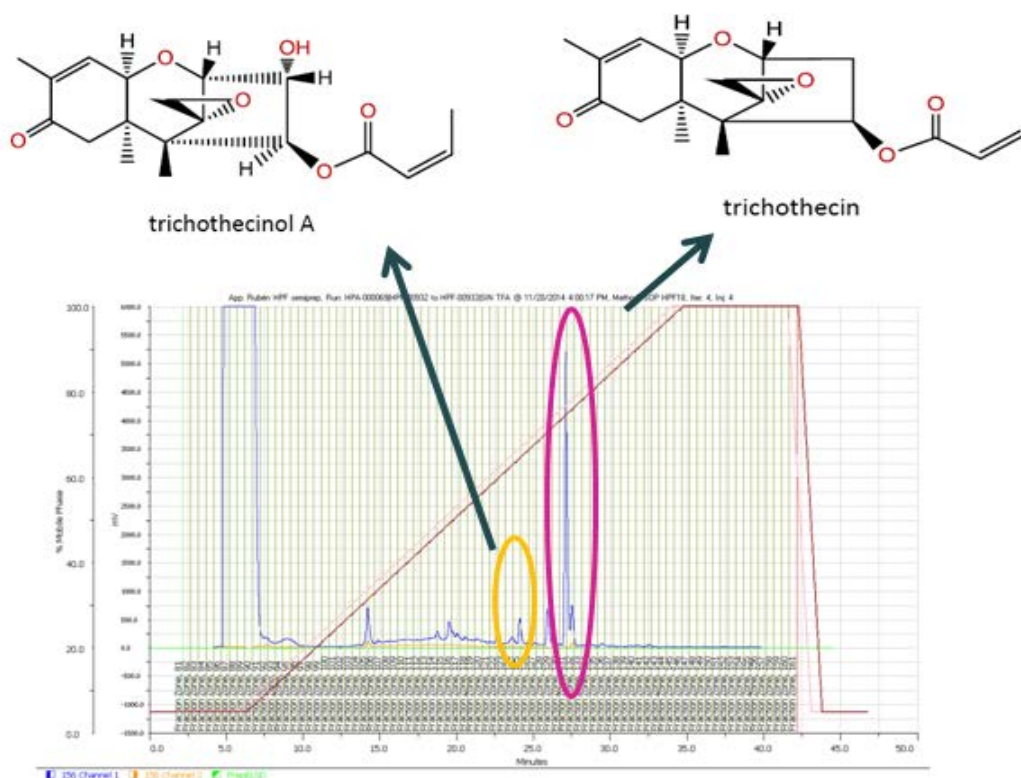
Figure 12. **(A)** Extract CF-090067 shows two activity peaks when the extract was treated with the bloodstream form of the parasite. **(B)** The graph from insect form showing two activity peaks at the same position as seen in the bloodstream form of the parasite. **(C)** The activity peaks were correlated with the chromatogram peaks and the molecules were identified as Trichothecinol A and Trichothecin by LC-HRMS.

The same protocol was performed in order to identify the molecules present in the extract CF-258252. The activity peaks and the molecules identified were shown in **figure 13**.

A,
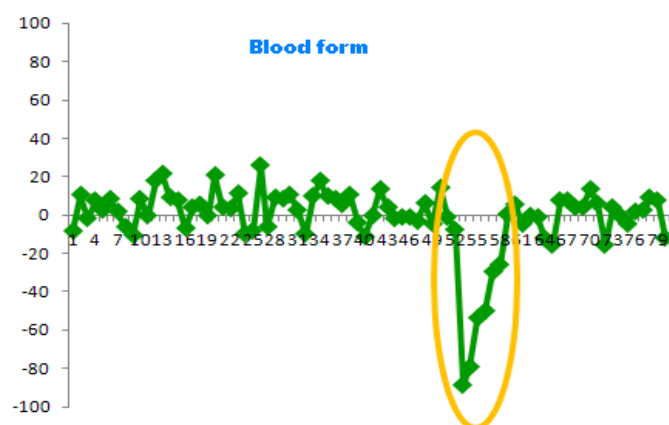
B,
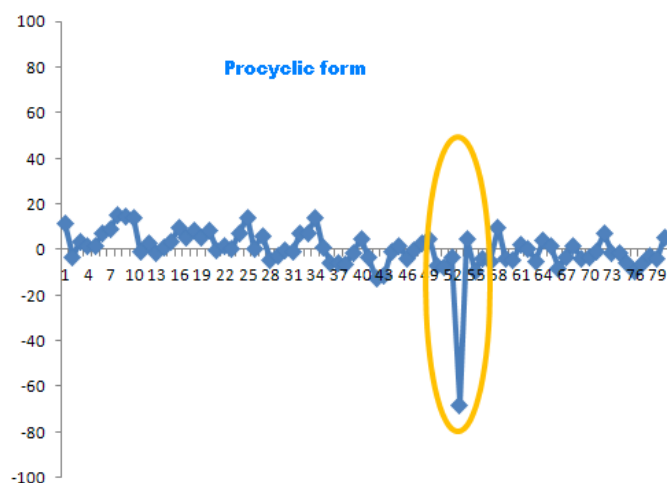
C,
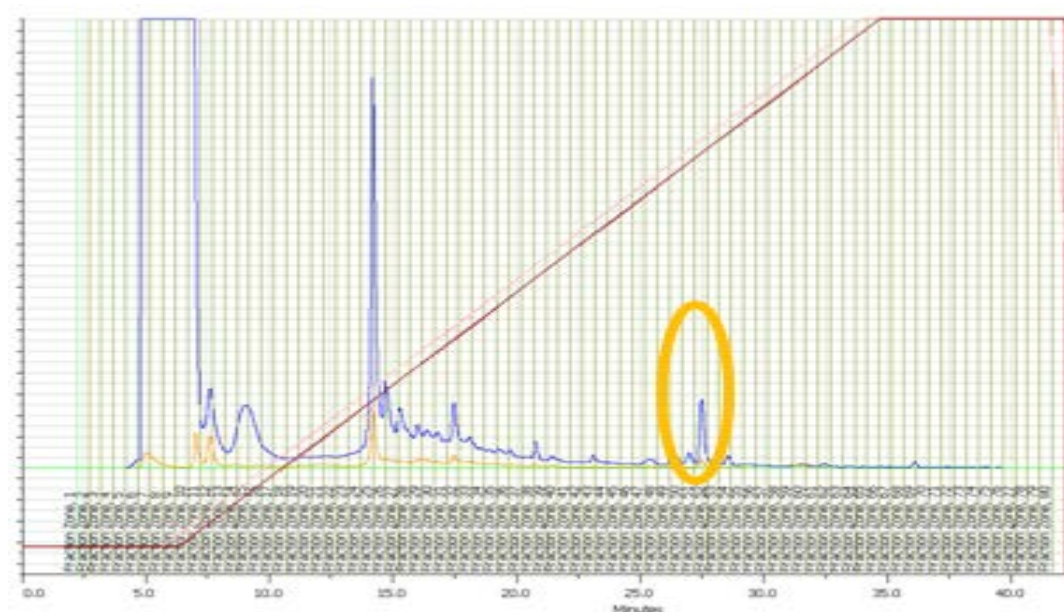
Figure 13. **(A)** The extract CF-252258 shows only one peak when treated with the blood form of the parasite**. (B)** The peak at the same position was also observed in the insect form of the parasite. **(C)** The molecules identified by HR-MS (Cordycepin, Curvicollide A, Chaetocin A, Chaetocin B and Chaetocin C).

2.3.1.4 Cytotoxicity study of two extracts on normal liver cells

In order to find out whether these extracts were toxic to normal human cells, we treated the extracts with liver THLE-2 cells. Extract CF-258252 showed no toxicity whereas extract CF-090067 did. The results were shown in **figure 14**.

So far, we have been discussing the screening of the extracts from fungi and actinomycetes; Chromatographic and mass spectrometric studies of these extracts and treatment of blood stream and insect form of the parasite with them. We found various molecules and from this group we selected Chaetocin for further studies. This choice is due to its commercial availability and previously-described anticancer activity. This is the first work to describe the antitrypanocidal activity of Chaetocin.

A   **B**
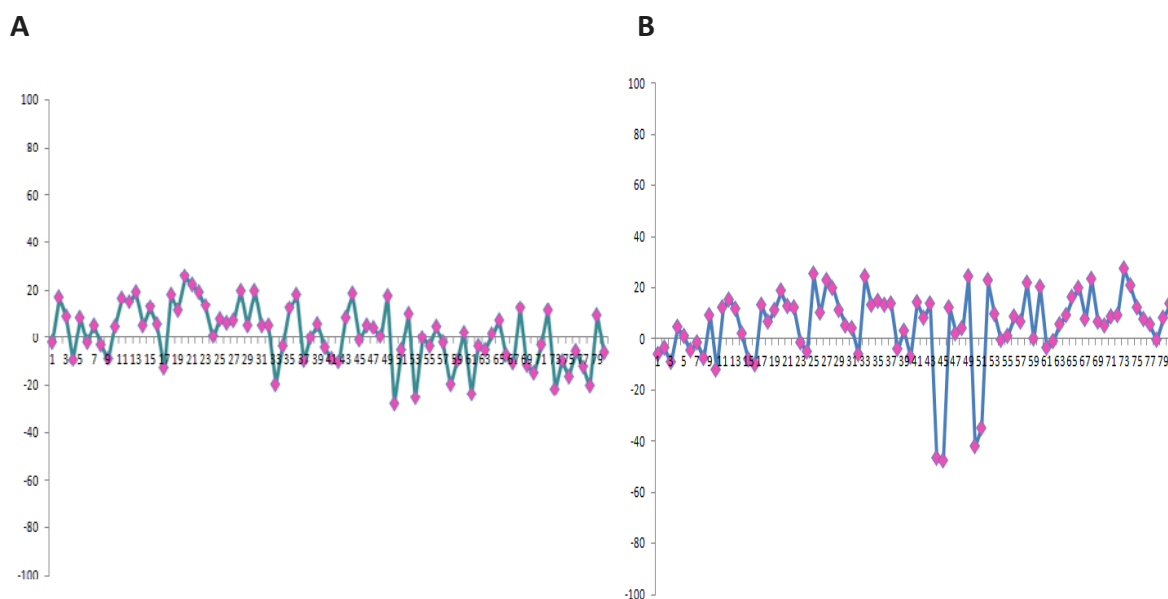
Figure 14. **(A)** Extract CF-258252 showed no toxicity. **(B)** Extract CF-090067 showed some toxicity.

2.3.2 Trypanocidal effect of Chaetocin in *T. brucei*

2.3.2.1 Anti-proliferative effect and calculation of IC50 value

The trypanocidal effect of *T. brucei* was evaluated by measuring the parasite-mediated reduction of Resazurin sodium dye. Chaetocin showed a dose-dependent effect on cell proliferation (**Figure 15**). Half-maximal inhibitory concentrations were 8.3 nM. After just 3 hours of incubation with chaetocin, the parasite started to change its morphology.
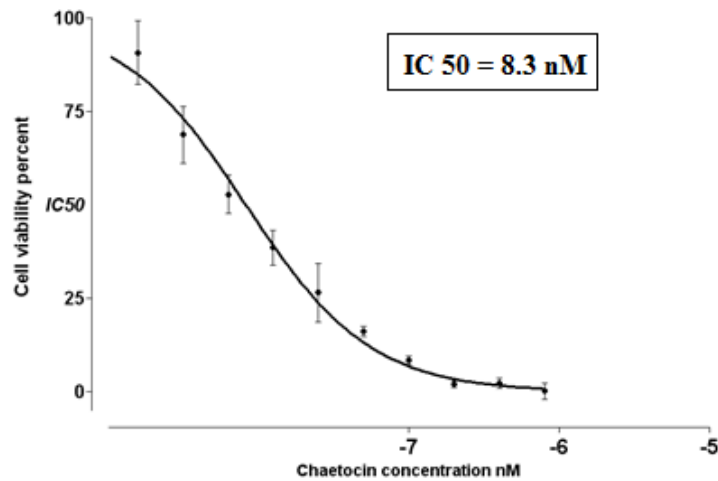
Figure 15. Trypanocidal activity of chaetocin at different concentrations. The graph shows the dose-response curve (cell viability percentage versus chaetocin concentration in nanomoles). The IC-50 value was determined by log inhibitors versus normalized response-variable slope using the GraphPad software.

2.3.2.2 Analysis of structural changes flourescence microscopy

The parasites were treated with chaetocin 1t 10 nM concentration and viewed by a Zeiss Axio Imager A.1 fluorescence microscope using Zen Blue software. A clear morphological change was observed after 3 hours of incubation when the parasite became spherical. After 6 and 24 hours of incubation, the parasite cell membrane was damaged and its DNA and kinetoplasts started to condense (**Figure 16**).
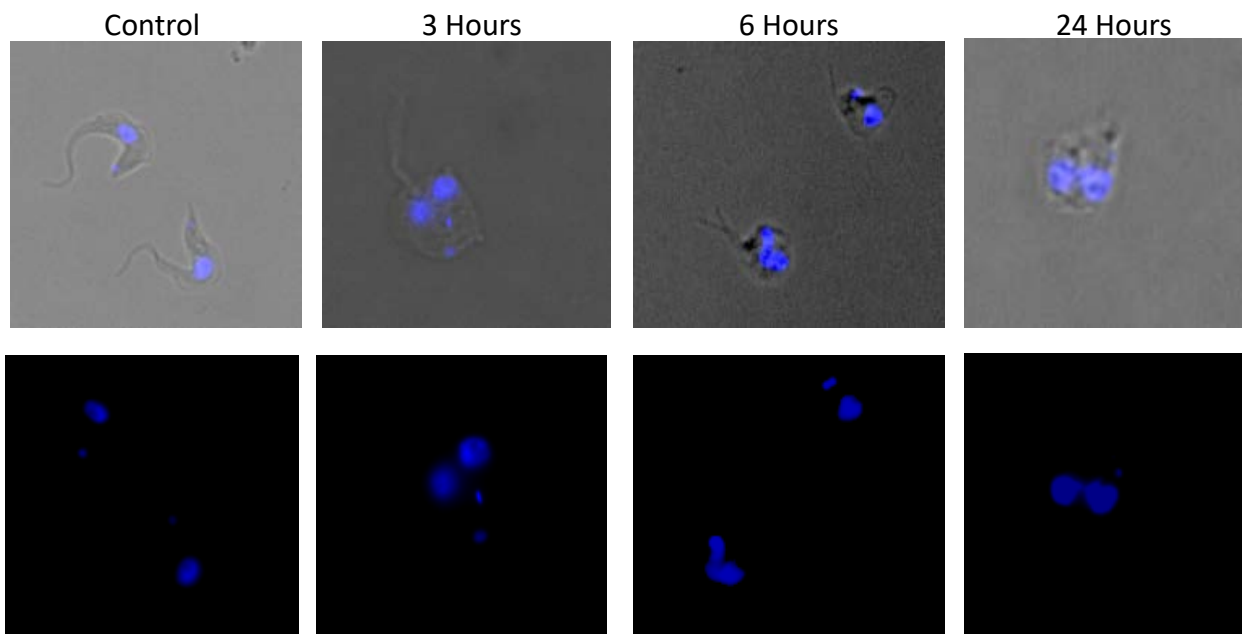
Figure 16. Analysis of the morphological phenotype after treatment with 10 nM Chaetocin at different time interval. Fixed parasites were stained with DAPI and observed by fluorescence microscopy.

2.3.2.3 Quantification of Normal and Abnormal cells

The parasites were treated with 8.3 nM (IC-50) chaetocin at different time intervals (3, 6, 10 and 24 hours). After that, the parasites were fixed and stained with DAPI and viewed by fluorescent microscope. Quantification of the abnormal and normal cells was performed by counting 100 cells per treatment. The results were shown in **figure 17**.

A,
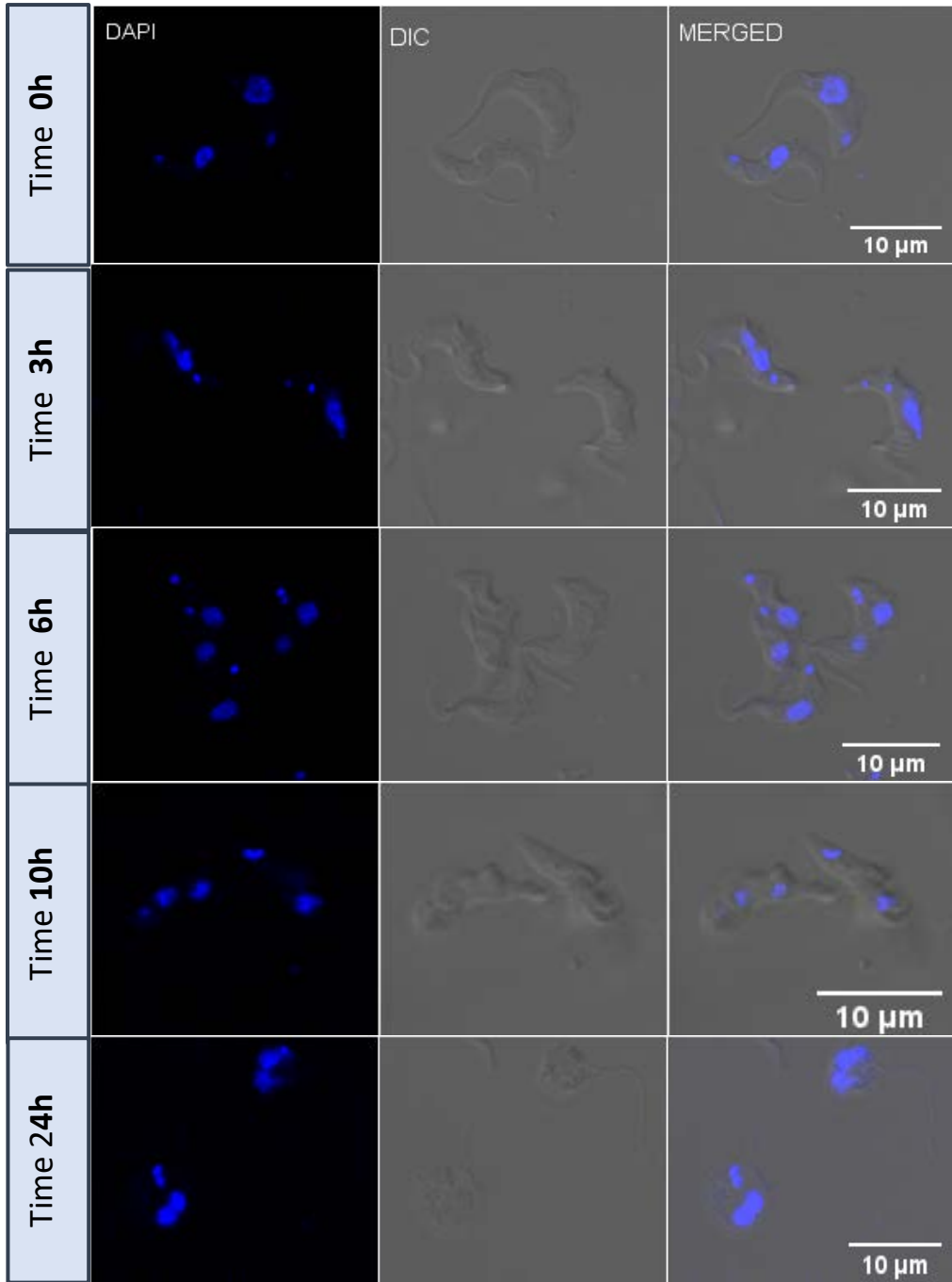
B,
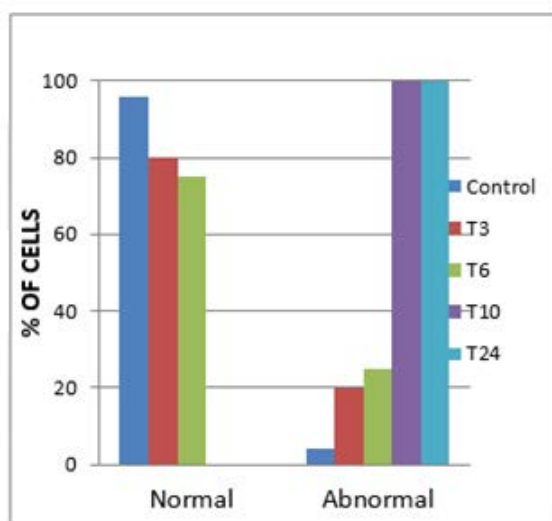
Figure 17. **(A)** Analysis of morphological phenotype at 3,6,10 and 24 hours of treatment with 8.3 nM chaetocin (IC-50 concentration), fixed with PFA and stained with DAPI. (1) DNA stained with DAPI, (2) Differential interference contrast (DIC) (3) Merge that evidences the parasites with morphological changes in DNA. **(B)** Quantification of normal and abnormal cell morphology. % of normal and abnormal cell morphology were determined by counting at least 100 cells per sample.

2.3.2.4 Effect of IC50 treatment on number of nucleus (N) and kinetoplasts (K)

The different cell-cycle phases of African trypanosomes were measured by the quantification of Nuclei (N) and mitochondrial DNA genome fragments known as Kinetoplasts (K). Cells containing one nucleus and one kinetoplast (1N1K) are in phase G1. A configuration of two kinetoplasts and one nucleus will be in the synthesis (S phase) or in the Mitotic phase (M phase). Post-mitotic phases of cells have 2N and 2K (2N2K). 100 cells were counted using the DAPI stain (**Figure 18**). This graph showed that the ratio of the cells with one nucleus and one kinetoplast (1N1K) decreased from 83.8 % (Standard deviation [SD] $\pm$ 5, n=100) in control cells to 59.9% (SD $\pm$ 8, n=100) and 46.6 (SD $\pm$ 7, n=100) after 6 and 12 hours of treatment with the chaetocin, at IC50 concentration. Cells with two nuclei and two kinetoplasts (2N2K) increased in parasites treated for 6 and 24 hours with respect to the control. Finally, aberrant cells containing several nuclei and kinetoplasts increased from 0.7 % (SD $\pm$ 0.93, n=100) to 10.2 % (SD $\pm$ 0.33, n= 100). This result indicates that the treated population of parasites was arrested in cytokinesis after completing several rounds of synthesis and mitotic phases.
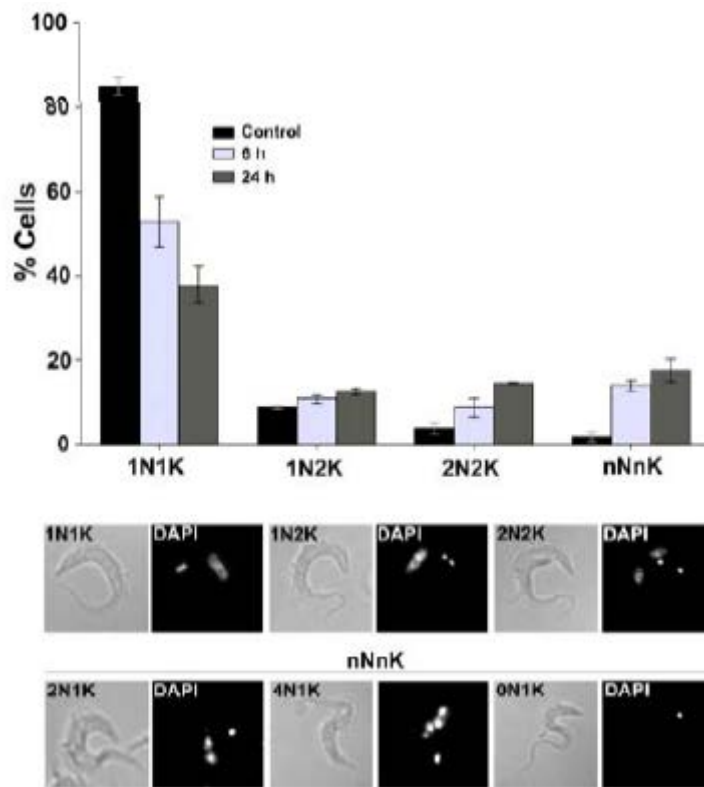
Figure 18. Paraformaldehyde-fixed parasites counterstained with DAPI after treatment with 8.3 nM chaetocin. Results are analysed as mean $\pm$ SD of three experiments. The top panel of the graph shows the normal types, plus 1N1K, 1N2K and 2N2K, while the three types of aberrant cells are shown in the bottom panel.

2.3.2.5 Chaetocin causes cell cycle arrest at G2 phase and ultimately cell death

The increase in the number of aberrant cells after treatment with chaetocin at different time intervels suggested that this compound causes an undesirable effect to the cell cycle phases. Inorder to further investigate exactly at what pahses of cell cycle is effected by chaetocin, the blood stream forms of parasites are incubated with chaetocin at different time intervels . Later the DNA content was measured by using Propidium iodide(PI) by flow cytometry analysis. The percentage of the of the different phases of cell cycle in the untreated trypanosomes exhibited a major G0/G1 population (42%) ,a lower S phase (38%) and a mitotic phase (20%). But with 6 ,10 and 24 hours of treatemnt the G2/M phase started to increase from 20 % to 30 %, 52 % and 77 % for treatment of 6hour 10 hour and 24 hours (**Figure 19**). The population in the G0/G1 phase decreased from 42 % in the untreated to 16 %, 24 % and 4 % with the treatment of 6,10 and 24 hours respectively. These results made it clear that the chaetocin treatment block the cell cycle at the G2 phase.
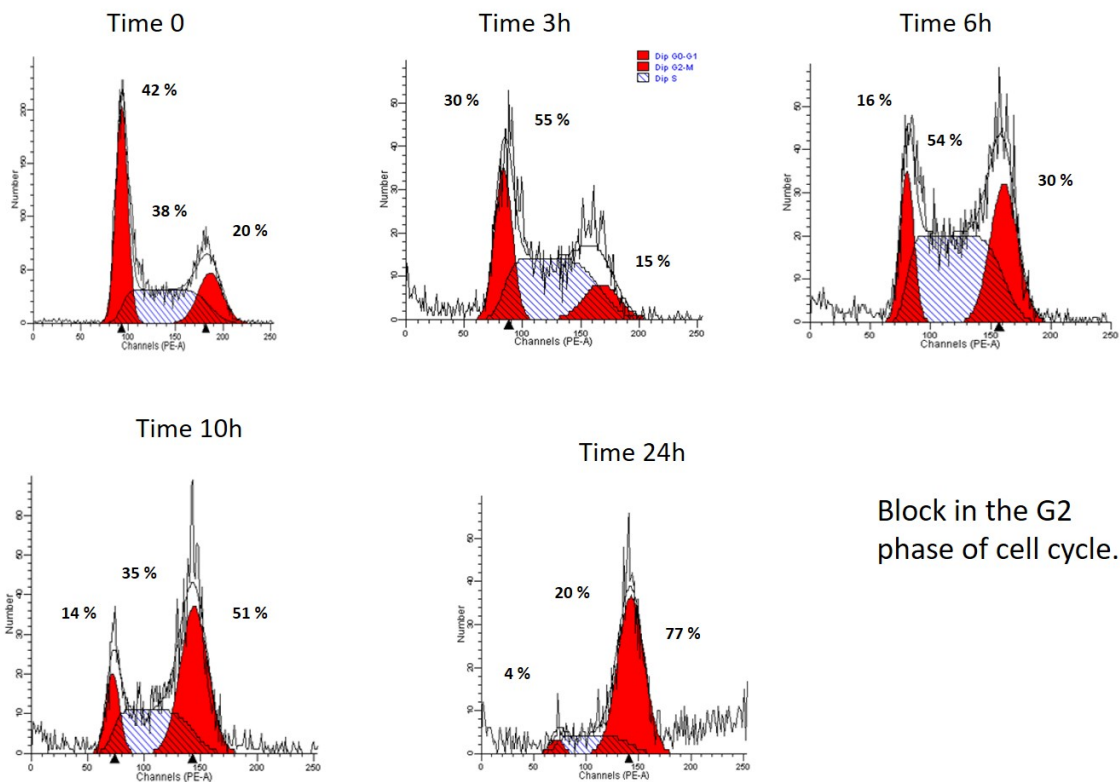
Figure 19. Cell-cycle analysis by FACS: Analysis of the bloodstream forms of the parasite treated with 8.3 nM chaetocin at different time intervals. Cells were stained with PI and the percentages of each cell-cycle phase were calculated.

2.3.2.6 Chaetocin uptake by trypanosomes

In order to understand the mechanism of chaetocin uptake by trypanosomes, we performed two set of experiments, one at 37°C and another at 4°C, where the parasites were treated with 8.3 nM chaetocin for different durations (1 hr and 2 hr). Pentamidine and suramin were used as model drugs. Pentamidine uptake is carried out by a transporter present in the cell membrane of the parasite, while suramin uptake is by endocytosis. At 37°C, the parasites died when treated with 8.3 nM chaetocin and this may be due to drug uptake by endocytosis. When we treated the parasites with the same dose of chaetocin at 4°C, they remained alive as the endocytosis process will be inhibited at 4°C resulting in no drug uptake. In case of pentamidine treatment, the parasites died irrespective of the incubation temperature. This proved our hypothesis that chaetocin uptake is by endocytosis. The experimental results were shown in **figure 20**.

A, PENTAMIDINE at 37°C
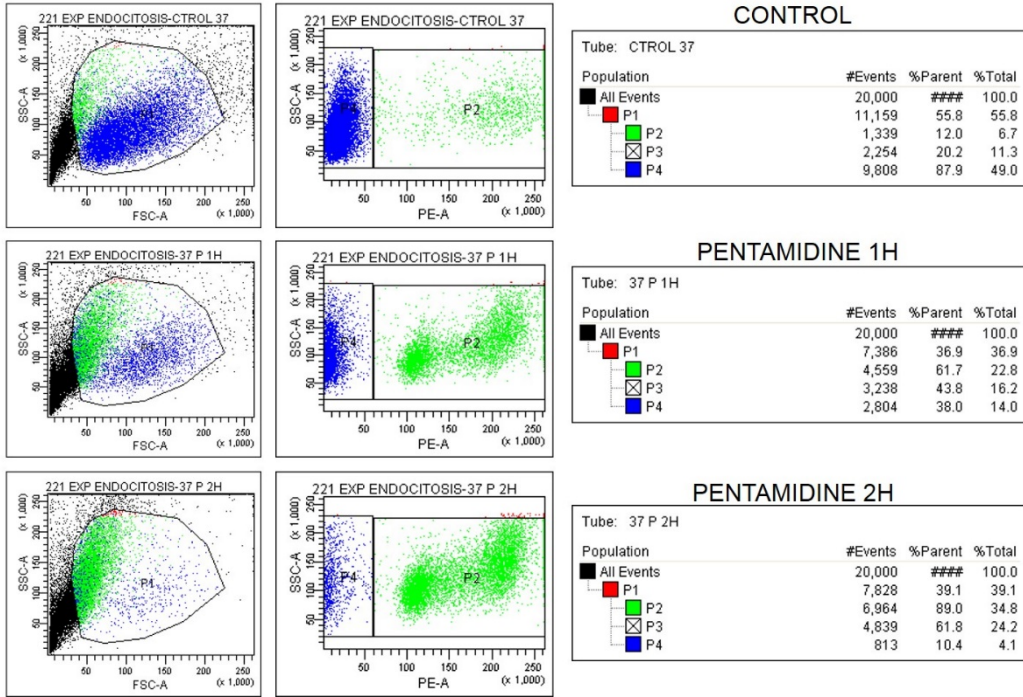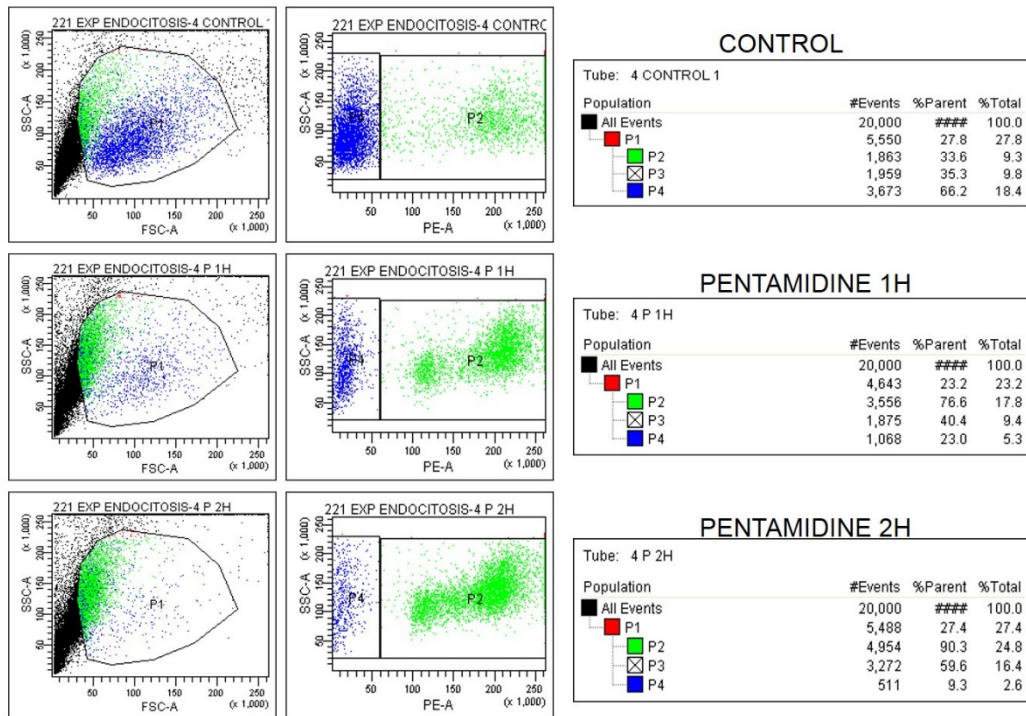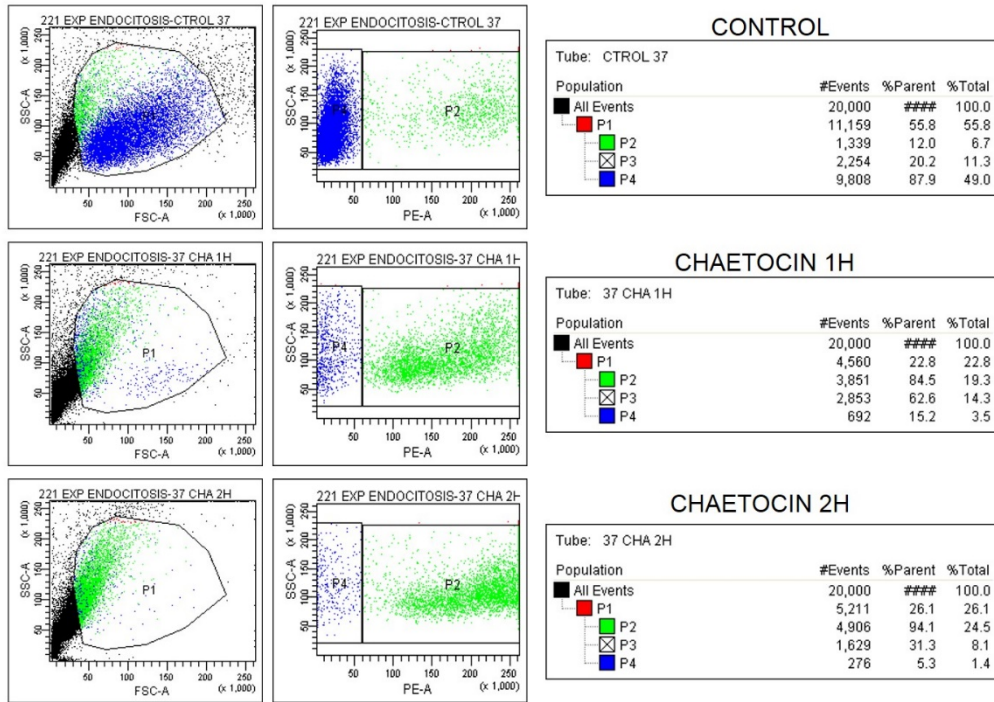
B, PENTAMIDINE at 4°C
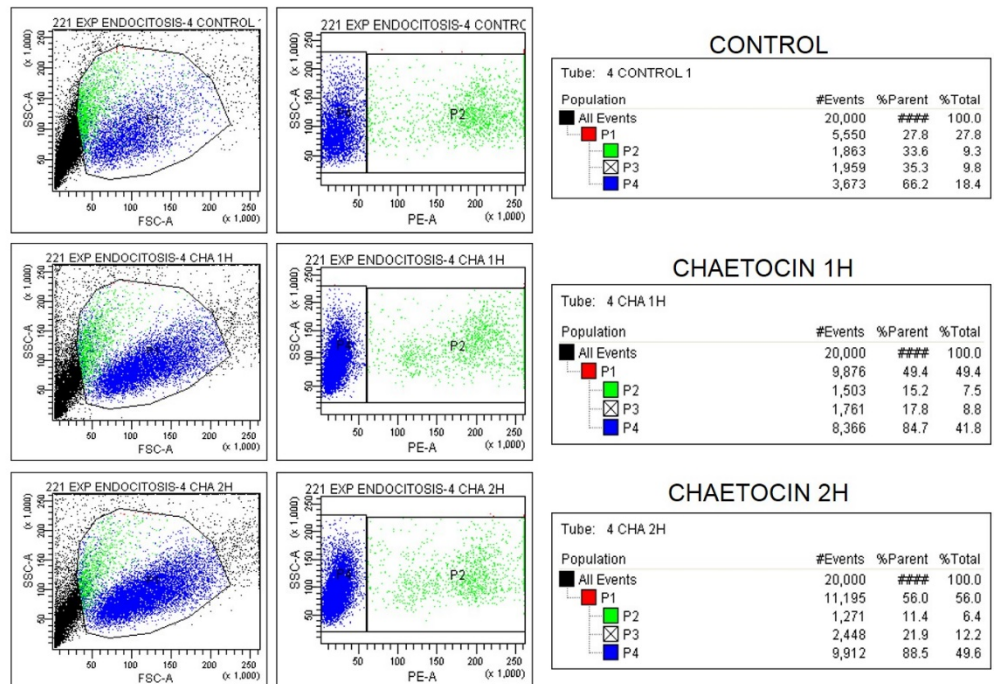
Figure 20. FACS analysis of the trypanosomes stained with PI as described in section **2.2.2.4** to analyse the cell population after treating the parasite with pentamidine at different durations (1 hr and 2 hr) at 37˚C **(A)** and 4˚C **(B)**. The parasites died at both temperatures. FACS analysis of the chaetocin-treated parasites stained with PI to quantify the cell population. The parasites incubated at 37˚C **(C)** died but at 4˚C **(D)** they remained alive. This made it clear that chaetocin uptake is by endocytosis.

2.3.2.7 Study of the cytotoxicity in normal liver cells

Cytotoxicity in normal liver cells was studied by treating THLE-2 cells with different concentrations of chaetocin, by MTT assay. The IC-50 was calculated to be 112.71 nM.
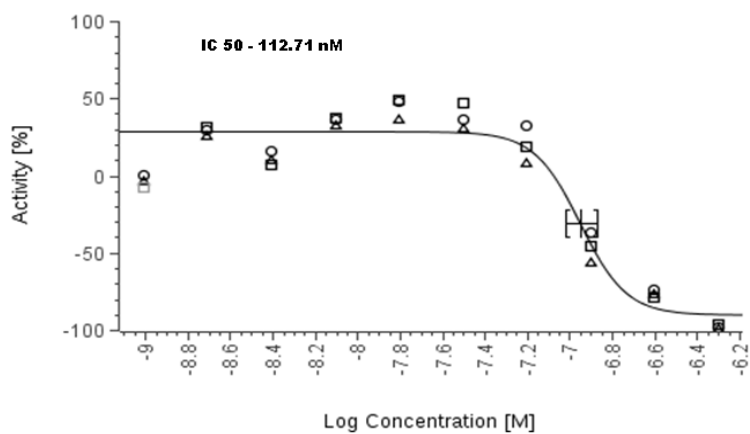
Figure 21. Chaetocin-treated normal liver cells (THLE-2). IC50 value was 112.71 nM.

The above result showed that chaetocin inhibit the normal cell lines only in the higher concentration with respect to parasitic cells (**Figure 21**).

2.4 CONCLUSION

Human African trypanosomiasis is a parasitic disease with a devastating socio-economic impact in sub-Saharan Africa through the direct infection of human and livestock. This disease is caused by a protozoan parasite *Trypanosoma brucei gambiense* and *Trypanosoma brucei rhodesiense*. This disease is truly fatal if left untreated. Current chemotherapeutics rely on five drugs with many limitations, ranging from acute toxicity and poor oral absorption to the need for costly machinery and parasitic resistance. The main reason for resistance is due to the loss of cell surface transporters for the drug. Therefore, the main reason for not finding a new therapeutic agent is that this parasite can easily escape from the host immune system.

The pharmaceutical corporations are reluctant to develop new drugs against this disease because of the low return on investment. It is therefore really important to come up with a solution to this problem, i.e. to find a cost-effective, novel, safe drug for this deadly disease. Natural extracts always contain new molecules, which can act inside a host human. As part of our investigation, we started to work on some microbial extracts such as fungi and actinomycetes. Initial screening found some molecules which can inhibit the bloodstream form of African trypanosomes *in vitro*. From those, we selected chaetocin for further studies. Chaetocin is already an antibacterial and anticancer agent, but we are the first to study its anti-parasitic action.

In this work, we have described the trypanocidal activity of the fungal metabolite chaetocin. It is noted that this fungal toxin exhibits strong cytotoxicity against HeLa cells and it is a specific inhibitor of the lysine-specific histone methyltransferase, an important epigenetic enzyme. We carried out experiments to understand chaetocin's antiparasitic activity, against trypanosomes. Our outcomes demonstrated that chaetocin displayed antiparasitic activity by blocking either cell cycle during the G2 phase and cytokinesis. Interestingly, chaetocin displayed a very low IC-50 value (8.3 nM) and its activity was selective against trypanosome. Indeed, the IC-50 value, in normal liver cells, was found many times more than those established in tripanosome cultures.

Moreover, we were able to picturize the morphological changes as well as quantify the DNA content in trypanosomes treated with chaetocin; particularly, the parasite's

morphology started to change even after 3 hours of incubation with chaetocin. We detected, also, the presence of aberrant cells harbouring numerous nuclei and kinetoplasts, after treatment.

Finally, our results showed that chaetocin uptake occurs via endocytosis, so even if there is a problem of drug transporter molecules as part of resistance, chaetocin can enter through an endocytotic process.

For all these reasons, this drug appears to be promising for use against trypanosomiasis. Further studies will be required to check this drug's ability to cross the blood-brain barrier. If this is possible, chaetocin may inhibit trypanosomes both in the primary and in the final stages of infection.

2.5 BIBLIOGRAPHY

1. Barrett MP, Burchmore RJ, Stich A, Lazzari JO, Frasch AC, Cazzulo JJ and Krishna S. (2003) The trypanosomiases. *Lancet.* 362(9394):1469-80.

2. Steverding D. (2008) The history of African trypanosomiasis. *Parasit Vectors*. 1(1):3

3. Stich A, Abel PM and Krishna S. (2002) Human African trypanosomiasis. *BMJ.* 325(7357):203-206.

4. Blum J, Schmid C and Burri C. (2006) Clinical aspects of 2541 patients with second stage human African trypanosomiasis. *Acta Trop*. 97(1):55-64.

5. Checchi F, Filipe JA, Haydon DT, Chandramohan D and Chappuis F. (2008) Estimates of the duration of the early and late stage of gambiense sleeping sickness. *BMC Infect Dis*. 8:16.

6. Franco JR, Simarro PP, Diarra A and Jannin JG. (2014) Epidemiology of human African trypanosomiasis. *Clin Epidemiol*. 6:257-75.

7. Brun R, Blum J, Chappuis F and Burri C. (2010) Human African trypanosomiasis. *Lancet.* 375: 148-159.

8. Third WHO report on neglected tropical diseases. (2015) Investing to overcome the global impact of neglected tropical diseases: third WHO report on neglected diseases.

9. Simarro PP, Diarra A, Ruiz Postigo JA, Franco JR and Jannin JG. (2011) The human African trypanosomiasis control and surveillance programme of the World Health Organization 2000-2009: the way forward. *PLoS Negl Trop Dis*. 5(2):1007.

10. Squarre D, Kabongo I, Munyeme M, Mumba C, Mwasinga W, Hachaambwa L, Sugimoto C and Namangala B. (2016) Human African Trypanosomiasis in the Kafue National Park, Zambia. *PLoS Negl Trop Dis*. 10(5):0004567.

11. WHO Report Report of the first WHO stakeholders meeting on rhodesiense human African trypanosomiasis (2014).

12. Namangala B, Hachaambwa L, Kajino K, Mweene AS, Hayashida K, Simuunza M, Simukoko H, Choongo K, Chansa P, Lakhi S, Moonga L, Chota A, Ndebe J, Nsakashalo-Senkwe M, Chizema E, Kasonka L and Sugimoto C. (2012) The use of Loop-mediated Isothermal Amplification (LAMP) to detect the re-emerging Human African Trypanosomiasis (HAT) in the Luangwa and Zambezi valleys. *Parasit Vectors*. 5:282.

13. Pays E, Vanhamme L and Pérez-Morga D. (2004) Antigenic variation in Trypanosoma brucei: facts, challenges and mysteries. *Curr Opin Microbiol*. (4):369-74.

14. Tiengwe C, Muratore KA and Bangs JD. (2016) Surface proteins, ERAD and antigenic variation in Trypanosoma brucei. *Cell Microbiol*. 18(11):1673-1688.

15. Song J, Baker N, Rothert M, Henke B, Jeacock L, Horn D and Beitz E. (2016) Pentamidine Is Not a Permeant but a Nanomolar Inhibitor of the Trypanosoma brucei Aquaglyceroporin-2. *PLoS Pathog.* 12(2):e1005436.

16. Munday JC, Eze AA, Baker N, Glover L, Clucas C, Aguinaga Andrés D, Natto MJ, Teka IA, McDonald J, Lee RS, Graf FE, Ludin P, Burchmore RJ, Turner CM, Tait A, MacLeod A, Mäser P, Barrett MP, Horn D and De Koning HP. (2014) Trypanosoma brucei aquaglyceroporin 2 is a high-affinity transporter for pentamidine and melaminophenyl arsenic drugs and the main genetic determinant of resistance to these drugs. *J Antimicrob Chemother*. 69(3):651-63.

17. De Koning HP (2001). Uptake of pentamidine in Trypanosoma brucei brucei is mediated by three distinct transporters: implications for cross-resistance with arsenicals. *Mol Pharmacol*. 59(3):586-92.

18. Delespaux V and de Koning HP. (2007) Drugs and drug resistance in African trypanosomiasis. *Drug Resist Updat*. 10(1-2):30-50.

19. Jacobs RT, Nare B and Phillips MA. (2011) State of the art in African trypanosome drug discovery. *Curr Top Med Chem.* 11(10):1255-74.

20. Ortiz D, Sanchez MA, Quecke P and Landfear SM. (2009) Two novel nucleobase/pentamidine transporters from Trypanosoma brucei. *Mol Biochem Parasitol*. 163(2):67-76.

21. Barrett MP, Boykin DW, Brun R and Tidwell RR. (2007) Human African trypanosomiasis: pharmacological re-engagement with a neglected disease. *Br J Pharmacol*. 152(8):1155-71.

22. Sanderson L, Dogruel M, Rodgers J, De Koning HP and Thomas SA. (2009) Pentamidine movement across the murine blood-brain and blood-cerebrospinal fluid barriers: effect of trypanosome infection, combination therapy, P-glycoprotein, and multidrug resistance-associated protein. *J Pharmacol Exp Ther*. 329(3):967-77.

23. Carter NS, Berger BJ and Fairlamb AH. (1995) Uptake of diamidine drugs by the P2 nucleoside transporter in melarsen-sensitive and -resistant Trypanosoma brucei brucei. *J Biol Chem*. 270(47):28153-7.

24. Matovu E, Stewart ML, Geiser F, Brun R, Mäser P, Wallace LJ, Burchmore RJ, Enyaru JC, Barrett MP, Kaminsky R, Seebeck T and de Koning HP. (2003) Mechanisms of arsenical and diamidine uptake and resistance in Trypanosoma brucei. *Eukaryot Cell*. 2(5):1003-8.

25. Bernhard SC, Nerima B, Mäser P and Brun R. (2007) Melarsoprol- and pentamidine-resistant Trypanosoma brucei rhodesiense populations and their cross-resistance. *Int J Parasitol*. 37(13):1443-8.

26. Bridges DJ, Gould MK, Nerima B, Mäser P, Burchmore RJ and de Koning HP. (2007) Loss of the high-affinity pentamidine transporter is responsible for high levels of cross-resistance between arsenical and diamidine drugs in African trypanosomes. *Mol Pharmacol*. 71(4):1098-108.

27. Alsford S, Eckert S, Baker N, Glover L, Flores AS, Leung KF, Turner DJ, Filed MC, Berriman M and Horn D. High-throughput decoding of anti-trypanosomal drug efficacy and resistance. *Nature.* 482(7384):232–236.

28. Baker N, Glover L, Munday JC, Aguinaga Andrés D, Barrett MP, de Koning HP and Horn D. (2012) Aquaglyceroporin 2 controls susceptibility to melarsoprol and pentamidine in African trypanosomes. *Proc Natl Acad Sci USA*. 109(27):10996-1001.

29. Uzcategui NL, Szallies A, Pavlovic-Djuranovic S, Palmada M, Figarella K, Boehmer C, Lang F, Beitz E and Duszenko M. (2004) Cloning, heterologous expression, and characterization of three aquaglyceroporins from Trypanosoma brucei. *J Biol Chem*. 279(41):42669-76.

30. Wille U, Schade B and Duszenko M. (1998) Characterization of glycerol uptake in bloodstream and procyclic forms of Trypanosoma brucei*. Eur J Biochem*. 256(1):245-50.

31. Bassarak B, Uzcátegui NL, Schönfeld C and Duszenko M. (2011) Functional characterization of three aquaglyceroporins from Trypanosoma brucei in osmoregulation and glycerol transport. *Cell Physiol Biochem.* 27(3-4):411-20.

32. Opoku-Temeng C and Sintim HO. (2016) Potent inhibition of cyclic diadenylate monophosphate cyclase by the antiparasitic drug, suramin. *Chem Commun (Camb).* 52 (19):3754-7.

33. Denise H and Barrett MP. (2001) Uptake and mode of action of drugs used against sleeping sickness. *Biochem Pharmacol*. 61(1):1-5.

34. Pyana Pati P, Van Reet N, Mumba Ngoyi D, Ngay Lukusa I, Karhemere Bin Shamamba S and Büscher P. (2014) Melarsoprol sensitivity profile of Trypanosoma brucei gambiense isolates from cured and relapsed sleeping sickness patients from the Democratic Republic of the Congo. *PLoS Negl Trop Dis.* 8(10):3212.

35. Raber G, Raber T, Raml R, Murko M, Magnes C and Francesconi KA. (2013) Determination of the trypanocidal drug melarsoprol and its conversion products in biological fluids with HPLC-ICPMS/ESMS. *Talanta*. 116:876-81.

36. Babokhov P, Sanyaolu AO, Oyibo WA, Fagbenro-Beyioku AF and Iriemenam NC. (2013) A current analysis of chemotherapy strategies for the treatment of human African trypanosomiasis. *Pathog Glob Health*. 107(5):242-52.

37. Baker N, de Koning HP, Mäser P and Horn D. (2013) Drug resistance in African trypanosomiasis: the melarsoprol and pentamidine story. *Trends Parasitol*. 29 (3):110-8.

38. Kennedy PG. (2012) An alternative form of melarsoprol in sleeping sickness. *Trends Parasitol*. 28(8):307-10.

39. Priotto G, Kasparian S, Mutombo W, Ngouama D, Ghorashian S, Arnold U, Ghabri S, Baudin E, Buard V, Kazadi-Kyanza S, Ilunga M, Mutangala W, Pohlig G, Schmid C, Karunakara U, Torreele E and Kande V. (2009) Nifurtimox-eflornithine combination therapy for second-stage African Trypanosoma brucei gambiense trypanosomiasis: a multicentre, randomised, phase III, non-inferiority trial. *Lancet.* 374(9683):56-64.

40. Vincent IM, Creek D, Watson DG, Kamleh MA, Woods DJ, Wong PE, Burchmore RJ and Barrett MP. (2010) A molecular mechanism for eflornithine resistance in African trypanosomes*. PLoS Pathog.* 6(11):1001204.

41. Wilkinson SR, Taylor MC, Horn D, Kelly JM and Cheeseman I. (2008) A mechanism for cross-resistance to nifurtimox and benznidazole in trypanosomes*. Proc Natl Acad Sci USA.* 105(13):5022-7.

42. Matthews KR. (2005) The developmental cell biology of Trypanosoma brucei. *J Cell Sci.* 118(Pt 2):283-90.

43. McKean PG. (2003) Coordination of cell cycle and cytokinesis in Trypanosoma brucei. *Curr Opin Microbiol*. 6(6):600-7.

44. Overath P and Engstler M. (2004) Endocytosis, membrane recycling and sorting of GPI-anchored proteins: Trypanosoma brucei as a model system. *Mol Microbiol*. 53(3):735-44.

45. Hammarton TC. (2007) Cell cycle regulation in Trypanosoma brucei. *Mol Biochem Parasitol*. 153(1):1-8.

46. De Silva Rodrigues JH, Stein J, Strauss M, Rivarola HW, Ueda-Nakamura T, Nakamura CV, and Duszenko M. (2016) Clomipramine kills Trypanosoma brucei by apoptosis. *Int J Med Microbiol*. 306(4):196-205.

47. Tibodeau JD, Benson LM, Isham CR, Owen WG and Bible KC. (2009) The anticancer agent chaetocin is a competitive substrate and inhibitor of thioredoxin reductase. *Antioxid Redox Signal.* 11(5):1097-106.

48. Lee YM, Lim JH, Yoon H, Chun YS and Park JW. (2011) Antihepatoma activity of chaetocin due to deregulated splicing of hypoxia-inducible factor 1α pre-mRNA in mice and in vitro. *Hepatology*. 53(1):171-80.

49. Jung HJ, Seo I, Casciello F, Jacquelin S, Lane SW, Suh SI, Suh MH, Lee JS and Baek WK. (2016) The anticancer effect of chaetocin is enhanced by inhibition of autophagy. *Cell Death Dis*. 7:2098.

50. Räz B, Iten M, Grether-Bühler Y, Kaminsky R and Brun R. (1997) The Alamar Blue assay to determine drug sensitivity of African trypanosomes (*T. b. rhodesiense* and *T. b. gambiense*) in vitro. *Acta Trop*. 68(2):139-47.

CHAPTER 3

MUTP: A Synthetic Phosphonium Salt with Potential Anticancer Activity

3.1 INTRODUCTION

3.1.1 Breast cancer

Nowadays in most people's mind there is no scarier diagnosis than that of cancer. Cancer is often thought of as an untreatable, unbearably painful disease with no cure. Cancer is undoubtedly a serious and potentially life-threatening illness. In particular breast cancer is the most common type of cancer in the world wide, especially in ladies after the age of 50.

3.1.1.1 Anatomy and physiology of the mammary gland

Mammary glands are exocrine glands, also classified as tube alveolar glands. They are present in males and females; however, they normally function in the latter gender only. The biological role of the mammary glands is to produce milk to nourish a newborn baby and to pass antibodies needed for baby's protection against infections (passive immunity) while the immature immune is initiating its function.

The normal breast (**Figure 1**) is internally composed of the following parts.

a. Lobes and lobules: It contains 15-20 lobes that radiated around the nipple. Each lobe contains 20-40 lobules

b. Glandular tissue: Glandular tissues are responsible for milk production and transportation which is composed of alveoli, ductules, lactiferous ducts and lactiferous sinuses.

c. Connective tissue: It supports the breast.

d. Blood: Nourishes the breast and supplies the nutrients.

e. Nerves: It makes the breast sensitive to touch.

f. Lymph node: Remove the waste products.

g. Adipose tissue: Protects from injury.

h. Areola: Pigmented area at the center of the breast.

i. Nipple: Protruding area at the center of each breast.

Milk production is regulated by different hormones. Stimulation of estrogen, a female sex hormone causes the development of glandular tissue in the female breast during puberty. Breast size increases in size because of the increased level of estrogen during the time of pregnancy due to the accumulation of adipose tissue. Another hormone important for the

implementation of the mammary gland function is the prolactin (PRL) and oxytocin. Prolactin from the anterior pituitary gland stimulates the production of milk in the glandular tissues while oxytocin causes the ejection of milk from the glands.
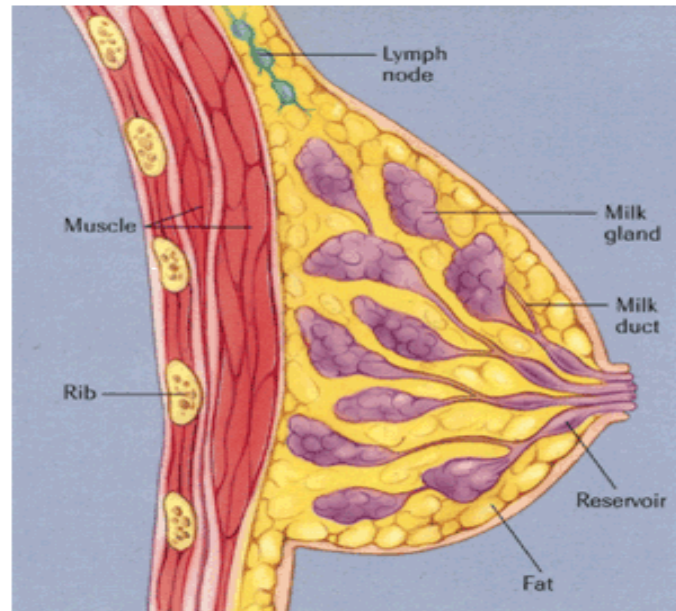
Figure 1. Structure of the normal breast.

3.1.1.2 Epidemiology

Breast cancer is the most diagnosed cancer in women in Italy (29% of all diagnosed cancers) and is the leading cause of cancer death. Indeed, breast cancer is ranks first in all age groups with 28% of deaths among young people, 21% among adult and finally 14% among women over the age of 70 years. However, by the late eighties it was detected a moderate and continuous downward trend in mortality from breast cancer, due to the greater development in diagnostic and therapeutic field. Recent data shows that approximately 12 % of women develop breast cancer. There were 231,840 new cases of breast cancer identified in the United States in 2015 [1].

The risk factors associated with breast cancer are:

- Age.
- Previous thoracic radiotherapy or previous breast diseases.
- Early starting of menstruation and late menopause.
- Having no child or having child after the age of 30 s.

- Lack of breast feeding.

- Lifestyle (obesity, low physical activity, high consumption of alcohol, carbohydrates and saturated fats).

- Hormone replacement therapy.

- Genetic factors and inheritance: Mutations in the BRCA-1 gene [Breast Cancer susceptibility gene 1] located on chromosome 17 and BRCA-2 gene [breast cancer susceptibility gene 2] located on chromosome 13 are responsible for two thirds of breast cancers. The gene expression products of BRCA-1 and BRCA-2 are two proteins that participate in cell repair response following DNA damage. Mutations in these genes can lead to altered expression of these proteins or protein expression with impaired functionality, thus predisposing the individual to cancer onset. Moreover, breast cancer risk in BRCA-1/2-mutation carriers is also influenced by environmental and lifestyle factors [2].

3.1.1.3 Classification of breast cancer

Based on the **histological classification**, the breast cancer is divided into four categories:

- **Epithelial**: Arising from epithelial cell and glandular lining of the inside of the ducts and lobules.

- **Fibroepithelial**: Consist of an epithelial component and from mesenchymal or stromal components.

- **Mesenchymal**: Pseudo tumoral or cancers that are not exclusively breast.

- **Miscellaneous**: Rare cancers, not grouped in previous classes.

If the disease has acquired the ability to invade the surrounding tissue and spread outside of the breast then it is classified as invasive carcinoma. The **figure 2** shows the steps in breast cancer development.
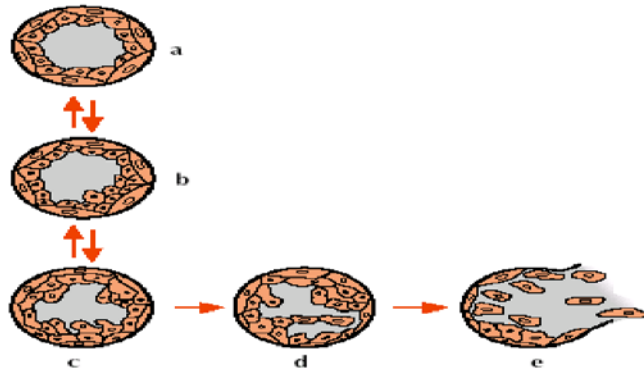
Figure 2. Steps involved in breast cancer development.

Breast cancer can be further classified according to the **classification system of TMN tumors**. The TNM system is the international system of classification of a tumor (staging), which takes account of its evolution. This classification takes into account three parameters:

- Size (**T** stands for tumor)
- Lymph node involvement (**N** stands for node)
- Whether the tumor has metastasized (**M** stands for metastasis)

The T (size) category describes the original (primary) tumor. **T1, T2, T3 and T4:** These numbers are based on the size of the tumor and the extent to which it has grown into neighboring breast tissue. The higher the T number, the larger the tumor and/or the more it may have grown into the breast tissue.

The N (lymph node involvement) category describes whether or not the cancer has reached nearby lymph nodes: **N1, N2 and N3:** These numbers are based on the number of lymph nodes involved and how much cancer is found in them. The higher the N number, the greater the extent of the lymph node involvement.

The M (metastasis) category tells whether or not there is evidence that the cancer has traveled to other parts of the body: **M1** means that distant metastasis is present.

The sum of the elements T, N and M can be associated with any form of cancer, in a particular stage. Indeed, there are four stages which are indicated by 0 to 4 [3]. **Figure 3** shows the different stages of breast cancer.
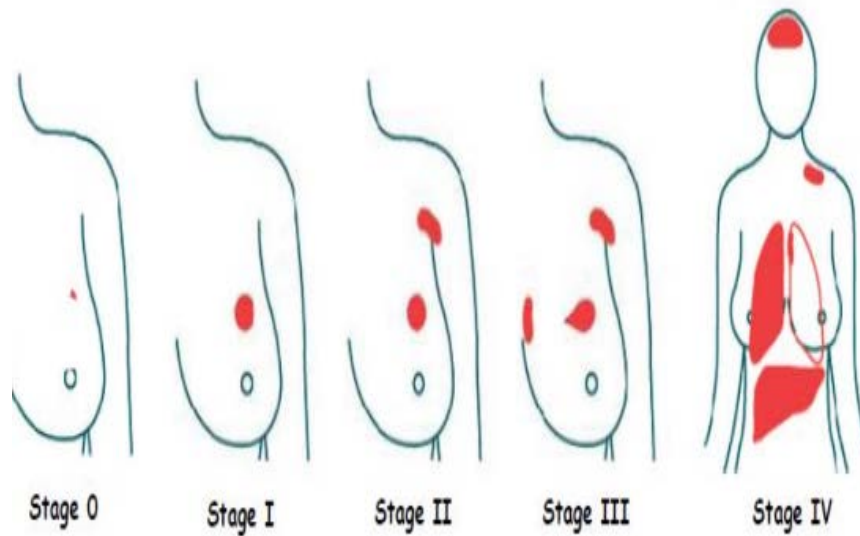
Figure 3. Stages of breast cancer.

In the last few years, the biological and molecular characterization of breast cancer has offered innovative elements with regard to the prognostic and therapeutic aspects. By using different molecular biology techniques now it is possible to perform a **molecular classification** (**Figure 4**), into five different subtypes based on the expression of some specific receptors.
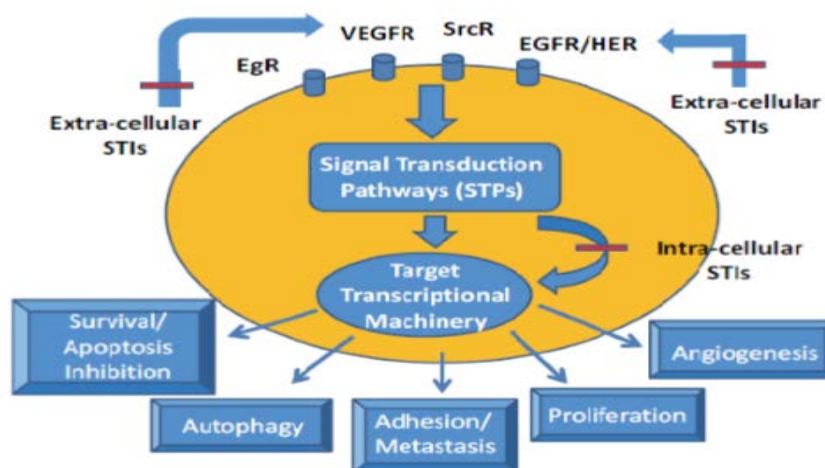
Figure 4. Principal Pathways involved in breast cancer.

- **Luminal A:** Cancers characterized by the presence of estrogen receptor (ER) and progesterone receptor (PR) with no HER2 (Human epidermal growth factor receptor) expression.
- **Luminal B**: Cancer characterized by the presence of hormonal receptors.
- **Luminal B (HER2) positive:** Neoplasm characterized by the presence of estrogen receptors and expression of HER2 receptors.
- **HER2 positive (non-luminal**): Neoplasm characterized by the presence of HER2 receptors but without the expression of hormonal receptors.
- **Basal like:** There is no presence of hormonal receptors or HER2 receptors.

The estrogen receptor (ER) and progesterone (PR), belong to the family of nuclear receptors and are able to regulate gene expression by interacting with specific DNA sequences localized at the level of the target genes. The activation of these intracellular receptors can take place with different mechanisms (**Figure 5**):

i. **Via ligand dependent**: In the absence of ligand, the receptor is sequestered in the nucleus of the target cells and is complexed with heat shock proteins (heat shock proteins, HSP) that keep the inactive conformation. Upon binding with specific ligand, the receptor undergoes a conformational change that causes detachment of HSP and facilitates dimerization and binding of the receptor to the response elements on DNA located on the target genes.

ii. **Via ligand independent**: The activation of the receptor may occur in the absence of ligand, as a result of receptor phosphorylation by kinases involved in different pathways of signal transduction, the activity of which is in turn stimulated by various types of substrates.
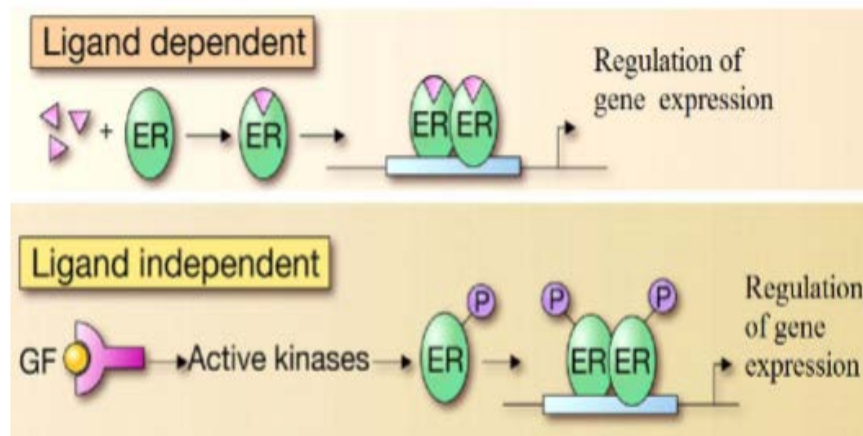
Figure 5. Mechanism of activation of estrogen receptor.

HER2 (Human Endothelial Factor Receptor) (**Figure 6**) belongs to the family of membrane receptors with tyrosine kinase activity, and in particular to the family of receptors for growth factors that includes ErbB1 (EGFR), ErbB3 (HER3), and ErbB4 (HER4). HER2 is not

able to bind to endogenous factors (orphan receptor), but form dimers with other family receptors, already linked with their specific ligands, stabilizing them and triggering the signal transduction pathways of kinase-mediated signal which regulate the processes of proliferation and cell differentiation.
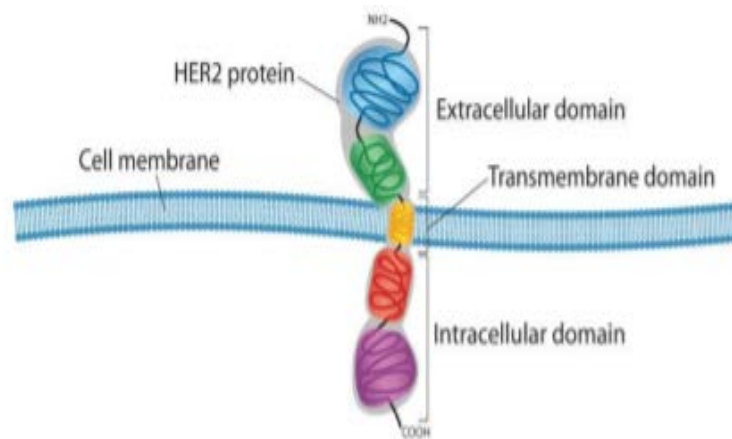
Figure 6. Structure of HER2 receptor.

3.1.1.4 Treatment

Taking into account the fact that the breast cancer can occur in several forms, the customization of therapy is the most demanding challenge. The choice of treatment must take into account several factors that greatly affect the response to treatment, such as the histological characteristics, molecular characteristics and tumor staging. The main therapeutic strategies consist of loco-regional treatments such as surgery and radiotherapy, and systemic pharmacological treatments, such as chemotherapy and monoclonal antibody therapy (immunotherapy). In surgery, two distinct types are in practice: radical and conservative surgery. The conservative surgery expected the removal of tumor nodule with a small portion of the surrounding healthy breast tissue or the removal of the entire breast quadrant affected by cancer.

3.1.1.5 Radiotherapy

Radiation therapy also called radiotherapy is a highly targeted and highly effective way to destroy cancer cells in the breast that may stick around after surgery. It uses the high energy radiation to kill cancer cells and prevent the growth. The main purpose of preoperative radiotherapy is to reduce the volume of the tumor and prevent the infiltration of surrounding

structures. Postoperative radiotherapy, or adjuvant, is instead adopted as a result of conservative surgery or treatments in order to reduce the risk of recurrence.

3.1.1.6 Chemotherapy

For the treatment of breast cancer, different chemotherapies are available either single or in combination with other therapies.

- Anthracyclines (Doxorubicin and Epirubicin): Anticancer drugs belonging to the class of cytotoxic antibiotics, whose antineoplastic action is due to their intercalation between the nitrogenous bases of DNA and inhibition of type II topoisomerases, mechanisms that bring instability and DNA damage with resulting induction of apoptosis.

- Taxanes (paclitaxel and docetaxel): Drugs that exert their anticancer action to stabilize microtubules, following the binding subunit of β-tubulin, and preventing their de polymerization.

- 5-fluorouracil: Drug belonging to the class of anti-metabolites of pyrimidine analogs. The antineoplastic effect is due to a threefold mechanism of action. The fluorodeoxyuridine monophosphate (FdUMP), the ribonucleotide that is generated by an enzyme from this analogue of uracil, inhibits thymidylate synthase, the enzyme responsible for synthesis of thymidine, interfering with DNA synthesis. Furthermore, the fluorouracil inhibits the enzyme uracil phosphatase preventing the use uracil in RNA synthesis, and, finally, is incorporated, for a small fraction, RNA, producing an abnormal RNA.

- Methotrexate: Drug that inhibits dihydrofolate reductase (DHFR), an enzyme that participates in the synthesis of tetrahydrofolate, necessary for the synthesis of thymidine and purine.

- Cyclophosphamide: A prodrug inactive until converted by P450-dependent hepatic oxidase in 4-Hydroxycyclofosfamide. The antineoplastic effect is due to the alkylating capacity of this metabolite active against of the nitrogenous bases of the DNA, and in particular of guanine.

- Platinum compounds (cisplatin and carboplatin): Drugs capable of binding to the nitrogen bases of nucleic acids, causing the formation of cross-links (cross-links) between the two filaments that form the double helix of DNA.

The side effects of chemotherapy depend on the fact that the cytotoxic action of these antineoplastic agents is not limited to cancer cells but also extends to healthy cells of actively proliferating tissues, such as the cells of the oral and intestinal mucosa, the cells of the bladder, embryonic cells and bone marrow precursors [4].

3.1.1.7 Immunotherapy

Immunotherapy is a therapeutic approach that is based on the use of monoclonal antibodies directed against specific molecular targets, and is a drug targeted therapy, which reduces the side effects of traditional chemotherapy. For the treatment of breast cancer, the most used are the monoclonal antibodies of Herceptin and Avastin. Herceptin is a recombinant humanized monoclonal antibody directed against the extracellular domain of the HER2 receptor. The binding of Herceptin with the receptor present on the tumor cell membrane determines a dual effect: in the first place prevents stimulation of the receptor, its dimerization and initiation of signal transduction pathways responsible for cell proliferation; also, it stimulates the immune response and antibody-dependent cell-mediated cytotoxicity. Herceptin therapy is well tolerated and the most common side effects usually occur in the first administration of the drug and are represented by flu-like symptoms.

Avastin is a humanized monoclonal antibody that binds to vascular endothelial growth factor, VEGF-A which is a mediator involved in the angiogenesis process that exerts its action by binding receptors VEGFR-1(Vascular endothelial growth factor receptor 1) and VEGFR-2. The binding of avastin to vascular endothelial growth factor does that itself less the interaction between VEGF-A and receptor and which has an inhibition of the angiogenesis process, necessary for the survival and the proliferation of cancerous cells and for the progression of the cancer. The treatment was well tolerated, with side effects consisting of hypertension, drowsiness, headache and nausea [5].

3.1.2 Cervical cancer

3.1.2.1 Symptoms and causes

The cervical cancer is a cancer arising from the cervix part of the human body (**Figure 7**). The cervix is the lower part of the uterus that opens into the vagina. No symptoms are seen in the early stages of diseases. Later symptoms may include abnormal vaginal bleeding and pelvic pain. Symptoms of very advanced cervical cancer may include: loss of appetite,

weight loss, fatigue, pelvic pain, back pain, leg pain, swollen legs, heavy vaginal bleeding, bone fractures, and (rarely) leakage of urine or feces from the vagina. In advanced disease, metastases may be present in the abdomen, lungs, or elsewhere. Human papillomavirus (HPV) infection appears to be involved in the development of more than 90% of cases [6]. Other risk factors include smoking, a weak immune system, birth control pills, smoking etc. Cervical cancer typically develops from precancerous changes over 10 to 20 years. About 90% of cervical cancer cases are squamous cell carcinomas, 10% are adenocarcinoma, and a small number are other types.
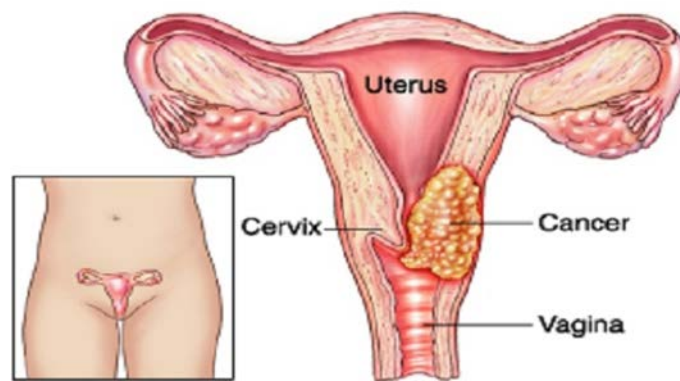
Figure 7. Illustration of cervical cancer.

3.1.2.2 Diagnosis

Diagnosis is typically by cervical screening followed by a biopsy. Pap test is also using to detect the changes in the pancreatic tissue. Medical imaging is then done to determine whether or not the cancer has spread. Confirmation of the diagnosis of cervical cancer or pre-cancer requires a biopsy of the cervix. Further diagnostic and treatment procedures are loop electrical excision procedure and conization, in which the inner lining of the cervix is removed to be examined pathologically. These are carried out if the biopsy confirms severe cervical intraepithelial neoplasia.

3.1.2.3 Epidemiology

Worldwide, cervical cancer is both the fourth-most common cause of cancer and the fourth-most common cause of death from cancer in women. About 70% of cervical cancers occur in developing countries. In medical research, the most famous cell line known as HeLa.

Cancer cervix occupies either the top rank or second among cancers in women in the developing countries, whereas in the affluent countries, cancer cervix does not even find a place in the top 5 leading cancers in women [7]. In the United States, an estimated 12,900 new cervical cancers and 4,100 cervical cancer deaths will occur in 2015. In the European Union, about 34,000 new cases per year and over 16,000 deaths due to cervical cancer occurred in 2014. Though squamous cell carcinoma posses more incidence, adenocarcinoma is also increasing recently [8].

3.1.2.4 Staging

Cervical cancer is staged by the International Federation of Gynecology and Obstetrics (FIGO) staging system, which is based on clinical examination, taking account both its evolution and the three parameters (T, L, and M), estimated in breast cancer.

3.1.2.5 Treatment

The main therapeutic strategies consist of loco-regional treatments such as surgery and radiotherapy, and systemic pharmacological treatments, such as chemotherapy and monoclonal antibody therapy (immunotherapy).

3.1.2.6 Surgery

Different types of surgical procedures may be used;

- **Radical hysterectomy**: Surgery to remove the uterus, cervix, ovaries and part of the vagina.

- **Radical trachelectomy**: Surgery to remove the cervix and the upper part of the vagina. The uterus and ovaries are not removed.

3.1.2.7 Chemotherapy and Immunotherapy

The same chemotherapeutic and immunotherapeutic agents, used for breast cancer treatment, are available for the cervical cancer. Avastin is the main monoclonal antibody utilized.

3.1.3 Structure and chemical synthesis of phosphonium salts

Phosphonium salts are salts containing a phosphonium (PH_4^+) ion and it refers to a quaternary organic derivative such as Tetraphenyl phosphonium chloride, $(C_6H_5)_4P^+$ Cl^- and

Tetra methyl phosphonium iodide [P(CH$_3$)$_4$]$^+$I$^-$ etc. The phosphonium salts present as a cation, a tetravalent phosphorus which bears a partial positive charge and defined as phosphonium ion. It is generally coordinated halide ions such Cl-, Br- and I-.
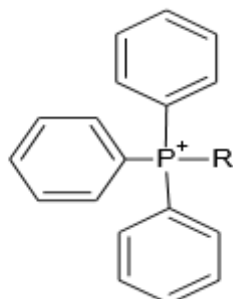
Figure 8. General molecular structure of phosphonium salts.

Alkyl triphenyl phosphonium salts are widely used for the preparation of reagents used in the Wittig reaction. Such salts are readily made by the reaction of triphenyl phosphine with an alkyl halide as shown in **figure 9**.
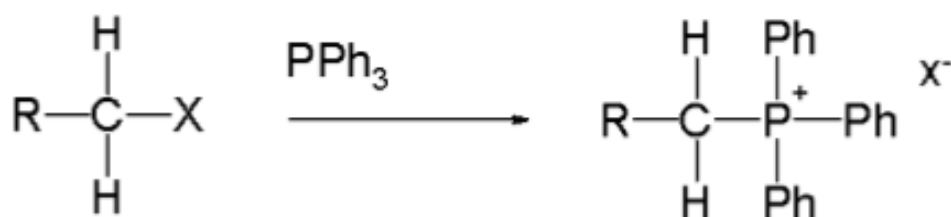
Figure 9. Preparation of phosphonium salts. (Ph: Phenyl, X: Alkyl)

The phosphonium salt is a stable compound which can often be purified by re-crystallization from ethanol.

3.1.4 Phosphonium salts

Phosphonium salts have wide range of applications in the area of Chemistry, Biology and Pharmacology. Phosphonium salts are a class of lipophilic cationic molecules that accumulate preferentially in mitochondria and inhibit the growth of human and rodent carcinoma cells in vitro and in animal models. They are promising potential anticancer agents for their interesting biological properties and easy synthesis of analogues [9]. Recently many

literatures described about the promising anticancer activity in cell and animal based systems. As pharmacological agents, phosphonium salts demonstrated antiglycemic properties in animal models, anti-proliferative activity in vitro and in vivo models and anti-microbial activity against Gram -ve, Gram +ve bacteria and parasite *T. cruzi* [10-12]. Phosphonium salts are promising anticancer agents, in the diagnosis and treatment, due their selective accumulation in the carcinoma cells. Indeed, several reports evidenced the selective cytotoxicity of cationic lipophilic compounds against cancer cells, compared to normal cells [13-18] and their mitochondrial localization [19]. Interestingly phosphonium salts have been reported to show anti-proliferative activity in several cancer cell lines and in xenograft model of ovarian cancer based on their ability to disrupt mitochondrial membrane ultrastructure and the lipid content [20-22]. Mitochondrial localization of this compound had been used to develop probes for mitochondrial function, also [23]. It has been shown that the different anti-proliferative effect is due to characteristic elevated plasma membrane potentials of neoplastic cells [24-26]. Even though the reasons are not fully understood, it's believed that carcinoma cells have a higher membrane potential than that of normal cells [27, 28]. The mechanism by which the phosphonium salts are able to cross plasma membranes are described [29, 30]. Charged molecules are generally unable to traverse cell membrane without the use of a transporter proteins due to the large amount of activation energies needed to remove associated water molecules. The distribution of charge across the large lipophilic surface of the phosphonium ion significantly lowers the energy requirement facilitating passage across lipid membranes.

Traditional chemotherapies achieved limited success in the treatment of carcinomas, due to their lack of specificity for tumorigenic cells. It is important, therefore, to discover anticancer agents for selective tumor cell killing. The special trait of the phosphonium salts can be exploited to allow selective delivery to tumor cells while sparing normal cells for both imagining and treatment purpose.

Recent studies showed that a phosphonium salt, namely TP-187, displayed low IC 50 value in different cell lines, related to an arrest in different phases of cell cycle. In particular, after TP-187 treatment, an arrest in the S phase of cell cycle was detected, in p53 mutant cell line (MDA-MB-435). The mechanism of action of this compound was further characterized "in vitro" evidencing mitochondrial localization, decreased oxygen consumption, increased production of superoxide radicals and inhibition of components involved in oxidative

phosphorylation mechanism [31, 32]. Moreover, in xenograft model of mice, TP-187 activates the caspase dependent mitochondrial apoptosis pathway [25].

The aim of the present study was to investigate the effects of lipophilic phosphonium salt, (11-methoxy, 11-oxoundecyl)triphenylphosphonium bromide (MUTP) as well as of two new phosphine oxide salts, 3,3'-(methylphosphoryl)dibenzenaminium chloride and 3,3'-(phenylphosphoryl)dibenzenaminium chloride (SBAMPO and SBAPPO) (**Figure 11, 12**) on the proliferation of two human cancer cell lines, MCF-7 and human uterine cervix adenocarcinoma (HeLa) cells. We compared these results with an chemotherapeutic agent, 5-fluorouracil (5-FU), and with the commercial analogue phosphonium salt, tetraphenylphosphonium bromide (TPP) (*Fig.10*)
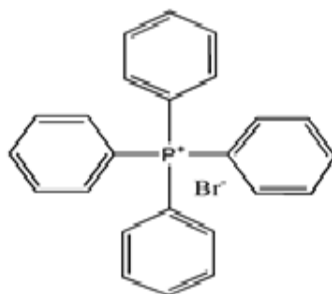
Figure 10. Structure of tetra phenyl phosphonium bromide (TPP)**.**
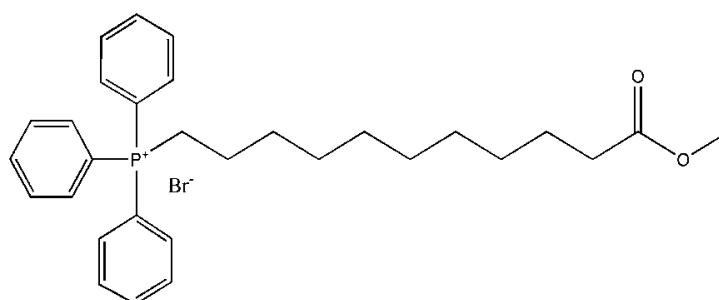
Figure 11. Structure of 11-Methoxy-11-Oxoundecyl-Triphenyl-Phosphonium Bromide (MUTP).
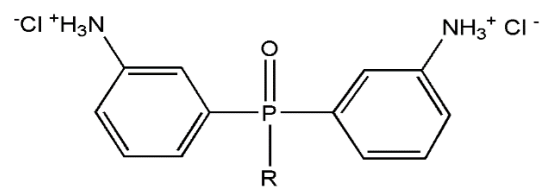
R = - CH$_3$ **sBAMPO**
R = - Ph   **sBAPPO**

Figure 12. Structure of Bis(3-aminophenyl)-methyl-phosphine oxide chloride (sBAMPO) and Bis(3-aminophenyl)-phenyl phospine oxide chloride (sBAPPO).

3.2 MATERIALS AND METHODS

3.2.1 Cell culture

The following cell lines were used in this study,

- **MCF-7**: Human breast cancer cellular line that expresses the estrogen receptor ERα (ER

  +) were obtained from the American Type Culture Collection (ATCC), Manassas, VA, USA and maintained in monolayer cultures in Dulbecco's Modified Eagle's Medium/Nutrient Mixture F-12 Ham (DMEM/F12) and supplemented with 10% Fetal bovine serum(FBS), 1% glutamine, 2% penicillin/streptomycin [33].

- **HeLa**: Human uterine cervix adenocarcinoma (HeLa) cells were obtained from the American Type Culture Collection (ATCC) (Manassas, VA). The cells were maintained in MEM medium containing 10% FBS, 1% L-glutamine, 1% Eagle's non-essential amino acids and 1% penicillin-streptomycin.

- **MCF-10A**: Human mammary epithelial cells, obtained from American Type Culture Collection (ATCC, Manassas, VA, USA), were maintained in DMEM-F12 supplemented with 10% horse serum (HS), 1% glutamine, 1% penicillin/streptomycin, 0.5 mg/ml hydrocortisone, 20 ng/ml HEGF (human epidermal growth factor) and 0.1 mg/ml cholera enterotoxin (Sigma–Aldrich, Milano, Italy) (complete medium).

All the cell lines were cultured at 37°C in 5% CO_2 in a humidified atmosphere. All salts tested were dissolved in dimethyl sulfoxide (DMSO) (Sigma, St. Louis, Missouri, USA) and diluted in appropriate medium supplemented with 2% DCC-FBS (dextran-coated charcoal-treated newborn calf serum serum) to obtain the working concentration. Each experiment was performed using multi-well plates in which the cells were plated in a defined quantity, after trypsinization. The treatments were carried out in DMEM/F12 w/o phenol red containing 2% NCS

3.2.2 Synthesis of sBAMPO and sBAPPO

Bis-(3-aminophenyl)-methyl-phosphine-oxide **(1)** (BAMPO) and Bis-(3-aminophenyl)-phenyl-phosphine-oxide **(2)** (BAPPO) were synthesized as reported in the literature [34]. A diethyl ether solution of **1** or **2** respectively was treated with a solution of hydrogen chloride

(1M in diethyl ether) to precipitate the product hydrochloride salt as a powder. The salt was collected by filtration and washed with diethyl ether.

3.2.3 Characterization of sBAMPO and sBAPPO

sBAMPO

^{1}H-NMR(400 MHz, DMSO-d6, ppm): 7.63-7.43 (m, 8H), 2.06 (d, 3H)
^{31}P NMR (161.97 MHz, DMSO-d6, ppm) 32.1 (s)
BAMPO **1**: ^{31}P NMR (161.97 MHz, DMSO-d6, ppm) 33.6 (s)

sBAPPO

^{1}H-NMR(300 MHz, DMSO-d6, ppm): 7.57 (m, 6H) 7.39 (s, 2H) 7.27-7.09 (m, 5H)
^{31}P NMR: (161.97 MHz, DMSO-d6, ppm) 30.9 (s)
BAPPO **2**: ^{31}P NMR :(161.97 MHz, DMSO-d6, ppm) 32.2 (s)

3.2.4 Trypsinization

Trypsinization is the technique used to detach the adherent cells from the bottom of the maintenance plate. The culture medium is aspirated from the plate and are were carried out three washes with phosphate buffered saline (PBS) in order to remove serum residue. After that add the trypsin, a proteolytic enzyme which facilitates the detachment of the cells from the substrate to which they are immobilized. The plate then left a few minutes in the incubator until the cells begin to detach. Then, the cells are re-suspended in medium containing serum to neutralize the trypsin, counted and used appropriately.

3.2.5 Cell counting

The cell count is based on the exclusion of Trypan Blue dye by viable cells, unlike the dead cells, possessing an intact cytoplasmic membrane, do not allow its penetration into the cytoplasm. A portion of the cell suspension, obtained after trypsinization, is suitably diluted in the dye, and this dilution is loaded in the Burker chamber, to allow the microscopic counting of cells. The number of cells/ml was calculated using the equation:

Avg. # of cells counted / # of squares*dilution factor*factor of the counting chamber (10^{4})

3.2.6 Cell viability assay (MTT assay)

Cell viability was determined by using the 3-(4,5-dimethylthiazol-2-y1)-2,diphenyl tetrazolium (MTT, Sigma) assay, as previously described [33, 35-37]. The MTT-assay is a cell proliferation assay, which allows to evaluate the viability of cultured cells. It is based on the ability of viable cells to reduce MTT to its corresponding insoluble form formazan catalysed by mitochondrial reductase (**Figure 13**).
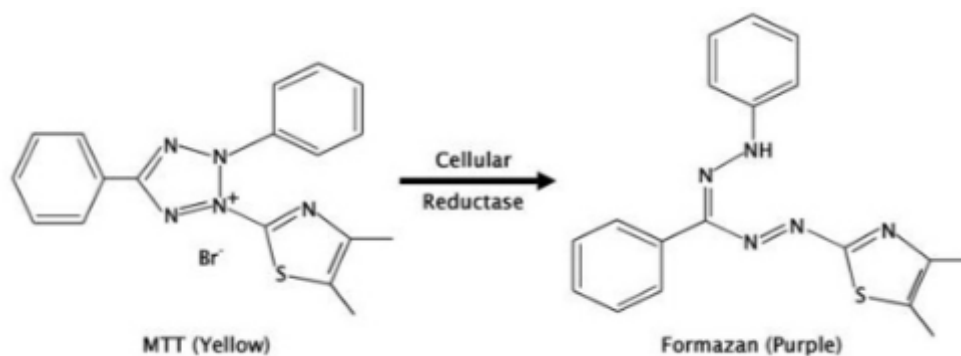
Figure 13. Reduction of MTT to corresponding formazan.

Briefly, Mcf-7, HeLa and Mcf-10A cells (3×10^4 cells/ well) were seeded in a 24-well plate and cultured in complete medium overnight. Before treatment, the culture medium was switched to DMEM F-12 or MEM supplemented with 2% charcoal-stripped (CS) FBS and cells were untreated or treated with different concentrations of MUTP. DMSO (Sigma-Aldrich) was used as the vehicle control. After 72 hours, the fresh MTT reagent 100µL (final concentration 2 mg/mL) was added and incubation was continued for 2 h. The metabolically active cells convert MTT, yellow, insoluble formazan in color, purple. The medium is aspirated from each well, and the formazan crystals present within the cells are solubilized with 500 µL of dimethyl sulfoxide (DMSO). The intensity of the staining solution of the formazan is directly proportional to the number of viable cells, and measured in a spectrophotometer at a wavelength of 570 nM. A minimum of three experiments, containing 5 different doses of phosphonium salts and 5-fluorouracil in triplicate was combined for IC_{50} calculations. The absorbance readings were used to determine the IC_{50} using Graph Pad Prism 6 Software (Graph Pad Inc., San Diego, CA). Briefly, values were log-transformed, normalized, and nonlinear regression analysis was used to generate a sigmoidal dose-response curve to calculate IC_{50} values for each cell line [38].

3.2.7 Cell cycle analysis

This is a method used in order to distinguish cells in different phases of the cell cycle, by flow cytometry. Before the analysis, the cells were permeabilized and treated with fluorescent dye that can quantitatively stain the DNA, propidium iodide. The fluorescence intensity of the stained cells at certain wavelengths will therefore correlate with the amount of DNA they contain. As the DNA content of cells duplicates during the S phase of the cell cycle, the fluorescence will be higher in S phase. MCF 7 cells were plated, non-treated and treated with 0.5 µM and 2 µM MUTP for 24 hours and 72 hours. After the treatment, the cells were trypsinized, collected and centrifuged at 2000 rpm for 5 minutes. Then, the supernatant was removed and the pellet washed 2 times with PBS and centrifuged at the same rpm for 5 minutes. The supernatant was removed and in the pellet added 500 µL of a solution consisting of: sodiumcitrate (0.1% in distilled H20) and propidium iodide (50 ug / ml). For each tube was, then, added 10 µL of RNase (0.5 g / ml) and 6.25 µL of IGEPAL (0.1%). The tubes were agitated by vortexing and incubated in the dark at 37 ° C for one hour. Then, the samples were read for cytometric analysis. At least $2x10^4$ cells/sample were measured. FACS analysis was performed using Mod Fit LT software (Becton Dickinson, NJ). The experiment was repeated three times.

3.2.8 Preparation of total protein extract

Cells were plated in well multi- well plates in complete culture medium and treated with the compounds. The lysis was started by addiction of lysis buffer (50 mM (4-(2-hydroxyethyl)-1-piperazineethanesulfonic acid (HEPES) pH 7.5, 150 mM sodium chloride (NaCl), 1.5 mM magnesium chloride (MgCl2), 1 mM Ethylene glycol tetra acetic acid (EGTA), 10% glycerol, Triton-X-100 1%, Phenylmethane sulfonyl fluoride (PMSF) 1 mM, 0.2 mM aprotinin, Na ortovanadate 0.2 mM) into each of the well. The lysis buffer distributed uniformly in the well disrupt the cell membranes, allowing the recovery of cellular protein content. The protease activity was inhibited by PMSF, aprotinin and sodium orthovanadate, protease inhibitors added in the lysis buffer. After 5 minutes the cell was scraped, collected, transferred to an Eppendorf tube and kept it in ice for 30 minutes, vortexing every 5 minutes. The content of each Eppendorf was then centrifuged at 14000 rpm for 10 minutes, at 4°C.

The pellet was formed from cell membranes, while the supernatant, the soluble protein extract, was transferred to new Eppendorf and kept at -80°C.

3.2.9 Determination of protein concentration

The total protein concentration was quantified by using spectrophotometric method of Bradford. The absorbance was read by spectrophotometer at a wave length of 595nm.

3.2.10 Electrophoresis of protein under denaturing condition (SDS-PAGE)

The total protein concentration was quantified by using spectrophotometric method of Bradford. The absorbance was read by spectrophotometer at a wave length of 595nm. 25 µg of protein from each sample, was separated by electrophoresis on SDS-polyacrylamide gels.

Prior to electrophoretic separation, the samples were added to Laemmli sample buffer (4% SDS, 20% glycerol, β-mercaptoethanol 10%, bromophenol blue 0.004%, Tris-HCl (0.125%) and brought to the same final volume by the addition of the same buffer used for the extraction of proteins. The protein contained in each sample were subjected to thermal denaturation treatment, at 100 ° C for 5 minutes. Simultaneously one well should be loaded with a marker of known molecular weights (Precision Plus Protein All Blue ™ Standards, Bio-Rad) essential for the identification of the protein of interest. The electrophoresis was carried out in a vertical apparatus for electrophoresis in the presence of a running buffer (25 mM Tris, 1.4% glycine, 0.1% SDS, pH 8.3), 100 volts for about 120 minutes. This operation allows separation of the proteins, negatively charged, as a function of their molecular weight [39]. The composition for preparing 15% stacking and resolving gel is given in **table 1**.

| Reagents | Stacking gel | Resolving gel |
	15%	15%
Water	2.160 mL	1.8 mL
AA/BIS AA (30/0.2)	500 µL	1.8 mL
TRIS/HCl (1.876 Mm)	300 µL	4.93 mL
SDS 10%	30 µL	83.33 µL
APS 10 %	15 µL	66 µL
TEMED	7 µL	7 µL

TRIS HCl, pH 6.8 for stacking gel and pH 8.8 for resolving gel.

Table 1. Composition of stacking gel and resolving gel.

3.2.11 Immunoblotting

The proteins separated on polyacrylamide gels are transferred by means of "electro-transfer" of a nitrocellulose membrane using a semi-dry transfer apparatus (BIORAD). The gel and the membrane are soaked in transfer buffer (Tris 20 mM, Glycine 150 mM, SDS 0.5% and methanol 20%). A "sandwich" is then set up the transfer apparatus, consisting of two sponges, nitrocellulose, gel, and two sponges. The transfer chamber is formed by two parallel electrodes and the nitrocellulose membrane must be placed between the gel and the anode. The transfer chamber with an electric current (25 volts is applied for 1 h) perpendicular to the gel, and negatively charged proteins migrate from the gel towards the positive pole, moving on nitrocellulose membrane. The quality of the transfer can be verified through the reversible staining of the membrane with Ponceau Red (1% solution of Ponceau Red in acetic acid at 5%). The membrane is bleached by washing with 1X TBST (Tris buffer saline - Tween: 0.1% Tween-20, Tris / HCl 10 mM and 100 mM NaCl).

3.2.12 Immunodetection

The nitrocellulose membrane was agitated for 60 minutes at room temperature in blocking solution, 10X solution of TBST (Tris / HCl, 100mM, 1M NaCl and 1% Tween-20) with the addition of milk powder to 5%. The function of the blocking solution is to block all of the hydrophobic sites present on the membrane, in order to reduce the non-specific interactions with the antibody. Subsequently, the membrane was rinsed three times, for five minutes,

with TBST 1X and is incubated overnight at 4 ° C with the solution of 1X TBST with 5% BSA contains the primary antibody specific for the protein of interest. The excess antibody is subsequently removed by three washes in 1X TBST, the next day. The antigen-antibody complexes are detected after incubation for one hour at room temperature with a specific secondary antibody (1X solution in TBST with 5% milk powder), able to recognize the constant portion of the IgG molecule used as primary antibody. The secondary antibody is conjugated with horseradish peroxidase, an enzyme capable of catalyzing, in basic conditions, the oxidation of a chemo luminescent substrate, Enhanced Chemiluminescence Substrate (ECL), in a product able to impress a photographic plate [39, 40].

Primary antibodies used:

- Antibody anti p53   Dilution (1:2000)

- Antibody anti p21 (SC-756)   Dilution (1:2000)

- Antibody anti-Bax   Dilution (1:2000)

- Antibody anti β-actine   Dilution (1:2000)

- Antibody total OXPHOS Dilution (1:500)

- Antibody Caspase 3 (1:2000)

- Antibody Caspase 9 (1:2000)

Secondary antibodies used:

- Antibody goat anti-rabbit IgG (Santa Cruz Biotechnology), Dilution 1:7000.

- Antibody goat anti-mouse IgG (Thermo Scientific), Dilution 1:5000.

3.2.13 Real time RT-PCR

Cells were grown in 10 cm dishes to 70% to 80% confluence and exposed to treatments with MUTP, 0.5 µM and 2 µM for 24 hours. Total cellular RNA was extracted using TRIZOL reagent (Invitrogen) as suggested by the manufacturer. The purity and integrity were checked spectroscopically and by gel electrophoresis before carrying out the analytical procedures. Analysis of p53 and p21 gene expression was performed by real time reverse transcription-PCR in the iCycler iQ Detection System (BioRad), using SYBR Green Universal PCR Master Mix (BioRad), following the manufacturer's recommendations. Each sample was normalized on its GAPDH content. Primers used for the amplification were: forward 5'-

TCAGTCTACCTCCCGCCATA-3' and reverse 5'-TTACATCTCCCAAACATCCCT-3' (p53); forward 5'-GCATGACAGATTTCTACCACTCC -3' and reverse 5'- AAGATGTAGAGCGGGCCTTT -3' (p21); forward 5'-CCCACTCCTCCACCTTTGAC-3' and reverse 5'-TGTTGCTGTAGCCAAATTCGTT-3' (GAPDH, house-keeping gene).

3.2.14 Mitochondrial staining

Mitochondrial activity was determined by Mito tracker Orange dye (M7510, Invitrogen) which was an orange fluorescent dye that stains mitochondria in live cells and its accumulation is dependent upon membrane potential. The dye is well-retained after aldehyde fixation. Mito Tracker Deep Red (M22426, Invitrogen), localizing inside the mitochondria irrespective of membrane potential, was used to assess mitochondrial mass as described by Fiorillo M, et al.[41]. Mcf-7 cells were treated with 4μM of MUTP for 48 hours. Vehicle alone (DMSO) control cells were processed in parallel. After 48 hours, cells were incubated with Mito Tracker staining solution (diluted in PBS/CM to a final concentration of 10 nM) for 30-60 minutes at 37°C. All subsequent steps were performed in the dark. Cells were washed in PBS, harvested and re-suspended in 300 μL of PBS/CM. Cells were then analyzed by Flow Cytometry using BD FACS Jazz™ Cell Sorter (Becton Dickinson and Co) [42].

3.2.15 Mitochondrial ROS production

Mitochondrial Reactive oxygen species (ROS) are ROS produced inside the mitochondria through oxidative phosphorylation. The effects of MUTP treatment on mitochondrial ROS production were examined as previously described in the paper [43]. Briefly, MCF-7 cells were treated with 4 μM MUTP for 24 hours. Vehicle-alone (DMSO) control cells were processed in parallel. At the end of treatment, cells were washed in PBS and incubated with CM-H$_2$DCFDA (diluted in PBS at a final concentration of 1 μM) for 20 minutes at 37°C. This step and all subsequent ones were performed in the dark to prevent the oxidation of the probe. The CM-H$_2$DCFDA is a cell-permeable probe that is non-fluorescent until oxidation occurs within the cells. After 20 minutes, cells were washed, harvested, re-suspended in 300 μL of PBS and analyzed by Flow Cytometry, using BD FACS Jazz™ Cell Sorter (Becton Dickinson and Co).

3.2.16 DNA Extraction

The cells were plated in 100 mm petri dishes in desired confluence. Treatment was carried out with two different concentration of MUTP. After 48 hours, the cells, immobilized on the bottom of the plate were detached by using trypsin, subsequently neutralized by the addition of plain medium. The cell suspensions were transferred into the tubes and centrifuged at 2500 rpm for 5 minutes. In each tube, 100µL of lysis buffer (Tris / HCl 50µM, 20nm EDTA, 1% NP-40) was added and it was left to act overnight at -80 ° C. The samples were subjected to centrifugation at 3000 rpm for 5 minutes and the supernatant removed. The proteins and the RNAses were denatured by addition of SDS and RNAse-A, respectively.

The lysates were incubated at 56 ° C for 2 hours, in order to leave all the residues of enzyme RNAase-A, at the same time inhibiting the activity of the DNAse, possibly present in the sample. Thereafter was added proteinase-K in order to degrade the proteins and the samples were incubated for 2 hours at 37°C.

Subsequently 500 µl of absolute ethanol and 65 µl of 3M sodium acetate were added in order to precipitate the DNA. After incubation at -80 ° C, overnight, it was proceeded to centrifuge samples for 20 minutes at 12000 rpm at 4 ° C. The supernatant was removed and the pellet, represented by the DNA precipitated, was washed with cold 75% ethanol to solubilize the precipitated salts and the DNA. Following centrifugation at 12000 rpm for 20 minutes at 4 ° C, the supernatant was removed and the pellets, the DNA, was suspended in 50 µl of TE-buffer (10 mM Tris-HCl, 1 mM EDTA, pH 8.0).

3.2.17 DNA electrophoresis on agarose gel

The agarose gel electrophoresis is a technique that allows to separate the DNA molecules according to their size, by exploiting their different migration speed through the agarose gel, subjected to an electric field. The agarose gel was prepared at the concentration of 2% in TBE buffer (Tris-borate-EDTA) with the addition of ethidium bromide, an intercalating agent that makes visible the DNA by fluorescence emission following exposure to the UV lamp. On the agarose gel, it was loaded a marker, consisting of a mixture of DNA fragments of known molecular weight, and the different samples mixed with a loading buffer, containing thickeners and dyes to facilitate the loading of samples and monitor the progress of the electrophoresis run.

3.2.18 TUNEL assay

Terminal deoxynucleotidyl transferase dUTP nick end labelling is an assay to evaluate apoptotic cells in population by measuring the DNA fragments that are formed. A hallmark of late apoptosis is extensive genomic DNA fragmentation that generates a multitude of DNA double-strand breaks (DSBs) with accessible 3'-hydroxyl (3'-OH) groups. This 3'-OH free terminal become the substrate for the recombinant enzyme terminal deoxynucleotidyl transferase (rTdT), which catalyzes the reaction of incorporation of fluorescein-12-deoxy-uridine-5' -triphosphate (fluorescein-12-dUTP) to the free 3'-OH. The fluorescein-12-dUTP linked to the DNA is displayed directly using a fluorescence microscope (**Figure 14**). The assay was performed by using the Click-iT® TUNEL Alexa Fluor® Imaging Assay (Invitrogen) according to the manufacturer's protocol. The Mcf-7 cells were plated in a 6 well plates incorporated with a coverslip on which the cells grow in their regular growth medium in a specific confluence. The cells were treated with desired concentrations of MUTP for a desired period of time. After, the wells were washed 3 times, with PBS. The cells were fixed with 4% paraformaldehyde solution in PBS for 15 minutes at room temperature and   washed 3 times with PBS. Later the cells were permeabilized with a solution 0.52% Triton X100, in PBS, for 4 minutes at room temperature and washed 3 times with PBS.

After that, 100µl of TdT reaction buffer were added to each coverslip. The cover slips were incubated for 10 minutes at room temperature. During the incubation time, it was prepared the TdT reaction cocktail, according to the instructions, in the kit. After incubation, the TdT reaction buffer was removed from the slides.

Then, 100 µl of TdT reaction cocktail was added to each coverslip and allowed the solution to spread all over the coverslip. The cover slips were incubated for 60 minutes at 37°C, in a humidified chamber to protect against evaporation. The coverslips were washed with BSA 3 % in PBS for 2 minutes. The Click-It reaction cocktail was prepared, according to the instruction provided in the kit, added (100 µl) to each coverslip and allowed the solution to spread completely over the surface. The slides were incubated for 30 minutes at room temperature in the dark. Then, the solution was removed and the slides washed with 3% BSA in 1x PBS, for 5 minutes. Next, DNA staining was conducted to analyze the nuclear morphology of the cells, after treatment. The Hoechst 33342 reagent was diluted in PBS, added (100 µl) on each cover slip and incubated for 15 minutes at room temperature, in the dark. The

solution was removed from the coverslip by washing well twice with PBS. The Cell nuclei were analyzed and photographed by using a fluorescent microscope (4×magnification). Images are representative of three separate experiments.
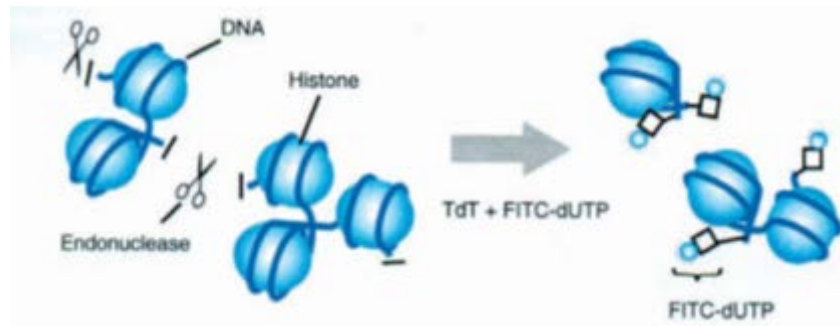
Figure 14. Mechanism by which the recombinant enzyme (terminal deoxynucleotidyl transferase) catalyzes the reaction of incorporation of fluorescein-12-dUTP at the free 3'OHT.

3.2.19 Statistical analysis

Data is represented as the mean ± standard deviation (S.D.), taken over ≥ 3 independent experiments, with ≥ 3 technical replicates per experiment, unless otherwise stated. Statistical significance was measured using the analysis of variance (ANOVA) or student t-test. p ≤ 0.05 was considered significant and all statistical tests were two-sided.

3.3   RESULTS AND DISCUSSION

3.3.1   MUTP elicits anti-proliferative effect on MCF-7 and HeLa cell lines

In order to investigate the effects on cancer cell proliferation of the aforementioned compounds, we have performed an MTT assay to assess their cytotoxic potential against two human cancer cell lines: the estrogen receptor-positive (ER+) human breast cancer cell line MCF-7, and human uterine cervix adenocarcinoma (HeLa) cells (**Figure 15** and **16**). The anti-proliferative effect was evaluated after a treatment period of three days. The absorbance read at 590nm. The compounds were solubilized in DMSO in 5 different concentrations (0.1, 0.5, 1, 5, 10 µM). The cells were also exposed to 5-fluorouracil (5-FU), in order to compare the compounds' anti-proliferative effects with the widely used anti-cancer drug. TPP is a novel phosphonium salts which is already proven to have the anticancer activity.
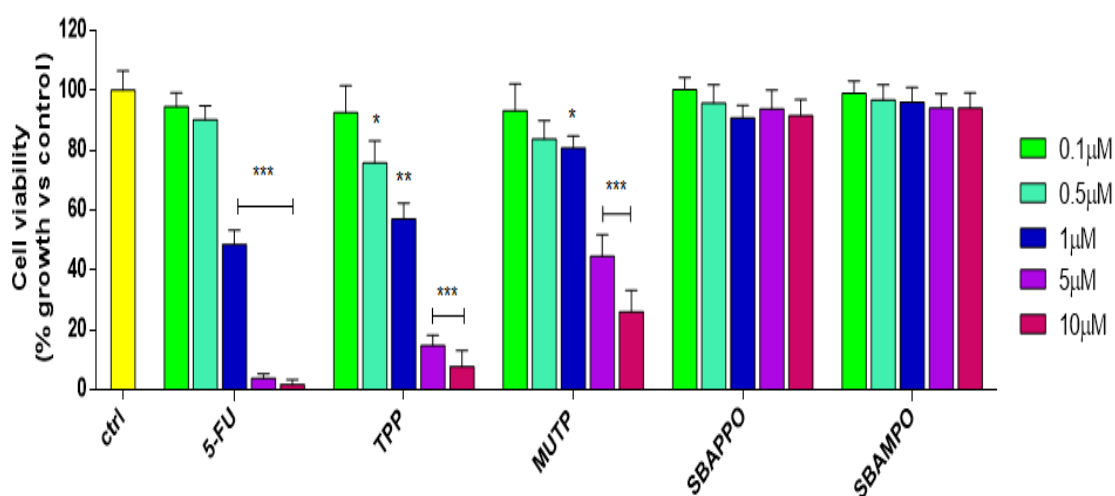
Figure 15. Effects induced by the treatment of different complexes on proliferation of anchorage dependent MCF-7 cancer cell lines.
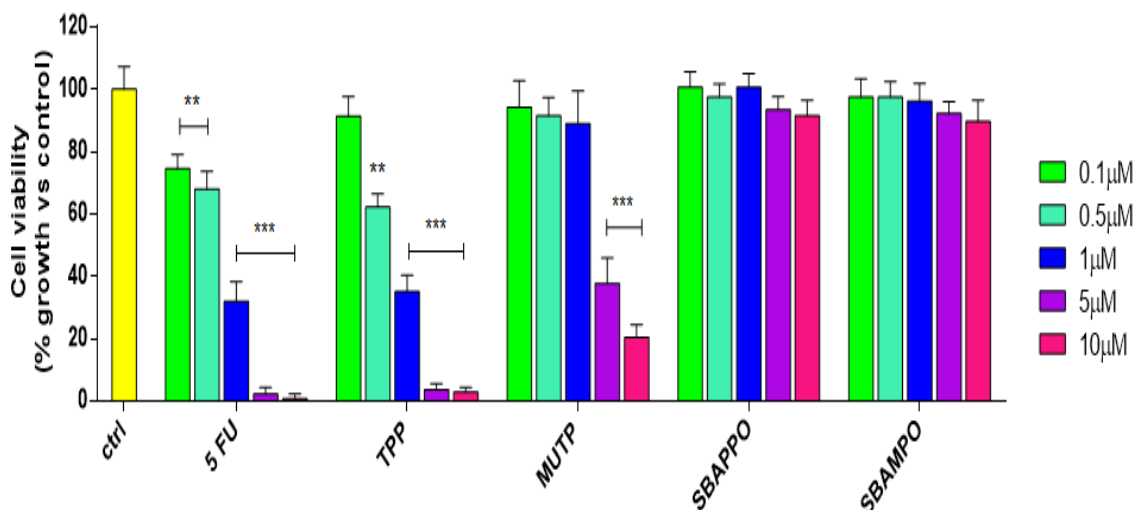
Figure 16. Effects induced by the treatement of complexes on HeLa cell lines.

Results showed that TPP and MUTP elicited anti-proliferative effects on both cancer cell lines. According to prevoius studies carried out on anti-proliferative activity of TPP [21], we observed that TPP reduced MCF-7 and HeLa cell viability on a dose dependent manner (**Figure 15** and **16**) with IC50 values equal to 1.25 and 0.65 µM, respectively (**Table 2**). Moreover, on both cell lines, TPP showed similar cytotoxic activity to 5-FU, whose IC50 values were found to be 1.16 and 0.58 µM, respectively (**Table 2**). MUTP showed an inhibitory effect on a dose dependent manner in both cell lines (**Figure 15** and **16**). SBAMPO and SBAPPO treatments showed no inhibitory effects on both cell lines (**Figure 15** and **16**).

In order to evaluate the toxicity of these compounds on normal cellular line, subsequently we have treated the compounds against normal breast glandular epithelial cell lines, MCF-10 A (**Figure 17**). The results obtained have shown that MUTP did not induce any anti-proliferative effects on this cell lines and 10 µM concentration showed a slight inhibitory effect. Also, we observed that treatment with 5-FU showed a significant inhibitory effect on MCF-10 A cell lines at 1, 5 and 10 µM.
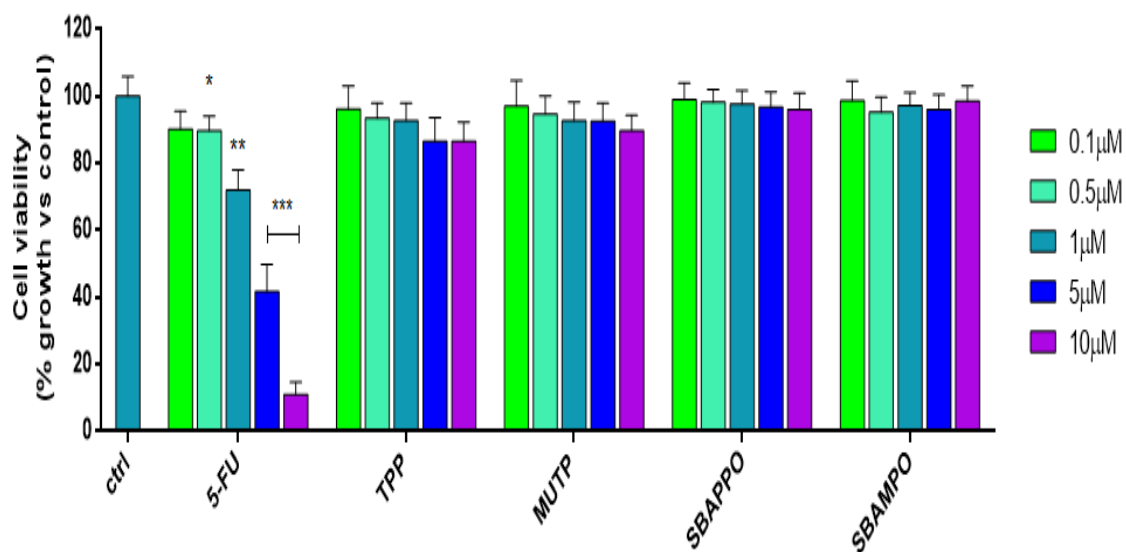
Figure 17. Effects induced by the treatment of complexes on MCF-10 A cell lines.

Compounds	MCF-7		HeLa		MCF-10A	
	IC-50 (µM)	95% confidence intervels	IC-50 (µM)	95% confidence intervels	IC-50 (µM)	95% confidence intervels
5-FU	1.16	0.81 to 1.66	0.58	0.43 to 0.77	2.72	2.14 to 3.45
TPP	1.25	1.04 to 1.51	0.65	0.53 to 0.77	48.34	31.07 to 75.21
MUTP	3.71	3.06 to 4.51	3.59	2.762 to 4.67	>50	>50
SBAMPO	>50	>50	>50	>50	>50	>50
SBAPPO	>50	>50	>50	>50	>50	>50

Table 2. IC 50 value of 5-fluorouracil, TPP, MUTP, sBAMPO and sBAPPO for MCF-7, HeLa and MCF-10A cells.

The results obtained showed that MUTP did not induce anti-proliferative effects on this cell line; 10 µM MUTP elicited a slight inhibitory effect. Therefore, conversely to the 5-FU treatment, the two phosphonium salts tested showed specific anti-proliferative, effect on MCF-7 breast cancer cells, revealing a higher IC50 value than 5-FU on non-tumorigenic MCF-

10A cells line (**Table 2**). Note that, as reported in Table 2, MUTP displayed an IC50 value > 50 μM.

3.3.2 MUTP-induced cell cycle arrest at G1 phase of MCF-7 cells

Previous study showed that MUTP analogue (TPP) showed a cell cycle arrest at G2/M phase [28]. The biological responses elicited by MUTP in MCF-7 cell, prompted us to investigate whether MUTP treatment could affect the MCF-7 cell cycle progression. Therefore, we evaluated the distribution of cells within the three major phases of the cycle, analyzing by PI staining with FACS. MCF-7 cells were treated with either vehicle (DMSO) or two different concentrations of MUTP (0.5 and 2 μM) for 24 h (**Figure 19A**) or 72 h (**Figure 19B**) and analyzed.
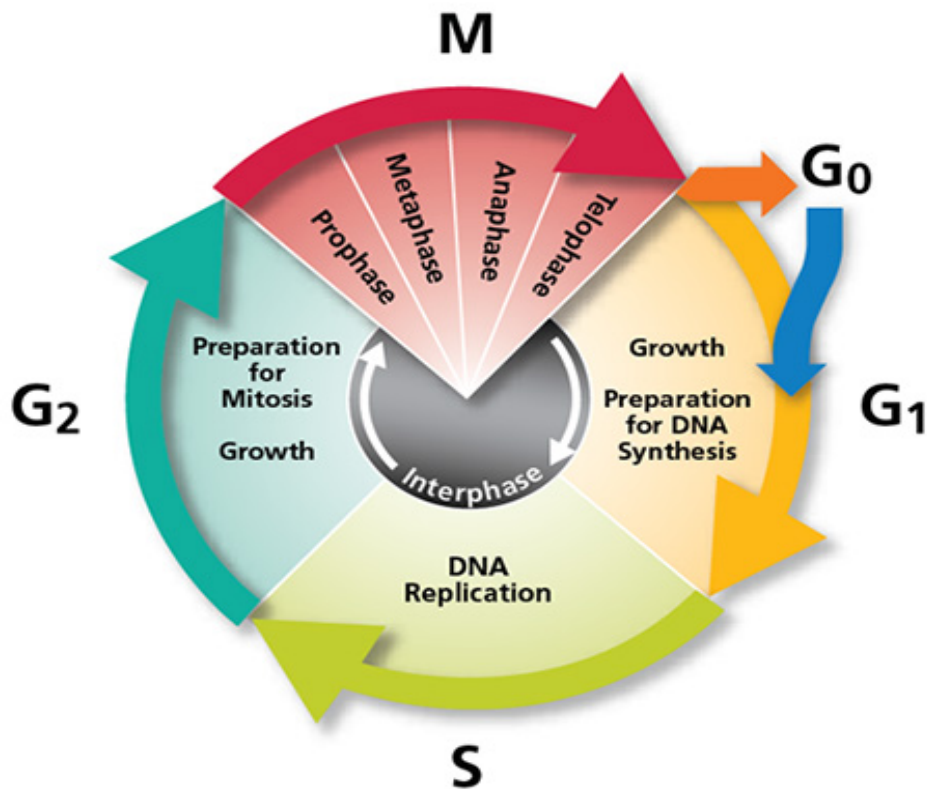
Figure 18. Different phases in a eukaryotic cell cycle.

The molecular events that control the cell cycle are ordered and directional: each process is a direct result of the previous event and is the cause of the next. It is characterized by the following stages, G1 phase, S phase, G2 phase and M, which are schematically summarized in **figure 18**. There is also a further extra cyclic phase which is indicated by G0,

during which the cells are temporarily in a state of quiescence. Using propidium iodide, it is possible to assess the cell cycle of a cell. Propidium iodide (3,8-diamino-5 dietilmetilamminopropil- 6 fenilfenantridin diiodide) (PI) is a synthetic dye characterized by a low fluorescence (red-orange), able to bind selectively to nucleic acids. The PI binding stoichiometrically to double-stranded DNA provides information on the amount of DNA contained in cells; in relation to the intensity of fluorescence. It is well known that the DNA content varies depending on the stage of the cycle in which the cell is located. In particular, the cells have a double amount of DNA in G2 and S phase when compared to that of the G1 phase. While during the period of DNA synthesis (S phase), the amount of DNA appears to be intermediate between the content in the G1 and G2 phase. Thus the assessment of the amount of DNA can be traced back to the percentage of cells in different cell cycle phases: G0 / G1, S and G2 / M [44, 45].
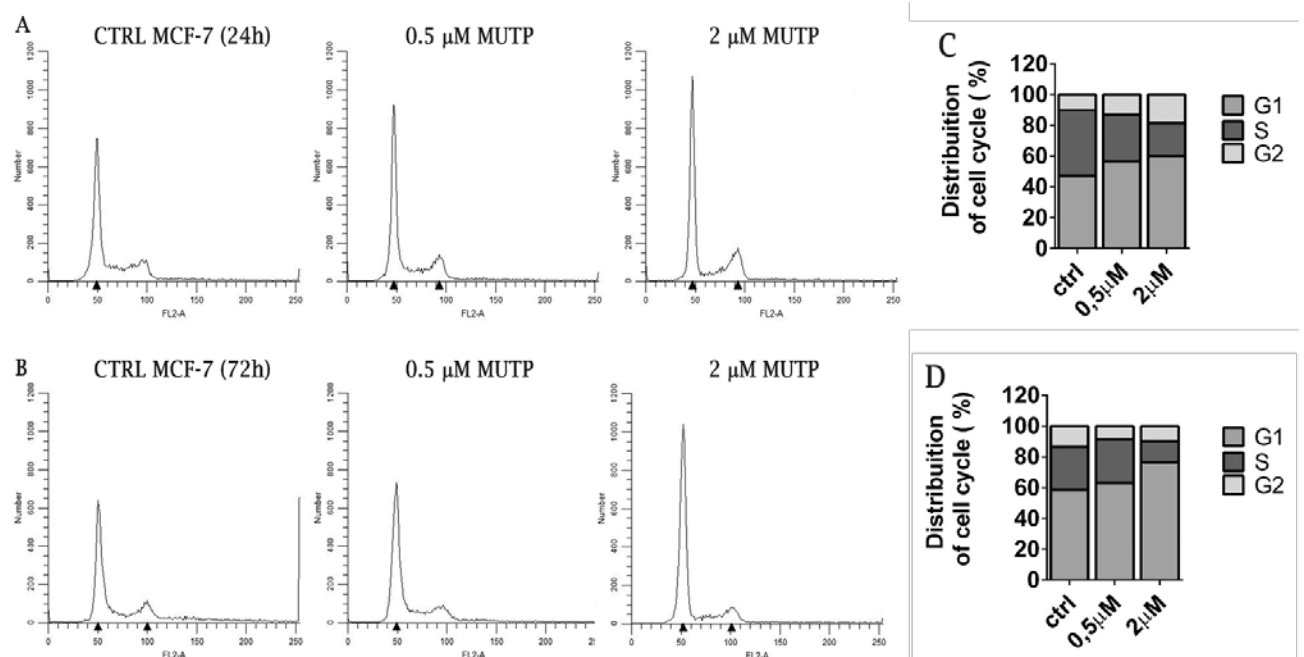
FIGURE 19: MUTP impairs G1/S transition of MCF-7 breast cancer cells. Exponentially growing MCF-7 cells were treated either with DMSO (Ctrl) or two different concentrations of MUTP (0.5 and 2 µM). After 24h **(A)** or 72h **(B)**, the cells were stained with Propidium Iodide (see Material and Methods), and analyzed by FACS. The graph shows the distribution MCF-7 cell population (%) in the various phases of cell-cycle. Quantitative analysis of percentage gated cells at G0/G1, S and G2/M phases, after 24h **(C)** and 72h **(D)** of treatment, were shown.

The results revealed that MUTP treated cells accumulated in the G1 phase of the cell cycle, while the fraction of cells in S phase decreased, compared with vehicle treated cells, in dose and time/dependent **(Figure 19, A-D).**

3.3.3 MUTP-induced cell cycle arrest through increased p21 and p53 expression

In order to shed light on the molecular mechanisms involved in MUTP-dependent cell cycle arrest, changes in levels of protein involved in cell cycle regulation were investigated, by Western blotting analysis. G1/S cell cycle arrest has been shown to be mediated by cyclin-dependent kinase inhibitors, such as p21 [46, 47]. Thus, we considered its expression as candidate mediator of the anti-proliferative response.

The p53 protein is a transcription factor at the center of a vast network of signals to detect cellular stress, such as DNA damage, telomere shortening and hypoxia. The p53 tumor suppressor gene is considered to be a "master gene of the cellular regulation" which in stress stimulation becomes activated and promotes cell cycle arrest and apoptosis [48]. In healthy cells, not subjected to stress, p53 has a short half-life (20 minutes), due of its association with the MDM2 (Mouse double minute 2 homolog) protein. If the cell is in stress conditions, p53 undergoes post-transcriptional modifications that determine the release of MDM2 and the increase of its half-life. The p53 protein counteracts the neoplastic transformation by three mechanisms that are linked: the temporary cell cycle arrest (quiescence), the permanent cell cycle arrest (senescence) and programmed cell death (apoptosis). The cell cycle arrest mediated by p53, can be considered as the first response to DNA damage. As a result of cell damage, such as DNA damage, p53 is activated and stimulates the transcription of many genes including the one for the p21 protein. This protein is able to bind the complex cyclin-CDK2 and cyclin-CDK4 and inhibit its activity, thus regulating the cell cycle progression at the G1 phase.

The expression levels of these two proteins in MCF-7 cells were evaluated after 72 hours of MUTP treatment, at two different concentrations (0.5 and 2 μM). The results obtained (**figure 20**) shown that p21 protein levels were significantly enhanced by 2 μM MUTP; in addition, the MUTP induced higher p53 expression, in dose/dependent manner, in all treated cells.

Accordingly, realtime (RT)-PCR revealed an induction of both p53 and p21 mRNA levels in MCF-7 cells after 24 hour treatment with two different doses of MUTP (**Figure 21**).
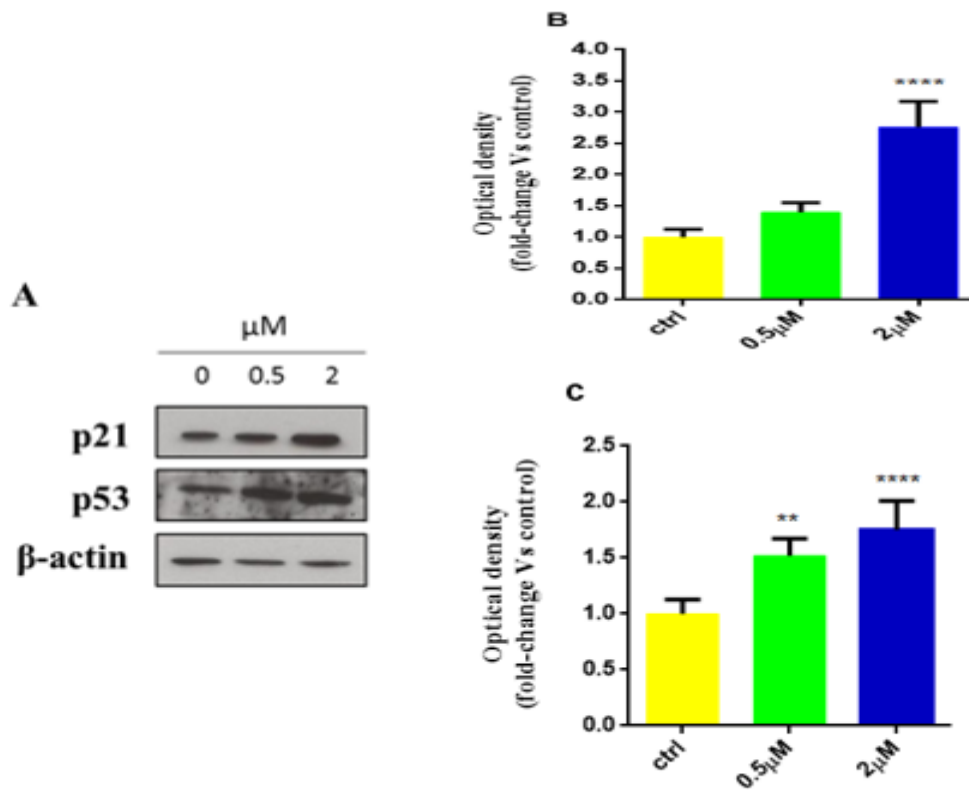
Figure 20. Effects of treatment with MUTP on the levels of expression of the p53 and p21 proteins in the MCF-7 cell lines. **(A)** Immunoblots of p53, and p21 from extracts of MCF-7 cells treated with DMSO (0) or two different concentrations of MUTP (0.5 and 2µM), for 24 hours. B-actin was used as a control for equal loading and transfer. The histograms represent the mean ± S.D. of three separate experiments in which band intensities of p21 **(B)** and p53 **(C)** were evaluated as optical density arbitrary units and expressed in terms of fold change compared to DMSO-treated samples (Ctrl) and normalized for β-actin content. (** p<0.001, **** p<0.00001, one-way ANOVA and Student's t-test calculations).
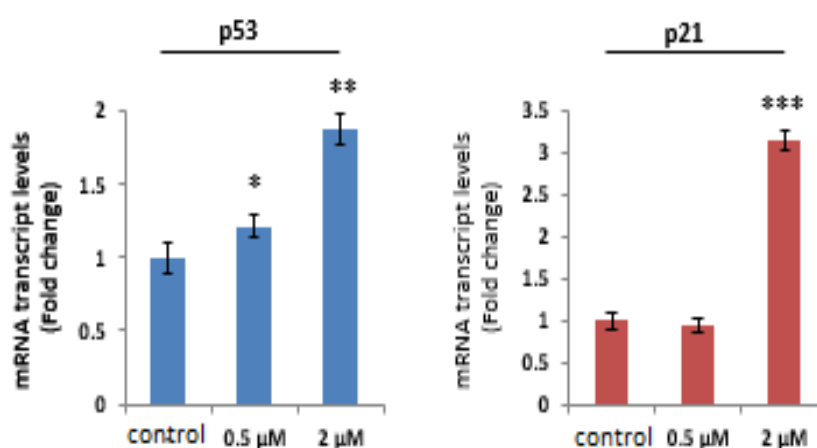
Figure 21. Realtime (RT)-PCR revealed an induction of both p53 and p21 mRNA expression, evaluated by (RT)-PCR , in MCF-7 cells treated with vehicle (control) or MUTP (0.5 and 2 µM) for 24 hours. Each sample was normalized to its GAPDH mRNA content. *, $P < 0.01$; ***, $P < 0.0001$.

3.3.4 MUTP reduces mitochondrial membrane potential with significant increase in ROS levels

Previous studies reported that cytotoxic action of phosphonium salts such as TPP and its derivatives would seem to be due to the disruption of the mitochondrial membrane potential, which is essential for the production of ATP. Moreover, TPP has been shown to damage the mitochondrial membrane, in hypopharyngeal FaDu cells [49-51]. Therefore in order to characterize the metabolic function of MCF-7 cells after treatment with the MUTP, MCF-7 cell lines were stained with different metabloic probes and analysed by FACS. The results showed that MUTP decresed mitochondrial mass, as assessed with Mitochondrial deep red (**Figure 22A**), and mitochondrial membrane potential as assessed with Mitotracker orange (**Figure22B**). The ratio of mitochondrial membrane potential and mitochondrial mass were calculated, showed that treatment with MUTP decreases mitochondrial membrane potential per mitochondria (**Figure 22C**). Its well known that the the reduction and disruption of mitochondrial membrane potential will ultimately leads to the production of reactive oxygen species (ROS). In this regard ROS levels were evaluated by FACS analysis, using the CM-H2DCFDA probe (**Figure 22D**). We demonstarted that ROS levels increase after the treatment with MUTP.
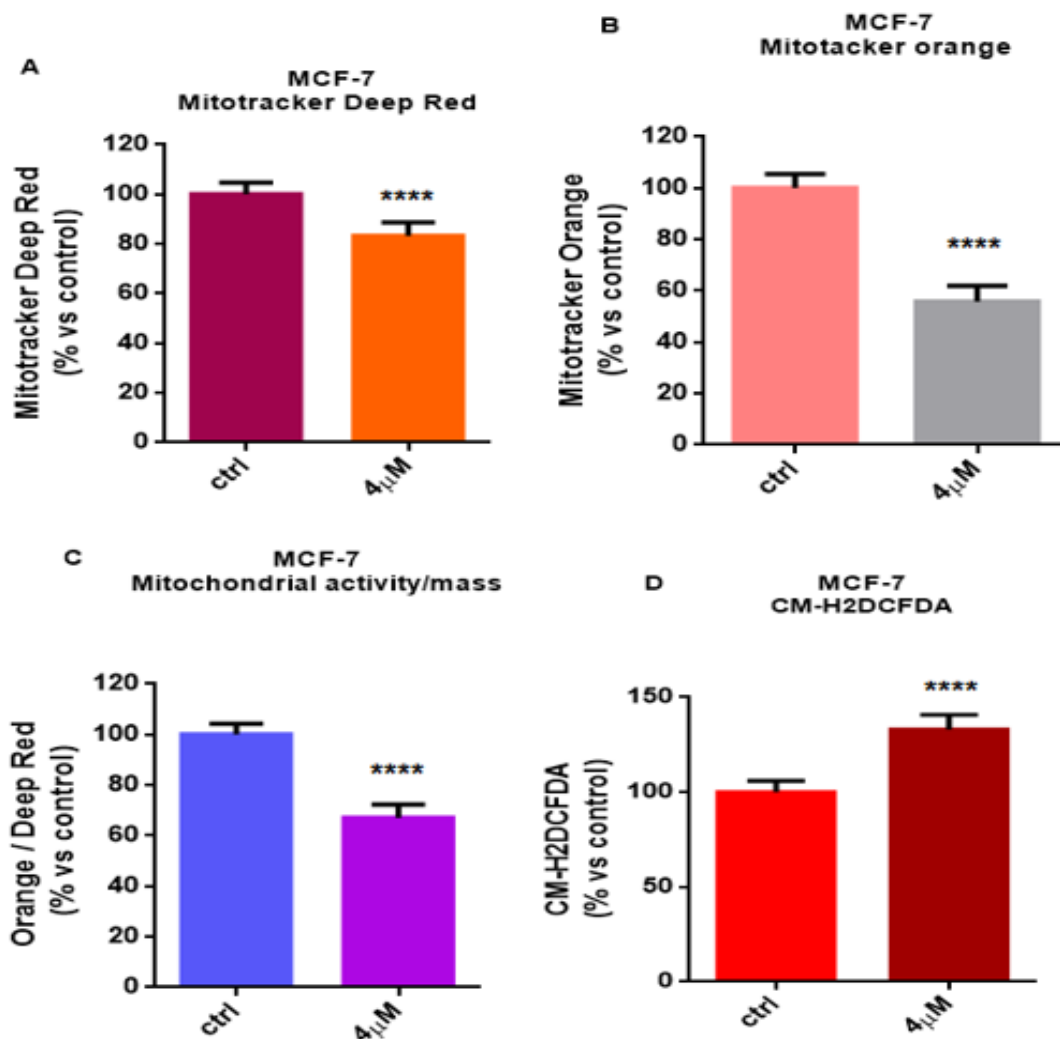
Figure 22. MUTP treatment decreases mitochondrial mass and mitochondrial membrane potential with increase in ROS levels. MCF-7 cells were treated with MUTP at 4 μM concentration for 48 hours. After that cells were stained with different metablic probes and analyzed by FACS. **(A)** MUTP decrease mitochondrial mass(mitotracker deep red) and **(B)** MUTP decreases mitochondrial membrane potential(Mitotracker orange). **(C)** The ratio of mitochondrial membrane potential (Mito Tracker Orange) versus mitochondrial mass (Mito Tracker Deep-Red) was calculated, showing that MUTP decreases mitochondrial membrane potential per mitochondria. **(D)** Cells were treated with **CM-H$_2$DCFDA** probe and analyzed by FACS to determine ROS levels. ROS increased after the treatment with 4 μM of MUTP. (****p < 0.00001, one-way ANOVA and Student's t-test calculations).

3.3.5 MUTP treatment blocks respiratory chain complex in MCF-7

Phosphonium salts reduce the cellular oxygen consumption in a dose dependent manner, by determining as result a decrease in oxidative phosphorylation efficiency [28]. Moreover, we have been observed that MUTP treatment significantly decreases the mitochondrial membrane potential per mitochondria, followed by a significant increase in

119

ROS levels. Based on these observations, we considered to assess what effect MUTP might have on mitochondrial oxidative pathway (OXPHOS) enzymes. The protein complexes, localized in the inner mitochondrial membrane, ultimately, serve as the major source of cellular energy. Towards this aim, MCF-7 cells were left untreated or treated with 0.5 and 2 μM MUTP for 24 h. Results from Western blotting analysis showed that 2 μM MUTP treated cells display a substantial reduction of the II and IV complexes (**Figure 23**) while, slight decrease was observed for the complex III.

Taken together our current data, in agreement with the literature data [49-51], showed that cytotoxic action of MUTP would seem to be due to the mitochondrial damage that it was manifested with a significant decrease in mitochondrial mass, mitochondrial membrane potential as well as substantial reduction in expression levels of the main proteins, involved in cellular energy production (OXPHOS enzymes).
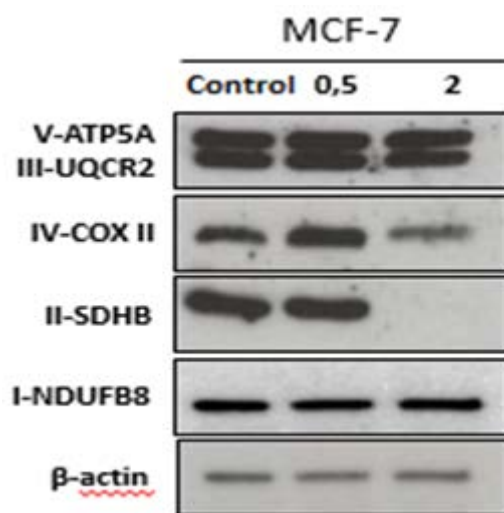
Figure 23. MUTP decreased OXPHOS protein content in MCF-7 cells. Total protein extracts from MCF-7 cells left untreated (control) or treated for 24 h with 0.5 and 2 μM MUTP, were analyzed by Western blot analysis using antibodies against OXPHOS subunits. β-Actin was used as loading control. Blots are representative of three independent experiments with similar results. The OXPHOS antibody cocktail recognizes nuclear-encoded components of Complex I (NDUFB8, NADPH-ubiquinone oxidoreductase 1 beta sub complex 8), Complex II (SDHB, succinate dehydrogenase complex, subunit B), Complex III (UQCRC2, ubiquinol-cytochrome c reductase core protein II), and Complex V ATPase (ATP5A, ATP synthase, alpha subunit), and mitochondrial encoded MTCO2 (mitochondrial-encoded cytochrome c oxidase subunit II) in Complex IV.

3.3.6 MUTP induce apoptosis in MCF-7 cells

The mitochondrial ROS excess induce oxidative modification of cellular macromolecules, inhibit protein function and promote cell death. Additionally, various redox systems, such as the glutathione, thioredoxin, and pyridine nucleotide redox couples, participate in cell signaling and modulation of cell function, including apoptotic cell death. Cell apoptosis is initiated by signals via two main pathways, the extrinsic pathway (receptor-mediated) or the intrinsic pathway (mitochondria-mediated) [52]. Furthermore, it has been observed that the tetraphenyl phosphonium bromide structural analogues, are able to trigger the process of apoptosis "in vivo" [25]. Starting from these observations, and by considering that our previous results showed p53 modulation, after MUTP treatment in MCF-7 cells, we asked if the anti-proliferative activity displayed by MUTP could be due to apoptosis induction (intrinsic pathway). The impact of MUTP on apoptosis was assessed by using different approaches.

First, we evaluated the expression levels of several protein involved in this pathway, Bax, Caspase-3 and Caspase-9, by immunoblot analysis. The Bax protein is specifically attached to mitochondrial membranes which may indicate a role in the regulation of mitochondrial function during apoptosis [53]. Mitochondria have been shown to play a key function in the events leading to caspase activation in cell-free systems as well as in many cell types undergoing apoptosis. Induction of apoptosis is, in some cells, associated with a loss of cytochrome C. In the cytosol, cytochrome C forms a complex with Apaf1 and Caspase-9, which triggers caspase activation and cell death [54]. Activated Caspase-9 in turn cleaves and activates Caspase-3 (**Figure 24**) [55].
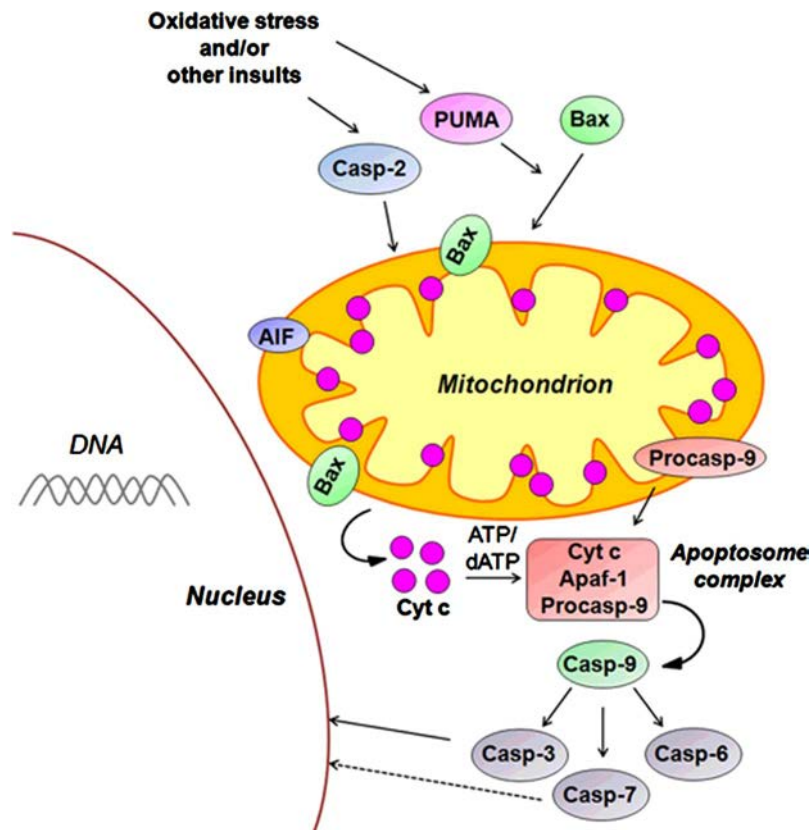
Figure 24. Intrinsic apoptosis pathway.

The results obtained (**Figure 25**) revealed an increase in the levels of BAX, Cas-9 and Cas-3 with increasing MUTP concentration (0.5 and 2 µM) upon treatment in MCF-7 cells. This modulation was in agreement with the hypothesis that an intrinsic apoptotic process was involved in MUTP anti-proliferative activity.
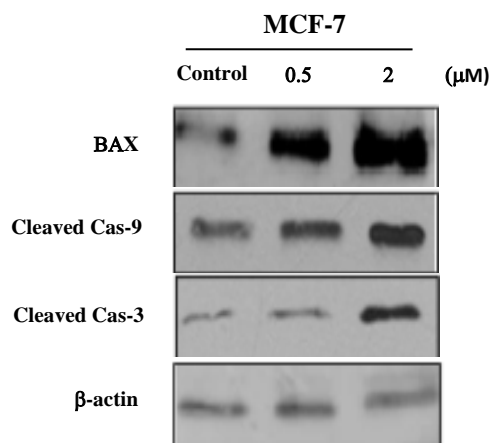
Figure 25. Induction of apoptosis by MUTP in MCF-7 cells. Immunoblots of Bax, cleaved Caspase-3 and cleaved Caspase-9 from extracts of MCF-7 cells treated with vehicle (Control) or MUTP (0.5 and 2 µM) for 24 hr. β-Actin was used as loading control.

3.3.7 DNA laddering

Second approach we used was to evaluate the inter nucleosomal fragmentation profile of genomic DNA, a diagnostic hallmark of cells undergoing apoptosis. MUTP treatment induced a marked DNA fragmentation in MCF-7 cells (**Figure 26**). For this purpose the MCF-7 cells were treated for 24 hours with 0.5 and 2µM MUTP, then DNA was extracted and subjected to electrophoresis on agarose gel. The results obtained have been reported in **figure 26**.
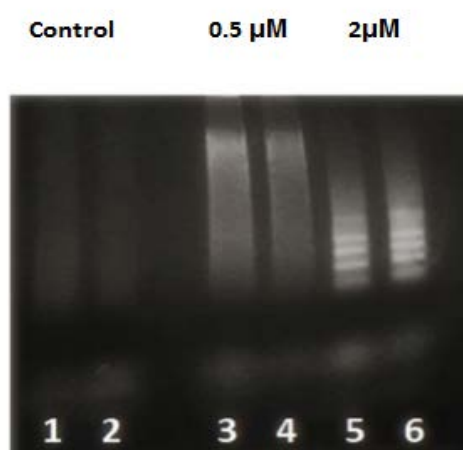
Figure 26. DNA laddering by agarose electrophoresis gel.

After the electrophoresis, in lines 5 and 6, in which it was loaded the DNA extracted from cells, after treatment with 2 µM MUTP, was detected a distinct and marked DNA fragmentation, to confirm the mechanism of apoptosis. On the contrary, no fragmentation could be observed in lines 3 and 4 where we loaded the DNA extracted from cells after treatment with MUTP 0.5 µM. Lines 1 and 2 are the control (DNA extracted from cells without treatment).

3.3.8 TUNEL assay further confirms apoptosis

Finally, inorder to confirme the apoptotic effect of MUTP on MCF-7 cells, we performed TUNEL assay. The reults obtained showed a strong induction of the apoptotic cells after MUTP exposure (**Figure 27**).
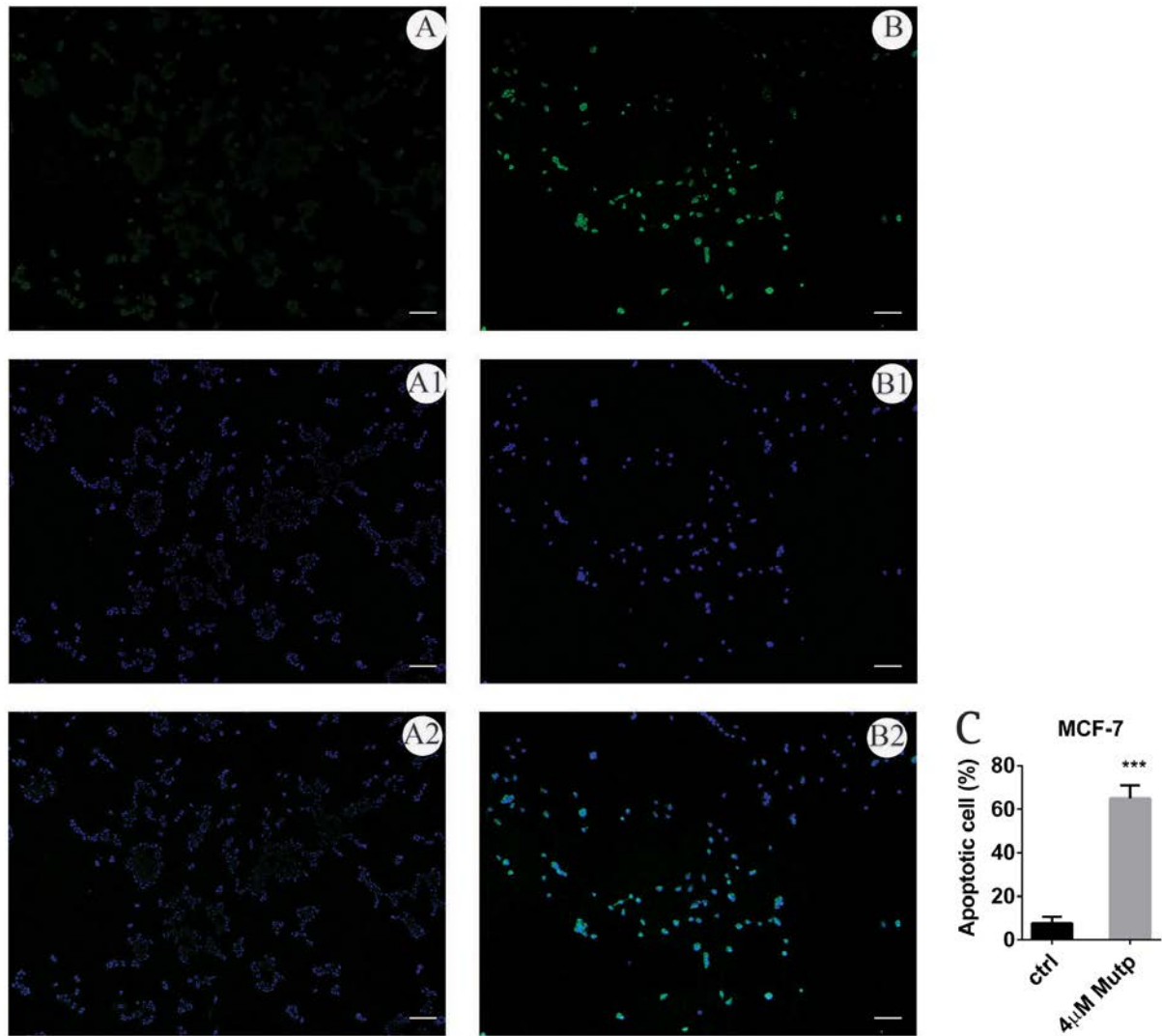
Figure 27: MUTP triggers apoptotic cell death in MCF-7 cells. Terminal deoxynucleotidyl transferase-mediated dUTP Nick End Labeling (TUNEL) staining in MCF-7 cells. The cells treated with DMSO (control, ctrl) (panels A, A1, A2) or 4μM MUTP (panels B, B1, B2), for 48 h, were washed with PBS, paraformaldehyde fixed and subjected to TUNEL assay (panels A, B); after removal of enzyme and buffer, fixed cells were Hoechst 33342 stained to visualize the cell nucleus (panels A1, B1). Merge (panels A2, B2) was also shown. The images were taken on Olympus BX41 microscope with CSV1.14 software using a CAMXC-30 for image acquisition. Scale Bars 125μm. **(C)** The histograms represent the means ± S. D. of apoptotic cells from three independent experiments performed in triplicate. *** $p < 0.0001$ versus control, one-way ANOVA and Student's t-test calculations).

3.4 CONCLUSION

In the present work we evaluated the invitro anticancer activities of nelwy synthetized phosphonium salts, at different concentrations (0.1, 0.5, 1,5 and 10 µM). Specifically, (11-methoxy, 11-oxoundecyl)triphenylphosphonium bromide (MUTP) as well as two new phosphine oxide salts, 3,3'-(methylphosphoryl)dibenzenaminium chloride and 3,3'-(phenylphosphoryl)dibenzenaminium chloride (SBAMPO and SBAPPO) on proliferation of two human cancer cell lines (Human breast cancer cell lines, Mcf-7 and Human uterine cervix adenocarcinoma,HeLa). Cell viability was determined by using the 3-(4,5-dimethylthiazol-2-y1)-2,5-diphenyltetrazolium (MTT) assay. The results obtained showed that MUTP elicited promising anti-proliferative activity against the two cell lines tested. The results were further confirmed by calculating the IC-50 value, that was found to be 3.71 µM and 3.59 µM for Mcf-7 and HeLa cells, respectively. We have compared the results with the commercial anticancer drug, 5-Fluorouracil and a typical phoshonium salt Tetraphenyl phosphonium bromide (TPP). More surprisingly we found that the MUTP treatment in normal breast epithelial cells (Mcf-10 A) didn't show any toxicity. The obtained IC-50 value was higher than 50 µM, while the commercial drug was found really toxic to healthy cells, indeed its IC-50 value was very low (2.72µM).

The good biological responses elicited by MUTP, prompted us to investigate the underlying mechanism of action. Literature data reported that Tetraphenyl phosphonium bromide (TPP) and its structural analogues [25], block cell cyle in G2/M phase. Therefore we evaluated if MUTP behaved in the same way and we evaluated the distribution of cells within the three major phases of cell cycle. FACS analysis revealed that MUTP treated cells accumulated in the G1/GS-phase of the cell cycle compared with vehicle treated cells. This block was confirmed by an increased expression level of two proteins involved in cell cycle regulation, p21 e p53.

Recently, there has been a surge of interest in developing compounds selectively targeting mitochondria for the treatment of neoplasms [56, 57].

The critical role of mitochondria in cellular metabolism and respiration supports this therapeutic rationale. Dysfunction in the processes of energy production and metabolism

contributes to attenuation of response to pro-apoptotic stimuli and increased ROS production both of which are implicated in the initiation and progression of most human cancers.

Therefore, in order to characterize the mitochondrial function in MCF7 cells, after MUTP treatment, the cells were stained with specific metabolic probes and analyzed by FACS. The results showed that MUTP treatment decreased mitochondrial mass and mitochondrial membrane potential and increased the ROS production. In agreement with these findings, the reduction in the expression of the mitochondrial oxidative pathway (OXPHOS) enzymes revealed a bioenergetics failure, induced by MUTP, in treated cells.

Next, we hypothesized that the mitochondrial damage could determine the triggering of apoptotic events; therefore, we assessed the impact of MUTP on apoptosis by using different approaches: immunoblot analysis of several protein involved in this pathway, Bax, Caspase-3 and Caspase-9, DNA laddering and Tunel assay.

Our outcomes demonstrated that MUTP treatment inhibited MCF-7 proliferation, inducing apoptosis.

Taken together all the data we have got from the experimental section confirmed that MUTP coud be considered a promising anticancer agent.

Hence, the capability of this phosphonium salt to elicit selective inhibitory effects on cancer cell growth, probably caused by a mitochondrial function inhibition, could be taken into account towards novel pharmacological approaches in cancer therapy. The different activities of the phosphonium salts and phosphine oxides (sBAMPO and sBAPPO) suggests that the phosphorus compounds, capable of exerting anti-tumor action, must have the oxidation state 3 and therefore a free electron-pair, electron pair that the phosphorus does not possess in oxidation state 5. However further studies will be helpful to better define the molecular mechanism involved.

3.5 BIBLIOGRAPHY

1. Fraser VJ, Nickel KB, Fox IK, Margenthaler JA and Olsen MA. (2016) The epidemiology and outcomes of breast cancer surgery. *Trans Am Clin Climatol Assoc.* 127:46-58.

2. Van EA, Derks L, Sie AS, Egbers L, Woldringh G, Prins JB, Manders P and Hoogerbrugge N. (2016) Lifestyle Risk Factors for Breast Cancer in BRCA1/2-Mutation Carriers Around Childbearing Age*. J Genet Couns*.

3. Sanguinetti, Bistoni and Aventa. (2010) Breast surgery, atlas text, Terni, *Morphena Publishing.* ISBN 978-88-96051-07-8.

4. Brunton L, Chabner BA, Knollmann BC, Goodman and Gilman. The pharmacoloical basics of therapy. 12th edition.

5. Manfred Kaufmann (2009). Management of Breast Diseases, *Springer.*

6. Huh WK, Ault KA, Chelmow D, Davey DD, Goulart RA, Garcia FA, Kinney WK, Massad LS, Mayeaux EJ, Saslow D, Schiffman M, Wentzensen N, Lawson HW and Einstein MH. (2015) Use of primary high-risk human papillomavirus testing for cervical cancer screening: interim clinical guidance. *Gynecol Oncol.* 136(2):178-82.

7. Shanta V , Krishnamurthi S , Gajalakshmi CK , Swaminathan R and Ravichandran K. (2000) Epidemiology of cancer of the cervix: global and national perspective. *Journal of the Indian Medical Association*. 98(2):49-52.

8. Kumar V, Abbas AK, Fausto N and Mitchell RN. (2007) Robbins Basic Pathology (8th ed.). *Saunders Elsevier.* 718–721.

9. Rideout D, CalogeropoulouT, Jaworski J and McCarthy M. (1990) Synergism through direct covalent bonding between agents: a strategy for rational design of chemotherapeutic combinations. *Biopolymers*. 29:247-62.

10. Bergeron KL, Murphy EL, Majofodun O, Muñoz LD, Williams JC Jr and Almeida KH. (2009) Arylphosphonium salts interact with DNA to modulate cytotoxicity. *Mutat Res*. 673(2):141-8.

11. Kinnamon KE, Steck EA, Hanson WL and Chapman WL Jr. (1977) In search of anti-Trypanosoma cruzi drugs: new leads from a mouse model*. J Med Chem.* 20(6):741-4.

12. Blank B, DiTullio NW, Deviney L, Roberts JT and Saunders HL. (1975) Synthesis and hypoglycemic activity of phenacyltriphenylphosphoranes and phosphonium salts. *J Med Chem*. 18(9):952-4.

13. Rideout DC, Calogeropoulou T, Jaworski JS, Dagnino RJ and McCarthy MR. (1989). Phosphonium salts exhibiting selective anti-carcinoma activity in vitro. *Anticancer Drug,* 4:265-80.

14. Rideout D, Bustamante A and Patel J. (1994) Mechanism of Inhibition of Fadu Hypopharyngeal Carcinoma Cell-Growth by Tetraphenylphosphonium Chloride. *International Journal of Cancer*. 57:247-253.

15. Weisberg EL, Koya K, Modica-Napolitano J, Li Y and Chen L B. (1996) In vivo administration of MKT-077 causes partial yet reversible impairment of mitochondrial function. *Cancer Res*. 56:551-5.

16. Bernal SD, Lampidis TJ, McIsaac RM and Chen LB.(1983) Anticarcinoma activity in vivo of rhodamine 123, a mitochondrial-specific dye. *Science*, 222:169-72.

17. Herr HW, Huffman JL, Huryk R, Heston WD, Melamed MR and Whitmore WF. (1988) Anticarcinoma activity of rhodamine 123 against a murine renal adenocarcinoma. *Cancer Res.* 48:2061-3.

18. Weiss MJ, Wong JR, Ha CS, Bleday R, Salem R, Steele GD and Chen LB. (1987) Dequalinium, a topical antimicrobial agent, displays anticarcinoma activity based on selective mitochondrial accumulation. *Proceedings of the National Academy of Sciences of the United States of America .* 84:5444-8.

19. Koya K, Li Y, Wang H, Ukai T, Tatsuta N, Kawakami M and Shishido Chen LB. (1996) MKT-077, a novel rhodacyanine dye in clinical trials, exhibits anticarcinoma activity in preclinical studies based on selective mitochondrial accumulation. *Cancer Res,* 56:538-43.

20. Ross MF, Kelso GF, Blaikie FH, James AM, Cochemé HM, Filipovska A, Da Ros T, Hurd TR, Smith RA and Murphy MP. (2005) Lipophilic triphenylphosphonium cations as tools in mitochondrial bioenergetics and free radical biology. *Biochemistry (Mosc)*. 70(2):222-30.

21. Cooper WA, Bartier WA, Rideout DC and Delikatny EJ. (2001) 1H NMR visible lipids are induced by phosphonium salts and 5-fluorouracil in human breast cancer cells. *Magn Reson Med*. 45(6):1001-10.

22. Manetta A, Gamboa G, Nasseri A, Podnos YD, Emma D, Dorion G, Rawlings L, Carpenter PM, Bustamante A, Patel J and Rideout D. (1996) Novel phosphonium salts display in vitro and in vivo cytotoxic activity against human ovarian cancer cell lines*. Gynecol Oncol*. 60(2):203-12.

23. Murphy MP. (2008) Targeting lipophilic cations to mitochondria. *Biochim Biophys Acta*. 1777(7-8):1028-31.

24. Davis S, Weiss MJ, Wong JR, Lampidis TJ and Chen LB. (1985) Mitochondrial and plasma membrane potentials cause unusual accumulation and retention of rhodamine 123 by human breast adenocarcinoma-derived MCF-7 cells. *J Biol Chem.* 260:13844-50.

25. Chen LB. (1988) Mitochondrial membrane potential in living cells. *Annu Rev Cell Biol.* 4:155-81.

26. Dubois RJ, Lin CC and Beisler JA. (1978) Synthesis and antitumor properties of some isoindolylalkylphosphonium salts. *J Med Chem*. 21(3):303-6.

27. Modica-Napolitano JS and Aprille JR. (2001) Delocalized lipophilic cations selectively target the mitochondria of carcinoma cells. *Adv Drug Deliv Rev*. 49(1-2):63-70.

28. Millard M, Pathania D, Shabaik Y, Taheri L, Deng J and Neamati N. (2010) Preclinical evaluation of novel triphenylphosphonium salts with broad-spectrum activity. *PLoS One*. 5(10).

29. Wang J, Yang CT, Kim YS, Sreerama SG, Cao Q, Li ZB, He Z, Chen X and Liu S. (2007) Cu-Labeled triphenylphosphonium and triphenylarsonium cations as highly tumor-selective imaging agents. *J Med Chem*. 50(21):5057-69.

30. Kim YS, Yang CT, Wang J, Wang L, Li ZB, Chen X and Liu S. (2008) Effects of targeting moiety, linker, bifunctional chelator, and molecular charge on biological properties of 64Cu-labeled triphenylphosphonium cations. *J Med Chem*. 51(10):2971-84.

31. DeBerardinis RJ, Lum JJ, Hatzivassiliou G and Thompson CB. (2008) The biology of cancer: metabolic reprogramming fuels cell growth and proliferation. *Cell Metab*. 7(1):11-20.

32. Gatenby RA, Gawlinski ET, Gmitro AF, Kaylor B and Gillies RJ. (2006) Acid-mediated tumor invasion: a multidisciplinary study. *Cancer Res*. 66(10):5216-23.

33. Casaburi I, Avena P, De Luca A, Chimento A, Sirianni R, Malivindi R, Rago V, Fiorillo M, Domanico F, Campana C, Cappello AR, Sotgia F, Lisanti MP & Pezzi V . Estrogen related receptor α (ERRα) a promising target for the therapy of adrenocortical carcinoma (ACC). Oncotarget. 2015. 22;6(28):25135-48

34. Raimondo M, Russo S, Guadagno L, Longo P, Chirico S, Mariconda A, Bonnaud L, Murariu O and Dubois P. (2015) Effect of incorporation of POSS compounds and phosphorous hardeners on thermal and fire resistance of nanofilled aeronautic resins. *Rsc Advances.* 5:10974-10986.

35. Palma G, Frasci G, Chirico A, Esposito E, Siani C, Saturnino C, Arra C, Ciliberto G, Giordano A and D'Aiuto M. (2015) Triple negative breast cancer: looking for the missing link between biology and treatments. *Oncotarget*. 26560-74.

36. Carocci A, Catalano A, Bruno C, Lovece A, Roselli M G, Cavalluzzi M M and De Santis F, De Palma A, Rusciano MR, Illario M, Franchini C and Lentini G. (2013) N-(Phenoxyalkyl)amides as MT(1) and MT(2) ligands: antioxidant properties and inhibition of Ca(2+)/CaM-dependent kinase II. *Bioorg Med Chem.* 21:847-51.

37. Caruso A, Sinicropi MS, Lancelot JC, El-Kashef H, Saturnino C, Aubert G, Ballandonne C, Lesnard A, Cresteil T, Dallemagne P and Rault S. (2014) Synthesis and evaluation of cytotoxic activities of new guanidines derived from carbazoles. *Bioorg Med Chem Lettrs*. 24:467-72.

38. Fiorillo M, Verre AF, Iliut M, Peiris-Pages M, Ozsvari B, Gandara R, Cappello AR, Sotgia F, Vijayaraghavan A and Lisanti MP. (2015) Graphene oxide selectively targets cancer stem cells, across multiple tumor types: implications for non-toxic cancer treatment, via "differentiation-based nano-therapy. *Oncotarget.* 6:3553-62.

39. Burnette WN. (1981) Western Blotting electrophoretic transfer of proteins from sodium dodecyl sulphate-polyacrylamide gels to unmodified nitrocellulose and radiographic detection with antibody and radioiodinated protein. *Analitical Biochemistry*. 112:195-203.

40. Cappello AR, Guido C, Santoro A, Santoro M, Capobianco L, Montanaro D, Madeo M, Andò S, Dolce V and Aquila S. (2012) The mitochondrial citrate carrier (CIC) is present and regulates insulin secretion by human male gamete. *Endocrinology*. 153(4):1743-54.

41. Fiorillo M, Lamb R, Tanowitz HB, Mutti L, Krstic-Demonacos M, Cappello AR, Martinez-Outschoorn UE, Sotgia F and Lisanti MP. (2016) Repurposing atovaquone: targeting mitochondrial complex III and OXPHOS to eradicate cancer stem cells. *Oncotarget.* 7(23):34084-99.

42. De Luca A, Fiorillo M, Peiris-Pages M, Ozsvari B, Smith DL, Sanchez-Alvarez R, Martinez-Outschoorn UE, Cappello AR, Pezzi V, Lisanti MP and Sotgia F. (2015) Mitochondrial biogenesis is required for the anchorage-independent survival and propagation of stem-like cancer cells. *Oncotarget*. 6:14777-95.

43. Fiorillo M, Lamb R, Tanowitz HB, Cappello AR, Martinez-Outschoorn UE, Sotgia F and Lisanti MP. (2016) Bedaquiline, an FDA-approved antibiotic, inhibits mitochondrial

function and potently blocks the proliferative expansion of stem-like cancer cells (CSCs). *Aging* (*Albany NY).* 8(8):1593-607.

44. Luchetti F, Canonico B, Curci R, Battistelli M, Mannello F, Papa S, Tarzia G and Falcieri E. (2006) Melatonin prevents apoptosis induced by UV-B treatment in U937 cell line. *J Pineal Res*. 40(2):158-67.

45. Luchetti F, Canonico B, Mannello F, Masoni C, D'Emilio A, Battistelli M, Papa S and Falcieri E. (2007) Melatonin reduces early changes in intramitochondrial cardiolipin during apoptosis in U937 cell line*. Toxicol In Vitro*. 21(2):293-301.

46. Gartel AL and Radhakrishnan SK. (2005) Lost in transcription: p21 repression, mechanisms, and consequences. *Cancer Res*. 65(10):3980-5.

47. Rizza P, Pellegrino M, Caruso A, Iacopetta D, Sinicropi MS, Rault S, Lancelot JC, El-Kashef H, Lesnard A, Rochais C, Dallemagne P, Saturnino C, Giordano F, Catalano S and Andò S. (2016) 3-(Dipropylamino)-5-hydroxybenzofuro[2,3-f]quinazolin-1(2H)-one (DPA-HBFQ-1) plays an inhibitory role on breast cancer cell growth and progression. *Eur J Med Chem*. 107:275-87.

48. Laptenko O and Prives C. (2006) Transcriptional regulation by p53: one protein, many possibilities. *Cell Death Differ.* 13(6):951-61.

49. Chimento A, Sala M, Gomez-Monterrey IM, Musella S, Bertamino A, Caruso A, Sinicropi MS, Sirianni R, Puoci F, Parisi OI, Campana C, Martire E, Novellino E, Saturnino C, Campiglia P and Pezzi V. (2013) Biological activity of 3-chloro-azetidin-2-one derivatives having interesting anti-proliferative activity on human breast cancer cell lines*. Bioorg Med Chem Lett*. 23(23):6401-5.

50. Sirignano E, Saturnino C, Botta A, Sinicropi MS, Caruso A, Pisano A, Lappano R, Maggiolini M and Longo P. (2013) Synthesis, characterization and cytotoxic activity on breast cancer cells of new half-titanocene derivatives. *Bioorg Med Chem Lett*. 23(11):3458-62 .

51. Paesano N, Marzocco S, Vicidomini C, Saturnino C, Autore G, De Martino G and Sbardella G. (2005) Synthesis and biological evaluation of 3-benzyl-1-methyl- and 1-methyl-3-phenyl-isothioureas as potential inhibitors of iNOS. *Bioorg Med Chem Lett*. 15(3):539-43.

52. Circu ML and Aw TY. (2010) Reactive oxygen species, cellular redox systems, and apoptosis. *Free Radic Biol Med*. 48(6):749-62.

53. Um HD. (2017) Bcl-2 family proteins as regulators of cancer cell invasion and metastasis: a review focusing on mitochondrial respiration and reactive oxygen species. *Oncotarget.* 7(5):5193-203.

54. Li P, Nijhawan D, Budihardjo I, Srinivasula SM, Ahmad M, Alnemri ES and Wang X. (1997) Cytochrome c and dATP-dependent formation of Apaf-1/caspase-9 complex initiates an apoptotic protease cascade. *Cell.* 91(4):479-89.

55. Czabotar PE, Lessene G, Strasser A and Adams JM. (2014) Control of apoptosis by the BCL-2 protein family: implications for physiology and therapy. *Nat Rev Mol Cell Biol*. 15(1):49-63.

56. Fiorillo M, Lamb R, Tanowitz HB, Mutti L, Krstic-Demonacos M, Cappello AR, Martinez-Outschoorn UE, Sotgia F and Lisanti MP. (2016) Repurposing atovaquone: targeting mitochondrial complex III and OXPHOS to eradicate cancer stem cells. *Oncotarget.* 7(23):34084-99.

57. Lamb R, Fiorillo M, Chadwick A, Ozsvari B, Reeves KJ, Smith DL, Clarke RB, Howell SJ, Cappello AR, Martinez-Outschoorn UE5, Peiris-Pagès M, Sotgia F and Lisanti MP. (2015) Doxycycline down-regulates DNA-PK and radiosensitizes tumor initiating cells: Implications for more effective radiation therapy. *Oncotarget.* 6(16):14005-25.

Proteomic Applications of Polymeric Nanoparticles with Engineered Affinity towards Select Target

Abstract

Complexity in biological samples pose a greater challenge for proteomic analysis. In order to overcome this issue, separation or fractionation is often a prerequisite to qualitative or quantitative proteomic approaches. Affinity chromatography is a method for separating biochemical mixture based on a highly specific interaction similar to the one between receptor and ligand. This mini-review discuss the use of polymeric nanoparticles as an alternative matrix support in affinity purification. The nanoparticle-based purification have the potential to selectively target the protein of interest from a complex pool. This strategy could be applied as sample purification step prior to mass spectrometry-based proteomic analyses.

Keywords: Polymeric nanoparticles; Proteomics; Affinity purification; Mass spectrometry

Hariprasad Thangavel[1]* and Dhanya Dhanyalayam[2]

[1]Department of Biology and Biochemistry, University of Houston, USA

[2]Department of Pharmacy, Health and Nutritional Sciences, University of Calabria, Italy

*Corresponding author: Hariprasad Thangavel, Center for Nuclear Receptors and Cell Signaling, Department of Biology and Biochemistry, University of Houston, Houston, TX 77204, USA, Tel: 832-230-6465; Email: hariprasadslm@gmail.com

Abbreviations: MS: Mass Spectrometry; NPs: Nanoparticles; PNIPAm: poly-N-isopropylacrylamide; GPER: G-protein coupled Estrogen Receptor; HPLC: High Performance Liquid Chromatography

Introduction to Affinity Purification

Proteins and other macromolecules of interest can be purified from crude extracts or other complex mixtures by a variety of methods. Selective precipitation is perhaps the simplest method for separating one type of macromolecule from another. Most purification methods, however, involve some form of chromatography whereby molecules in solution (mobile phase) are separated based on differences in chemical or physical interaction with a stationary material (solid phase). Gel filtration (also called size-exclusion chromatography or SEC) uses a porous resin material to separate molecules based on size (i.e., physical exclusion). In ion exchange chromatography, molecules are separated according to the strength of their overall ionic interaction with a solid phase material (i.e., nonspecific interactions).

By contrast, affinity chromatography (also called affinity purification) makes use of specific binding interactions between molecules. It is a variant of chromatography based on the ability of biomolecules (analytes) to bind certain ligands specifically and reversibly. These unique features of the analyte and the ligand interaction are then utilized for the separation of the analyte of interest from a complex mixture. From the first protein-protein interaction studies done in the late 1990´s [1,2], affinity separations have experienced a true renaissance in proteomics. A complete parade of affinity matrices and affinity-based experimental approaches has been developed that has found numerous applications ranging from subtraction of highly abundant proteins to study of drug target profiles to large scale mapping of posttranslational modifications. In the classical setup, a relevant ligand is attached to a solid, inert resin creating an affinity stationary phase (affinity matrix). When a sample containing desired analyte is passed over such affinity matrix, the analyte having specific binding affinity to the ligand become bound and retained by the matrix while the other molecules stay apart. After the other unwanted molecules are washed away, the bound analyte is stripped from the affinity matrix, resulting in its purification from the original sample (Figure 1). This principle was discovered by Cuatrecasas and Wilchek [3,4], who applied it to the purification of Staphylococcal nuclease and avidine. Since their discovery, numerous specialized affinity purification techniques appeared, but notably even today more than 90% of them apply the same general principles as reported in 1968 [5]. Each specific affinity system requires its own set of conditions and presents its own peculiar challenges for a given research purpose [6].
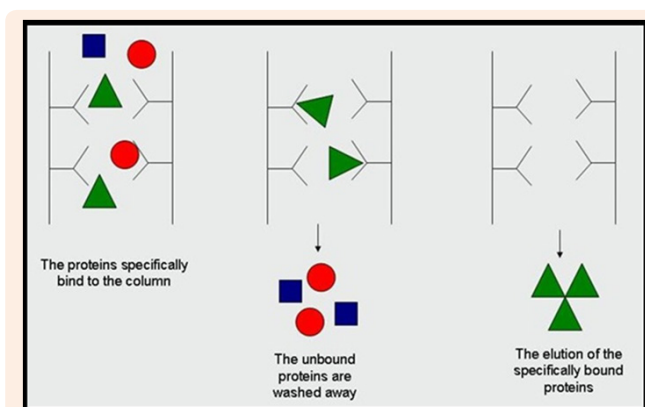
Figure 1: Protein purification using affinity chromatography [7].

Basically, there are two main modes of affinity chromatography - a 'subtraction' mode and an 'enrichment' mode. If the aim of the purification is to specifically remove protein species that would hamper characterization of the sample, then affinity chromatography is employed in subtraction mode. Traditionally, the main purpose of affinity subtraction is the elimination of highly abundant proteins like albumin, immunoglobulin, etc., to achieve broader coverage of proteomes that suffer from wide dynamic range such as human body fluids (blood plasma, cerebrospinal fluid, urine, saliva). Whereas, enrichment mode is applied for the isolation of selected protein species. At the protein level, the enrichment affinity chromatography permits the purification of a particular protein of interest or a group of low abundant proteins and/or proteins that share a specific structural feature. At peptide level, the enrichment affinity chromatography has attained an essential position in the purification of post-translationally modified species.

Moreover, the enrichment affinity chromatography of proteins can be used as a tool to obtain an information on specific protein affinities. In short, the basic principle of affinity chromatography allows to utilize the method for the isolation of protein partners of selected molecules [7,8]. During the affinity purification, the molecule of interest represents a 'bait' that is bound by its cellular protein counterparts, its 'preys'. These (protein) preys are then easily purified and consequently identified by MS [9,10], generating thus a map of the bait-protein interaction network. In this setup, affinity chromatography has facilitated the discernment of many different molecular relationships from protein-protein interactions to drug selectivity profiles [11-13].

Engineered polymeric nanoparticles for affinity purification

The support or matrix in affinity purification is any material to which a bio-specific ligand is covalently attached. Typically, the material to be used as an affinity matrix is insoluble in the system in which the target molecule is found. Usually, but not always, the insoluble matrix is a solid. Hundreds of substances have been described and utilized as affinity matrices, including agarose, cellulose, dextran, polyacrylamide, latex and controlled pore glass [14-16]. Useful affinity supports are those with a high surface-area to volume ratio, chemical groups that are easily modified for covalent attachment of ligands, minimal nonspecific binding properties, good flow characteristics and mechanical and chemical stability.

Over the last decade, the use of magnetic nanoparticles [17-20] and polymer nanoparticles [21-24] for protein affinity purification have been widely reported. Engineered synthetic nanoparticles (NPs) with an intrinsic affinity and selectivity for target biomacromolecules are significant interest for use in diagnostics [25], therapeutics [26-28] and protein purification [29-30], and as a tool to investigate biochemical processes [31-32]. Recent studies show that synthetic NPs (Figure 2) incorporating functional groups complementary to a surface domain of a target biomacromolecule can result in a high intrinsic affinity for target peptides [28], proteins [26,33], and polysaccharides [34,35].

These materials are attractive as an inexpensive and robust alternative to affinity reagents of biological origin, including antibodies [36].
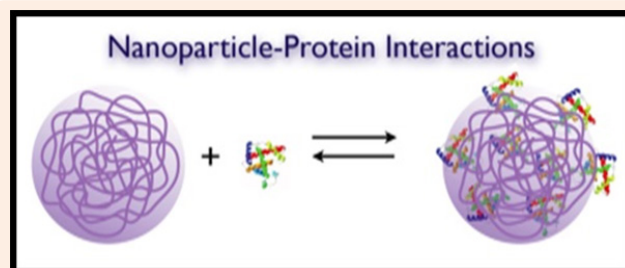
Figure 2: Synthetic polymer nanoparticles for protein purification.

PNIPAm-based nanoparticles for GPER purification

G-protein coupled Estrogen Receptor may play a significant role in tamoxifen resistance in breast cancer cells. Although it is believed to be a key player in several other cancers, the background information at the molecular level is still limited. In order to study the complete proteome, post translational modifications, mutations and to better understand their molecular interactions with various other receptors and ligands, it is necessary to isolate pure GPER from crude cell lysate. The lack of promising separation and purification tools peaked our interest towards designing NPs that can capture this target biomolecule. In recent years, NPs with an intrinsic affinity have shown to be successful in binding biomacromolecules like melittin [37,38], immunoglobulin G [39], histone [40], fibrinogen [40] and lysozyme [29] by controlling and optimizing the functional monomers composition.

In our study, we adopted a similar approach in an effort to capture GPER with high affinity and selectivity among a mixture of proteins that are expressed in various breast cancer cell lines. Considering the fact that GPER is a membrane protein with many hydrophobic amino acid residues on the surface, a candidate NP was chosen from a library of nanoparticles that were prepared by combining different populations of functional groups on a poly-N-isopropylacrylamide (PNIPAm)-based polymer backbone. The synthesis of the candidate NPs was illustrated below (Figure 3). We started our experiment with GPER peptide selection and synthesis. Then, we evaluated the interaction between truncated-GPER (short peptide epitopes) and NPs by high performance liquid chromatography (HPLC). Finally, we moved on to evaluate the interaction between GPER (whole protein) and NPs by immunoblot analysis. After evaluating the results, the nanoparticle-based purification approach turned out to be the method of choice to enrich GPER prior to mass spectrometry analysis.

Conclusion

Recently, nanoparticles with an intrinsic affinity have shown to be successful in binding biomacromolecules like melittin, immunoglobulin G, histone, fibrinogen and lysozyme by controlling and optimizing the functional monomers composition.

We tested a similar approach in an effort to capture GPER with high affinity and selectivity among a mixture of proteins that are expressed in various cancer cell lines. We anticipate to use this strategy as a sample purification step before mass spectrometry-based proteomic analysis. Similar approach could be applied to study a number complex targets that are difficult to purify or lack separation tools with current proteomic technologies.
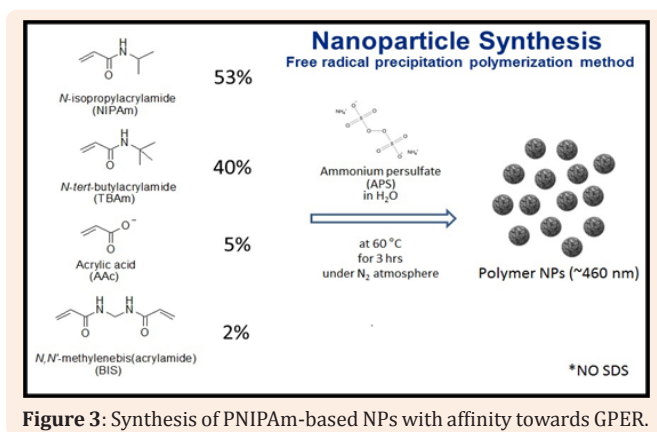
Figure 3: Synthesis of PNIPAm-based NPs with affinity towards GPER.

Acknowledgement

References

1. Neubauer G, Gottschalk A, Fabrizio P, Séraphin B, Lührmann R, et al. (1997) Identification of the proteins of the yeast U1 small nuclear ribonucleoprotein complex by mass spectrometry. Proc Natl Acad Sci USA 94(2): 385-390.

2. Gitte Neubauer, Angus King, Juri Rappsilber, Cinzia Calvio, Mark Watson, et al. (1998) Mass spectrometry and EST-database searching allows characterization of the multi-protein spliceosome complex. Nat Genet 20(1): 46-50.

3. Cuatrecasas P, Wilchek M, Anfinsen CB (1968) Selective enzyme purification by affinity chromatography. Proc Natl Acad Sci USA 61(2): 636-643.

4. Cuatrecasas P, Wilchek M (1968) Single-step purification of avidine from egg white by affinity chromatography on biocytin-Sepharose columns. Biochem Biophys Res Commun 33(2): 235-239.

5. M Wilchek (2004) My life with affinity. Protein Sci 13(11): 3066-3070.

6. Cuatrecasas P, Anfinsen CB (1971) Affinity Chromatography. Annual Review of Biochemistry 40: 259-278.

7. Tőzsér J, Emri T, Csősz É (2011) Protein purification (chromatographic techniques) and analysis (SDS-PAGE, 2DE, mass spectrometry). Protein Biotechnology, Hungary.

8. Muronetz VI, Sholukh M, Korpela T (2001) Use of protein-protein interactions in affinity chromatography. J Biochem Biophys Methods 49(1-3): 29-47.

9. Bauer A, Kuster B (2003) Affinity purification-mass spectrometry: Powerful tools for the characterization of protein complexes. Eur J Biochem 270(4): 570-578.

10. Dunham WH, Mullin M, Gingras AC (2012) Affinity-purification coupled to mass spectrometry: Basic principles and strategies. Proteomics 12(10): 1576-1590.

11. Belanger KD (2009) Using affinity chromatography to investigate novel protein-protein interactions in an undergraduate cell and molecular biology lab course. CBE Life Sci Educ 8(3): 214-225.

12. Hutchens TW, Yip TT, Porath J (1988) Protein interaction with immobilized ligands: Quantitative analyses of equilibrium partition data and comparison with analytical chromatographic approaches using immobilized metal affinity adsorbents. Analytical Biochemistry 170(1): 168-182.

13. Hoffmann A, RG Roeder (1991) Purification of his-tagged proteins in non-denaturing conditions suggests a convenient method for protein interaction studies. Nucleic Acids Res 19(22): 6337-6338.

14. Cuatrecasas P (1970) Protein Purification by Affinity Chromatography: derivatizations of agarose and polyacrylamide beads The Journal of Biological Chemistry 245: 3059-3065.

15. Porath J (1992) Immobilized metal ion affinity chromatography. Protein Expression and Purification 3(4): 263-281.

16. Porath J, B Olin (1983) Immobilized metal affinity adsorption and immobilized metal affinity chromatography of biomaterials. Serum protein affinities for gel-immobilized iron and nickel ions. Biochemistry 22(7): 1621-1630.

17. Safarik I, Safarikova M (2004) Magnetic techniques for the isolation and purification of proteins and peptides," BioMagnetic Research and Technology 2(7): 1-17.

18. Franzreb F, Siemann-Herzberg M, Hobley TJ, Thomas ORT (2006) Protein purification using magnetic adsorbent particles. Applied Microbiology and Biotechnology 70(5): 505-516.

19. Peter JF, Otto AM (2010) Magnetic particles as powerful purification tool for high sensitive mass spectrometric screening procedures. Proteomics 10(4): 628-633.

20. Fischer I, Hsu CC, Gärtner M, Müller C, Overton TW, et al. (2013) Continuous protein purification using functionalized magnetic nanoparticles in aqueous micellar two-phase systems. J Chromatogr A 1305: 7-16.

21. Kim JH, Yoon JY (2002) Protein adsorption on polymer particles. Surface and Colloid Science, pp. 4373-4381.

22. Hoshino Y, Haberaecker WW, Kodama T, Zeng Z, Okahata YS (2010) Affinity Purification of Multifunctional Polymer Nanoparticles. J Am Chem Soc 132(39): 13648-13650.

23. Boyer C, X Huang, Whittaker MR, V Bulmus, Davis TP (2011) An overview of protein-polymer particles. Soft Matter 7: 1599-1614.

24. Hoshino Y, Lee H, Y Miura (2014) Interaction between synthetic particles and biomacromolecules: fundamental study of nonspecific interaction and design of nanoparticles that recognize target molecules. Polymer Journal 46: 537-545.

25. Saha K, Agasti SS, Kim C, Li X, Rotello VM (2012) Gold nanoparticles in chemical and biological sensing. Chem Rev 112(5): 2739-2779.

26. Khandare J, Calderón M, Dagia NM, Haag R (2012) Multifunctional dendritic polymers in nanomedicine: opportunities and challenges. Chem Soc Rev 41(7): 2824-2848.

27. Smith MH, Lyon LA (2012) Multifunctional nanogels for siRNA delivery. Acc Chem Res 45(7): 985-993.

28. Hoshino Y, Koide H, Furuya K, Haberaecker WW, Lee SH, et.al. (2012) The rational design of a synthetic polymer nanoparticle that neutralizes a toxic peptide *in vivo*. Proc Natl Acad Sci U S A 109(1): 33-38.

29. Yoshimatsu K1, Lesel BK, Yonamine Y, Beierle JM, Hoshino Y, et al. (2012) Temperature-Responsive "Catch and Release" of Proteins by using Multifunctional Polymer-Based Nanoparticles. Angew Chem Int Ed Engl 51(10): 2405-2408.

30. Yonamine Y, Yoshimatsu K, Lee SH, Hoshino Y, Okahata Y, et al. (2013) Polymer nanoparticle-protein interface. Evaluation of the contribution of positively charged functional groups to protein affinity. ACS Appl Mater Interfaces 5(2): 374-379.

31. Monopoli MP, C Aberg, A Salvati, Dawson KA (2012) Biomolecular coronas provide the biological identity of nanosized materials. Nat Nanotechnol 7(12): 779-786.

32. Kim ST, Saha K, Kim C, Rotello VM (2013) The role of surface functionality in determining nanoparticle cytotoxicity. Acc Chem Res 46(3): 681-691.

33. Fischer NO, McIntosh CM, Simard JM, Rotello VM (2002) Inhibition of chymotrypsin through surface binding using nanoparticle-based receptors. Proc Natl Acad Sci USA 99(8): 5018-5023.

34. Zeng Z, Patel J, Lee SH, Mc Callum M, Tyagi A, et al. (2012) Synthetic Polymer Nanoparticle-Polysaccharide Interactions: A Systematic Study. J Am Chem Soc vol 134(5): 2681-2690.

35. Sun W, H Bandmann, T Schrader (2007) A Fluorescent Polymeric Heparin Sensor. Chemistry A European Journal 13(27): 7701-7707.

36. Yoshimatsu K, Yamazaki T, Hoshino Y, Rose PE, Epstein LF, et.al. (2014) Epitope Discovery for a Synthetic Polymer Nanoparticle: A New Strategy for Developing a Peptide Tag. J Am Chem Soc 136(4): 1194-1197.

37. Hoshino Y, Urakami T, Kodama T, Koide H, Oku N, et.al. (2009) Design of synthetic polymer nanoparticles that capture and neutralize a toxic peptide. Small 5(13): 1562-1568.

38. Hoshino Y, Koide H, Urakami T, Kanazawa H, Kodama T, et.al. (2010) Recognition, neutralization and clearance of target peptides in the blood stream of living mice by molecular imprinted polymer nanoparticles: a plastic antibody. J Am Chem Soc 132(19): 6644-6645.

39. Shih Hui Lee, Yu Hoshino, Arlo Randall, Zhiyang Zeng, Piere Baldi, et al. (2012) Engineered synthetic polymer nanoparticles as IgG affinity ligands. Journal of the American Chemical Society 134(38): 15765-15772.

40. Yonamine Y, Hoshino Y, Shea KJ (2012) ELISA-mimic screen for synthetic polymer nanoparticles with high affinity to target proteins. Biomacromolecules 13(9): 2952-2957.

Biopolymeric self-assembled nanoparticles for enhanced antibacterial activity of Ag-based compounds

CrossMark

Dhanya Dhanyalayam[a,1], Luca Scrivano[a,1], Ortensia Ilaria Parisi[a],
Maria Stefania Sinicropi[a], Antonietta Fazio[a], Carmela Saturnino[b,*],
Maria Rosaria Plutino[c], Francesca Di Cristo[d], Francesco Puoci[a,*], Anna Rita Cappello[a,2],
Pasquale Longo[e,2]

[a] Department of Pharmacy, Health and Nutritional Sciences, University of Calabria, 87036 Rende (CS), Italy
[b] Department of Sciences, University of Basilicata, Potenza, Italy
[c] Institute for the Study of Nanostructured Materials, ISMN-CNR, O.U. Palermo, Deptartment of ChiBioFarAm, University of Messina, Viale F. Stagno d'Alcontres 31, Vill. S. Agata, 98166 Messina, Italy
[d] Department of Pharmaceutical and Biomedical Sciences, University of Salerno, Fisciano (SA) Italy
[e] Department of Chemistry and Biology, University of Salerno, Fisciano (SA), Italy

A R T I C L E   I N F O

A B S T R A C T

Microbial infections still remain one of the main issues for human health. The rapid development of resistance towards the most common antimicrobial drugs in bacteria represents today a challenge in the infections management. In the present work we have investigated the antibacterial activity of a group of compounds, namely silver N-heterocyclic carbene complexes, against a broad spectrum of bacteria. For the most promising compound, a biopolymeric nanocarrier has been developed, in order to potentiate the metal complex activity against both Gram +ve and Gram −ve. The polymeric nanovehicle is based on dextran, modified with oleic acid residues, that confer amphiphilic properties to the polysaccharide. We have characterized the obtained biomaterial and studied its ability to self-assemble into nanoparticles in aqueous environment. Next, the transdermal diffusion analyses have been carried out to evaluate the ability of the polymeric particles to penetrate tissues. Thanks to the strategy adopted, we have fabricated an antibacterial system to which K. pneumoniae and E. coli are the most sensitive.

© 2016 Published by Elsevier B.V.

1. Introduction

Microbial infections are still one of the major causes of death among world population. It is estimated that 26% of the total global deaths are caused by infectious diseases (IDs) and in sub-Saharan Africa, in particular, deaths for IDs reach 50–52% (Becker et al., 2006). Antibiotics are certainly an important weapon against IDs, however, their wide use to control microbial infections in humans, animals and in agriculture has caused the development of resistance in bacterial populations. Over time, this phenomenon has enabled the selection of drug-resistant bacteria, acquiring survival ability through three main mechanisms: the capture by bacteria of resistance genes from the surrounding environment; the freezing of polymorphism in antibiotic target genes that imparts drug-resistance (Andersson and Hughes, 2011); and the up-regulation of proteins involved in drug efflux (Cox and Wright, 2013; Fajardo et al., 2008) or enzymatic inactivation (Abraham and Chain, 1940). Besides this the infections, caused by Gram −ve bacteria, are difficult to treat because these organisms have a protective outer membrane consisting of lipopolysaccharides (Pagès et al., 2008).

For this reason, there is an urgent need of new antimicrobial agents that express antibacterial activity, particularly against Gram −ve pathogens and that could be used to fight drug resistance.

Metallic silver, silver salts and silver complexes have been used since antiquity in a variety of applications like water purification, wound management, eye-drops, anti-infective coatings in medical devices and in burn treatment because they have potent antimicrobial properties but low human toxicity (Clement and Jarrett, 1994; Klasen, 2000a; Tambe et al., 2001). Several silver

compounds have been proven to be effective also in the treatment of open wounds, and suppurating wounds, chronic osteomyelitis, and urinary tract infections (De Gracia, 2001; Silver et al., 2006) and, among the various silver containing species, silver complexes are particularly interesting since the antimicrobial activity can be changed by varying type of ligands coordinated to silver (Özdemir et al., 2010). For example, the Ag(I) imidazolate complex has antibacterial and antifungal properties (Nomiya et al., 1997).

Nowadays among the silver derivatives, silver sulfadiazine remains one of the most common drug used in wound therapy and medicinal devices, although it causes severe adverse effects, and it delays wound healing due to its cytotoxicity towards fibroblasts and keratinocytes (Kalinowska-Lis et al., 2016).

Although the cytotoxic effects of silver compounds against Gram +ve and Gram −ve bacteria have long been established, the exact mechanisms of action are not completely understood (Kyros et al., 2014). It has been reported that Ag$^+$-treated bacterial cells show destabilization of the cellular envelope and increased membrane permeability (Morones-Ramirez et al., 2013); moreover, their cytoplasm displays molecules of condensed DNA that lose their ability to replicate. Another mechanism suggests that the silver binds to some components within the bacterial cell, inducing the subsequent inhibition of bacterial growth (Kyros et al., 2014; Modak and Fox, 1973). These changes can potentiate the activity of a broad range of antibiotics against Gram −ve bacteria as well as restore the antibiotic susceptibility of resistant bacterial strains (Morones-Ramirez et al., 2013).

In view of this, new and effective antimicrobial agents are required urgently. In recent years, there has been a considerable trend toward the development of metal complexes having biological properties (Chimento et al., 2015; Napoli et al., 2011; Saturnino et al., 2014; Sirignano et al., 2013a).

Metal *N*-heterocyclic carbene (M-NHC) complexes have appeared as an emerging field of research in medicinal chemistry where NHC complexes of coinage metals (Cu, Au, and Ag) proved to be better anticancer and antimicrobial agents (Iqbal et al., 2013; Melaiye et al., 2004; Tan et al., 2010).

For their excellent chemical properties and quite easy synthesis, different examples of NHC complexes of silver, gold platinum or other transition metals have been biologically evaluated, and they seem to have promising properties in biomedical sciences. (Bruno et al., 1995; Oehninger et al., 2013; Patil et al., 2015; Saturnino et al., 2010, 2014; Sirignano et al., 2013b). In particular, Ag-NHCs have long been used as antimicrobial agents for their high stability (Klasen, 2000b), as they can overcome the drawbacks associated with conventional silver antibiotics including resistance and fast loss of activity (Sinicropi et al., 2010a, 2010b).

Silver-*N*-heterocyclic carbene complexes can, in fact, slowly release silver ions into the wound, enabling better prevention of infection and promoting healing (Hindi et al., 2008).

Herein we have investigated the in vitro efficacy against a broad spectrum of bacteria of a small library of silver *N*-heterocycles carbene complexes, Ag(1)-NHC, synthesized from some of us (Napoli et al., 2013).

The studied silver carbene complexes are of type [AgL$_2$]$^+$[AgI$_2$]$^-$ (Mariconda et al., 2014). In particular we have studied: Iodide[*N*-methyl-*N*-(2-hydoxy-cyclopentyl-imidazole-2-ylidine)]silver(I), Iodide[*N*-methyl-*N*-(2-hydoxy-cyclohexyl)-imidazole-2-ylidine]silver(I) and Iodide[*N*-methyl-*N*-(2-hydoxy-2-phenyl)ethyl-imidazole-2-ylidine]silver(I), namely AgL6, AgL18 and AgL20 respectively (Fig. 1). For AgL6, in particular, also a polymeric nanocarrier has been developed, in order to increase its efficacy.

Nanosystems have been proven to be successful antimicrobial carrier due to targeted drug delivery at infection sites, reduced drug-resistance by microbial organism and increased therapeutic
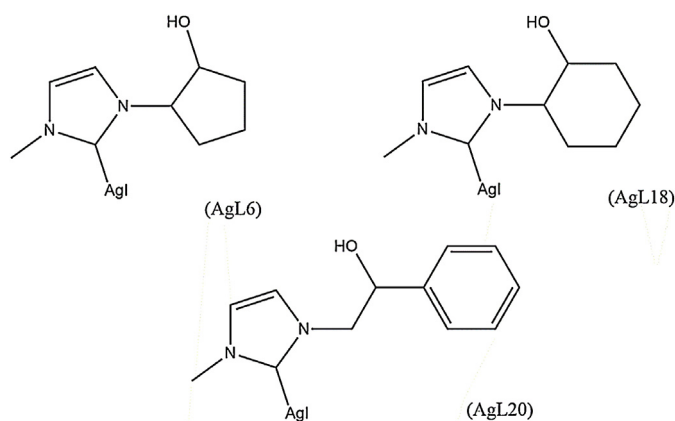
Fig. 1. Chemical structures of AgL6, AgL18 and AgL20.

index. These actions reduce side effects and improve patient compliance thanks to the decreased frequency of administrations.

Many materials can be used to prepare nanocarriers, such as lipids, polymers or inorganic particles. Among these, polymers are greatly interesting, due to the possibility of modification of their physico-chemical properties. Many polymeric particles can be produced, each characterized by peculiar properties. Hydrogels, dendrimers, drug-polymer conjugates and polymer vesicles represent few examples of nanosized particles based on polymeric materials and used as drug delivery systems.

Polymer nanovesicles are nanosized drug carriers, auto-assembled from amphiphilic block copolymers. They are organized in nanostructures in which the hydrophobic parts are inserted in the middle of the membrane, while the hydrophilic parts are exposed on both the inner and outer surfaces, delimiting a central aqueous core separated from the outside environment (Levine et al., 2008). This organization represents the major advantage of this kind of nanostructures, that can encapsulate hydrosoluble drugs in the aqueous core, and also hydrophobic or amphiphilic compounds in the thick membrane. Although they are generally identified as an individual type of drug nanocarriers, they should be considered as being a category of nanoparticles with a 'reservoir' architecture type (nanocapsules). The diversity of the building blocks can also be used to impart properties such as responsiveness to environmental stimuli, either endogenous (i.e. pH, enzymes, oxidative stress, etc.) or exogenous (i.e. temperature, magnetic field, light, ultrasound) (Ahmed et al., 2006a, 2006b; Discher and Ahmed, 2006; Onaca et al., 2009). Polymeric nanovesicles can also be engineered for selective delivery through targeting molecules linkage to outer surface (Meng et al., 2005).

Despite a large number of scientific papers describing the development of polymer nanovesicles as drug delivery systems, only few have explored their application to antimicrobials (Geilich et al., 2015; Wayakanon et al., 2013).

Therefore, here we describe for the first time the production of polymer nanostructured in which dextran, a biopolymer widely used in the pharmaceutical field (Vittorio et al., 2012), and oleate residues represents the hydrophilic and the hydrophobic parts, respectively. The nanoparticles were loaded with one of the synthesized Ag-based drug, whose antimicrobial activity was not investigated yet.

2. Materials and methods

2.1. Materials

Dextran, sodium oleate, disodium hydrogen phosphate, sodium dihydrogen phosphate, potassium bromide (KBr), pyrene,

dicyclohexyl carbodiimide (DCC), dimethylaminopyridine (DMAP), methanol, ethanol absolute, dimethyl sulfoxide (DMSO) and tetrahydrofuran (THF) were purchased by Sigma-Aldrich (Sigma Chemical Co., St. Louis, MO, USA). Dialysis tube (MWCO: 12000–14000 Da) were also provided by Sigma-Aldrich.

2.2. Instrumentations

Absorption spectra were recorded with a UV–vis JASCO V-530 spectrometer using 1 cm quartz cells.

Particles size and distribution were determined by Dynamic Light Scattering (DLS) analyses using a 90 Plus particle size analyzer (Brookhaven Instruments Corporation, New York, NY USA), at $25.0 \pm 0.1\,°C$ by measuring the autocorrelation function at $90°$. The laser was operating at 658 nm. The distribution size was directly obtained from the instrument fitting data by the inverse "Laplace transformation" method and by Contin methods (Provencher, 1982). The polydispersity index (P.I.) was used as a measure of the width of size distribution. P.I. less than 0.3 indicates a homogenous population of particles.

Each sample was measured three times and the results are expressed as mean $\pm$ standard deviation. IR spectra were recorded as KBr pellets on a Jasco FT-IR 4200.

2.3. Dextran-oleate synthesis

The coupling of dextran and sodium oleate was achieved as follows: 500 mg of dextran were dissolved in 50 mL of DMSO. After complete dissolution, 100 mg of sodium oleate, 68 mg of DCC and 40 mg of DMAP, were added to the solution and left under magnetic stirring, for 4 h at 60 °C, and at room temperature overnight. In order to recover the oleate-grafted dextran, the purification step was performed by precipitating the reaction mixture in cold ethanol. Then the product was collected in dialysis membrane and dialyzed against a mixture ethanol/water 50:50 for 24 h and against distilled water for further 48 h. Finally, dextran oleate was recovered and freeze-dried to a powder.

2.4. Determination of the critical aggregation concentration

The critical aggregation concentration (CAC) of the dextran oleate aqueous solution was determined by fluorescence method using pyrene as a nonpolar fluorescent probe. 24.0 μL of pyrene solution (2.5×10^{-5} M) in acetone were added in vials and evaporated under vacuum. Amounts of dextran oleate solution at various concentrations were added to the pyrene vials leading to a final pyrene concentration of 6.0×10^{-7} M. The mixture was kept under agitation for 4–5 h. Fluorescence measurements were conducted on each sample (excitation = 333 nm, emission = 350–500 nm) at a $90°$ angle in a 1 cm quartz cuvette. The average ratio of the intensity of the vibronic bands at 372 nm (I_1) over 383 nm (I_3), obtained from the fluorescence emission spectra of pyrene recorded at 25 °C, was plotted vs. log of the concentration for each sample. The CAC was determined as the polymer concentration at the intersection point of two regression lines.

2.5. Self-assembling of the polymer vesicle

5 mg of dextran oelate was dissolved in 10 mL of THF in a 50 mL round bottom flask. Next, 10 mL of phosphate buffer saline solution (0.01 M, pH 7.4) were gently poured along the flask walls. The organic solvent was removed using a rotary evaporator, under reduced pressure at 40 °C and 40 rpm, yielding the dextran oleate vesicles suspension. AgL6 loaded vesicles were prepared as described above, by adding 1 mL of AgL6 solution to the phosphate buffer.

2.6. Drug encapsulation efficiency

Drug encapsulation efficiency was determined using the dialysis method for separating the non-entrapped drug from dextran oleate vesicles (DOVs) (Maestrelli et al., 2005). According to this technique, 3 mL of AgL6-loaded DOVs dispersion were dropped into a dialysis bag immersed in 10 mL of distilled water and magnetically stirred. Free drug was dialyzed for 30 min each time and the dialysis was complete when no drug was detectable in the recipient solution. The encapsulation efficiency was expressed as the percentage of the drug entrapped into DOVs referred to the total amount of drug that is present in the non-dialyzed sample. It was determined by diluting 1 mL of dialyzed and 1 mL of non-dialyzed DOVs in 25 mL of methanol and obtaining two solutions whose concentrations are represented in equation 1 by [ND] and [D], respectively. The concentrations of AgL6 where calculated by measuring the absorbance of the two solutions between 200 nm and 400 nm. This procedure was necessary to breakdown DOVs.

$$Encapsulation\ efficiency\ (\%) = \frac{[ND] - [D]}{[ND]} \times 100 \tag{1}$$

2.7. In vitro diffusion study

In vitro diffusion studies were performed at $37 \pm 0.5\,°C$ using Franz diffusion cells (Disa, Milan, Italy; permeation area $0.4614\,cm^2$).

For this purpose, Strat-M® membrane (Merck-Millipore) was placed between the donor and receptor compartments of the Franz cells and, then, the compartments were clamped together ensuring that the shiny side of the membrane was facing the donor compartment.

The receptor compartment was filled with 5.5 mL of phosphate buffer at pH 7.4 (1.0×10^{-3} M) and, after 20–30 min when the receptor solution reached 37 °C, 0.5 mL of the AgL6-loaded DOVs suspension were added to the donor compartment, which was covered with Parafilm™ in order to prevent any loss. The content of the receptor compartment was removed at 1, 2, 4, 6, 8 and 24 h for UV–vis analysis and, at each time point, the amount withdrawn was replaced with fresh phosphate buffer. The in vitro diffusion experiments were performed in triplicate.

2.8. Bacterial strains

The strains *Escherichia coli* (ATCC 25922), *Klebsiella pneumoniae* (ATCC 13883), *Pseudomonas aeruginosa* (ATCC 27853), *Staphylococcus aureus* (ATCC 25923) and *Streptococcus pyogenes* (ATCC 19615) were provided by REMEL. The cells were grown in Müller-Hinton broth II (MHB; Difco, Detroit, MI, USA) containing 2 g/L beef infusion solids, 17.5 g/L casein hydrolysate, 1.5 g/L starch. The final pH was adjusted to 7.4.

2.9. Antimicrobial tests

2.9.1. Disc-diffusion susceptibility testing

The antimicrobial susceptibilities of the Ag-NHCs complexes were evaluated using the Kirby-Bauer disc-diffusion method (Bauer et al., 1966; Benson, 1998; Benson2002), performed according to CLSI guidelines and results were interpreted using CLSI breakpoints (Clinical and Laboratory Standards Institute, 2012a, 2013). Cefotaxime discs (10 μg; from Oxoid™) and silver sulfadiazine (AgSD) discs (32 μg) were used as positive controls. The stock solutions of AgSD (from Sigma/Aldrich Company; St. Louis, MO, USA) and of all complexes were prepared by dissolving them in dimethyl sulfoxide (DMSO, from Sigma/Aldrich Company;

St. Louis, MO, USA) and were utilized to impregnate the Blank Antimicrobial Susceptibility Disks (Oxoid[TM]).

Specifically, overnight cultures of bacteria tested were adjusted to a turbidity of 0.5 McFarland standards (10^6 CFU/mL) before inoculation onto agar plates with sterile cotton swabs. A cotton swab dipped in the cell culture was streaked onto an agar plate surface in such a way as to obtain a uniform layer of bacteria across the whole surface. After 10–15 min, the cefotaxime or AgSD or novel complex discs were laid on the inoculated surface of the agar plates; then, all agar plates were incubated at 37 °C, overnight. The diameters of inhibition were measured and susceptibility was expressed in terms of resistance (R), moderate susceptibility (I) and susceptibility (S).

Agar plates inoculated with bacteria tested with impregnated DMSO discs were used as controls. Analysis for each combination of bacteria tested and discs with positive controls and with several new compounds were repeated three times.

2.9.2. Determination of MIC and MBC values

The minimum inhibitory concentration (MIC) of the antibacterial compounds was determined using the broth dilution method, according to CLSI guidelines (Clinical and Laboratory Standards Institute, 2012b). Briefly, a solution of each Ag complex was diluted, serially, with MHB medium. Then, the suspensions of the microorganisms, prepared from overnight cultures of bacteria in the MHB medium, at a concentration of 10^6 cfu mL^{-1}, were added to each dilution in a 1:1 ratio. Growth (or lack thereof) of the microorganisms was determined visually after incubation for 24 h at 37 °C. AgSD and cefotaxime were also included as positive controls. The lowest concentration at which there was no visible growth (turbidity) was considered as the MIC value.

In order to determine the minimum bactericidal concentration (MBC), 10 μL aliquots of dilution representing the MIC value, and at least three of the more concentrated dilutions of the Ag-NHCs, cefotaxime and AgSD, were plated on Müller-Hinton agar. Then, the plates were incubated for 24 h, at 37 °C. The MBC values were determined as the lowest concentration that causes at least a 99.9%
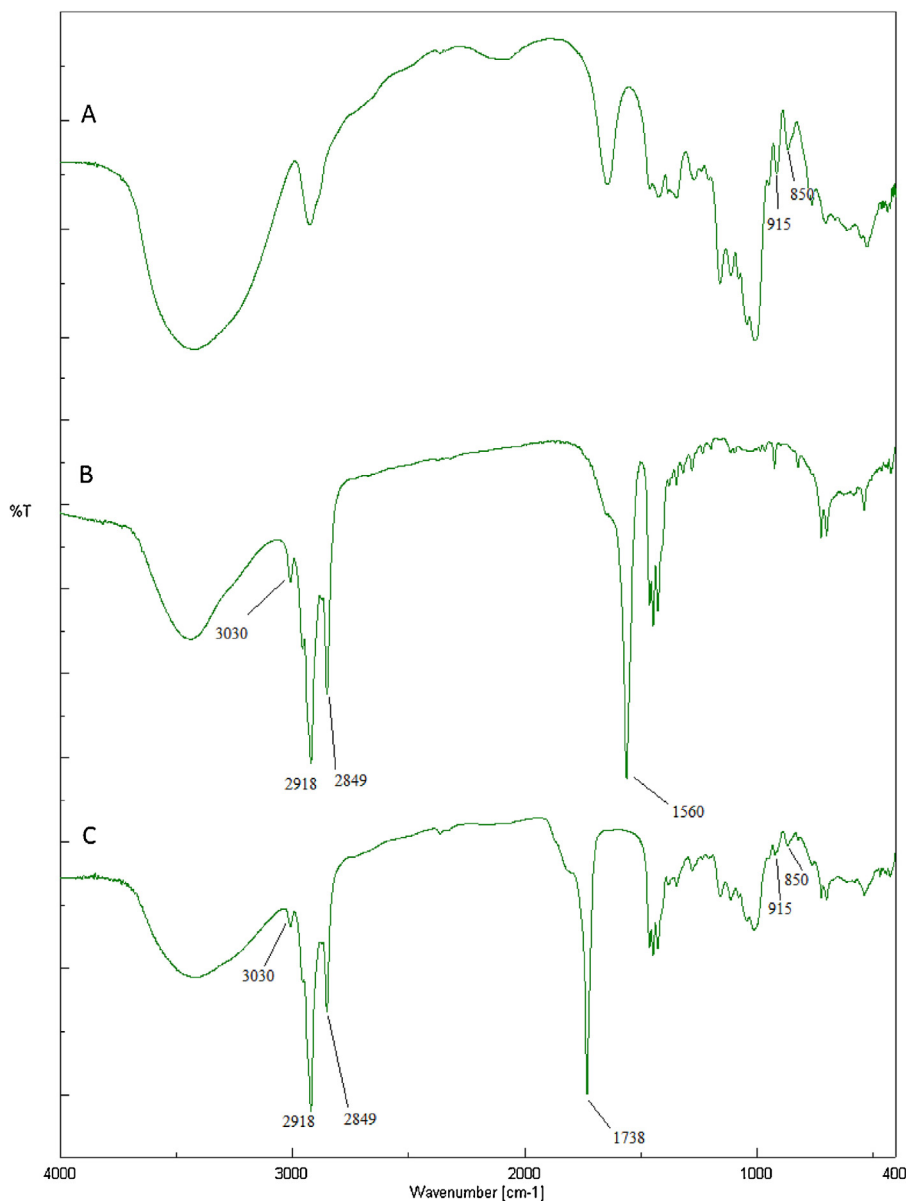

Fig. 2. FT-IR apectra of (A) dextran, (B) sodium oleate and (C) dextran oleate.

decrease in cfu mL^{-1} relative to the initial concentration (Kalinowska-Lis et al., 2014).

The negative control tubes did not contain bacterial inoculum while the positive control (or turbid) tubes were free of the compounds and contained only DMSO. The tests were repeated in triplicate.

3. Results and discussion

3.1. Polymer vesicles characterization

Evaluation by FT-IR spectra analyses has been performed in order to verify the coupling of oleate onto dextran backbone, comparing the FT-IR spectra of sodium oleate, dextran and dextran oleate conjugate. The sodium oleate spectrum (Fig. 2—Trace B) shows a strong peak at 1560 cm^{-1}, which is the typical signal of the C=O stretching vibration of the carboxylic salt group. It can be also observed the presence of strong signals between 2849 and 2950 cm^{-1} corresponding to stretching vibration of the C—H bond of the alkane portion of the molecule; while the double bond can be identified thanks to the band at 3030 cm^{-1}, corresponding to the stretching vibration of =C—H bond. Dextran spectrum (Fig. 2—Trace A), on the contrary, does not show any signal that can be ascribed to C=O double bond, which is obviously absent in dextran structure. But information about the conformation of the polysaccharide can be acquired in the region 600–950 cm^{-1}. A peak in the 885–925 cm^{-1} region is the evidence of two CH in the axial position (AA), in the 825–855 cm^{-1} region the equatorial-axial position (EA), in the 790–825 cm^{-1} region in the equatorial–equatorial position (EE) and in 860–885 cm^{-1} region in the axial-equatorial position (AE). The bands around 915 cm^{-1} and 850 cm^{-1}, indicating AA and EA fragments, confirm the glucopyranosyl conformation, which is not affected by oleate conjugation. In dextran oleate spectrum (Fig. 2—Trace C), in fact, these peaks are preserved, while a new strong band appeared. It can be found around 1740 cm^{-1} indicating the presence of C=O bond stretching vibration of an ester group. This group came from the oleate moieties, but its spectroscopic signal has been shifted towards higher frequencies. This is certainly due to the new formation of the ester bond.

The polymer nanovesicles were prepared by self-assembling procedure and their dimensions were analyzed by dynamic light scattering.

Table 1
Dimensional data. DOVs size and size distribution of both empty and AgL6-loaded DOVs are expressed as mean diameter ± standard deviation and polydispersity index (P.I.).

	Mean diameter	Polydispersity index
DOVs	525 ± 14 nm	0.214
DOVs-AgL6	613 ± 17 nm	0.268

The self-assembling technique involves the dissolution of the amphiphilic polymer in organic solvent, followed by the introduction of the aqueous phase, represented by phosphate buffer saline (PBS) solution at pH = 7.4. The apolar organic phase is then removed under reduced pressure decreasing the dissolution of the hydrophobic block of dextran oleate. This led to the increase of hydrophilicity of the phase and, consequently, to the self-assembly of the nanosized DOVs.

The dimensional characterization of DOVs and DOVs-AgL6 was performed with DLS, putting a small amount of polymer vesicles in the PBS solution at pH 7.4. The mean hydrodynamic diameter found was different for the two polymer batches: 525 nm and 613 nm for DOVs and DOVs-AgL6, respectively (Fig. 3). Data collected in Table 1, shows the presence of monodisperse homogeneous population of both empty and AgL6-loaded vesicles. Polydispersity index value is, in fact, below 0.3 and the mean diameter is below 700 nm.

There is a difference of almost 100 nm between the two systems and that can be ascribed to the presence of encapsulated drug. It seems that the presence of AgL6 in solution negatively affects the self-assembling of dextran oleate vesicles, resulting in larger nanoparticles. In particular, the Ag atoms can interfere with vesicles formation, due to its nature. However, the negative effect on DOVs dimension does not compromise their formation maintaining a mean diameter far below 1 μm.

The amphiphilic character was conferred to dextran thanks to the conjugation with a hydrophobic group, i.e. the oleate residue. The so modified polysaccharide acquired the ability to self-assemble in an aqueous environment via hydrophobic interaction between lipid moieties.

The critical aggregation concentration (CAC) of dextran oleate in water was estimated from the dependence of pyrene fluorescence spectra (I_{372}/I_{383} ratio) as a function of the polysaccharide-
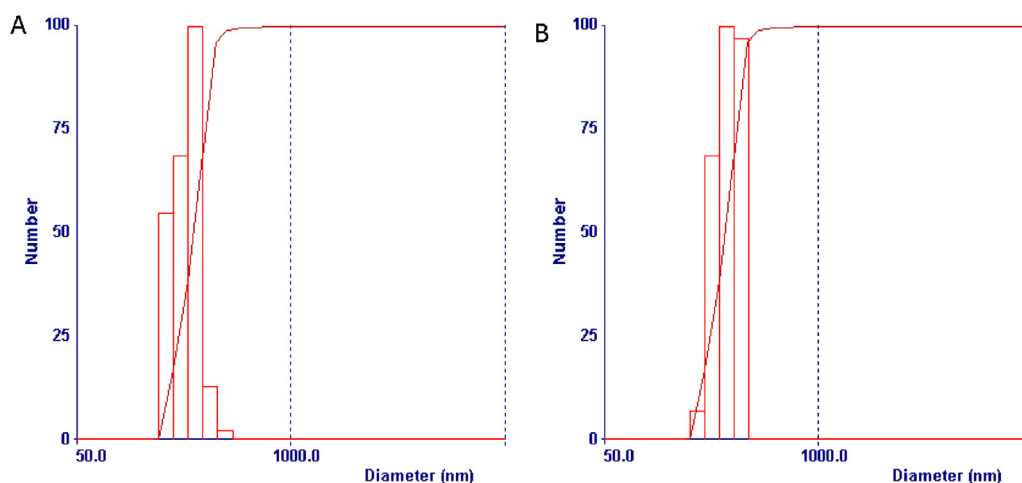
Fig. 3. Graph of size and size distribution obtained by DLS analysis of DOVs (Panel A) and DOVs-AgL6 (Panel B).
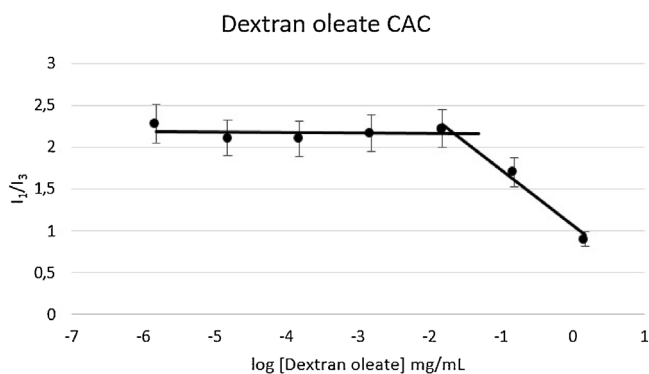
Fig. 4. Ratio of pyrene I_1/I_3 band fluorescence at various concentrations of dextran oleate in water. The critical aggregation concentration was calculated as the intersection point of the two linear regions of the plots.

lipid concentration (Fig. 4). A sharp change was observed from 14 μg/mL, which was considered to be the CAC.

3.2. Drug encapsulation and release profile

Polymer nanovesicles possess the advantage of being optimal carrier for both hydrophobic and hydrophilic drugs, which can be loaded in the lipophilic membrane or in the aqueous core, respectively.

Dextran oleate vesicles (DOVs) were loaded with AgL6 during self-assembling and drug encapsulation was measured by UV–vis spectrophotometry after dialysis against distilled water. The encapsulation efficiency has been calculated according to the equation 1 reported in the experimental method section. The obtained value for AgL6 was ca. 76%, supporting the vesicular structure of the carrier.

Strat-M® membranes, which are a synthetic model that is predictive of diffusion in human skin, were employed for transdermal diffusion testing. The diffusion of AgL6-loaded DOVs was compared to free AgL6 and the results are reported in Fig. 5. From the release profile depicted in the figure, it is evident an increased amount of AgL6 recovered in the acceptor compartment of Franz diffusion cells from DOVs-AgL6, since the time point of 2 h, if compared to free AgL6. The trend is much more evident in the following hours, when DOVs-AgL6 released almost 95% of its payload after 24 h. On the other hand, free AgL6 diffusion is limited and it is not complete at the end point. The data confirmed that DOVs enhance drug penetration through limiting barriers, such as

the skin. AgL6 incomplete penetration is certainly due to the chemical properties of the compound, which possesses a partial hydrophilicity that inhibits the absorption of the entire amount of drug (Saturnino et al., 2016).

3.3. Antimicrobial activity

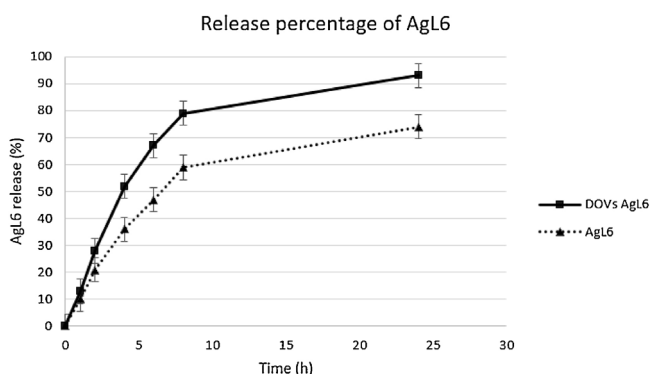The antimicrobial activity of the Ag-NHCs was measured against two Gram +ve (*S. aureus* and *S. pyogenes*) and three Gram −ve bacterial strains (*E. coli, K. pneumoniae* and *P. aeruginosa*). The inhibition ratios of the silver carbene complexes against pathogenic strains were calculated from inhibition diameters values, measured at 32, 64 and 128 μg of each tested compound. The average of three inhibition zone diameter measurements was compared against commercial drugs (commercial cephalosporin cefotaxime and silver sulfadiazine (AgSD), commonly used in the treatment of skin infections), using the disc-diffusion susceptibility test (Kirby-Bauer test) (Bauer et al., 1966).

Final interpretation of the measurements enabled all of the bacteria strains tested to be grouped into three categories (Sensitive, Intermediate and Resistant) as summarized in Table 2. No inhibition zone was seen in the control (DMSO) (Data not shown).

The antibiotic sensitivity profile of the bacterial strains showed that, among the Ag-NHCs complexes tested, only AgL6 displayed antimicrobial activity against the microorganisms, but only when tested in large amounts, in comparison with cefotaxime. Indeed, a comparison of data obtained on the inhibition zones of the pathogenic bacteria proved that all five bacterial strains were Sensitive to 32 and 128 μg AgL6. Moreover, this compound was more effective than AgSD toward the Gram −ve pathogens tested. However, it may be said that AgL18 and AgL20 were much less effective than AgL6 and only against the Gram −ve strains; indeed *E. coli, K. pneumoniae* and *P. aeruginosa* were intermediate to 128 μg AgL18 and AgL20.

The Kirby-Bauer test could only test the bacterial susceptibility to various antimicrobial reagents at pre-designed dosage. Such information as minimal inhibitory concentration (MIC) of a specific compound could not be obtained from this test. Therefore, in order to determine MIC values for AgL6, the broth dilution method was performed. As expected, the MIC determination results were in good agreement with the disc-diffusion susceptibility test (Table 3). For example, in the disc-diffusion test, all five bacteria were found to be Sensitive to AgL6; in the dilution experiment, the MIC of this compound was found to be very high against all the strains, particularly against Gram +ve bacteria (MIC values were 32 μg/mL). The values obtained were greater than those reported for the commercial drugs Cefotaxime (MIC ranging between 0.5 and 4 μg/mL) and AgSD (MIC ranging between 8 and 32 μg/mL). Both of these commercial drugs were found to be Sensitive according to the Kirby-Bauer test.

Similarly, minimal bactericidal concentration (MBC) values for AgL6 were also determined in bacterial cultures; the values were higher against Gram +ve bacteria than against Gram −ve bacteria.

Since limited cellular penetration could reduce the effectiveness of many antimicrobial treatments, we hypothesized that incorporating AgL6 into a "pharmaceutically-oriented device", such as DOVs, could improve its cellular uptake and, consequently, its antimicrobial activity.

Literature data reported that the incorporation of novel synthetic compounds into suitable drug carriers can improve their antimicrobial effect and, consequently, may be a very promising strategy to enhance their cellular uptake (Parisi et al., 2014).

The MIC and MBC values for Ag-NHCs, after its incorporation into the carrier, confirmed our hypothesis, evidencing improved activity against all the bacteria strains (Table 3). Indeed, all MIC and

Fig. 5. Transdermal diffusion profile of AgL6 and DOVs-AgL6.

Table 2
Antibiotic susceptibility profiles.

Compounds	µg	Bacterial strains				
		Staphylococcus aureus ATCC 25923	*Streptococcus pyogenes* ATCC 19615	*Escherichia coli* ATCC 25922	*Klebsiella pneumoniae* ATCC 13883	*Pseudomonas aeruginosa* ATCC 27853
Cefotaxime	10	S	S	S	S	S
Silver sulfadiazine (AgSD)	32	S	S	S	S	S
AgL6	32	S	S	S	S	S
	64	S	S	S	S	S
	128	S	S	S	S	S
AgL18	32	R	R	R	R	R
	64	R	R	R	R	R
	128	R	R	I	I	I
AgL20	32	R	R	R	R	R
	64	R	R	R	R	R
	128	R	R	I	I	I

S: Sensitive; R: Resistant; I: Intermediate.

Table 3
MIC (top rows) and MBC (bottom rows) values of the investigated compounds.

Compounds	MIC MBC (µg/mL)	Bacterial strains				
		Staphylococcus aureus ATCC 25923	*Streptococcus pyogenes* ATCC 19615	*Escherichia coli* ATCC 25922	*Klebsiella pneumoniae* ATCC 13883	*Pseudomonas aeruginosa* ATCC 27853
Cefotaxime	MIC	1	0.5	2	2	4
	MBC	1	1	4	2	8
Silver sulfadiazine (AgSD)	MIC	32	16	8	8	16
	MBC	32	32	16	16	16
AgL6	MIC	32	32	16	16	32
	MBC	64	64	32	32	32
DOVs	MIC	>128	>128	>128	>128	>128
	MBC	>128	>128	>128	>128	>128
DOVs-AgL6	MIC	8	8	4	4	8
	MBC	16	16	8	8	16

MBC values decreased four times against all bacteria tested, while only the MBC value, against *P. aeruginosa*, was reduced twofold.

These values were found to be closer to those for cefotaxime and, surprisingly, twofold lower than for AgSD. In contrast, the vehicle alone did not exhibit antibacterial activity (Table 3).

Finally, our outcomes showed *K. pneumoniae* and *E. coli* to be the most sensitive microorganisms to AgL6, followed by *P. aeruginosa* while the Gram +ve bacteria were less sensitive to the prepared complex.

4. Conclusion

The present study was aimed at investigating the antibacterial activity of silver *N*-heterocyclic carbene complexes. They were tested against both Gram +ve and Gram −ve bacteria. One of the compounds was found to be the most active (AgL6), while there is a natural bacterial resistance towards AgL18 and AgL20. The biopolymeric nanocarrier developed for AgL6 delivery, was successfully obtained by self-assembly of dextran oleate conjugate, in which dextran chain and oleic residues represent the hydrophilic and the hydrophobic parts of the amphiphilic material, respectively. The nanometric dimension of the particles have been confirmed by DLS analyses (mean diameter ranging between 500 and 600 nm). Finally, we have demonstrated that this nanosystem is an excellent tool that can greatly improve antibiotic activity of compounds, such as AgL6, reducing both MIC and MBC.

References

Özdemir, İ., Özcan, E.Ö., Günal, S., Gürbüz, N., 2010. Synthesis and antimicrobial activity of novel Ag-N-hetero-cyclic carbene complexes. Molecules 15, 2499–2508.

Abraham, E.P., Chain, E., 1940. An enzyme from bacteria able to destroy penicillin. Nature 146, 837.

Ahmed, F., Pakunlu, R.I., Brannan, A., Bates, F., Minko, T., Discher, D.E., 2006a. Biodegradable polymersomes loaded with both paclitaxel and doxorubicin permeate and shrink tumors, inducing apoptosis in proportion to accumulated drug. J. Control. Release 116, 150–158.

Ahmed, F., Pakunlu, R.I., Srinivas, G., Brannan, A., Bates, F., Klein, M.L., Minko, T., Discher, D.E., 2006b. Shrinkage of a rapidly growing tumor by drug-loaded polymersomes: pH-triggered release through copolymer degradation. Mol. Pharm. 3, 340–350.

Andersson, D.I., Hughes, D., 2011. Persistence of antibiotic resistance in bacterial populations. FEMS Microbiol. Rev. 35, 901–911.

Bauer, A., Kirby, W., Sherris, J.C., Turck, M., 1966. Antibiotic susceptibility testing by a standardized single disk method. Am. J. Clin. Pathol. 45, 493.

Becker, K., Hu, Y., Biller-Andorno, N., 2006. Infectious diseases—a global challenge. Int. J. Med. Microbiol. 296, 179–185.

Benson, H., 2002. Appendix A. Microbiological Applications: Laboratory Manual in General Microbiology. 8th ed. McGraw Hill, Boston, Massachusetts, pp. 432.

Benson, H., 1998. Antimicrobial Sensitivity Testing: The Kirby-Bauer Method. Microbiological Applications: Laboratory Manual in General Microbiology, 7th ed. McGraw Hill, Boston, Massachusetts, pp. 139–141.

Bruno, G., Nicolo, F., Loschiavo, S., Sinicropi, M.S., Tresoldi, G., 1995. Synthesis and spectroscopic properties of di-2-pyridyl sulfide (Dps) compounds—crystal-structure of [Ru(Dps)2cl2]. J. Chem. Soc. Dalton 17–24.

Chimento, A., Saturnino, C., Iacopetta, D., Mazzotta, R., Caruso, A., Plutino, M.R., Mariconda, A., Ramunno, A., Sinicropi, M.S., Pezzi, V., 2015. Inhibition of human topoisomerase I and II and anti-proliferative effects on MCF-7 cells by new titanocene complexes. Bioorg. Med. Chem. 23, 7302–7312.

Clement, J.L., Jarrett, P.S., 1994. Antibacterial silver. Met. Based Drugs 1, 467–482.

Clinical and Laboratory Standards Institute, 2012a. Performance Standard for Antimicrobial Disk Susceptibility Tests; Approved Standard, vol. 32. CLSI, PA, USA (Document M02-A11, No. 1).

Clinical and Laboratory Standards Institute, 2012b. Methods for Dilution Antimicrobial Susceptibility Test for Bacteria That Grow Aerobically; Approved Standards, 9th ed. CLSI, Wayne, PA (Document M07-A9).

Clinical and Laboratory Standards Institute, 2013. Performance Standards for Antimicrobial Susceptibility Testing. Twentieth Informational Supplement M100-S23. CLSI, Wayne, PA.

Cox, G., Wright, G.D., 2013. Intrinsic antibiotic resistance: mechanisms, origins, challenges and solutions. Int. J. Med. Microbiol. 303, 287–292.

De Gracia, C., 2001. An open study comparing topical silver sulfadiazine and topical silver sulfadiazine–cerium nitrate in the treatment of moderate and severe burns. Burns 27, 67–74.

Discher, D.E., Ahmed, F., 2006. Polymersomes. Annu. Rev. Biomed. Eng. 8, 323–341.

Fajardo, A., Martínez-Martín, N., Mercadillo, M., Galán, J.C., Ghysels, B., Matthijs, S., Cornelis, P., Wiehlmann, L., Tümmler, B., Baquero, F., 2008. The neglected intrinsic resistome of bacterial pathogens. PLoS One 3, e1619.

Geilich, B.M., van de Ven, A.L., Singleton, G.L., Sepúlveda, L.J., Sridhar, S., Webster, T.J., 2015. Silver nanoparticle-embedded polymersome nanocarriers for the treatment of antibiotic-resistant infections. Nanoscale 7, 3511–3519.

Hindi, K.M., Siciliano, T.J., Durmus, S., Panzner, M.J., Medvetz, D.A., Reddy, D.V., Hogue, L.A., Hovis, C.E., Hilliard, J.K., Mallet, R.J., 2008. Synthesis, stability, and antimicrobial studies of electronically tuned silver acetate N-heterocyclic carbenes. J. Med. Chem. 51, 1577–1583.

Iqbal, M.A., Haque, R.A., Ahamed, M.B.K., Majid, A.A., Al-Rawi, S.S., 2013. Synthesis and anticancer activity of para-xylyl linked bis-benzimidazolium salts and respective Ag (I) N-heterocyclic carbene complexes. Med. Chem. Res. 22, 2455–2466.

Kalinowska-Lis, U., Szewczyk, E.M., Chęcińska, L., Wojciechowski, J.M., Wolf, W.M., Ochocki, J., 2014. Synthesis, characterization, and antimicrobial activity of silver (I) and copper (II) complexes of phosphate derivatives of pyridine and benzimidazole. ChemMedChem 9, 169–176.

Kalinowska-Lis, U., Felczak, A., Chęcińska, L., Szabłowska-Gadomska, I., Patyna, E., Małecki, M., Lisowska, K., Ochocki, J., 2016. Antibacterial activity and cytotoxicity of silver (I) complexes of pyridine and (Benz) imidazole derivatives. X-ray crystal structure of [Ag (2, 6-di (CH2OH) py) 2] NO3. Molecules 21, 87.

Klasen, H., 2000a. Historical review of the use of silver in the treatment of burns. I. Early uses. Burns 26, 117–130.

Klasen, H.J., 2000b. A historical review of the use of silver in the treatment of burns. II. Renewed interest for silver. Burns 26, 131–138.

Kyros, L., Banti, C., Kourkoumelis, N., Kubicki, M., Sainis, I., Hadjikakou, S., 2014. Synthesis, characterization, and binding properties towards CT-DNA and lipoxygenase of mixed-ligand silver (I) complexes with 2-mercaptothiazole and its derivatives and triphenylphosphine. JBIC J. Biol. Inorg. Chem. 19, 449–464.

Levine, D.H., Ghoroghchian, P.P., Freudenberg, J., Zhang, G., Therien, M.J., Greene, M. I., Hammer, D.A., Murali, R., 2008. Polymersomes: a new multi-functional tool for cancer diagnosis and therapy. Methods 46, 25–32.

Maestrelli, F., González-Rodríguez, M.L., Rabasco, A.M., Mura, P., 2005. Preparation and characterisation of liposomes encapsulating ketoprofen–cyclodextrin complexes for transdermal drug delivery. Int. J. Pharm. 298, 55–67.

Mariconda, A., Grisi, F., Costabile, C., Falcone, S., Bertolasi, V., Longo, P., 2014. Synthesis, characterization and catalytic behaviour of a palladium complex bearing a hydroxy-functionalized N-heterocyclic carbene ligand. N. J. Chem. 38, 762–769.

Melaiye, A., Simons, R.S., Milsted, A., Pingitore, F., Wesdemiotis, C., Tessier, C.A., Youngs, W.J., 2004. Formation of water-soluble pincer silver (I)-carbene complexes: a novel antimicrobial agent. J. Med. Chem. 47, 973–977.

Meng, F., Engbers, G.H., Feijen, J., 2005. Biodegradable polymersomes as a basis for artificial cells: encapsulation, release and targeting. J. Control. Release 101, 187–198.

Modak, S.M., Fox, C.L., 1973. Binding of silver sulfadiazine to the cellular components of Pseudomonas aeruginosa. Biochem. Pharmacol. 22, 2391–2404.

Morones-Ramirez, J.R., Winkler, J.A., Spina, C.S., Collins, J.J., 2013. Silver enhances antibiotic activity against gram-negative bacteria. Sci. Transl. Med. 5 190ra181–190ra181.

Napoli, M., Saturnino, C., Sirignano, E., Popolo, A., Pinto, A., Longo, P., 2011. Synthesis, characterization and cytotoxicity studies of methoxy alkyl substituted metallocenes. Eur. J. Med. Chem. 46, 122–128.

Napoli, M., Saturnino, C., Cianciulli, E.I., Varcamonti, M., Zanfardino, A., Tommonaro, G., Longo, P., 2013. Silver (I) N-heterocyclic carbene complexes: synthesis, characterization and antibacterial activity. J. Organomet. Chem. 725, 46–53.

Nomiya, K., Tsuda, K., Sudoh, T., Oda, M., 1997. Ag (I)□N bond-containing compound showing wide spectra in effective antimicrobial activities: polymeric silver (I) imidazolate. J. Inorg. Biochem. 68, 39–44.

Oehninger, L., Rubbiani, R., Ott, I., 2013. N-Heterocyclic carbene metal complexes in medicinal chemistry. Dalton Trans. 42, 3269–3284.

Onaca, O., Enea, R., Hughes, D.W., Meier, W., 2009. Stimuli-responsive polymersomes as nanocarriers for drug and gene delivery. Macromol. Biosci. 9, 129–139.

Pagès, J.-M., James, C.E., Winterhalter, M., 2008. The porin and the permeating antibiotic: a selective diffusion barrier in Gram-negative bacteria. Nat. Rev. Microbiol. 6, 893–903.

Parisi, O.I., Fiorillo, M., Caruso, A., Cappello, A.R., Saturnino, C., Puoci, F., Panno, A., Dolce, V., El-Kashef, H., Sinicropi, M.S., 2014. Enhanced cellular uptake by pharmaceutically oriented devices of new simplified analogs of Linezolid with antimicrobial activity. Int. J. Pharm. 461, 163–170.

Patil, S.A., Patil, S.A., Patil, R., Keri, R.S., Budagumpi, S., Balakrishna, G.R., Tacke, M., 2015. N-heterocyclic carbene metal complexes as bio-organometallic antimicrobial and anticancer drugs. Future Med. Chem. 7, 1305–1333.

Provencher, S.W., 1982. A constrained regularization method for inverting data represented by linear algebraic or integral equations. Comput. Phys. Commun. 27, 213–227.

Saturnino, C., Napoli, M., Paolucci, G., Bortoluzzi, M., Popolo, A., Pinto, A., Longo, P., 2010. Synthesis and cytotoxic activities of group 3 metal complexes having monoanionic tridentate ligands. Eur. J. Med. Chem. 45, 4169–4174.

Saturnino, C., Sirignano, E., Botta, A., Sinicropi, M.S., Caruso, A., Pisano, A., Lappano, R., Maggiolini, M., Longo, P., 2014. New titanocene derivatives with high antiproliferative activity against breast cancer cells. Bioorg. Med. Chem. Lett. 24, 136–140.

Saturnino, C., Barone, I., Iacopetta, I., Mariconda, A., Sinicropi, M.S., Rosano, C., Campana, A., Catalano, S., Longo, P., Andò, S., 2016. N-heterocyclic carbene complexes of silver and gold as novel tools against breast cancer progression. Future Med. Chem. 8, 2213–2229.

Silver, S., Phung, L.T., Silver, G., 2006. Silver as biocides in burn and wound dressings and bacterial resistance to silver compounds. J. Ind. Microbiol. Biotechnol. 33, 627–634.

Sinicropi, M.S., Amantea, D., Caruso, A., Saturnino, C., 2010a. Chemical and biological properties of toxic metals and use of chelating agents for the pharmacological treatment of metal poisoning. Arch. Toxicol. 84, 501–520.

Sinicropi, M.S., Caruso, A., Capasso, A., Palladino, C., Panno, A., Saturnino, C., 2010b. Heavy metals: toxicity and carcinogenicity. Pharmacology 2, 329–333.

Sirignano, E., Saturnino, C., Botta, A., Sinicropi, M.S., Caruso, A., Pisano, A., Lappano, R., Maggiolini, M., Longo, P., 2013a. Synthesis, characterization and cytotoxic activity on breast cancer cells of new half-titanocene derivatives. Bioorg. Med. Chem. Lett. 23, 3458–3462.

Sirignano, E., Saturnino, C., Botta, A., Sinicropi, M.S., Caruso, A., Pisano, A., Lappano, R., Maggiolini, M., Longo, P., 2013b. Synthesis, characterization and cytotoxic activity on breast cancer cells of new half-titanocene derivatives. Bioorg. Med. Chem. Lett. 23, 3458–3462.

Tambe, S., Sampath, L., Modak, S., 2001. In vitro evaluation of the risk of developing bacterial resistance to antiseptics and antibiotics used in medical devices. J. Antimicrob. Chemother. 47, 589–598.

Tan, S.J., Yan, Y.K., Lee, P.P.F., Lim, K.H., 2010. Copper, gold and silver compounds as potential new anti-tumor metallodrugs. Future Med. Chem. 2, 1591–1608.

Vittorio, O., Cirillo, G., Iemma, F., Di Turi, G., Jacchetti, E., Curcio, M., Barbuti, S., Funel, N., Parisi, O.I., Puoci, F., Picci, N., 2012. Dextran-catechin conjugate: a potential treatment against the pancreatic ductal adenocarcinoma. Pharm. Res. 29, 2601–2614.

Wayakanon, K., Thornhill, M.H., Douglas, C.I., Lewis, A.L., Warren, N.J., Pinnock, A., Armes, S.P., Battaglia, G., Murdoch, C., 2013. Polymersome-mediated intracellular delivery of antibiotics to treat Porphyromonas gingivalis-infected oral epithelial cells. FASEB J. 27, 4455–4465.

Bergamot (*Citrus bergamia* Risso) Flavonoids and Their Potential Benefits in Human Hyperlipidemia and Atherosclerosis: An Overview
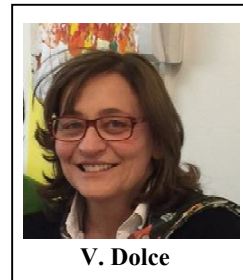
A.R. Cappello*,#, V. Dolce*,#, D. Iacopetta, M. Martello, M. Fiorillo, R. Curcio, L. Muto and D. Dhanyalayam

Department of Pharmacy, Health and Nutritional Sciences, University of Calabria, 87036 Arcavacata di Rende (Cosenza) Italy

A.R. Cappello

V. Dolce

Abstract: Elevated serum cholesterol, triglycerides and LDL levels are often associated with an increased incidence of atherosclerosis and coronary artery disease. The most effective therapeutic strategy against these diseases is based on statins administration, nevertheless some patients, especially those with metabolic syndrome fail to achieve their recommended LDL targets with statin therapy, moreover, it may induce many serious side effects. Several scientific studies have highlighted a strong correlation between diets rich in flavonoids and cardiovascular risk reduction. In particular, *Citrus bergamia* Risso, also known as bergamot, has shown a significant degree of hypocholesterolemic and antioxidant/radical scavenging activities. In addition, this fruit has attracted considerable attention due to its peculiar flavonoid composition, since it contains some flavanones that can act as natural statins. Hence, the study of bergamot flavonoids as metabolic regulators offers a great opportunity for screening and discovery of new therapeutic agents. Cholesterol metabolism, flavonoid composition and potential therapeutic use of *C. bergamia* Risso will be discussed in the following review.

Keywords: Bergamot fruit, flavonoids, hyperlipidemia, atherosclerosis, 3-hydroxy-3-methylglutaryl-CoA reductase enzyme.

INTRODUCTION

The risk for atherosclerosis and coronary heart disease is increased in patients with elevated serum concentrations of low-density lipoproteins cholesterol (LDL), total cholesterol (TC) and triglicerides (TG) [1-5]. Several meta-analysis studies showed that statin therapy can reduce the 5-year incidence of cardiovascular diseases, by about one fifth per mmol/L reduction in LDL cholesterol [6-8].

It is well-known that statins are able to inhibit 3-hydroxy-3-methylglutaryl-CoA reductase (HMGR) activity, the rate-limiting enzyme of cholesterol biosynthesis [9]. Statin administration is one of the most widely used approaches to lower serum LDL level and to reduce cardiovascular event rates [10-12]. However, many patients, especially those with the dyslipidemia associated with metabolic syndrome, are unable to reach their lipid treatment goals on statins alone [2]. Furthermore, patients might be statin-intolerant and experience significant side-effects [3], hence the importance of finding new drugs acting as statins.

Some foods were shown to possess these therapeutic properties; in particular, daily consumption of *Citrus* fruit

juice was shown to positively influence serum lipid levels and to decrease coronary heart disease risk [13]. Their hypolipidemic effects can be due to the presence of flavonoids, pectins and ascorbic acid, which have a high antioxidant potential and may interfere with cholesterol metabolism [14-19].

Flavonoids are aromatic secondary plant metabolites, having strong antioxidant and radical scavenging activities [15, 20]. Their intake was associated with a reduced risk for certain chronic diseases such as cardiovascular disorders and cancerous processes [21-23]. Flavonoids exhibited antiviral, antimicrobial and anti-inflammatory activities [23-25], moreover, they were able to inhibit human platelet aggregation [26] and to support a correct immune response [27].

Bergamot, the common name of *Citrus bergamia* Risso, belongs to the family Rutaceae, subfamily Esperidea and it has been widespread in the Mediterranean area for centuries. Over the past few years, thanks to the growing interest in bioactive compounds, bergamot fruit has attracted attention for its remarkable flavonoid composition. The first part of this review will report an overview on cholesterol metabolism, in the second part, literature data regarding flavonoid composition and distribution in bergamot fruit will be analysed. The last part will focus on the scientific evidence concerning the bioactivities of bergamot flavonoids and their potential utility for human health as well as their uses in atherosclerosis and coronary heart disease treatments.

*Address correspondence to these authors at the Department of Pharmacy, Health and Nutritional Sciences, University of Calabria 87036 Arcavacata di Rende (Cosenza) Italy; Tel: +39 0 984493177; Fax: +39 0 984493107; E-mail: annarita.cappello@unical.it; and Tel: +39 0 984493119; Fax: +39 0 984493107; E-mail: vincenza.dolce@unical.it;

#These authors contributed equally to this work.

1. CHOLESTEROL HOMEOSTASIS AND REGULATION

Cholesterol body homeostasis is mainly due to the regulation of its endogenous synthesis, intestinal absorption, excretion and hepatic conversion (Fig. **1**).

Cholesterol *de novo* synthesis occurs mainly in the liver and, in human, it accounts for more than 70% of body cholesterol. Cholesterol intestinal absorption depends on diet composition. Excess liver cholesterol can be directly excreted as biliary sterols or converted into bile acids, both are eliminated via feces.

Cholesterol absorption is controlled by at least two types of transporters, Niemann-Pick C1-Like 1 (NPC1L1) as influx transporter and ATP-Binding Cassette (ABC) proteins as efflux transporters [28]. NPC1L1 transports cholesterol from intestinal lumen into enterocytes and it reabsorbs free

cholesterol back into hepatocyte from bile [29]. ABCG5 and ABCG8 reduce cholesterol absorption in the intestinal lumen and exclude cholesterol from liver to the bile duct (Fig. **1**). ABCG1 and ABCA1 are involved in reverse cholesterol transport, the pathway by which peripheral cell cholesterol can be returned to the liver for excretion [30].

Regulation of cholesterol homeostasis is achieved by proteins such as sterol regulatory element-binding proteins (SREBPs) and AMP-Activated Protein Kinase (AMPK); by nuclear receptors such as peroxisome proliferator activated receptors (PPARs) and liver X receptors (LXRs); by microRNAs (miRNAs).

SREBPs are key transcription regulators encoded by two genes, SREBP-1 and SREBP-2. SREBP-1 upregulates the transcription of some hepatic lipogenic genes [31-35]. SREBP-2 modulates the transcription of some sterol
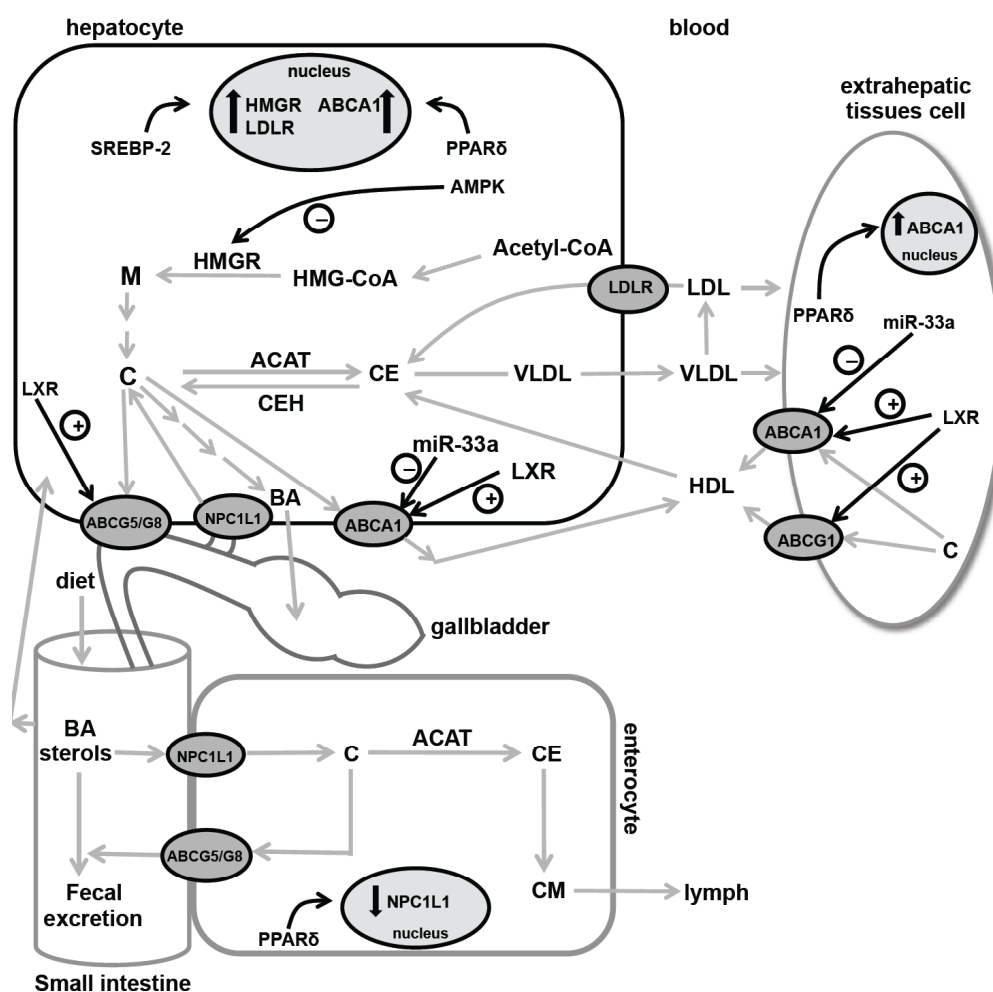
Fig. (1). Overview of cholesterol homeostasis and regulation in liver, small intestine, extraepatic tissues, and plasma. The regulation is indicated with black arrows. ⊕ indicates activation while ⊖ indicates inhibition. ABCA1, ABCG1, and ABCG5/G8: ATP-binding cassette transporters; ACAT: acyl CoA:cholesterol acyltransferase; AMPK: AMP-activated protein kinase; BA: bile acid; C: cholesterol; CE: cholesteryl ester; CEH: cholesteryl ester hydrolase; CM: chylomicrons; HDL: high-density lipoprotein; HMGR: 3-hydroxy-3-methylglutaryl-CoA reductase; LDL: low-density lipoprotein; LDLR: low-density lipoprotein receptor; LXR: liver X receptor; M: mevalonate; miR-33a: microRNA-33a; MTP: microsomal triglyceride transfer protein; NPC1L1: Niemann-Pick C1-Like 1; PPAR∂: peroxisome proliferator activated receptor delta; SREBP2: sterol regulatory element binding protein-2; VLDL: very low density lipoprotein.

biosynthetic genes [36], for instance, when hepatocyte cholesterol content is low, expressions of HMGR and LDLR are upregulated [36] (Fig. **1**).

AMPK is a critical player in energy homeostasis at both cellular and whole body levels. An increased AMP to ATP ratio leads to AMPK activation through phosphorylation by at least three different upstream kinases [37]; in particular, when cellular cholesterol content is high, AMPK inactivates HMGR by phosphorylation (Fig. **1**) [38].

PPARs are members of nuclear hormone receptors superfamily that act as ligand-dependent transcription factors [39, 40]. PPARα directly upregulates the transcription of genes involved in cholesterol catabolism [41]. PPARγ integrates the control of energy, lipid and glucose homeostasis [42-44] and its activation also redirects effluxed cholesterol from liver toward adipose tissue uptake via scavenger receptor type-BI [45]. PPARδ activation elevates serum HDL levels by increasing the expression of ABCA1 [30], it can reduce cholesterol absorption by decreasing NPC1L1 intestinal expression [29] and it also potentiates fecal neutral sterol secretion by increasing transintestinal cholesterol efflux [46].

LXRs play a primary role in reverse cholesterol transport, modulating the expression of several target genes as ABCA1, ABCG1, ABCG4 ABCG5, ABCG8 and apoE [47-50]. In the liver, when cellular cholesterol content is high, LXRs activation induces cholesterol excretion and/or efflux [50, 51].

MicroRNAs promote the down-regulation of their target genes by binding to specific regions located in the 3' UTR of their target mRNA [52]. MIR-33a is believed to minimize cholesterol export by the post-transcriptional repression of ABCA1 transporter (Fig. **1**) [53, 54].

2. FLAVONOIDS IN BERGAMOT TISSUES

Plant flavonoids are a large group of very different compounds sharing the common feature of phenolic moieties [55]. The presence of a relatively large number of flavonoids is the result of many different possible combinations among polyhydroxylated aglycones and a limited number of mono- and disaccharides. The most commonly found sugars are hexoses, such as glucose, galactose and rhamnose or pentoses such as arabinose and xylose. They are, with a few notable exceptions, plant metabolites deriving from the shikimate pathway and the phenylpropanoid metabolism [56]. In recent years, flavonoids have attracted tremendous attention due to the protection that they provide against some types of cardiovascular diseases [57]. As a consequence, many studies have been directed to the characterization of the flavonoid fractions and to the isolation of the most representative flavonoids present in the most common *Citrus* species, as well as of flavonoids present in many local species such as *C. bergamia* Risso [58, 59]. Bergamot fruit presents an external part, epicarp or flavedo yellow coloured; a middle part, mesocarp or albedo, that is a spongy white inner layer and an inner part, endocarp or pulp. Albedo and flavedo peeled off together are called peel. Bergamot

essential oil is obtained from this fraction by cold press; it is composed of a volatile (93–96%) and a non-volatile fraction (4–7%).

The classes of flavonoids present in *C. bergamia* Risso fractions are flavanones and flavones. Flavanones are present as flavanone-O-glycosides, recently, flavanones diglycosides carrying the 3-hydroxy-3-methylglutaric acid (HMG) moiety have also been detected [60-62]. Flavones are present as flavone-O-glycosides, flavone-C-glycosides or polymethoxy-flavones (Table **1**).
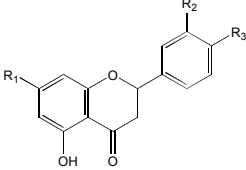
A comparative study on flavonoid composition in fruit tissues of different *Citrus* species has been reported by Nogata *et al.* [59], showing that bergamot fruit has a peculiar flavonoid composition. In particular, it contains neoeriocitrin in exceptionally large amount (288 mg/100 g fresh weight) and it is relatively rich in neohesperidin, naringin, poncirin, rhoifolin, and neodiosmin (590, 438, 1240, 43 and 33 mg/100 g fresh weight, respectively) with respect to the other *Citrus* fruits analyzed. Furthermore, it contains very little amount of hesperidin (2 mg/100 g fresh weight).

Table **1** lists structure and tissue distribution of flavonoids, in *C. bergamia* Risso as described in literature.
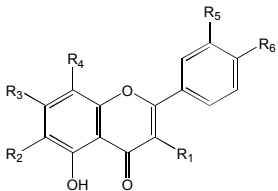
Flavanone-O-glycosides are present in all the analysed parts, in particular the most abundant are naringin, neoeriocitrin, neohesperidin and poncirin, whereas hesperidin and neoponcirin have been detected in a very low amount [59]. They are also present in the peel, but it could be noted that when it is splitted into albedo and flavedo, these compounds are mainly present in albedo [59]. Moreover, poncirin, which is present in huge amount in hand-squeezed juice, is absent in industrial juice, this may be due to the pressing process used to extract industrial juices [58]. In addition, three acylated flavanones, which seem to correspond to di-oxalate derivatives of neoeriocitrin, naringin and neohesperidin, have been identified in bergamot juice [63]. The HMG-conjugated flavanones, brutieridin, melitidin and HMG-neoeriocitrin have also been detected at different concentrations depending on the ripening stage; they may be found in bergamot fruit either in juice or in albedo and flavedo [60-62].

Flavone-O-glycosides present a different tissue distribution. All these compounds are present in the peel, with the exception of chrysoeriol 7-O-neohesperidoside, chrysoeriol 7-O-neohesperidoside-4'-glucoside and rhoifolin 4'- glucoside [59, 64]. Diosmetin mono-glucoside, diosmetin mono-rhamnoside and apigenin mono-glucoside/mono-rhamnoside has been detected in bergamot peel [64] but not in albedo and flavedo. It could be explained because, according to this author, bergamot peel is a mix of seeds, pulp and deoiled flavedo after essential oil and juice extraction. Furthermore, rutin, that is absent in albedo, has been found in large amount in flavedo [64]. All these compounds have been revealed in the juice [58, 59, 63, 65-67], with the exception of diosmetin mono-rhamnoside and diosmetin mono-glucoside; this latter has been detected in industrial juice, probably because fruit industrial processing leads to juices contaminated with peel constituents [58].
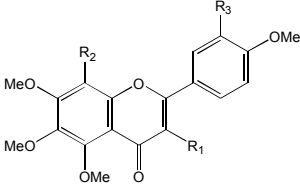
Table 1. Flavonoids identified in bergamot fruit.

Flavanone-O-glycosides	Peel	Albedo	Flavedo	Juice	Industrial juice
	[59, 84, 92]	[59, 60, 79]	[59, 60, 79]	[58-60, 64-67, 79]	[58]
Eriocitrin (eriodictyol 7-O-rutinoside) R_1=O-rutinose, R_2=OH, R_3=OH	X	X	X	X	X
Eriodictyol mono-rhamnoside Most likely 7-O-substituted	X				
Hesperidin (hesperetin 7-O-rutinoside) R_1=O-rutinose, R_2=OH, R_3=OCH$_3$	X	X		X	
Hesperetin mono-rhamnoside Most likely 7-O-substituted	X				
Naringin (naringenin 7-O-neohesperidoside) R_1=O-neohesperidose, R_2=H, R_3=OH	X	X	X	X	X
Naringenin mono-rhamnoside Most likely 7-O-substituted	X	X	X	X	X
Narirutin (naringenin 7-O-rutinoside) R_1=O-rutinose, R_2=H, R_3=OH	X	X	X	X	
Neoeriocitrin (eriodictyol 7-O-neohesperidoside) R_1=O-neohesperidose, R_2=OH, R_3=OH	X	X	X	X	X
Neohesperidin (hesperetin 7-O-neohesperidoside) R_1=O-neohesperidose, R_2=OH, R_3=OCH$_3$	X	X	X	X	X
Neoponcirin (isosakuranetin 7-O-rutinoside) R_1=O-rutinose, R_2=H, R_3=OCH$_3$	X	X	X	X	
Poncirin (isosakuranetin 7-O-neohesperidoside) R_1=O-neohesperidose, R_2=H, R_3=OCH$_3$	X	X	X	X	
Neoeriocitrin di-oxalate R_1=O-neohesperidose -di-oxalate, R_2=OH, R_3=OH				X	
Naringin di-oxalate R_1=O-neohesperidose-di-oxalate R_2=OH, R_3=OH				X	
Neohesperidin di-oxalate R_1=O-neohesperidose -di-oxalate R_2=OCH$_3$, R_3=OH				X	
Brutieridin (hesperetin 7-2''-α-rhamnosyl-6''-3'''''-hydroxy-3'''''-methylglutaryl)-β-glucoside) R_1=O-rhamnosyl-HMG, R_2=OH, R_3=OCH$_3$		X	X	X	
Melitidin (naringenin 7-2''-α-rhamnosyl-6''-3'''''-hydroxy-3'''''-methylglutaryl)-β -glucoside) R_1=O-rhamnosyl-HMG, R_2=H, R_3=OH		X	X	X	
Neoeriocitrin HMG conjugated		X	X	X	

Flavone O-glycosides and C-glycosides	Peel	Albedo	Flavedo	Juice	Industrial juice
	[59, 84, 92]	[59, 60, 79]	[59, 60, 79]	[58-60, 64-67, 79]	[58]
Apigenin **Mono-glucoside/mono-rhamnoside**	X				
Chrysoeriol 7-O-neohesperidoside R_1=H, R_2=H, R_3=O-neohesperidose, R_4=H, R_5=OCH$_3$, R_6=OH				X	X
Chrysoeriol 7-O-neohesperidoside-4'-glucoside R_1=H, R_2=H, R_3=O-neohesperidose, R_4=H, R_5=OCH$_3$, R_6=O-glucoside				X	X
Diosmetin mono glucoside	X				X
Diosmetin mono rhamnoside	X				
Diosmin (diosmetin 7-O-rutinoside) R_1=H, R_2=H, R_3=O-rutinose, R_4=H, R_5=OH, R_6=OCH$_3$	X	X	X	X	
Neodiosmin (diosmetin 7-O-neohesperidoside) R_1=H, R_2=H, R_3=O-neohesperidose, R_4=H, R_5=OH, R_6=OCH$_3$	X	X	X	X	X
Rhoifolin (apigenin 7-O-neohesperidoside) R_1=H, R_2=H, R_3=O-neohesperidose, R_4=H, R_5=OH, R_6=OH	X	X	X	X	X
Rhoifolin 4'-glucoside (apigenin 7-O-neohesperidoside 4'-glucoside) R_1=H, R_2=H, R_3=O-neohesperidose, R_4=H, R_5=OH, R_6=O-glucoside				X	X
Rutin (quercetin 3-O- rutinoside) R_1=O-rutinose, R_2=H, R_3=OH, R_4=H, R_5=OH, R_6=OH	X		X	X	
Isovitexin (apigenin 6-C-glucoside) R_1=H, R_2=glucoside R_3=OH, R_4=H, R_5=H, R_6=OH				X	X
Luteolin **Mono-glucoside/mono-rhamnoside**	X				
Lucenin-2 (luteolin 6,8-di-C-glucoside) R_1=H, R_2=glucoside, R_3=OH, R_4=glucoside, R_5=OH, R_6=OH				X	X
Lucenin-2 4'-methyl ether (diosmetin 6,8-di-C-glucoside) R_1=H, R_2=glucoside, R_3=OH, R_4=glucoside, R_5=OH, R_6=OCH$_3$	X			X	X
Stellarin-2 (chrysoeriol 6,8-di-C-glucoside) R_1=H, R_2=glucoside, R_3=OH, R_4=glucoside, R_5=OCH$_3$, R_6=OH				X	X
Scoparin (chrysoeriol 8-C-glucoside) R_1=H, R_2=H, R_3=OH, R_4=glucoside, R_5=OCH$_3$, R_6=OH				X	X
Orientin 4'-methyl ether (diosmetin 8-C-glucoside) R_1=H, R_2=H, R_3=OH, R_4=glucoside, R_5=OH, R_6=OCH$_3$				X	
Vicenin-2 (apigenin 6,8-di-C-glucoside) R_1=H, R_2=glucoside, R_3=OH, R_4=glucoside, R_5=H, R_6=OH	X			X	

(Table 1) Contd.…

Polymethoxy flavones	Peel	Albedo	Flavedo	Juice	Industrial juice
	[59, 84, 92]	[59, 60, 79]	[59, 60, 79]	[58-60, 64-67, 79]	[58]
Sinensetin (3',4',5,6,7-pentamethoxyflavone) R$_1$=H, R$_2$=H, R$_3$=OCH$_3$	X		X		
Nobiletin (3',4',5,6,7,8,-esamethoxyflavone) R$_1$=H, R$_2$=OCH$_3$, R$_3$=OCH$_3$	X	X	X		
Tangeretin (4',5,6,7,8-pentamethoxyflavone) R$_1$=H, R$_2$=OCH$_3$, R$_3$=H	X		X		

Flavone-C-glycosides are mainly present in the juice, similarly to flavanone-O-glycosides some of these compounds lack in industrial juice [58, 63, 65-68]. In bergamot essential oil (data not showed) only two flavonoids have been detected: sinensetin and tetra-O-methylscutellarein. This latter has been detected in essential oil [69].

3. HYPOLIPIDEMIC AND ANTIATHEROSCLERO-TIC PROPERTIES OF BERGAMOT DERIVATIVES

Hypolipidemic effects of *Citrus* species are due to several components, such as flavonoids, pectins and ascorbic acid. Flavonoids are believed to inhibit LDL oxidation and to increase LDL reuptake, furthermore, they can interfere with fecal excretion of bile acids and with HMGR, LDLR and FASN functions [14, 70-72]. In particular, naringin seems to be active on atherosclerosis, as demonstrated by animal studies [73], neoeriocitrin is believed to strongly inhibit LDL oxidation [74] whereas, HMG-flavonoids could be able to inhibit HMGR [60]. These observations have provided the rationale to investigate the protective hypolipidemic effect of bergamot extracts in animal models and in human patients.

Miceli *et al.* [75] demonstrated that daily administration of bergamot juice to hypercholesterolemic rats caused a significant reduction in TC, TG and LDL levels, an increase in serum HDL levels and a protective effect on hepatic parenchyma. In addition, fecal output of total bile acids and neutral sterols was enhanced in the bergamot juice treated group in comparison with the hyperlipidemic group. These results are in agree with previous studies, which hypothesized that pectins and flavonoids were able to lower serum cholesterol levels by modulating hepatic HMG-CoA concentration. It could be noted that in this study, the potential side-effect due to bergamottin presence in bergamot juice was not investigated. Bergamot juice is rich in bergamottin (ranging from 18 to 61 mg/L) [63, 66], a furanocoumarin compound that inhibits cytochrome P450 34A enzyme activity, significantly increasing the oral bioavailability of several drugs metabolized primarily by this cytochrome [74, 76].

This problem was overcome by Mollace *et al.* [77], that analyzed the hypolipidemic effect of a defurocoumarinized bergamot-derived polyphenolic fraction supplemented with ascorbic acid on animal models of diet-induced hyperlipidemia and in patients suffering from metabolic syndrome [77]. They found that oral administration of this fraction both in animal and in patients, caused a significant reduction of TC, TG and glycemia with a concomitant increase of HDL levels. In particular, in 59 patients with metabolic syndrome a 30-days treatment period with bergamot-derived polyphenolic fraction, administred at the dose of 1 g/die, reduced the serum levels of TC, LDL and TG by 30%, 33% and 41%, respectively [26]. This effect was associated with a significant improvement in vascular reactivity in patients with both hyperlipidemia and hyperglycemia, suggesting a potential protective role for the use of bergamot-derived polyphenolic fraction in these patients.

Recent prospective studies, led on patients with hyperlipidemia demonstrated that administration of a defurocoumarinized bergamot-derived polyphenolic fraction was able to reduce TC level by 31%. In the same conditions, rosuvastatin administration (10 mg/die) caused a similar reduction of TC content (30%). Their association produced a considerable enhancement of rosuvastatin hypolipidemic effect, causing a reduction of TC level by 38%, normalizing the serum lipid profile [78].

The authors suggested that the observed hypolipidemic effect could be mainly due to the presence in bergamot-derived polyphenolic fraction of melitidin, brutieridin and HMG-neoeriocitrin. This hypothesis was investigated by Di Donna *et al.* [79] in a hypercholesterolemic rat model, by measuring the effects on lipid profile of administration of HMG-flavanones enriched fraction (62% of brutieridin, 14% of melitidin and 15% of HMG-neoeriocitrin), extracted from bergamot fruit, in comparison with simvastatin. HMGR, LDLR and FASN transcription levels and their correlated protein amounts were evaluated.

In this study, simvastatin and HMG-flavanones enriched fraction singularly administrated reduced levels of TC (30%, 20% respectively), TG (32%, 20% respectively), VLDL (33%, 28% respectively) and LDL (24%, 40% respectively), whereas an increase of 20% in HDL content was observed exclusively in rats treated by HMG-flavanones enriched fraction [61]. Furthermore, according to the previously published data, HMGR, LDLR and FAS transcription levels were found up-regulated. An increased amount of their corresponding proteins was detected [80]. Genotoxicity and toxicity were not observed by testing HMG-flavanones enriched fraction *in vitro*. The authors hypothesized that HMGR inhibition leads to a reduction of endogenous cholesterol level which, in turn, is responsible of HMGR and LDLR transcriptional up-regulation, as well of the higher LDLR exposure within the hepatocytes membrane, through a compensatory mechanism based on SREBPs pathway. Furthermore, it was highlighted that cholesterol depletion below a certain threshold is known to be responsible for FASN genic transcription increase, via SREBPs activation, which is one of the observed effects. It was suggested that transcriptional up-regulation of these genes and the corresponding increased protein amounts could be occurred via SREBPs pathway (Fig. **2**).

Beside the already described hypolipidemic effect, flavonoids, in particular naringin, have received considerable attention because of their antioxidant/radical scavenging properties [15, 20]. Increasing clinical evidences support the hypothesis that phospholipid oxidation products may play a role in atherosclerosis. This was firstly suggested by demonstrating that mildly oxidized LDL proatherogenic activities were present in the fraction containing oxidized phospholipids. Subsequently, phospholipid oxidation products were reported to accumulate in hyperlipidemic plasma, atherosclerotic lesions and in several diseases that predispose to stroke [81-83].

Trombetta *et al.* [84] reported that two flavonoid-rich extracts from bergamot peel, endowed with radical-scavenging properties and lacking genotoxic activity, were able to prevent alterations induced by the pleiotropic inflammatory cytokine tumor necrosis factor-α (TNF-α) on human umbilical vein endothelial cells (HUVECs). This study was led by monitoring intracellular levels of malondialdehyde, reduced and oxidized glutathione levels, superoxide dismutase activity and the activation status of nuclear factor-κB. To clarify the mechanisms involved in flavonoid protective activity, flavonoid-rich extracts were tested in vitro for their ability to inhibit cyclooxygenase-1 (COX-1) and cyclooxygenase-2 (COX-2) activity, in a human whole blood model. Conversely to literature data [85], authors excluded that the protective effect of bergamot peel extracts against TNF-α-induced changes in HUVECs might be due to their capability to inhibit COX-1 or COX-2 pathways, because these phytocomplexes were unable to modify prostaglandin E2 and tromboxan B2 release when they were tested on human whole blood.

Several investigations suggested that phospholipid oxidation products may play a pathogenic role in progressive renal damage [86, 87]. A prominent mechanism probably involved in the deleterious effects of hypercholesterolemia on the kidney was an increased formation of reactive oxygen species. In addition, oxidized LDL particles were injurious to renal tubular epithelial cells and they might contribute to tubulointerstitial damage and glomerulosclerosis [88]. In an experimental model of short-term diet-induced
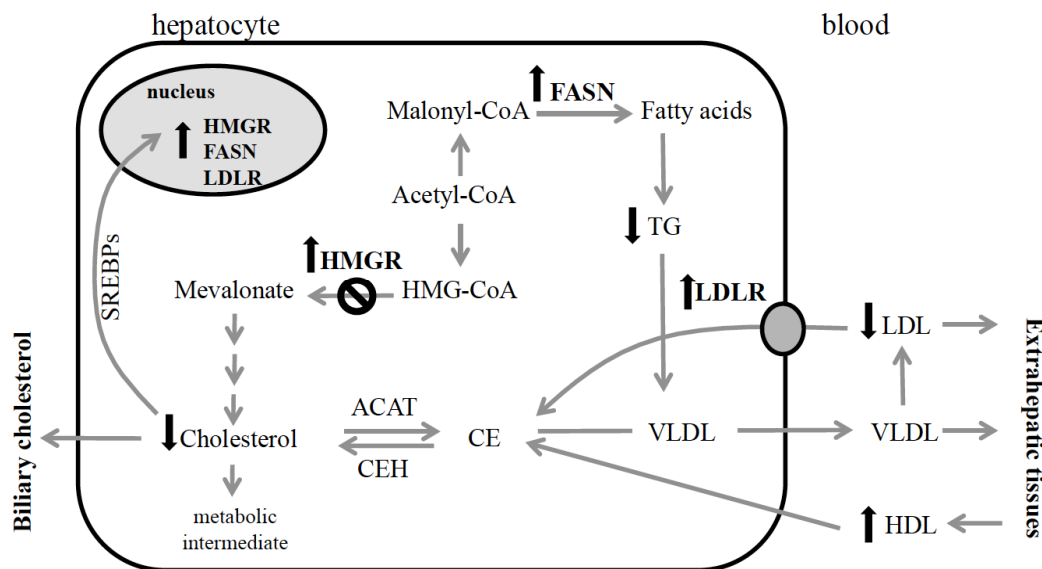
Fig. (2). Model depicting HMG flavanones enriched fraction effects on lipids metabolism elicited in rat hepatocytes (from Di Donna *et al* 2014 [61]). Black arrows indicate HMG flavanones enriched fraction effects on genes, enzymes and metabolites levels. ⊘ indicates enzymatic inhibition. ACAT: Acyl-CoA:cholesterol acyltransferase; CE: cholesteryl ester; CEH: cholesteryl ester hydrolase; FASN: fatty acid synthase; HDL: high-density lipoprotein; HMG-CoA: 3-hydroxy-3-methylglutaryl-CoA; HMGR: 3-hydroxy-3-methylglutaryl-CoA reductase; LDL: low density lipoprotein; LDLR: low density lipoprotein receptor; SREBPs: sterol response element binding proteins; TG: triglycerides; VLDL: very low density lipoprotein.

hypercholesterolemia [89], a significant decrease in renal lipid peroxidation was observed after bergamot juice administration, as shown by the low malondialdehyde levels found. Furthermore, analysis of kidney histopathological sections supported the biochemical data, indicating a protective effect of bergamot juice on the development of kidney injury induced by the hypercholesterolemic diet. The authors hypothesized that the beneficial effect on renal parenchyma was due to the great abundance of flavonoids in bergamot juice, believed to reduce oxidative damage *in vivo*.

CONCLUSION

HMGR inhibitors (statins) are the most effective, practical and largely prescribed class of drugs for reducing LDL concentrations [10, 11]. Nevertheless some patients, especially those with metabolic syndrome do not achieve their recommended LDL targets with statin therapy [77, 90]. Moreover, statins may induce many side effects, including myalgia, myopathy, liver diseases and rhabdomyolysis [91]. Many studies demonstrated a relationship between the intake of flavonoid-rich foods and a reduced risk for cardiovascular disease [13]. Bergamot fruit is very rich in many peculiar bioactive flavonoids compared to other *Citrus* fruits [15-18], hence their evaluation as metabolic regulators might represent an attractive strategy in drug discovery. The aim of this review is to provide an overview on all flavonoids detected in *C. bergamia* Risso and on the current knowledge of their hypolipidemic effects [58-69], summarizing the results obtained from different *in vivo* studies [61, 75, 77, 89].

All data reported suggest that *C. bergamia* Risso flavonoids might be used in nutraceutical products or in functional foods, even if additional studies are needed to fully reveal their interaction with upstream mediators of lipid metabolism pathways. Furthermore, since only few studies on flavonoids administration in humans are available, further clinical studies are required to focus on dose, bioavailability, efficacy and safety of this class of flavonoids in humans.

LIST OF ABBREVIATIONS

ABC   = ATP-Binding Cassette

AMPK   = AMP- activated protein kinase

COX-1   = Cyclooxygenase-1

COX-2   = Cyclooxygenase-2

FASN   = Fatty acid synthase

HDL   = High-density lipoprotein

HMG-CoA   = 3-hydroxy-3-methylglutaryl-CoA

HMGR   = 3-hydroxy-3-methylglutaryl-CoA reductase

HUVECs   = Human umbilical vein endothelial cells

LDL   = Low-density lipoprotein

LDLR   = Low-density lipoprotein receptor

LXRs   = Liver X receptors

microRNAs = miRNAs

NPC1L1   = Niemann-Pick C1-Like 1

PPARs   = Peroxisome proliferator activated receptors

SREBPs   = Sterol regulatory element-binding proteins

TC   = Total cholesterol

TG   = Triglycerides

TNF-α   = Tumor necrosis factor-α

VLDL   = Very low-density lipoprotein

CONFLICT OF INTEREST

The author(s) confirm that this article content has no conflict of interest.

ACKNOWLEDGEMENTS

SUPPLEMENTARY MATERIALS

Supplementary material is available on the publisher's web site along with the published article.

REFERENCES

[1]   Balbisi, E.A. Management of hyperlipidemia: new LDL-C targets for persons at high-risk for cardiovascular events. *Med. Sci. Monit.*, **2006**, 12(2), RA34-39.

[2]   Maxfield, F.R. Tabas, I. Role of cholesterol and lipid organization in disease. *Nature*, **2005**, 438(7068), 612-621.

[3]   Gielen, S.; Sandri, M.; Schuler, G. Teupser, D. Risk factor management: antiatherogenic therapies. *Eur. J. Cardiovasc. Prev. Rehabil.*, **2009**, 16 Suppl 2(S29-36.

[4]   Stamler, J.; Neaton, J.D.; Cohen, J.D.; Cutler, J.; Eberly, L.; Grandits, G.; Kuller, L.H.; Ockene, J.; Prineas, R. Group, M.R. Multiple risk factor intervention trial revisited: a new perspective based on nonfatal and fatal composite endpoints, coronary and cardiovascular, during the trial. *J. Am. Heart Assoc.*, **2012**, 1(5), e003640.

[5]   Stamler, J. Neaton, J.D. The Multiple Risk Factor Intervention Trial (MRFIT)--importance then and now. *JAMA*, **2008**, 300(11), 1343-1345.

[6]   Baigent, C.; Keech, A.; Kearney, P.M.; Blackwell, L.; Buck, G.; Pollicino, C.; Kirby, A.; Sourjina, T.; Peto, R.; Collins, R.; Simes, R. Cholesterol Treatment Trialists, C. Efficacy and safety of cholesterol-lowering treatment: prospective meta-analysis of data from 90,056 participants in 14 randomised trials of statins. *Lancet*, **2005**, 366(9493), 1267-1278.

[7]   Boekholdt, S.M.; Hovingh, G.K.; Mora, S.; Arsenault, B.J.; Amarenco, P.; Pedersen, T.R.; LaRosa, J.C.; Waters, D.D.; DeMicco, D.A.; Simes, R.J.; Keech, A.C.; Colquhoun, D.; Hitman, G.A.; Betteridge, D.J.; Clearfield, M.B.; Downs, J.R.; Colhoun, H.M.; Gotto, A.M., Jr.; Ridker, P.M.; Grundy, S.M. Kastelein, J.J. Very low levels of atherogenic lipoproteins and the risk for cardiovascular events: a meta-analysis of statin trials. *J. Am. Coll. Cardiol.*, **2014**, 64(5), 485-494.

[8]   Boekholdt, S.M.; Arsenault, B.J.; Mora, S.; Pedersen, T.R.; LaRosa, J.C.; Nestel, P.J.; Simes, R.J.; Durrington, P.; Hitman, G.A.; Welch, K.M.; DeMicco, D.A.; Zwinderman, A.H.; Clearfield, M.B.; Downs, J.R.; Tonkin, A.M.; Colhoun, H.M.; Gotto, A.M., Jr.; Ridker, P.M. Kastelein, J.J. Association of LDL cholesterol, non-HDL cholesterol, and apolipoprotein B levels with risk of cardiovascular events among patients treated with statins: a meta-analysis. *JAMA*, **2012**, 307(12), 1302-1309.

[9]   Goldstein, J.L. Brown, M.S. Regulation of the mevalonate pathway. *Nature*, **1990**, 343(6257), 425-430.

[10]　Ross, S.D.; Allen, I.E.; Connelly, J.E.; Korenblat, B.M.; Smith, M.E.; Bishop, D. Luo, D. Clinical outcomes in statin treatment trials: a meta-analysis. *Arch. Intern. Med.*, **1999**, 159(15), 1793-1802.

[11]　Scharnagl, H.; Schinker, R.; Gierens, H.; Nauck, M.; Wieland, H. Marz, W. Effect of atorvastatin, simvastatin, and lovastatin on the metabolism of cholesterol and triacylglycerides in HepG2 cells. *Biochem. Pharmacol.*, **2001**, 62(11), 1545-1555.

[12]　Stone, N.J.; Robinson, J.G.; Lichtenstein, A.H.; Bairey Merz, C.N.; Blum, C.B.; Eckel, R.H.; Goldberg, A.C.; Gordon, D.; Levy, D.; Lloyd-Jones, D.M.; McBride, P.; Schwartz, J.S.; Shero, S.T.; Smith, S.C., Jr.; Watson, K.; Wilson, P.W.; Eddleman, K.M.; Jarrett, N.M.; LaBresh, K.; Nevo, L.; Wnek, J.; Anderson, J.L.; Halperin, J.L.; Albert, N.M.; Bozkurt, B.; Brindis, R.G.; Curtis, L.H.; DeMets, D.; Hochman, J.S.; Kovacs, R.J.; Ohman, E.M.; Pressler, S.J.; Sellke, F.W.; Shen, W.K.; Smith, S.C., Jr.; Tomaselli, G.F. American College of Cardiology/American Heart Association Task Force on Practice, G. 2013 ACC/AHA guideline on the treatment of blood cholesterol to reduce atherosclerotic cardiovascular risk in adults: a report of the American College of Cardiology/American Heart Association Task Force on Practice Guidelines. *Circulation*, **2014**, 129(25 Suppl 2), S1-45.

[13]　Assini, J.M.; Mulvihill, E.E. Huff, M.W. Citrus flavonoids and lipid metabolism. *Curr. Opin. Lipidol.*, **2013**, 24(1), 34-40.

[14]　Gorinstein, S.; Leontowicz, H.; Leontowicz, M.; Krzeminski, R.; Gralak, M.; Martin-Belloso, O.; Delgado-Licon, E.; Haruenkit, R.; Katrich, E.; Park, Y.S.; Jung, S.T. Trakhtenberg, S. Fresh Israeli Jaffa blond (Shamouti) orange and Israeli Jaffa red Star Ruby (Sunrise) grapefruit juices affect plasma lipid metabolism and antioxidant capacity in rats fed added cholesterol. *J. Agric. Food Chem.*, **2004**, 52(15), 4853-4859.

[15]　Gorinstein, S.; Leontowicz, H.; Leontowicz, M.; Krzeminski, R.; Gralak, M.; Delgado-Licon, E.; Martinez Ayala, A.L.; Katrich, E. Trakhtenberg, S. Changes in plasma lipid and antioxidant activity in rats as a result of naringin and red grapefruit supplementation. *J. Agric. Food Chem.*, **2005**, 53(8), 3223-3228.

[16]　Monforte, M.T.; Trovato, A.; Kirjavainen, S.; Forestieri, A.M.; Galati, E.M. Lo Curto, R.B. Biological effects of hesperidin, a Citrus flavonoid. (note II): hypolipidemic activity on experimental hypercholesterolemia in rat. *Farmaco*, **1995**, 50(9), 595-599.

[17]　Srinivasan, S. Pani, L. Antihyperlipidemic effect of diosmin: A citrus flavonoid on lipid metabolism in experimental diabetic rats. *Journal of Functional Foods*, **2013**, 5(1), 484–492.

[18]　Marounek, M.; Volek, Z.; Synytsya, A. Copikova, J. Effect of pectin and amidated pectin on cholesterol homeostasis and cecal metabolism in rats fed a high-cholesterol diet. *Physiol. Res.*, **2007**, 56(4), 433-442.

[19]　Lappano, R.; Rosano, C.; Madeo, A.; Albanito, L.; Plastina, P.; Gabriele, B.; Forti, L.; Stivala, L.A.; Iacopetta, D.; Dolce, V.; Ando, S.; Pezzi, V. Maggiolini, M. Structure-activity relationships of resveratrol and derivatives in breast cancer cells. *Mol. Nutr. Food Res.*, **2009**, 53(7), 845-858.

[20]　Burda, S. Oleszek, W. Antioxidant and antiradical activities of flavonoids. *J. Agric. Food Chem.*, **2001**, 49(6), 2774-2779.

[21]　Peterson, J.J.; Dwyer, J.T.; Jacques, P.F. McCullough, M.L. Associations between flavonoids and cardiovascular disease incidence or mortality in European and US populations. *Nutr. Rev.*, **2012**, 70(9), 491-508.

[22]　Garcia-Lafuente, A.; Guillamon, E.; Villares, A.; Rostagno, M.A. Martinez, J.A. Flavonoids as anti-inflammatory agents: implications in cancer and cardiovascular disease. *Inflamm. Res.*, **2009**, 58(9), 537-552.

[23]　Kim, H.P.; Son, K.H.; Chang, H.W. Kang, S.S. Anti-inflammatory plant flavonoids and cellular action mechanisms. *J. Pharmacol. Sci.*, **2004**, 96(3), 229-245.

[24]　Yin, D.; Li, J.; Lei, X.; Liu, Y.; Yang, Z. Chen, K. Antiviral Activity of Total Flavonoid Extracts from Selaginella moellendorffii Hieron against Coxsackie Virus B3 In Vitro and In Vivo. *Evid. Based Complement Alternat. Med.*, **2014**, 2014(950817.

[25]　Mandalari, G.; Bennett, R.N.; Bisignano, G.; Trombetta, D.; Saija, A.; Faulds, C.B.; Gasson, M.J. Narbad, A. Antimicrobial activity of flavonoids extracted from bergamot (Citrus bergamia Risso) peel, a byproduct of the essential oil industry. *J. Appl. Microbiol.*, **2007**, 103(6), 2056-2064.

[26]　Tijburg, L.B.; Mattern, T.; Folts, J.D.; Weisgerber, U.M. Katan, M.B. Tea flavonoids and cardiovascular disease: a review. *Crit. Rev. Food Sci. Nutr.*, **1997**, 37(8), 771-785.

[27]　Peluso, I.; Miglio, C.; Morabito, G.; Ioannone, F. Serafini, M. Flavonoids and immune function in human: a systematic review. *Crit. Rev. Food Sci. Nutr.*, **2015**, 55(3), 383-395.

[28]　Matsuo, M. ATP-binding cassette proteins involved in glucose and lipid homeostasis. *Biosci. Biotechnol. Biochem.*, **2010**, 74(5), 899-907.

[29]　Jia, L.; Betters, J.L. Yu, L. Niemann-pick C1-like 1 (NPC1L1) protein in intestinal and hepatic cholesterol transport. *Annu. Rev. Physiol.*, **2011**, 73(239-259.

[30]　Attie, A.D. ABCA1: at the nexus of cholesterol, HDL and atherosclerosis. *Trends Biochem. Sci.*, **2007**, 32(4), 172-179.

[31]　Sampath, H. Ntambi, J.M. Polyunsaturated fatty acid regulation of genes of lipid metabolism. *Annu. Rev. Nutr.*, **2005**, 25(317-340.

[32]　Santolla, M.F.; Lappano, R.; De Marco, P.; Pupo, M.; Vivacqua, A.; Sisci, D.; Abonante, S.; Iacopetta, D.; Cappello, A.R.; Dolce, V. Maggiolini, M. G protein-coupled estrogen receptor mediates the up-regulation of fatty acid synthase induced by 17beta-estradiol in cancer cells and cancer-associated fibroblasts. *J. Biol. Chem.*, **2012**, 287(52), 43234-43245.

[33]　Dolce, V.; Capobianco, L. Cappello, A.R. Mitochondrial tricarboxylate and dicarboxylate-tricarboxylate carriers: from animals to plants. *IUBMB Life*, **2014**, 66(7), 462-671.

[34]　Dolce, V.; Cappello, A.R.; Lappano, R. Maggiolini, M. Glycerophospholipid synthesis as a novel drug target against cancer. *Curr. Mol. Pharmacol.*, **2011**, 4(3), 167-175.

[35]　Cappello, A.R.; Guido, C.; Santoro, A.; Santoro, M.; Capobianco, L.; Montanaro, D.; Madeo, M.; Ando, S.; Dolce, V. Aquila, S. The mitochondrial citrate carrier (CIC) is present and regulates insulin secretion by human male gamete. *Endocrinology*, **2012**, 153(4), 1743-1754.

[36]　Goldstein, J.L. Brown, M.S. The LDL receptor. *Arterioscler. Thromb. Vasc. Biol.*, **2009**, 29(4), 431-438.

[37]　Steinberg, G.R. Kemp, B.E. AMPK in Health and Disease. *Physiol. Rev.*, **2009**, 89(3), 1025-1078.

[38]　Steck, T.L. Lange, Y. Cell cholesterol homeostasis: mediation by active cholesterol. *Trends Cell Bio.l*, **2010**, 20(11), 680-687.

[39]　Desvergne, B. Wahli, W. Peroxisome proliferator-activated receptors: nuclear control of metabolism. *Endocr. Rev.*, **1999**, 20(5), 649-688.

[40]　Braissant, O.; Foufelle, F.; Scotto, C.; Dauca, M. Wahli, W. Differential expression of peroxisome proliferator-activated receptors (PPARs): tissue distribution of PPAR-alpha, -beta, and -gamma in the adult rat. *Endocrinology*, **1996**, 137(1), 354-366.

[41]　Bensinger, S.J. Tontonoz, P. Integration of metabolism and inflammation by lipid-activated nuclear receptors. *Nature*, **2008**, 454(7203), 470-477.

[42]　Chawla, A.; Repa, J.J.; Evans, R.M. Mangelsdorf, D.J. Nuclear receptors and lipid physiology: opening the X-files. *Science*, **2001**, 294(5548), 1866-1870.

[43]　Bonofiglio, D.; Santoro, A.; Martello, E.; Vizza, D.; Rovito, D.; Cappello, A.R.; Barone, I.; Giordano, C.; Panza, S.; Catalano, S.; Iacobazzi, V.; Dolce, V. Ando, S. Mechanisms of divergent effects of activated peroxisome proliferator-activated receptor-gamma on mitochondrial citrate carrier expression in 3T3-L1 fibroblasts and mature adipocytes. *Biochim. Biophys. Acta*, **2013**, 1831(6), 1027-1036.

[44]　Francis, G.A.; Fayard, E.; Picard, F. Auwerx, J. Nuclear receptors and the control of metabolism. *Annu. Rev. Physiol.*, **2003**, 65(261-311.

[45]　Toh, S.A.; Millar, J.S.; Billheimer, J.; Fuki, I.; Naik, S.U.; Macphee, C.; Walker, M. Rader, D.J. PPARgamma activation redirects macrophage cholesterol from fecal excretion to adipose tissue uptake in mice via SR-BI. *Biochem. Pharmacol.*, **2011**, 81(7), 934-941.

[46]　Vrins, C.L.; van der Velde, A.E.; van den Oever, K.; Levels, J.H.; Huet, S.; Oude Elferink, R.P.; Kuipers, F. Groen, A.K. Peroxisome proliferator-activated receptor delta activation leads to increased transintestinal cholesterol efflux. *J. Lipid Res.*, **2009**, 50(10), 2046-2054.

[47]　Kennedy, M.A.; Venkateswaran, A.; Tarr, P.T.; Xenarios, I.; Kudoh, J.; Shimizu, N. Edwards, P.A. Characterization of the human ABCG1 gene: liver X receptor activates an internal

promoter that produces a novel transcript encoding an alternative form of the protein. *J. Biol. Chem.*, **2001**, 276(42), 39438-39447.

[48]   Wagner, B.L.; Valledor, A.F.; Shao, G.; Daige, C.L.; Bischoff, E.D.; Petrowski, M.; Jepsen, K.; Baek, S.H.; Heyman, R.A.; Rosenfeld, M.G.; Schulman, I.G. Glass, C.K. Promoter-specific roles for liver X receptor/corepressor complexes in the regulation of ABCA1 and SREBP1 gene expression. *Mol. Cell Biol.*, **2003**, 23(16), 5780-5789.

[49]   Laffitte, B.A.; Repa, J.J.; Joseph, S.B.; Wilpitz, D.C.; Kast, H.R.; Mangelsdorf, D.J. Tontonoz, P. LXRs control lipid-inducible expression of the apolipoprotein E gene in macrophages and adipocytes. *Proc. Natl. Acad. Sci. U S A*, **2001**, 98(2), 507-512.

[50]   Repa, J.J.; Berge, K.E.; Pomajzl, C.; Richardson, J.A.; Hobbs, H. Mangelsdorf, D.J. Regulation of ATP-binding cassette sterol transporters ABCG5 and ABCG8 by the liver X receptors alpha and beta. *J. Biol. Chem.*, **2002**, 277(21), 18793-18800.

[51]   Peet, D.J.; Turley, S.D.; Ma, W.; Janowski, B.A.; Lobaccaro, J.M.; Hammer, R.E. Mangelsdorf, D.J. Cholesterol and bile acid metabolism are impaired in mice lacking the nuclear oxysterol receptor LXR alpha. *Cell*, **1998**, 93(5), 693-704.

[52]   Shukla, G.C.; Singh, J. Barik, S. MicroRNAs: Processing, Maturation, Target Recognition and Regulatory Functions. *Mol. Cell Pharmacol.*, **2011**, 3(3), 83-92.

[53]   Najafi-Shoushtari, S.H.; Kristo, F.; Li, Y.; Shioda, T.; Cohen, D.E.; Gerszten, R.E. Naar, A.M. MicroRNA-33 and the SREBP host genes cooperate to control cholesterol homeostasis. *Science*, **2010**, 328(5985), 1566-1569.

[54]   Rayner, K.J.; Suarez, Y.; Davalos, A.; Parathath, S.; Fitzgerald, M.L.; Tamehiro, N.; Fisher, E.A.; Moore, K.J. Fernandez-Hernando, C. MiR-33 contributes to the regulation of cholesterol homeostasis. *Science*, **2010**, 328(5985), 1570-1573.

[55]   Harborne, J.B. Williams, C.A. Advances in flavonoid research since 1992. *Phytochemistry*, **2000**, 55(6), 481-504.

[56]   Vogt, T. Phenylpropanoid biosynthesis. *Mol. Plant*, **2010**, 3(1), 2-20.

[57]   Benavente-Garcia, O. Castillo, J. Update on uses and properties of citrus flavonoids: new findings in anticancer, cardiovascular, and anti-inflammatory activity. *J. Agric. Food Chem.*, **2008**, 56(15), 6185-6205.

[58]   Gattuso, G.; Barreca, D.; Gargiulli, C.; Leuzzi, U. Caristi, C. Flavonoid composition of Citrus juices. *Molecules*, **2007**, 12(8), 1641-1673.

[59]   Nogata, Y.; Sakamoto, K.; Shiratsuchi, H.; Ishii, T.; Yano, M. Ohta, H. Flavonoid composition of fruit tissues of citrus species. *Biosci. Biotechnol. Biochem.*, **2006**, 70(1), 178-192.

[60]   Di Donna, L.; De Luca, G.; Mazzotti, F.; Napoli, A.; Salerno, R.; Taverna, D. Sindona, G. Statin-like principles of bergamot fruit (Citrus bergamia): isolation of 3-hydroxymethylglutaryl flavonoid glycosides. *J. Nat. Prod.*, **2009**, 72(7), 1352-1354.

[61]   Di Donna, L.; Iacopetta, D.; Cappello, A.R.; Gallucci, G.; Martello, E.; Fiorillo, M.; Dolce, V. Sindona, G. Hypocholesterolaemic activity of 3-hydroxy-3- methyl-glutaryl flavanones enriched fraction from bergamot fruit (Citrus bergamia): ''In vivo'' studies. *J. Funct. Foods*, **2014**, 7(558-568).

[62]   Sindona, G.; Di Donna, L. Dolce, V. Natural molecules extracted from bergamot tissues, extraction process and pharmaceutical use., **April 15, 2010**, WO/2010/041290 A1(WO/2010/041290 A1).

[63]   Gardana, C.; Nalin, F. Simonetti, P. Evaluation of flavonoids and furanocoumarins from Citrus bergamia (Bergamot) juice and identification of new compounds. *Molecules*, **2008**, 13(9), 2220-2228.

[64]   Mandalari, G.; Bennett, R.N.; Bisignano, G.; Saija, A.; Dugo, G.; Lo Curto, R.B.; Faulds, C.B. Waldron, K.W. Characterization of flavonoids and pectins from bergamot (Citrus bergamia Risso) peel, a major byproduct of essential oil extraction. *J. Agric. Food Chem.*, **2006**, 54(1), 197-203.

[65]   Dugo, P.; Presti, M.L.; Ohman, M.; Fazio, A.; Dugo, G. Mondello, L. Determination of flavonoids in citrus juices by micro-HPLC-ESI/MS. *J. Sep. Sci.*, **2005**, 28(11), 1149-1156.

[66]   Gattuso, G.; Barreca, D.; Caristi, C.; Gargiulli, C. Leuzzi, U. Distribution of flavonoids and furocoumarins in juices from cultivars of Citrus bergamia Risso. *J. Agric. Food Chem.*, **2007**, 55(24), 9921-9927.

[67]   Gattuso, G.; Caristi, C.; Gargiulli, C.; Bellocco, E.; Toscano, G. Leuzzi, U. Flavonoid glycosides in bergamot juice (Citrus bergamia Risso). *J. Agric. Food Chem.*, **2006**, 54(11), 3929-3935.

[68]   Caristi, C.; Bellocco, E.; Gargiulli, C.; Toscano, G. Leuzzi, U. Flavone-di-C-glycosides in citrus juices from Southern Italy. *Food Chem.*, **2006**, 95(3), 431-437.

[69]   Dugo, P.; Mondello, L.; Dugo, L.; Stancanelli, R. Dugo. G. LC-MS for the identification of oxygen heterocyclic compounds in citrus essential oils. *J. Pharm. Biomed. Anal.*, **2000**, 24(1), 147-154.

[70]   Barreca, D.; Bellocco, E.; Caristi, C.; Leuzzi, U. Gattuso, G. Flavonoid composition and antioxidant activity of juices from Chinotto (Citrus x myrtifolia Raf.) fruits at different ripening stages. *J. Agric. Food Chem.*, **2010**, 58(5), 3031-3036.

[71]   Morin, B.; Nichols, L.A.; Zalasky, K.M.; Davis, J.W.; Manthey, J.A. Holland, L.J. The citrus flavonoids hesperetin and nobiletin differentially regulate low density lipoprotein receptor gene transcription in HepG2 liver cells. *J. Nutr.*, **2008**, 138(7), 1274-1281.

[72]   Kou, M.C.; Fu, S.H.; Yen, J.H.; Weng, C.Y.; Li, S.; Ho, C.T. Wu, M.J. Effects of citrus flavonoids, 5-hydroxy-3,6,7,8,3',4'-hexamethoxyflavone and 3,5,6,7,8,3',4'-heptamethoxyflavone, on the activities of macrophage scavenger receptors and the hepatic LDL receptor. *Food Funct.*, **2013**, 4(4), 602-609.

[73]   Choe, S.C.; Kim, H.S.; Jeong, T.S.; Bok, S.H. Park, Y.B. Naringin has an antiatherogenic effect with the inhibition of intercellular adhesion molecule-1 in hypercholesterolemic rabbits. *J. Cardiovasc. Pharmacol.*, **2001**, 38(6), 947-955.

[74]   Yu, J.; Wang, L.; Walzem, R.L.; Miller, E.G.; Pike, L.M. Patil, B.S. Antioxidant activity of citrus limonoids, flavonoids, and coumarins. *J. Agric. Food Chem.*, **2005**, 53(6), 2009-2014.

[75]   Miceli, N.; Mondello, M.R.; Monforte, M.T.; Sdrafkakis, V.; Dugo, P.; Crupi, M.L.; Taviano, M.F.; De Pasquale, R. Trovato, A. Hypolipidemic effects of Citrus bergamia Risso et Poiteau juice in rats fed a hypercholesterolemic diet. *J. Agric. Food Chem.*, **2007**, 55(26), 10671-10677.

[76]   Paine, M.F.; Criss, A.B. Watkins, P.B. Two major grapefruit juice components differ in time to onset of intestinal CYP3A4 inhibition. *J. Pharmacol. Exp. Ther.*, **2005**, 312(3), 1151-1160.

[77]   Mollace, V.; Sacco, I.; Janda, E.; Malara, C.; Ventrice, D.; Colica, C.; Visalli, V.; Muscoli, S.; Ragusa, S.; Muscoli, C.; Rotiroti, D. Romeo, F. Hypolipemic and hypoglycaemic activity of bergamot polyphenols: from animal models to human studies. *Fitoterapia*, **2011**, 82(3), 309-316.

[78]   Gliozzi, M.; Walker, R.; Muscoli, S.; Vitale, C.; Gratteri, S.; Carresi, C.; Musolino, V.; Russo, V.; Janda, E.; Ragusa, S.; Aloe, A.; Palma, E.; Muscoli, C.; Romeo, F. Mollace, V. Bergamot polyphenolic fraction enhances rosuvastatin-induced effect on LDL-cholesterol, LOX-1 expression and protein kinase B phosphorylation in patients with hyperlipidemia. *Int. J. Cardiol.*, **2013**, 170(2), 140-145.

[79]   Di Donna, L.; Iacopetta, D.; Cappello, A.R.; Gallucci, G.; Martello, E.; Fiorillo, M.; Dolce, V. Sindona, G. Hypocholesterolaemic activity of 3-hydroxy-3- methyl-glutaryl flavanones enriched fraction from bergamot fruit (Citrus bergamia): ''In vivo'' studies. *J. Funct. Foods*, **2014**, 7(558-568).

[80]   Kong, W.J.; Wei, J.; Zuo, Z.Y.; Wang, Y.M.; Song, D.Q.; You, X.F.; Zhao, L.X.; Pan, H.N. Jiang, J.D. Combination of simvastatin with berberine improves the lipid-lowering efficacy. *Metabolism*, **2008**, 57(8), 1029-1037.

[81]   Lee, S.; Birukov, K.G.; Romanoski, C.E.; Springstead, J.R.; Lusis, A.J. Berliner, J.A. Role of phospholipid oxidation products in atherosclerosis. *Circ. Res.*, **2012**, 111(6), 778-799.

[82]   Bochkov, V.N.; Oskolkova, O.V.; Birukov, K.G.; Levonen, A.L.; Binder, C.J. Stockl, J. Generation and biological activities of oxidized phospholipids. *Antioxid. Redox Signal*, **2010**, 12(8), 1009-1059.

[83]   Berliner, J.A.; Leitinger, N. Tsimikas, S. The role of oxidized phospholipids in atherosclerosis. *J. Lipid Res.*, **2009**, 50 Suppl(S207-212.

[84]   Trombetta, D.; Cimino, F.; Cristani, M.; Mandalari, G.; Saija, A.; Ginestra, G.; Speciale, A.; Chirafisi, J.; Bisignano, G.; Waldron, K.; Narbad, A. Faulds, C.B. In vitro protective effects of two extracts from bergamot peels on human endothelial cells exposed to tumor necrosis factor-alpha (TNF-alpha). *J. Agric. Food Chem.*, **2010**, 58(14), 8430-8436.

[85]   Kim, Y.S.; Ahn, Y.; Hong, M.H.; Joo, S.Y.; Kim, K.H.; Sohn, I.S.; Park, H.W.; Hong, Y.J.; Kim, J.H.; Kim, W.; Jeong, M.H.; Cho, J.G.; Park, J.C. Kang, J.C. Curcumin attenuates inflammatory

responses of TNF-alpha-stimulated human endothelial cells. *J. Cardiovasc. Pharmacol.*, **2007**, 50(1), 41-49.

[86]   Scheuer, H.; Gwinner, W.; Hohbach, J.; Grone, E.F.; Brandes, R.P.; Malle, E.; Olbricht, C.J.; Walli, A.K. Grone, H.J. Oxidant stress in hyperlipidemia-induced renal damage. *Am. J. Physiol. Renal Physiol.*, **2000**, 278(1), F63-74.

[87]   Chade, A.R.; Rodriguez-Porcel, M.; Grande, J.P.; Krier, J.D.; Lerman, A.; Romero, J.C.; Napoli, C. Lerman, L.O. Distinct renal injury in early atherosclerosis and renovascular disease. *Circulation*, **2002**, 106(9), 1165-1171.

[88]   Stulak, J.M.; Lerman, A.; Porcel, M.R.; Caccitolo, J.A.; Romero, J.C.; Schaff, H.V.; Napoli, C. Lerman, L.O. Renal vascular function in hypercholesterolemia is preserved by chronic

antioxidant supplementation. *J. Am. Soc. Nephrol.*, **2001**, 12(9), 1882-1891.

[89]   Trovato, A.; Taviano, M.F.; Pergolizzi, S.; Campolo, L.; De Pasquale, R. Miceli, N. Citrus bergamia Risso & Poiteau juice protects against renal injury of diet-induced hypercholesterolemia in rats. *Phytother. Res.*, **2010**, 24(4), 514-519.

[90]   Jones, P.H. Expert perspective: reducing cardiovascular risk in metabolic syndrome and type 2 diabetes mellitus beyond low-density lipoprotein cholesterol lowering. *Am. J. Cardiol.*, **2008**, 102(12A), 41L-47L.

[91]   Joy, T.R. Hegele, R.A. Narrative review: statin-related myopathy. *Ann. Intern. Med.*, **2009**, 150(12), 858-868.

UNIVERSITY OF CALABRIA

Ph.D. candidate : Dhanya Dhanyalayam

Academic tutor: Prof.ssa. Anna Rita Cappello.

Department of Pharmacy, Health and Nutritional Sciences

Title of the thesis:

STUDY OF ANTIMICROBIAL AND ANTICANCER ACTIVITY OF NEW SYNTHETIC AND NATURAL TOOLS

Curriculum: Basi molecolari della malattie e applicazioni terapeutiche innovative

05/E - BIOCHIMICA E BIOLOGIA MOLECOLARE SPERIMENTALI E CLINICHE

Settore Scientifico Disciplinare: Bio/10

REPORT ON THE ACTIVITIES OF SCIENTIFIC RESEARCH PERFORMED

My doctoral research was carried out under the supervision of Prof.ssa Anna Rita Cappello. My research project was aimed at studying pharmaceutical properties of new molecules with the aim of identifying some compounds with anticancer activity, as well as anti parasitic and antibacterial agents which are useful for the treatment of diseases caused by antibiotic resistant pathogens.

Infectious diseases and cancer are the two disease groups that representing the major cause of death worldwide. Unfortunately, antibiotic resistance is the biggest threat in the first case; in fact, new resistance mechanisms continuously are emerging and spreading globally, threatening the ability to treat common infectious diseases. A growing list of infections caused by bacteria, viruses, parasites etc. are becoming harder and harder to treat, and sometimes impossible, as antibiotics become less effective. Without urgent action, we are heading for a post-antibiotic era, in which common infections and minor injuries can once again kill the human population. Concerning cancer, Resistance to chemotherapy and molecularly targeted therapies is a major problem in current research. Drugs side effects and toxicity to normal body

cells is also an important threat in cancer treatments. In this regard, these problems are at the forefront of scientific research and technological innovation and are leading to the development of new therapeutic approaches against cancer and infectious disease with fewer side effects and lesser resistance problems.

The aim of the present study was to investigate on the new compounds in order to find new possible therapeutic agents against bacteria, parasites and cancer.

Infectious diseases are caused by microorganisms such as bacteria, parasites, viruses etc.; in particular, bacterial infectious diseases are caused by either Gram +ve or Gram -ve bacteria. Certainly, antibiotics are the main weapon against infectious bacterial diseases; however, the uncontrolled use of antibiotics to control infections in humans, animals and in agriculture caused the development of drug resistance by bacterial populations. Besides this, infections caused by Gram -ve bacteria are difficult to treat due to the presence of a protective outer membrane consisting of lipopolysaccharides. Therefore, it is clear that there is a need to develop novel classes of antibacterial agents capable of killing bacteria through mechanisms unlike those of the known classes of antibiotics. Then, scientists are currently searching for new approaches to treat infectious diseases, particularly those caused by Gram -ve bacteria, focusing on exactly how the pathogens change and how drug resistance evolves.

Since ancient times, metal complexes have been used as antibacterial compounds, metallic silver and silver salts are good examples of this. Silver compounds are particularly interesting since their antibacterial activity can be altered by changing the ligand associated with the silver complex. To date, among silver derivatives, silver sulfadiazine remains one of the most commonly-used antibacterial drugs. Therefore, metal N-heterocyclic carbene (M-NHC) complexes appeared as an emerging field of research in medicinal chemistry where NHC complexes of coinage metals (Cu, Au, and Ag) proved to be better antimicrobial agents. Herein, it was investigated the, in vitro, antibacterial activity of the newly synthesized silver (Ag) complexes, Iodide[N-methyl-N-(2-hydoxy-cyclopentyl-imidazole-2ylidine]silver(I), Iodide[N-methyl-N-(2-hydoxy-cyclohexyl)-imidazole-2-ylidine]silver(I) and Iodide[N-methyl-N-(2-hydoxy-2-phenyl)ethyl-imidazole-2-ylidine]silver(I), namely AgL6, AgL18 and AgL20, against two Gram +ve (Staphylococcus aureus, Streptococcus pyogenes) and three Gram -ve (Escherichia coli, Klebsiella pneumoniae and Pseudomonas aeruginosa) bacteria. Among these, AgL6 showed good antibacterial activity against both Gram +ve and Gram -ve bacteria. However, the minimum inhibitory concentration (MIC) value was 32 μg/mL for Gram +ve and

16 μg/mL for Gram -ve bacteria, which was higher than that displayed by commercial drug, used as control (Silver Sulfadiazine, AgSD).

We therefore hypothesized that the poor activity is due to the poor intake of the compound. In order to enhance its antibacterial activity, we have developed "a pharmaceutically-oriented device", a nanocarrier as a tool for targeted drug delivery. Here it was described, for the first time, the production of a polymer nanostructure in which dextran, a biopolymer, and oleate residues represent the hydrophilic and hydrophobic parts, respectively. This nanoparticle was loaded with AgL6 and the antibacterial activity has been investigated. The results were very interesting, with MIC values being reduced four-fold for both Gram +ve and Gram -ve bacteria. Surprisingly, these values were two-fold lower than for silver sulfadiazine. Briefly, our results showed that K. pneumoniae and E. coli are the most susceptible bacteria to AgL6, followed by P. aeruginosa.

In conclusion, the investigated compound AgL6 showed excellent potentiality against bacterial infections.

According to the World Health Organization (WHO), 17 diseases caused by bacteria and parasites have been classified as neglected tropical diseases (NTDs). NTDs are endemic in 149 tropical and subtropical countries and affect more than 1 billion people, including 875 million children. These diseases are responsible for over 500,000 deaths per year and are characterized by severe pain and long-term disability. Human African Trypanosomiasis (sleeping sickness) is an important disease among them and is caused by two parasites of the genus Trypanosome: Trypanosome brucei rhodesiense and Trypanosome brucei gambiense. Trypanosomiasis is a disease with a devastating socio-economic impact in sub-Saharan Africa through direct infection of humans and livestock. This disease is fatal if left untreated. Current therapy relies on five drugs that have many limitations among which acute toxicity, problems with oral absorption and emergence of trypanosomal resistance, this latter is a major concern owing to the absence of vaccines and therapeutic alternatives. Therefore, pharmaceutical research is aimed at the discovery of new drugs, although the investment in this therapeutic area is not attractive owing to the prospect of poor financial returns. Many pharmaceutical industries have already utilized an opportunistic approach by utilizing drugs long since used for other diseases, a process known as "repurposing" of the drug. It is estimated that over half of the drugs used today are derived from natural sources.

In the present study, in a search for molecules with trypanocida activity, it was screened 2000 natural extracts from Fungi and Actinomycetes. The extracts showing activity were selected, and the active compound was identified by liquid chromatography and mass spectroscopy. Chaetocin is one of the molecules identified which showed good trypanocidal activity when tested in vitro. Chaetocin is already used as an antibacterial and anticancer drug, here it was repurposed as drug against trypanosomiasis. The results were very surprising because the trypanocidal activity was in the nanomolar range; the IC50 value was found to be 8.3 nM.

Next, it was investigated on its mechanism of action. In chaetocin treated cells, morphological changes and chromatin degradation were identified, by immunofluorescence and cell-cycle arrest during the G2 phase was proven by cytometry analysis. Finally, it was hypothesized that the enzyme histone methyl transferase, an important enzyme acting in the G2 phase, could be the target for this drug. This study displayed that chaetocin could have great potentiality in the fight against the deadly trypanosomiasis. However, further studies will be needed to reveal whether this compound can cross the blood-brain barrier.

In the third part of this thesis it was evaluated the synthesis and anticancer activity of some phosphonium salts. Phosphonium salts are a class of lipophilic cationic molecules that accumulate preferentially in mitochondria and inhibit the growth of human cancer cell lines.

The aim of the present study was to investigate the effects of a lipophilic phosphonium salt, (11-methoxy, 11-oxoundecyl)triphenylphosphonium bromide (MUTP) along with two other newly synthesized phosphine oxide salts, 3,3'-(methylphosphoryl)dibenzenaminium chloride and 3,3'-(phenylphosphoryl)dibenzenaminium chloride (SBAMPO and SBAPPO) on proliferation, in two human cancer cell lines: human breast cancer cells (MCF-7) and human uterine cervix adenocarcinoma cells (HeLa) and to elucidate their mechanism. The cancer cell mitochondrial membrane potential is relatively high when compared to normal cells, this force the phosphonium salts to accumulate, preferencially, in the mitochondria and inhibit their function. The results showed that only MUTP exhibits anti-proliferative effects on both cell lines, without affecting normal breast epithelial cell proliferation. More specifically, it was demonstrated that MUTP treatment of breast cancer cells is associated with impaired cell cycle progression, as determined by cytometry analysis. The G1/S cell cycle arrest was confirmed by an increased expression level of two proteins involved in cell cycle regulation, p21 and p53.

Recently, there has been a surge of interest in developing compounds selectively targeting mitochondria for the treatment of neoplasms. The critical role of mitochondria in cellular metabolism and respiration supports this therapeutic rationale. Dysfunction in the processes of energy production and metabolism contributes to attenuation of response to pro-apoptotic stimuli and increased ROS production both of which are implicated in the initiation and progression of most human cancers. Therefore, in order to characterize the mitochondrial function in MCF7 cells, after MUTP treatment, the cells were stained with specific metabolic probes and analyzed by FACS.

The outcomes displayed that MUTP treatment decreased mitochondrial mass and mitochondrial membrane potential and increased the ROS production. In agreement with these findings, the reduction in the expression of the mitochondrial oxidative pathway (OXPHOS) enzymes revealed a bioenergetics failure, induced by MUTP, in treated cells. TUNEL assay, DNA Laddering and Western blot analysis of caspase-3, caspase-9 and Bax confirmed the apoptotic effect of MUTP treatment.

Taken together, all these data suggest that MUTP may be capable of selectively targeting neoplastic cell growth and therefore has potential applications as an anticancer agent.

Publications

- ✓ Thangavel H and **Dhanyalayam D**. (2017) Proteomic Applications of Polymeric Nanoparticles with Engineered Affinity towards Select Target. *Journal of Nanomedicine Research,* 5(4):00124.

- ✓ **Dhanyalayam D**, Palma G, Cappello AR, Mariconda A, Sinicropi MS, Giordano F, Del Vecchio V, Ramunno A, Arra C, Longo P and Saturnino C. (2017) Phosphonium Salt Displays Cytotoxic Effects Against Human Cancer Cell Lines. *Anti-Cancer Agents in Medicinal Chemistry.* (Under 2nd revision)

- ✓ **Dhanyalayam D**, Parisi OI, Scrivano L, Cappello AR, Puoci F, Sinicropi S and Saturnino C. (2017) Biopolymeric Self-assembled Nanoparticles for Enhanced Antibacterial Activity of Novel Ag- and Au-based Drugs. *International Journal of Pharm*, 517(1-2):395-402.

- ✓ Cappello AR, Dolce V, Iacopetta D, Martello M, Fiorillo M, Curcio R, Muto L and **Dhanyalayam D**. (2016) Bergamot (Citrus bergamia Risso) Flavonoids and Their

Potential Benefits in Human Hyperlipidemia and Atherosclerosis: an Overview. *Mini reviews in medicinal chemistry,* 16(8):619-29.

Poster communications

- ✓ Cappello Anna Rita, Caruso Anna, Iacopetta Domenico, **Dhanyalayam Dhanya**, Puoci Francesco, Parisi Ortensia Ilaria, Longo Pasquale, Sinicropi Maria Stefania and Saturnino Carmela. (2014) Metal complexes: synthesis and preliminary biological studies. In: Atti del congresso COSENZA 7-12 settembre 2014 cosenza univ Pag.342-342.

- ✓ Ortiz Gonzales Matilde, **Dhanyalayam Dhanya**, Depedro Nuria, Garcia Salcedo Jose A. (2016) "Búsqueda de nuevas moléculas con actividad terapéutica para el tratamiento de la tripanosomiasis Africana" Conference in University of Granada, Spagna In: Atti del congresso 20-05-2016.

Participation of conferences

- ✓ **"La chimica scienza della sicurezza e dello sviluppo sostenibile"** organized by SOCIETÀ DI CHIMICA ITALIANA, sezione Calabria, on 22-23 giugno 2015.

- ✓ "**FAO World food day**" congress organized by University of Calabria (23 october 2015, Aula magna, University of Calabria)

- ✓ "**III jornadas Cientificas de Genyo" organized by FIBAO & GENYO on 15 - 16 December**

- ✓ **2015, Granada, Spain.**

- ✓ **"Imaging, Genomica e nuove possibili Terapie",** congress organized by ECM XENIA EVENTI (Rende, 10 Giugno 2016).

International mobility program

- ✓ Completed an internship at "Instituto de Investigación Biosanitaria de Granada", University of Granada, Spain for 6 months from 01.11.2015 to 30.04.2016 under the supervision of Prof. Jose Antonio Garcia Salcedo.

Courses and workshop attended

- ✓ "Updating English testing frames for specialized language skills" by Prof.ssa Anna Franca Plastina on 27.01.2015 in Aula Circolare, University of Calabria.

- ✓ "Advanced English" containing 4 lessons (in between 26.01.205 to 16.02.2015) by Prof.ssa Anna Franca Plastina in Aula Seminari, University of Calabria. (2CFU)
- ✓ A course on Informatics containing 3 lessons (on 14.10.2015, 21.10.2015, 28.10.2015) by Andrea Tagarelli in aula of Centro Sanitario. (2CFU)
- ✓ "Percorso formative in materia di Innovazione, Ricerca etrasferimento Tecnologico" containing 9 modules from 02.07.2014 to 18.07.2014 organized by Liaison Office, UNICAL.

Participation of seminars

- ✓ **"Biomonitoraggio umano del mercurio"** by Prof.Nocola Pirrone on 07.03.2014 in Aula Circolare, University of Calabria.
- ✓ **"Le promesse della medicina genomica"** by Dott.Emiliano GIARDINA on 28.03.2014 in Aula Seminari, Centro Sanitario, University of Calabria.
- ✓ **"Salute e Donazione"** on 08.05.2014-09.05.2014 in Aula circolare, University of Calabria.
- ✓ "**Characterization of tryptophan metabolism in the central nervous system**" by Dott.ssa. Judit Heredy on 23.06.2014 in Aula Seminari, University of Calabria.
- ✓ **"Signaling pathways regulating breast cancer stem cell activity**" by Robert Bryan Clarke on 03.10.2014 in Aula Seminari, University of Calabria.
- ✓ "**Recent Advances in Computational Proteomics**" by Prof. Pedro A Fernandes on 11.12.2014 in cube 12C, University of Calabria.
- ✓ **"Epigenetic alteration and microRNA dysregulation in human cancers**" by Dott. Domenico Zito on 17.04.2015 in Aula Seminari, University of Calabria.
- ✓ **"Interaction of graphene with biological and biomimetic membranes**" by Dott. Arvind Vijayaraghavan on 15.06.2015 in Aula Circolare, Univeristy of Calabria.
- ✓ **" Sicurezza degli alimenti :il ruolo di accredia**" by Silvia Tramontin & "Accredia e laccreditamento dei laboratori" by Federico Pecoraro on 17.06.2015 in Aula Circolare, University of Calabria.
- ✓ **"Quantum chemistry applied to asymmetric homogeneous and enzymatic catalysis"** by Prof. Fahmi Himo on 11.09.2015 in cube 12C, University of Calabria.

- ✓ **"Salute dell'ambiente e salute umana: il caso del destino ambientale delle diossine in Campania"** by Dott. Nic Pacini on 08.10.2015 in Aula Seminari, University of Calabria.
- ✓ "**From systems biology to systems medicines-New approaches to neurodegenrative diseases"** by Prof. Rudi Balling on 12.01.2016 in Genyo, Granada, Spain.
- ✓ **"How to prevent dyslipidemia without causing hepatic steatosis or ketosis**" by Prof.Victor Zammit on 15.06.2016 in Centro Congressi, University of Calabria.